Enrichment of Low Grade Chromite Ore for the Recovery of Metal Values for Suitable Value added Product

Thesis Submitted

by

Amit Kumar Bhandary

DOCTOR OF PHILOSOPHY

School of Materials Science & Nano Technology
Faculty of Interdisciplinary Studies, Law & Management
Jadavpur University
Kolkata-700032
India

2024

- **TITLE OF THE THESIS:**

Enrichment of Low Grade Chromite Ore for the Recovery of Metal Values for Suitable Value added Product.

- **NAME, DESIGNATION & INSTITUTION OF SUPERVISORS:**

Dr. Mahua Ghosh Chaudhuri
Associate Professor
School of Materials Science and Nanotechnology
Jadavpur University
Kolkata- 700032

Prof. Rajib Dey
Professor
Department of Metallurgical & Material Engineering
Jadavpur University
Kolkata-700032

3.1 LIST OF PUBLICATION (Published):

- Amit Kumar Bhandary, Siddhartha Mukherjee, Rajib Dey, and Mahua Ghosh Chaudhuri, "Mineralogical studies and optimization of tabling parameters of low grade chromite ore by box behnken design of experiments", Journal of Metals, Materials and Minerals, Vol. 32, No. 4, pp. 174-185, 2022, https://doi.org/10.55713/jmmm.v32i4.1563.

- Amit Kumar Bhandary, Prithviraj Gupta, Siddhartha Mukherjee, Mahua Ghosh Chaudhuri, Rajib Dey, "Beneficiation of Low Grade Chromite Ore and Its Characterization for the Formation of Magnesia-Chromite Refractory by Economically Viable Process" , World Academy of Science, Engineering and Technology, International Journal of Chemical and Molecular Engineering, Vol: 10, No 8, 2016, doi.org/10.5281/zenodo.1126131

- Prithviraj Gupta, Amit Kumar Bhandary, Mahua Ghosh Chaudhuri, Siddhartha Mukherjee, Rajib Dey, "Kinetic Studies on the Reduction of Iron Oxides in Low-Grade Chromite. Ore by Coke Fines for Its Beneficiation", Arabian Journal for Science and Engineering, https://doi.org/10.1007/s13369-018-3324-x.

- Rajib Dey, Amit Kumar Bhandary, Maharshi Ghosh Dastidar, Siddhartha Mukherjee, Mahua Ghosh Chaudhuri, "Utilisation of Low Grade Chromite Ore for the Production of Carbon Free Ferrochrome" , mgmi_trans_vol_114_apr17_mar18.

3.2 LIST OF PUBLICATION (Communicated):

- **Amit Kumar Bhandary**, Santosh Khan, Sourav Adhikary, Rajib Dey, and Mahua Ghosh Chaudhuri, "Smelting of Pre-Heated Chromite Concentrate with Coke at Different Temperature and its Isothermal Kinetic Study", Journal of Iron and Steel Research International, Manuscript No. ISRI-D-24-00964.

4 LIST OF PATENTS:

- **NIL**

5. LIST OF PRESENTATION IN NATIONAL /INTERNATIONAL:

- Amit Kumar Bhandary, Rajib Dey, and Mahua Ghosh Chaudhuri,"Optimisation of Binder percentage to agglomerate chromite ore fines for using in SEAF in pre-reduced condition to produce ferrochrome", International seminar on prospects and challenges in metallurgical and allied industries with special emphasis on quality, safety and environment, Hotel Floatel, Kolkata on Ganges, February 22, 2019.

STATEMENT OF ORIGINALITY

I, Amit Kumar Bhandary, registered on 29th December 2017, do hereby declare that this thesis entitled "Enrichment of Low Grade Chromite Ore for the Recovery of Metal Values for Suitable Value Added Product" contains a literature survey and original research work conducted by me as part of my Doctoral studies.

All information in this thesis has been obtained and presented in accordance with existing academic rules and ethical conduct. I declare that, in compliance with these rules and conduct, I have fully cited and referenced all materials and results that are not original to this work.

Furthermore, I confirm that I have reviewed this thesis in accordance with the "Policy on Anti-Plagiarism, Jadavpur University, 2019", and the similarity level as verified by iThenticate software is 1%.

Signature of Candidate: Amit Kr. Bhandary

Date: 17.12.24

Certified by Supervisor(s):

(Signature with date, seal)

1. Rajib Dey
17/12/24

Professor
Metallurgical & Material Engg. Dept.
Jadavpur University
Kolkata - 700032

2. Mahua Ghosh Chaudhuri
17.12.24

Dr. (Ms) Mahua Ghosh Chaudhuri
Associate Professor
School of Materials Science and Nano Technology
Jadavpur University
Kolkata-700 032, India

CERTIFICATE FROM THE SUPERVISORS

This is to certify that the thesis entitled "**Enrichment of Low Grade Chromite Ore for the Recovery of Metal Values for Suitable Value Added Product**" submitted by **Amit Kumar Bhandary**, for the award of the **PhD (FISLAM)** degree of Jadavpur University, is entirely based on his own work conducted under the supervision of **Dr. Mahua Ghosh Chaudhuri and Prof. Rajib Dey**. Furthermore, neither this thesis nor any part of it has been submitted for any degree, diploma, or any other academic award elsewhere.

Mahua Ghosh Chaudhuri

Dr. Mahua Ghosh Chaudhuri

Associate Professor

School of Materials Science and Nanotechnology

Jadavpur University

Kolkata- 700032

Dr. (Ms) Mahua Ghosh Chaudhuri
Associate Professor
School of Materials Science and Nano Technology
Jadavpur University
Kolkata-700 032, India

Rajib Dey

Prof. Rajib Dey

Professor

Department of Metallurgical & Material Engineering

Jadavpur University

Kolkata-700032

Professor
Metallurgical & Material Engg. Dept,
Jadavpur University
Kolkata - 700032

Dedicated to My Family,

Friends, Mahua Mam

&

Rajib Sir

ACKNOWLEDGEMENT

I would like to express my deepest gratitude to all those who have supported and guided me throughout my PhD journey. Without their encouragement and assistance, this work would not have been possible.

First and foremost, I am profoundly grateful to my esteemed PhD guide, Dr. Mahua Ghosh Chaudhuri, for her exceptional guidance, support, and patience. Her insightful feedback and constructive criticism were invaluable in shaping this thesis. Her unwavering commitment to excellence and her meticulous attention to detail have greatly influenced my research and academic development. Similarly, I extend my heartfelt thanks to Prof. Rajib Dey for his invaluable contributions and guidance. His expertise and thoughtful advice have been crucial in refining my research and ensuring its rigor. His readiness to assist with complex problems and your commitment to my academic growth have made a significant impact on this thesis. His insights have been instrumental in shaping the direction of my work, and I am sincerely grateful for your mentorship. I would like to extend my heartfelt gratitude to Prof. Siddhartha Mukherjee, my project coordinator, for his exceptional support and guidance throughout my PhD journey. Prof. Mukherjee's expertise and commitment to excellence have significantly contributed to the successful completion of this research.

I would also like to extend my heartfelt appreciation to my wife, Pritha Pal, whose unwavering support, understanding, and encouragement have been my pillar of strength throughout this journey. Her sacrifices and patience have been a constant source of motivation, and her belief in me has been instrumental in my perseverance. Her presence has provided me with the emotional support needed to overcome the challenges faced during this research. I would also like to express my heartfelt love to my little son, whose presence has been a constant source of joy and motivation. His laughter and energy have reminded me of the beauty in life.

I would like to express my sincere appreciation to several faculty members of the department who have generously offered their support and valuable insights at various stages of my research. Their

willingness to assist and provide guidance whenever I sought their help has been instrumental in advancing my work. I am particularly grateful to Prof. M.K. Mitra, Prof. Gopes Chandra Das, Associate Professor Sathi Banerjee, Dr. C.K. Ghosh and Dr. S. Sarkar for their meaningful contributions and thoughtful suggestions.

To my friends, I am deeply thankful for their companionship and moral support. Their understanding and encouragement, especially during times of stress and fatigue, have been a great source of comfort. I appreciate their willingness to listen and provide perspective, which helped me navigate the complexities of my research and maintain a balanced outlook.

I would also like to extend my heartfelt thanks to my lab mates—Bitan, Maharshi, Chanchal da, Arnab da, Debarati, Prithviraj, Sourav, Sanjib, and Santosh—for their camaraderie and collaboration throughout my research. Their collective spirit and insightful discussions have significantly enriched my work and offered valuable perspectives.

Additionally, I am profoundly grateful to Anirban da, Anindya Roy, Saikat da, Supratim da, and Suparna di for providing instrumental facilities and offering valuable suggestions that have greatly contributed to the success of this research. Finally, I wish to acknowledge the administrative and technical staff at Jadavpur University for their assistance and support, which facilitated the smooth progress of my research.

I sincerely thank the Ministry of Mines for granting fellowship under their Science and Technology project scheme (2015–2017) and Tata Steel for providing the low-grade chromite ore essential for this research.

Thank you all for being an integral part of this journey. Your contributions have made this achievement possible, and I am sincerely grateful for your support.

Amit Kumar Bhandary

List of Contents

List of Figures

List of Tables

Chapter-1

Introduction

1.1 Background

Chromium is the first element found in group 6 of the periodic table. It is widely used in the metallurgical industry. Pure chromium cannot be found in nature. The only source of chromium metal is chromite ore ($FeOCr_2O_4$), an iron chromium oxide mineral. Steel is added with the qualities of hardness, toughness, and chemical resistance by the metal chromium. The resulting alloy is referred to as "stainless steel". Chromium content in stainless steel is at least 10.5%. These sources of chromium come from ferrochrome. 90 to 95% chromite ore is used for the production of ferrochrome. On the other hand, the stainless steel industry uses 80–90% of the FeCr produced. Thus, the need for stainless steel drives the need for chromite and FeCr. Global production of stainless steel is predicted to increase by 5.5% annually on average in 2013. Compared to 2020, the production of stainless steel rose by 13% in 2021 [1].

Ferrochrome is commercially produced from chromite ore. Chromite ore processing is difficult due to its spinal structure. Spinal structure is very complex in nature. Chromite ore is not found in its pure form in the Earth's crust. It is associated with different types of gangue minerals. The chemical formula of chromite ore is $FeCr_2O_4$. It is a member of the spinal group. AB_2O_4 is a common way to express it. In this formula, A and B represent divalent and trivalent cations respectively. In chromite ore trivalent cations B^{3+} can be Cr^{3+}, Al^{3+}, and Fe^{3+} present in octahedral sites, whereas divalent cations A^{2+} can be Fe^{2+} and Mg^{2+}present in tetrahedral sites. Two different sorts of structures result from the distribution of two different cations. One is common spinel, which has 16 trivalent cations and 8 divalent cations in the octahedral B sites. Second, inverse spinel, has eight of the sixteen trivalent cations in the tetrahedral A sites and eight trivalent and eight divalent cations in the octrahedral B sites. Due to the high density, divalent iron is typically replaced by magnesium, and chromium is replaced by aluminium, resulting in the formation of the minerals magnesiochromite ($MgCr_2O_4$) and hercynite ($FeAl_2O_4$). Spinel ($MgAl_2O_4$), magnetite (Fe_3O_4), and magnesioferrite ($MgFe_2O_4$) make up the other solid solutions found in chromite ore [2], [3]. Chromium metal is made using chromite as a raw material. Chromium increases a material's toughness, hardness, and strength. It exhibits resistance to steel abrasion and corrosion, lowers oxidation, and reduces electrical flow. Several important types of chromium steel are stainless steel, high-speed tool steel, and steel resistant to corrosion and heat. Ferrochrome comes

in three types: high carbon (4–8% carbon), medium carbon ferrochrome (2-4% carbon) and low carbon (up to 2% carbon). Different amounts of chromium are used in steel production [4].

The major source of chromite is ultra-mafic igneous rocks [5]. Different types of ultra-mafic igneous rock are present in the earth's crust. Peridotites, pyroxenites, amphibolites, and other ultra-mafic igneous rocks contain chromite ore. There are primarily two types of commercial chromite deposits: stratiform and podiform. In underground magma chambers, vast volumes of igneous rock cool very slowly to form stratiform deposits. Associated minerals including chromite crystallised early during this sluggish cooling. However, the magma was still extremely hot, causing the crystals to settle in the magma chamber based on their weight to create a stratified deposit. In this deposition, other minerals are associated with chromite ore. Minerals like olivine, magnetite, corundum, and serpentine are the major minerals associated with chromite ore. The size and reserve levels of the podiform deposit are small to medium. These types of ore are rich in magnesium and chromium. Podiform deposits are the most important source of metallurgical-grade chromite for high-carbon ferrochromium production. A stratiform deposit is where most of the chromite deposits are discovered. There are two types of mining used to extract chromite: open-pit and underground. Only stratiform deposits are suitable for underground mining [6], [7], [8], [9], [10].

1.2 Different Types of Chromite Ore

The grade of chromite ore is determined by the chromium-iron ratio. High-grade and low-grade chromite ore are the two categories into which it is separated based on the Cr: Fe ratio. High-grade chromite ore has a Cr: Fe ratio exceeding 1.5 whereas low-grade ore has a Cr: Fe ratio below 1.5. The grade of chromite ore is also thought to be characterized by the percentage of Cr_2O_3 contented. SK Tripathy et al. investigated the relation between Cr_2O_3% and Cr: Fe which is shown in Fig. 1 [11].

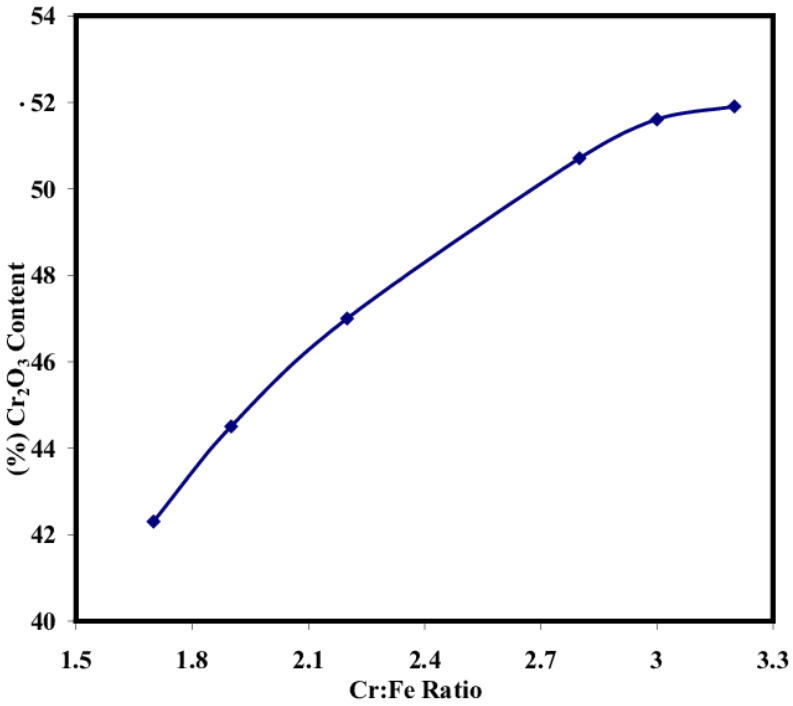

Figure 1: Relation Between Cr:Fe Ratio and (%) Cr_2O_3 Content.

The reduction of chromite ore requires a significant quantity of energy. Therefore, low-grade chromite ore cannot be used directly for the manufacturing of ferrochrome. In such cases, the beneficiation of low-grade chromite ore is crucial. Regarding total deposits of chromite ore, 24.90% of the ore in India is beneficiable [12]. Chromite ore is categorized according to how it is used as follows:

1. Metallurgical grade
2. Chemical grade
3. Foundry grade
4. Refractory grade

Chromite ore is called metallurgical grade if it contains a minimum of 40% Cr_2O_3, whereas 46%, 45%, and 46% Cr_2O_3 are required for chemical grade, foundry grade, and refractory grade, respectively.. Iron-rich chromite ore is suitable for the chemical grade, while chromite ore with high levels of aluminium and magnesium is optimal for the refractory grade. Ore of chromite with low silica content is appropriate for the foundry's application.

1.3 Applications and Types of Ferrochrome

Chromium metal is made using chromite as a raw material. Chromium increases a material's toughness, hardness, and strength. It exhibits resistance to steel abrasion and corrosion, lowers oxidation, and reduces electrical flow. Key types of chromium steel include stainless steel, high-speed tool steel, and steel resistant to corrosion and heat. To produce these types of chromium-based alloy steel ferrochrome is the most important raw material. Depending on the proportion of carbon in it, there are different types of ferrochrome on the market which is shown in Table 1 [13].

Table 1.1: Main Commercial Grades of FeCr According to ISO-Standard 54481-81 [13].

FeCr Grade	% Cr	% C	% Si	% P	**% S**
High-carbon	45-70	4-10	0-10	<0.05	**<0.10**
Medium-carbon	55-75	0.5-4	<1.5	<0.03	<0.05
Low-carbon	55-95	0.1-0.5	<1.5	<0.03	<0.03
Charge-grade	53-58	5-8	3-6		

Stainless steel, ball-bearing steel, tool steel, and other alloy steels are all produced using high-carbon ferrochrome. In contrast, acid-resistant steel, special steel, and super alloy are made using medium and low carbon ferrochrome. Nowadays, different ferrochrome grades are combined with nitrogen to create high-nitrogen ferrochrome, which is used to make high-chromium cast steels. High carbon ferrochrome is prepared by submerged electric arc furnace using metallurgical grade coke as a reductant. Carbothermic reduction is involved in that process. Due to its high production cost, medium to low-carbon ferrochrome is more expensive than high-carbon ferrochrome. Silicothermic reduction, which uses a lot of energy, is necessary for this process [5]. Ferrochrome slag is created during the extraction process of ferrochrome, which is used in ceramic, refractory, and other civil engineering applications.

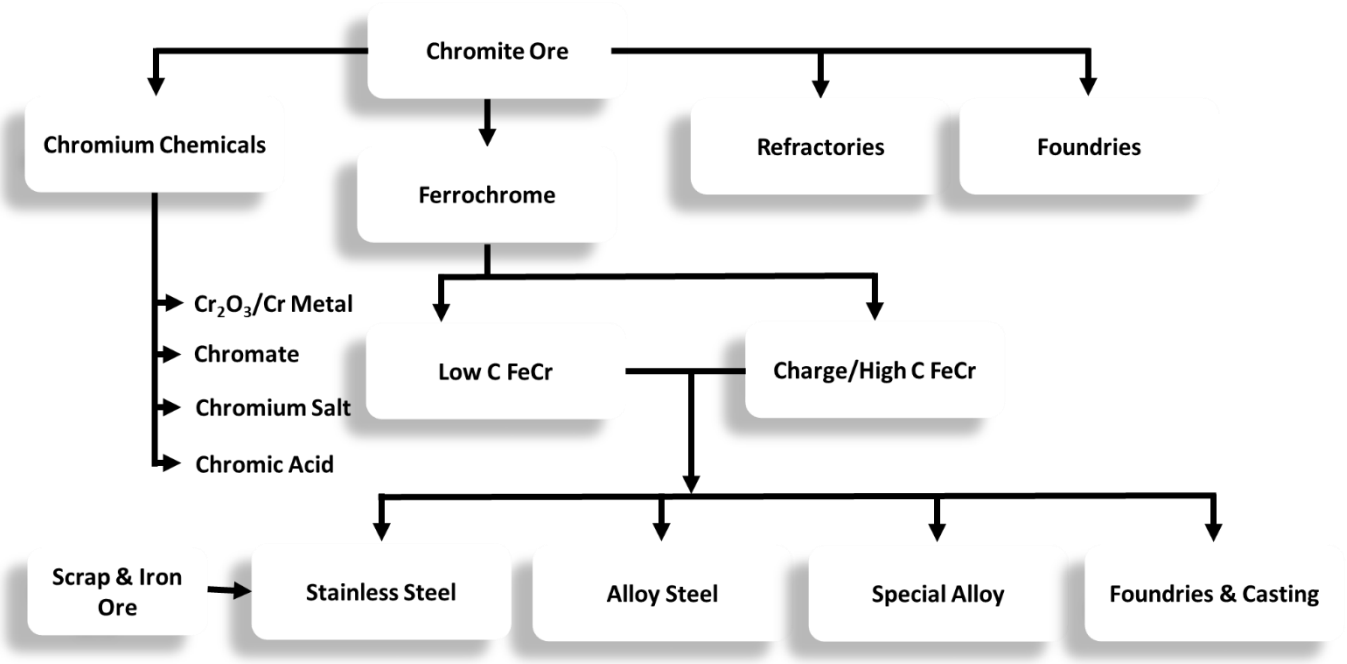

Figure 2: Applications of Chromite Ore.

Various amounts of chrome are utilized in steel industries. Chromite is an important refractory material to employ. Because of their superior corrosion resistance, mag-chrome refractories are used in non-ferrous metallurgy fields including copper, lead, and zinc refining. However, the bricks are still utilized in tap-hole plugs, argon-oxygen decarburizers (AODs), and steelmaking ladles. These refractories are used in cement and lime kilns. In high-temperature furnaces used in the glass industry, mag-chrome bricks are employed. Chromite ore is also used in chemical industries. Chromite is used to produce important chromium compounds like sodium and potassium chromates and bichromates. It is also utilized in the production of chromium pigments, including chromic oxide green and chromic acid. These compounds are employed in chromium-plating solutions. The various applications of chromite ore are summarized in Fig. 2.

1.4 Availability of Chromite Ore

South Africa, Kazakhstan, Turkiye, Finland, India, Brazil, and China all have significant resources of chromite ore. The majority of the world's reserves of chromite ore are in Kazakhstan and South Africa. Kazakhstan has the largest available reserves of chromite ore. There is a reserve of about 230 million tonnes of chromite ore in this nation. South Africa, with 200 million tonnes of chromite

ore reserves, ranks second. In terms of the reserve of chromite ore, India and Turkey are in third and fourth place, respectively [12], [14], [15] [6], [16].

South Africa is the world's largest producer of chromite, with an output of 18 million metric tons of chromite ore in 2024. In 2024, Turkey ranks as the second-largest producer of chromite, although its chromium production has declined compared to earlier years. With a production of roughly 4.2 million MT, India is the fourth-largest chromite ore producer in the world. The overall scenario of worldwide chromite ore reserves and chromite ore production is shown in Fig. 3 and Fig. 4.

Country	Reserves(Round off) (In "000 tonnes of Chromium Content)
Kazakhstan	**230000**
South Africa	**200000**
India	**100000**
Turkiye	**26000**
Finland	**13000**
United States	**620**
Other Countries	**0**
Total (Rounded)	**569620**

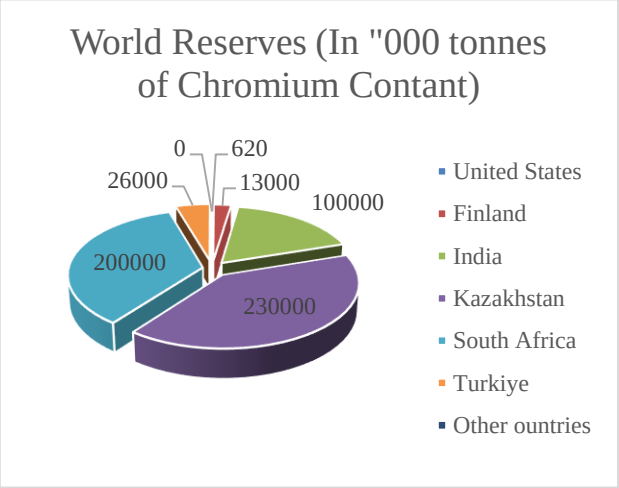

Figure 3: World Reserves of Shipping-Grade Chromite Ore.

Country	Chromite Ore Production (In tonnes)
South Africa	**18000000**
Turkiye	**6900000**
Kazakhstan	**6500000**
India	**4200000**
Finland	**2200000**
Others	**4000000**
World	**41800000**

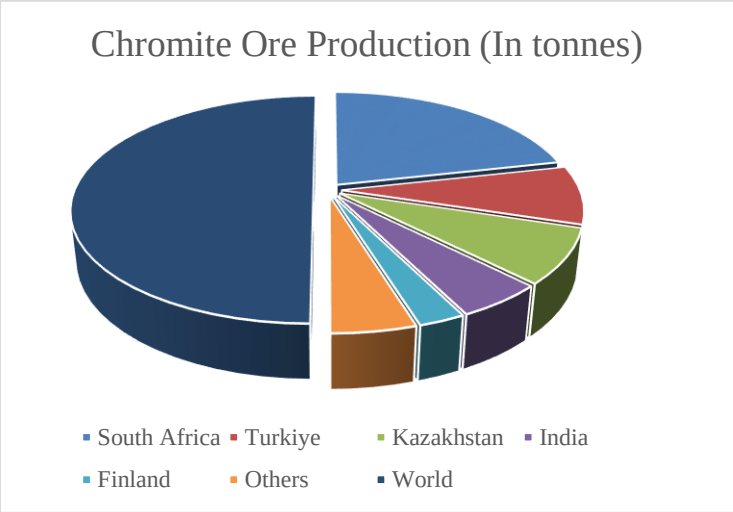

Figure 4: Worldwide Production of Chromite Ore.

1.5 Scenario of Chromite Ore in India

The Sukinda Valley in the Cuttak and Jajpur districts of Odisha is home to the majority of India's chromite ore reserve- more than 96% of it.

Table 1.2: State-Wise Chromite Ore Reserves in India.

State	**Reserves (In "000 tonnes)**	**Remaining Resources (In "000 tonnes)**	**Total (In "000 tonnes)**
Odisha	101412	229301	330713
Manipur	0	6657	6657
Nagaland	0	3200	3200
Karnataka	727	905	1632
Jharkhand	0	736	736
Maharashtra	71	538	609
Tamil Nadu	0	282	282
Telangana	0	186	186
Total	**102210**	**241805**	**344015**

Most of the ores in the Sukhinda Valley are of high-grade, soft, and friable composition. Minor deposits of chromite are found in Manipur, Nagaland, Karnataka, Jharkhand, Maharashtra, Tamil Nadu, and Andhra Pradesh. In India, there are 344.015 million tonnes of chromite ore reserves in total, of which 102.21 million tonnes are reserves (29.71%) and 241.805 million tonnes are reaming resources (70.329%) [6], [12]. The state-wise reserve of chromite ore in India is given in Table 2 and Fig. 5.

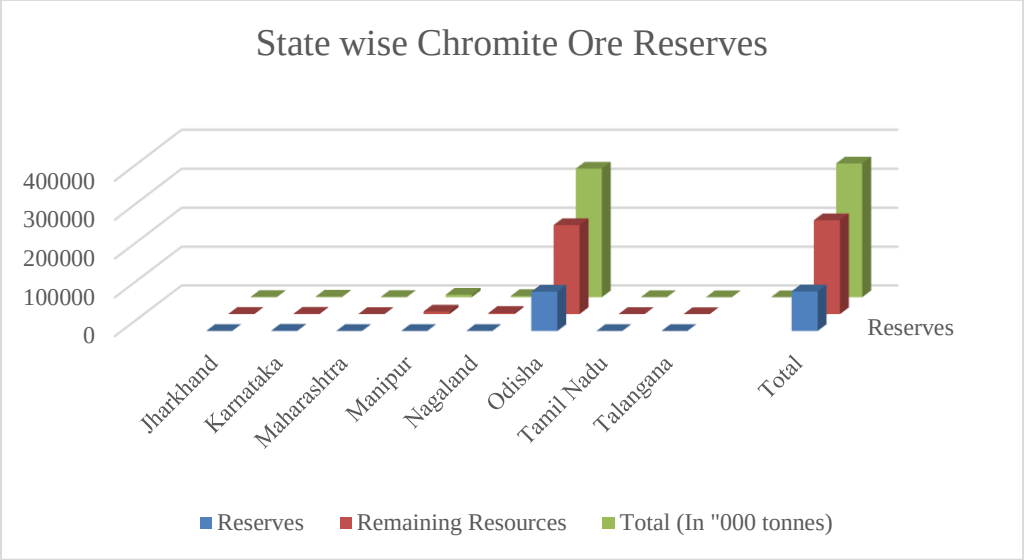

Figure 5: State-Wise Chromite Ore Reserves in India.

Table 1.3: Grade-Wise Chromite Ore Reserves in India.

Grade	**Reserves**	**Remaining Resources**	**Total (In "000 tonnes)**
Charge Chrome	25804	79905	105709
Beneficiable	31557	54139	85696
Ferrochrome	13842	47504	61346
Refractory	29978	17684	47662
Unclassified	896	37343	38239
Low	0	3765	3765
Other	133	740	873
Not-know	0	725	725
Total	**102210**	**241805**	**344015**

Charge-chrome grade accounts for 30.72% of the total, followed by ferrochrome grade at 17.83%, beneficiable grade at 24.90%, refractory grade at 13.85%, and other grades at 12.7%. In India, 25.99% of chromite ore has a low chromium-iron ratio. Grade-wise chromite ore reserve in India is shown in Table 3 and Fig. 6.

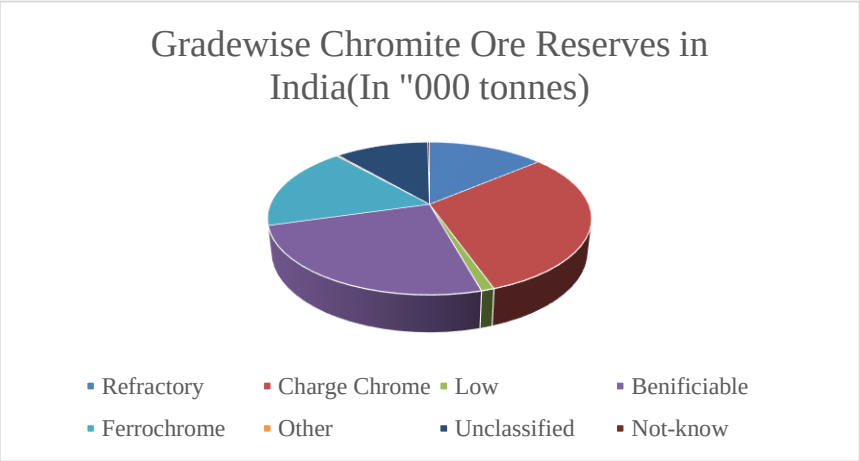

Figure 6: Grade-Wise Chromite Ore Reserves in India.

1.6 Grade-wise Production of Chromite Ore

Chromite ore mining produces lumps and fines with varying Cr:Fe ratios. Ferrochrome is directly derived from high-grade lumpy chromite ore. The issue appears while handling fines and low-grade chromite ore. There are a total of 22 chromite mines in India that process chromite ore in the 2019–20 academic year. The private sector is primarily responsible for producing chromite ore. The private sector owns and runs 13 of the 22 mines [12]**.** More than 90% of mines are located in the Odisha region. Table 4 reflects the overall grade-wise chromite ore production in different regions in India.

Table 1.4: Grade-Wise Production of Chromite, 2019-2020.

State/ District	Numbers of mines	Below 40% (In tonnes)		40-50% (In tonnes)		52% & Above (In tonnes)		Concentrates (In tonnes)	Total (In tonnes)
		Lumps	Fines	Lumps	Fines	Lumps	Fines		Quantity
India	**22**	**73044**	**830291**	**94838**	**1078617**		**1617150**	**235320**	**3929260**
Public Sector	9	320	314465	238	255292		225998	13409	809822
Private Sector	13	72724	515826	94600	823325		1391152	221911	3119538
Karnataka	**2**								
Hassan	2								
Odisha	**20**	**73044**	**830291**	**94838**	**1078617**		**1617150**	**235320**	**3929260**
Dhenkanal	3								
Jajpur	14	72724	830199	94600	1078617		1617150	235320	3928610
Keonjhar	3	320	92	238					650

Large amounts of fines are produced during the mining of chromite. Approximately 90% of the chromite ore is found as fines. Odisha is crucial to the exploitation of chromite ore. Out of the 20 chromite mines in Odisha, 14 are located in Jaipur. In 2019-20, Odisha will produce 3929260 tons of chromite ore, of which 3526058 tons are fines and 167882 tons are lumpy chromite ore.

1.7 Importance of Low-Grade Chromite Ore

Due to its capacity to impart a special corrosion resistance quality to a variety of alloying materials, chromium is becoming an increasingly essential element in the metal industry. Ferrochrome, which has a chromium content of more than 60% by weight, is the most widely exported chromium iron alloy. Since chromite ore is a widely accessible source of chromium, demand for it is rising daily. Chromite ore has a complicated mineral structure. Thus, the extraction of chromium from chromite ore requires a significant amount of electrical energy. For this reason, only high-grade chromite ore is utilized in the ferrochrome-making process. The current situation shows that the

growing need for ferrochrome is driving up the demand for high-grade chromite ore daily. However, the supply of high-grade chromite ore in the earth's crust is finite. In that case, using the low-grade reserves found in the earth's crust is crucial to maintaining the market's supply of ferrochrome. Because of its high power consumption, low-grade chromite ore cannot be immediately charged in a submerged electrical arc furnace used to produce ferrochrome in profitable volumes. Beneficiation is necessary to use those low-grade ore. Of India's total reserves of chromite ore, 25% are of a quality suitable for beneficiation. To upgrade low-grade ore, a variety of beneficiation processes are available; nevertheless, the selection of these techniques is crucial for both productivity and profitability [17], [18], [19].

1.8 Beneficiation Techniques

Additionally, significant amounts of subgrade ores containing 10 to 35% Cr_2O_3 are dug up. These low-grade ores are supplied to the plant for beneficiation. It is now more crucial than ever to use accessible lower-grade ores due to the progressive depletion of chromium-rich chromite ores. The run-of-mine ore (ROM) is typically first crushed and ground, and then the released ore is enhanced using a variety of methods. However, the Cr/Fe ratio cannot be raised through physical means. It requires pyro-metallurgical and/or hydrometallurgical treatment to upgrade to produce higher Cr/Fe ratios [5].

In the present scenario, different types of beneficiation techniques are used for the up-gradation of chromite ore. The most popular methods used in chromite ore beneficiation include gravity separation techniques, magnetic separation, froth flotation, flocculation, and electrostatic separation. Different techniques are adopted as per the chemical composition and gangue material associated with the chromite ore.

Magnetic separation is widely used in the beneficiation of ferruginous materials. To recover or enrich ferrous metals, magnetic separation is generally employed in solid waste treatment systems. The magnetic separation process can be used on a large scale. The method has been widely used in the beneficiation of iron-containing ore and beach sand [20], [21], [22], [23]. The froth flotation process enriches sulphur base minerals. The surface chemistry of the medium and ore particles served as the basis for the development of this approach. This commercially feasible method is used to beneficiate sulphide ore [24], [25], [26].

For significantly smaller particles, the flocculation beneficiation process is employed. Several flocculating chemicals aid in the coagulation of the particles in that procedure. Some uses for flocculation include water treatment facilities, sewage treatment facilities, drinking water purification facilities, and ore beneficiation plants [27], [28].

Gravity concentration techniques have been adopted worldwide. This classification technique uses the specific gravity difference between Chromite and gangue minerals. Chromite beneficiation generally has two main sections: communition and concentration. In a typical illustration, the feed preparation unit performs two-stage crushing, followed by grinding to a particle size of less than 1 mm. In the concentration section, the unit is upgraded by using traditional gravity techniques such as the wilfley table, hydrocyclones, spiral concentrators, and jigging. Each gravity separation method operates at its peak effectiveness throughout a narrow range of particle sizes. Spiral concentrators and hydrocyclones are frequently utilized in the chemical, agricultural, and metallurgical industries. Spiral hydrocyclones are used in metallurgical processes to remove impurities and silt from low-grade ore to enrich it. In the processing of ore, it is also used to separate particles of different sizes [29], [30], [31]. Jigging is one of the earliest ore treatment techniques and is now an essential part of the mining industry. It is a gravity separation technique that depends on the densities, sizes, and shapes of the particles [32].

In the gravity separation of low-grade chromite ore wilfley table plays a very important role. It separates various minerals present in ore by their different relative motion. Different materials in water move differently depending on their densities, gravitational forces, and other forces. It is mostly used to upgrade heavy minerals including chromite, ore rich in magnesium, iron, beach sand, and plant waste [33], [34]. The tabling process has a few benefits over other gravity separation methods for the beneficiation of chromite ore, which are listed below:

1. Unlike other mineral processing methods, the necessary grade can be readily attained when using the wilfley table by modifying the operating parameters.
2. Compared to other gravity separation methods, separation efficiency is substantially higher.
3. That method necessitates limited power usage.
4. The amount of raw material feed can be increased to meet production needs.
5. Concentrate, middling, and tailing and get at one single operation.

6. By changing riffle height and position in the wilfley Table different particle sizes of ore can be used for upgradation.
7. Wilfley table operation does not require any chemical reagent.

1.9 Agglomeration Processes

Beneficiated chromite ore fines cannot be directly charged for reduction melting because it results in limited gas permeability, stack formation in the furnace chamber, high power consumption, and other issues. For instance, processing lump chromite ore requires 4000KWh of power per tonne, while fines processing requires 4600KWh. The operation of fines requires an additional 600KWh of power. However, it is exceedingly challenging to transfer beneficiate chromite ore fines from one facility (plant) to another. Significant material loss happens during that process. Thus, in that perspective, the agglomeration of such fines is highly important [35].

A phenomenon known as agglomeration occurs when tiny solid particles stick together. It can also be a helpful procedure for improving powder characteristics and producing high-quality products by using controlled particle expansion. From a metallurgical perspective, the mining of ore results in significant fines production each year (lump-to-fine ratio: 2:3). As a result, fines are not charged directly into the furnace for reduction. Agglomeration is therefore essential for using these ore fines. Agglomeration is accomplished by heating or adding a binder to the ore particles. Depending on the size and makeup of the fines, the agglomeration process is essentially divided into pelletization, briquetting, and sintering. The main benefits of the pelletization process are (a) the relatively low consumption of energy and (b) the use of small particles [13], [36]. Typically, sintering is used for larger particle sizes. During that process, two or more particles fused together across the boundaries but avoided melting altogether. The benefits of that method include (a) good cold and hot strength, (b) the lack of a binder, and (c) good metallurgical performance [37], [38]. However, the briquetting technique is also quite effective at agglomerating chromite.

The briquettes' strong strength comes from the medium-sized particles, which range in size from 30 to 200 mesh. They are also referred to as nuggets. The technique of briquetting uses ore fines to create briquettes with pillow, almond, cylindrical, and other shaped components. Typically, bentonite, molasses, moisture, and iron oxides are present in briquettes. In this procedure, each

ingredient is added in the appropriate weight percentage at first. After mixing them, the mixture is put into the cylindrical die. The hydraulic press is filled with the mixture and the die. The die is put under pressure and allowed to rest for a period. Briquettes are extracted from the die after being driven out. The feed's bulk density rises during this procedure. Binders are crucial to the briquetting process. The briquettes' mechanical and physical strength comes from this binder. Both organic and inorganic binders exist. In the briquetting process, a variety of inorganic binders, including bentonite, lime, gypsum, clay, water glass, and cement, and organic binders, including tar, dextrin, resins, humic acid, and molasses, are utilized. A suitable water percentage frequently serves as both a lubricant and a green binder. Briquettes may be heated following the cold bonding procedure to give the joint extra durability [39], [40].

1.9.1 Advantages of Briquettes/Nuggets

A processing technique called briquetting includes combining fine ore, coal or coke, and binder particles. Utilizing pressure, those undergo compaction and transform into denser forms. Size fraction has no effect on briquetting. In contrast to sintering and pelletizing, which have substantial energy consumption and pollutants, this method is inexpensive, environmentally benign, and ambient.

The following are some briquettes' advantages:

- 1. The constituent raw materials' particle sizes are unrestricted.
- 2. That technique does not require a high temperature.
- 3. It is an agglomeration of high density.
- 4. Both high-grade and low-grade ore fines can be used in this method.
- 5. Briquettes are denser than sinters and pellets in terms of relative density.
- 6. The briquetting process makes use of ore fines, coke dust, non-coking coals, and by-products of metallurgical processing. Better ecological and environmental safety results from less solid waste in the steel industry.

1.10 Reduction and Smelting of Chromite Ore

The chromite ore is occasionally pre-reduced in a rotary kiln at a low temperature as part of the production process for ferrochrome. In that reduction, solid state reduction is used to partially reduce the chromite ore. The pre-reduction of ore in modern conventional procedures takes place

at temperatures between 1400 and 1500 °C, which is a pretty high temperature. In solid-state reduction, carbonaceous substances or CO gas produced by the Boudouard reaction are used to directly decrease the chromite ore. To produce ferrochrome, pre-reduced carbon chromite charge was used in a submerged electrical arc (SEAF). By using silicothermic reduction smelting and aluminothermic reduction smelting, respectively, low carbon (LC) and ultra-low carbon ferrochrome are produced. The manufacturing of LC ferrochrome in the condition of silicothermic reduction smelting now uses the argon-oxygen-decarburization (AOD) and vacuum-oxygen-decarburization (VOD) processes. The major applications for LC and ultra-LC ferrochrome are the production of superalloys and compositional finalization [41], [42], [43]. Different types of smelting processes of chromite ore are given in the Fig. 7.

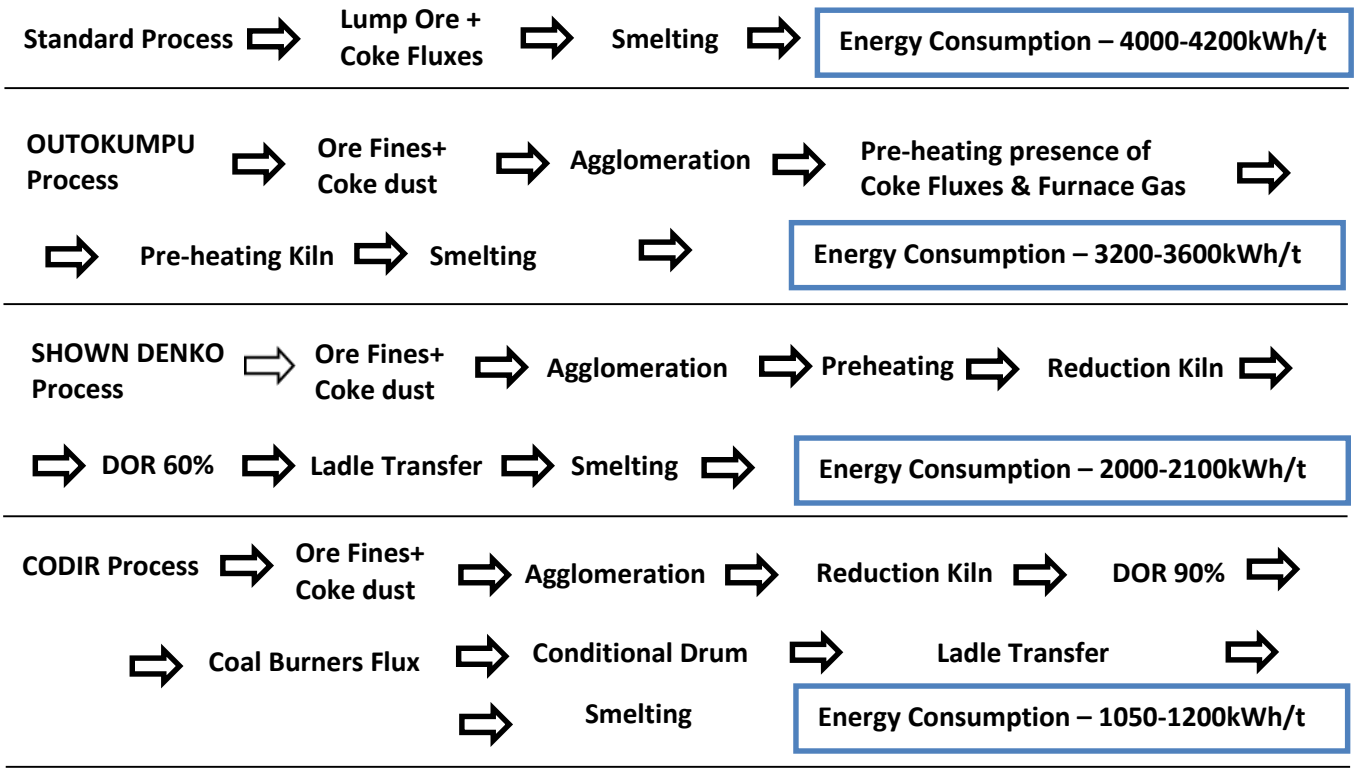

Figure 7: Types of Chromite Smelting Processes.

1.11 Isothermal Kinetic Study

A reaction that occurs in an experiment is described mathematically and theoretically by a kinetic study. When a solid-state reaction happens, different types of reactions take place. Different types of mathematical rate equations are present in order to determine the path of the reaction. These equations depict many kinetic models. These models are created using certain mechanistic presumptions. Equations 1 through 15 which is given in Table 5, are some of the solid state kinetic models that are currently in use. Calculating the reaction's rate constant defines the reaction's progression. After examining how the rate constant changes in relation to the various variables on which it depends, the reaction mechanism can be predicted. Temperature, pressure, and reactant or product concentration all affect the reaction's rate constant. Different reaction models provide different reaction mechanisms for the overall reaction in solid-state kinetics. For multi-step reaction process it is very difficult to get the reaction mechanism of individual steps. [44], [45], [46], [47].

Table 1.5: Summary of Different Kinetic Models with Their Equations.

$\alpha = kt$	Linear Growth (CG1)	1
$[1-(1-\alpha)^{1/2}] = kt$	Cylindrical (CG2)	2
$[1-(1-\alpha)^{1/3}] = kt$	Spherical (CG3)	3
$\alpha^2 = kt$	Parabolic (D1)	4
$\alpha + (1-\alpha)\ln(1-\alpha) = kt$	ValensiBarrer (D2)	5
$1-2/3\alpha - (1-\alpha)^{2/3} = kt$	GinstlingBrounstein(D3)	6
$[1-(1-\alpha)^{1/3}]^2 = kt$	Jander (D4)	7
$[(1+\alpha)^{1/3}-1]^2 = kt$	Anti Jander (D5)	8
$[(1-\alpha)^{1/3}-1]^2 = kt$	Zhuralevet al. (D6)	9
$[-\ln(1-\alpha)] = kt$	First-order reaction	10
$[(1-\alpha)^{-1/2}-1] = kt$	One & half order reaction	11
$[(1-\alpha)^{-1}-1] = kt$	Second order reaction	12
$[-\ln(1-\alpha)]^{2/3} = kt$	AvromiErofeev, n=1.5 (NG1)	13
$[-\ln(1-\alpha)]^{1/2} = kt$	AvromiErofeev, n=2 (NG2)	14
$[-\ln(1-\alpha)]^{1/3} = kt$	AvromiErofeev, n=3 (NG3)	15

In the kinetic equations above, the abbreviations D, CG, NG, and R denote diffusion, contracting geometry, nucleation growth, and chemical reaction-regulated mechanisms, respectively.

1.12 Response Surface Methodology (RSM) and Optimization Techniques

Response Surface Methodology (RSM) is a collection of statistical and mathematical methods that is used to analyze and model engineering challenges. In this method, the response is the output variable, while the input parameters are independent variables that can be given to the design. The goal of experimental design is to maximize a response that is affected by a number of independent variables. The generated response surfaces and the controlled input parameters are also quantified by RSM [48], [49]. The term "design of experiments" (DOE) refers to a statistical method that involves planning, evaluating, and interpreting controlled tests to assess the variables in an experiment. It functions as an analytical tool by gathering different types of data. Different types of designed experiments are present among this Box-Behnken Design is a very popular one. Box-Behnken statistical design with 3 factors and 3 levels has been chosen to reduce the number of experiments, giving a set of 17 runs for the optimization research. The center point of a multidimensional cube is copied, and a set of points located at the midpoints of each edge make up the experimental setup. A block of samples matching a two-level factorial design is repeated across several sets of parameters in Box-Behnken designs. For the duration of the block, the factorial design-exempt parameters remain constant at their mean value. The equation N = 2K (K-1) + C, where K stands for the number of factors and C for the number of central points, is used to determine the number of experiments (N) that BBD provides.

The following equation, which represents the interaction between the influencing factors and the response, is a second-order polynomial equation:

$$X\ (response) = Y + a_1A + a_2B + a_3C + a_4\,AB + a_5\,AC + a_6\,BC + a_7\,A_2 + a_8\,B_2 + a_9\,C_2$$

[Y is constant, a_i represents the regression coefficient, and A, B, and C represent independent variables]. Three variables and three levels of tests have been conducted using BBD. Instead of using 27, 17 sets of experiments were examined to optimize the process parameters. The relationship between the parameters and the reaction has been established with the aid of mathematical modeling. Response surface plots have been used to illustrate the interactions between input factors and the response.

1.13 Hydrometallurgy

The technique of extracting and recovering metal from ore while using wet media is known as hydrometallurgy. Aqueous solutions play a significant role in that process. This method is particularly efficient for obtaining various types of chemically graded compounds from their source. The primary benefits of hydrometallurgy are an exceptionally pure end product, low energy consumption, suitability for low-grade ore, ease of small-scale execution, and highly specialized process. Sometimes in hydrometallurgy, it is challenging to separate impurities, which creates distinct issues for subsequent operations. Since most hydrometallurgical processes take place at room temperature, they are considerably slower than pyrometallurgical processes. However, the operational cost of that process is low with respect to the pyrometallurgical process. Chromium has variable oxidation states, but the most commonly available oxidation states are +3 and +6. In chromium-bearing ore, Cr(III) is the most prevalent oxidation state because it is water-insoluble. In the typical hydrometallurgical process, chromite ore is roasted in the presence of oxygen at 1200 ^{o}C, and leached into water. In this process, trivalent chromium converts into hexavalent chromium, which is water-soluble [50], [51]. The following list of reactions involved in this process:

$$4FeCr_2O_4 + 8NaCO_3 + 7O_2 \rightarrow 8\ Na_2CrO_3 + 2\ Fe_2O_3 + 8CO_2$$

$$Fe_2O_3 + Na_2CO_3 \rightarrow 2\ NaFeO_2 + CO_2$$

$$4FeCr_2O_4 + 16NaFeO_2 + 7O_2 \rightarrow 8Na_2CrO_4 + 10Fe_2O_3$$

$$2Na_2CrO_4 + H_2SO_4 \rightarrow Na_2SO_4 + Na_2Cr_2O_7 + H_2O$$

Here, sodium chromate that dissolves in water is created, and it can be changed into sodium dichromate by adding sulfuric acid. Chromium oxide is produced through the reduction of $Na_2Cr_2O_7$, and additional reduction with silicon or aluminium yielded more than 99% pure chromium.

1.14 Bioleaching

Natural microorganisms play a role in the dissolving of metal from its ore body. This is the primary idea behind bioleaching or biohydrometallurgy. Different kinds of bacteria and fungi are utilized in that procedure as microbes that can create soluble metal compounds from their mineral supply.

In bioleaching, bacteria and fungi serve as biocatalysts. Acidolysis, Complexolysis, and Redoxolysis are generally the three principles on which the mineralytic effects of bacteria and fungi on minerals are founded. Microorganisms can solubilize metals by generating different types of organic and inorganic acids. They also participate in oxidation and reduction reactions & excrete complexing agents during the leaching process [52], [53]. The bioleaching method of upgrading low-grade chromite ore is quite effective, however the choice of microorganisms is crucial. This process produces upgraded material that can be used as secondary raw material in the metallurgical sector.

So from the above study, it may be inferred that low-grade chromite ore is now extremely important for the increase of productivity in many industries especially in the steel sector. In this thesis, an attempt has been made to enrich the low-grade chromite ore to increase the metal values for subsequent production of different value-added products like iron-chromium alloy, ferrochrome, magchrome, etc by proper optimization of mineral beneficiation, agglomeration, and reduction parameters in different ways.

1.15 Reference

[1] S. P. du Preez et al., “An Overview of Currently Applied Ferrochrome Production Processes and Their Waste Management Practices,” Jun. 01, 2023, MDPI. doi: 10.3390/min13060809.

[2] S. Sánchez-Ramos, A. Doménech-Carbó, J. V. Gimeno-Adelantado, J. Peris-Vicente, and F. M. Valle-Algarra, “Thermal decomposition of chromite spinel with chlorite admixture,” Thermochim Acta, vol. 476, no. 1–2, pp. 11–19, Sep. 2008, doi: 10.1016/j.tca.2008.07.003.

[3] M. Kadziałko-Hofmokl, K. Delura, P. Bylina, M. Jeleńska, and J. Kruczyk, “Mineralogy and magnetism of Fe-Cr spinel series minerals from podiform chromitites and dunites from Tapadła (Sudetic ophiolite, SW Poland) and their relationship to palaeomagnetic results of the dunites,” Geophys J Int, vol. 175, no. 3, pp. 885–900, 2008, doi: 10.1111/j.1365-246X.2008.03933.x.

[4] R. K. Singh, S. Dey, M. K. Mohanta, and A. Das, “Enhancing the Utilization Potential of a Low Grade Chromite Ore through Extensive Physical Separation,” Separation Science and Technology (Philadelphia), vol. 49, no. 12, pp. 1937–1945, 2014, doi: 10.1080/01496395.2014.903495.

[5] Y. R. Murthy, S. K. Tripathy, and C. R. Kumar, “Chrome ore beneficiation challenges & opportunities - A review,” 2011, Elsevier Ltd. doi: 10.1016/j.mineng.2010.12.001.

[6] R. B. Panda, “Environmental scenario of chromite ore mining at Sukinda valley beyond 2030,” 2012. [Online]. Available: www.ibm.nic.in

[7] D. A. Singer, “Podiform chromite deposits; database and grade and tonnage models,” 2012. [Online]. Available: https://www.researchgate.net/publication/233947458

[8] S. Septiana, A. Idrus, F. Zaccarini, G. Garuti, and L. D. Setijadji, “Ore mineralogy of podiform-type chromite deposit in Tedubara area and its vicinity, Kabaena Island, Indonesia,” in IOP Conference Series: Earth and Environmental Science, IOP Publishing Ltd, Oct. 2021. doi: 10.1088/1755-1315/851/1/012044.

[9] A. V. Mokrushin and V. F. Smol’kin, “Chromite mineralization in the sopcheozero deposit (Monchegorsk layered intrusion, fennoscandian shield),” Minerals, vol. 11, no. 7, Jul. 2021, doi: 10.3390/min11070772.

[10] R. Mukherjee and S. K. Mondal, “INDIAN CHROMITE DEPOSITS FROM A GLOBAL PERSPECTIVE,” 2009. Available: https://www.researchgate.net/publication/267799788

[11] S. K. Tripathy, V. Singh, and Y. Ramamurthy, “Improvement in Cr:Fe Ratio of Indian Chromite Ore for Ferro Chrome Production,” International Journal of M ining Engineering and M ineral Processing, vol. 2012, no. 3, pp. 101–106, 2012, doi: 10.5923/j.mining.20120103.01.

[12] I. Bhavan, “Indian Minerals Yearbook 2020 59 th Edition CHROMITE (ADVANCE RELEASE) GOVERNMENT OF INDIA MINISTRY OF MINES INDIAN BUREAU OF MINES,” 2022.

[13] E. L. J. Kleynhans, J. P. Beukes, P. G. Van Zyl, P. H. I. Kestens, and J. M. Langa, “Unique challenges of clay binders in a pelletised chromite pre-reduction process,” Miner Eng, vol. 34, pp. 55–62, Jul. 2012, doi: 10.1016/j.mineng.2012.03.021.

[14] N. Koleli and A. Demir, “Chromite,” in Environmental Materials and Waste: Resource Recovery and Pollution Prevention, Elsevier Inc., 2016, pp. 245–263. doi: 10.1016/B978-0-12-803837-6.00011-1.

[15] Y. R. Murthy and S. K. Tripathy, “Process optimization of a chrome ore gravity concentration plant for sustainable development,” The Journal of the Southern African Institute of Mining and Metallurgy, vol. 120, 2020, doi: 10.17159/2411.

[16] “Mineral Commodity Summaries 2022 - Chromium.”

[17] M. Motasim Hassan Al-Tigani, A. Awdekarim, A. Al-Gak Abdueldaem, and A. Abdullah Sadeek Seifelnasr, “Application of Response Surface Methodology on Beneficiation of Sudanese Chromite Ore via Pilot Plant Shaking Table Separator,” 2020. [Online]. Available: www.ijeais.org/ijamr

[18] G. Goswami and J. D. Panda, “Beneficiation of low grade chromite for preparation of charge-chrome.”

[19] A. K. Das et al., “Processing of Low-Grade Chromite Ore for Ferroalloy Production: A Case Study from Ghutrigaon, Odisha, India,” Transactions of the Indian Institute of Metals, vol. 73, no. 9, pp. 2309–2320, Sep. 2020, doi: 10.1007/s12666-020-02032-5.

[20] S. K. Tripathy, Y. R. Murthy, V. Singh, and N. Suresh, “Processing of Ferruginous Chromite Ore by Dry High-Intensity Magnetic Separation,” Mineral Processing and Extractive Metallurgy Review, vol. 37, no. 3, pp. 196–210, May 2016, doi: 10.1080/08827508.2016.1168418.

[21] “Magnetic and Electrostatic Separation,” in Mineral Processing Design and Operations, Elsevier, 2016, pp. 629–687. doi: 10.1016/b978-0-444-63589-1.00017-4.

[22] S. K. Tripathy, Y. R. Murthy, V. Singh, S. Farrokhpay, and L. O. Filippov, "Improving the quality of ferruginous chromite concentrates via physical separation methods," Minerals, vol. 9, no. 11, Nov. 2019, doi: 10.3390/min9110667.

[23] S. K. Tripathy, P. K. Banerjee, and N. Suresh, "Magnetic separation studies on ferruginous chromite fine to enhance Cr:Fe ratio," International Journal of Minerals, Metallurgy and Materials, vol. 22, no. 3, pp. 217–224, Mar. 2015, doi: 10.1007/s12613-015-1064-4.

[24] S. Sysila, H. Laapast, K. Heiskanen~, E. Ruokonen, and ¶ § Partek, "THE EFFECT OF SURFACE POTENTIAL ON THE FLOTATION OF CHROMITE," 1996.

[25] G. P. Gallios, E. A. Deliyanni, E. N. Peleka, and K. A. Matis, "Flotation of chromite and serpentine," Sep Purif Technol, vol. 55, no. 2, pp. 232–237, Jun. 2007, doi: 10.1016/j.seppur.2006.12.015.

[26] Q. I. Wesseldijk ~, M. A. Reuter, D. J. Bradshaw, and P. J. Harris, "The Flotation Behaviour of Chromite with Respect to the Beneficiation of UG2 Ore," Minerals Engineering, Vol. 12, No. 10, pp. 1177-1184, 1999.

[27] L. Panda, R. Venugopal, and N. R. Mandre, "Selective Flocculation of Chromite Tailings," Transactions of the Indian Institute of Metals, vol. 74, no. 3, pp. 619–628, Mar. 2021, doi: 10.1007/s12666-020-02175-5.

[28] R. K. Dwari, S. I. Angadi, and S. K. Tripathy, "Studies on flocculation characteristics of chromite's ore process tailing: Effect of flocculants ionicity and molecular mass," Colloids Surf A Physicochem Eng Asp, vol. 537, pp. 467–477, Jan. 2018, doi: 10.1016/j.colsurfa.2017.10.069.

[29] S. Özgen, "Clean Chromite Production from Fine Chromite Tailings by Combination of Multi Gravity Separator and Hydrocyclone," Separation Science and Technology (Philadelphia), vol. 47, no. 13, pp. 1948–1956, Aug. 2012, doi: 10.1080/01496395.2012.663445.

[30] S. K. Tripathy, S. K. Bhoja, and Y. R. Murthy, "Processing of chromite ultra-fines in a water only cyclone," Int J Min Sci Technol, vol. 27, no. 6, pp. 1057–1063, Nov. 2017, doi: 10.1016/j.ijmst.2017.06.015.

[31] S. ÖZGEN, "Modelling and optimization of clean chromite production from fine chromite tailings by a combination of multigravity separator and hydrocyclone," J. S. Afr. Inst. Min. Metall, vol.112, n.5, pp.387-394, 2012, ISSN 2411-9717.

[32] "Development and Research of Intelligent Algorithms for Controlling the Process of Ore Jigging," International Journal of Emerging Trends in Engineering Research, vol. 8, no. 9, pp. 6240–6246, Sep. 2020, doi: 10.30534/ijeter/2020/215892020.

[33] A. A. Seifelnasr, T. Tammam, and A.-Z. M. Abouzeid, "Gravity Concentration of Sudanese Chromite Ore using Laboratory Shaking Table," Physicochem. Probl. Miner. Process, vol. 48, no. 1, pp. 271–280, 2012.

[34] S. Khakmardan, R. J. Doodran, A. Shirazy, A. Shirazi, and E. Mozaffari, "Evaluation of Chromite Recovery from Shaking Table Tailings by Magnetic Separation Method," Open Journal of Geology, vol. 10, no. 12, pp. 1153–1163, 2020, doi: 10.4236/ojg.2020.1012055.

[35] P. V. T. Rao and A. I. Das, "Agglomeration of Chrome Ore Fines for Ferrochrome Making-A Step Towards Increased Competitiveness," NML Jamshedpur 831 007, p. 51-58, 1997.

[36] B. W. Neizel, J. P. Beukes, P. G. Van Zyl, and N. F. Dawson, "Why is CaCO3 not used as an additive in the pelletised chromite pre-reduction process?," Miner Eng, vol. 45, pp. 115–120, 2013, doi: 10.1016/j.mineng.2013.02.015.

[37] S. Agarwal, J. Pal, and D. Ghosh, "Development of chromite sinter from ultra-fine chromite ore by direct sintering," ISIJ International, vol. 54, no. 3, pp. 559–566, 2014, doi: 10.2355/isijinternational.54.559.

[38] Z. Deqing, L. Jian, P. Jian, and H. Aoping, "Sintering behaviours of chromite fines and the consolidation mechanism," Int J Miner Process, vol. 86, no. 1–4, pp. 58–67, Mar. 2008, doi: 10.1016/j.minpro.2007.11.002.

[39] Z. Rezvani, G. R. Chegini, A. Arabhosseini, M.H Kianmehr, "Natural Energy of Briquette, Definitions," Journal of Automotive & Applied Mechanies, Vol. 2, Issue 1, 2014.

[40] R. Sen, M. K. Mitra, S. Mukherjee, and R Dey, "Effect of Grading of Chromite Ores on the Quality of Briquettes," ISIJ International, Vol. 50, No. 2, pp. 200–206, 2010.

[41] D. Chakraborty, S. Ranganathan, and S. N. Sinha, "Reduction of Chromite Ore at Different Flow Rates of Inert Gas," INFACON XI, pp. 153-158, 2007.

[42] X. Hu, "Studies on Carbothermic Reduction of Chromite in the Presence of FeO x," Printed by Luleå University of Technology, 2016, ISBN 978-91-7583-742-0. Available: www.ltu.se.

[43] A. I. Fares, K. M. A. Sohel, K. Al-Jabri, and A. Al-Mamun, "Characteristics of ferrochrome slag aggregate and its uses as a green material in concrete – A review," Aug. 02, 2021, Elsevier Ltd. doi: 10.1016/j.conbuildmat.2021.123552.

[44] M. Kekkonen, Y. Xiao, and L. Holappa, “Kinetic Study on Solid State Reduction of Chromite Pellets,” INFACON 7, pp. 351-360, 1995.

[45] J. CHEN, S. bin WANG, M. ZHANG, J. ying LIU, and J. xiong ZHOU, “Kinetics of Voluminal Reduction of Chromium Ore Fines Containing Coal by Microwave Heating,” Journal of Iron and Steel Research International, vol. 15, no. 6, pp. 10–15, Nov. 2008, doi: 10.1016/S1006-706X(08)60258-7.

[46] R. Ochoa, A. Flores, J. Torres, J. Guía, and R. Muñiz, “Kinetic study on the metallothermic reduction of chromite ore using magnesium scrap,” Canadian Metallurgical Quarterly, vol. 55, no. 2, pp. 210–220, Apr. 2016, doi: 10.1080/00084433.2016.1146432.

[47] P. Gupta, A. K. Bhandary, M. G. Chaudhuri, S. Mukherjee, and R. Dey, “Kinetic Studies on the Reduction of Iron Oxides in Low-Grade Chromite Ore by Coke Fines for Its Beneficiation,” Arab J Sci Eng, vol. 43, no. 11, pp. 6143–6154, Nov. 2018, doi: 10.1007/s13369-018-3324-x.

[48] S. Samanli, O. Oney, and O. Osmanli, “Modeling of Knelson Concentrator Operating Parameters by Using Application of Box–Behnken Experimental Design for Chromite Ore,” Journal of Mining Science, vol. 59, no. 1, pp. 118–126, Feb. 2023, doi: 10.1134/S1062739123010131.

[49] S. K. Tripathy and Y. Rama Murthy, “Modeling and optimization of spiral concentrator for separation of ultrafine chromite,” Powder Technol, vol. 221, pp. 387–394, May 2012, doi: 10.1016/j.powtec.2012.01.035.

[50] Y. Zhang et al., “A clean and efficient leaching process for chromite ore,” Miner Eng, vol. 60, pp. 60–68, 2014, doi: 10.1016/j.mineng.2014.01.025.

[51] Y. Du and M. Chrysochoou, “Chemistry and leaching behavior of chromite ore processing residue from the soda ash process,” Environ Eng Sci, vol. 35, no. 11, pp. 1185–1193, Nov. 2018, doi: 10.1089/ees.2018.0047.

[52] V. Bolaños-Benítez et al., “(Bio)leaching behavior of chromite tailings,” Minerals, vol. 8, no. 6, Jun. 2018, doi: 10.3390/min8060261.

[53] S. Biswas, S. Samanta, R. Dey, S. Mukherjee, and P. C. Banerjee, “Microbial leaching of chromite overburden from Sukinda mines, Orissa, India using Aspergillus niger,” International Journal of Minerals, Metallurgy and Materials, vol. 20, no. 8, pp. 705–712, Aug. 2013, doi: 10.1007/s12613-013-0787-3.

Chapter-2

Scope of the Work

In conventional metallurgical processes, high-grade chromite ore is used to produce different value-added finished products like stainless steel, high-speed steel, etc but its deposition is restricted to a small region of the earth's crust. The demand for stainless steel and other chromium-containing metallurgical and chemical products is rising, while high-grade chromium ore deposits are correspondingly declining. In addition, chromite ore mining produces enormous amounts of fines. The utilization of those fines is very important these days from profitability and environmental viewpoints. These fines are also considered low-grade. Low-grade chromite ore has been the subject of research attention for some time. There are few research studies available that discuss the attempts to extract metal values from these low-grade ores. The current research work attempts elaborately to map out potential process technologies for utilizing low-grade ore in order to recover metal values and turn it into an economically viable one. To satisfy the domestic need for ferrochrome & other chromium-based intermediate products, pyrometallurgical and hydrometallurgical studies of the ore have been conducted to boost the productivity of metal sectors specially steel by proper utilization of low-grade chromite ore.

Chapter-3

Methodology

3.0 Methodology

For the past few years, researchers have been concerned about the use of low-grade chromite ore. Significant low-grade chromite ore deposition is found in Orissa's Sukinda Valley in India. The current study aims to develop an alternative method for utilizing Sukinda Valley's low-grade chromite ore. This chapter outlines the step-by-step methodology used to accomplish the research project's goal. Below is a description of the raw material collection process:

Chromite Ore: Collected from Sukinda mines with the help of Tata Steel Limited.

Source of Coke and Coal Dust: Vizag Steel Plant, India.

Source of Molasses: Tata Steel Plant, Jharkhand, India.

Source of Bentonite: Tata Steel Plant, Jharkhand, India.

3.1 Raw Materials Analysis

For the purpose of characterization and chemical analysis, chromite ore, coke, and coal will crushed and ground below 200 mesh using a jaw crusher (primary crusher) and a roll crusher (secondary crusher). The basis outline of the characterization of raw materials is shown in Fig. 3.1.

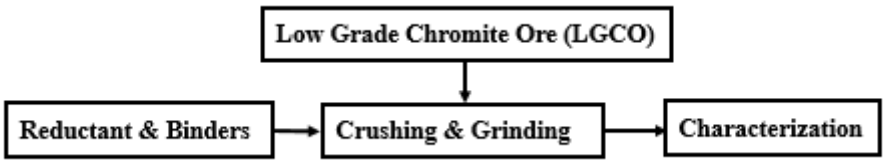

Figure 3.1: Flow Diagram of Characterization of Raw Materials.

Using Wavelength X-ray Florescence (WDXRF) analysis, the composition of chromite ore will investigated. An atomic absorption spectrophotometer (AAS) will be used to quantitatively analyze each element present in the ore. Using X-ray Diffraction (XRD) analysis, the various phases found in the ore will be observed. Scanning Electron Microscopy (SEM) analysis will be carried out for the morphological study.

Pyris Diamond Thermo Gravimetric/Differential Thermal Analysis (DTA) will examine the thermo-gravimetric analysis of the raw ore in a nitrogen atmosphere.

To determine the percentages of compositions, standard proximate analysis and TG/DTA analyses of lean-grade coal and coke dust will be carried out. With the aid of SEM-EDX, raw coke dust will be characterized.

The chemical composition and proximate analysis of binders (bentonite and molasses) will be investigated using the standard method.

3.2 Beneficiation of Low-Grade Chromite Ore Using Wilfley Table

After crushing and grinding the particle size distribution of chromite ore will be analyzed using BSS standard sieves with a vibrating mechanical shaker. The Cr_2O_3% will be calculated for each particle size fraction through AAS to get the distribution of chromium in the ore.

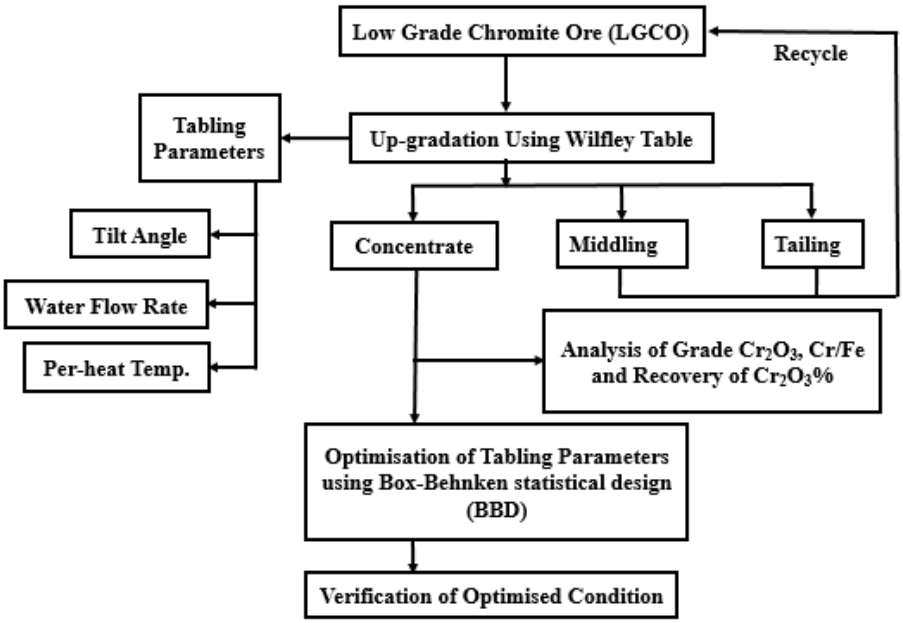

Figure 3.2: Flow Diagram of Beneficiation of Low-Grade Chromite Ore.

Particles larger than 75 μm will be ground once more until the chromite sample's total particle size is less than 75 μm. After mineralogical studies, the sample will be split into three parts and preheated in a raising hearth furnace at 28°C, 514°C, and 1000°C. Thermogravimetric and differential thermal analysis (TG-DTA) will be used to help determine the temperatures. Three different samples will be homogeneously mixed and subjected to laboratory scale wilfley Table for gravity separation using the parameters recommended by the Box-Behnken statistical design (BBD) model. For all the experiments the position of collection containers will be fixed for concentrate, middling, and tailing products. Samples will be taken from their designated locations for additional analysis following each experiment. Characterization of concentrate, middling, and tailing samples will be carried out with the help of AAS and identify the

optimized tabling parameters. Beneficiation and optimization technique is summarized in Fig. 3.2.

3.3 Effect of Pressure and Binder on Mechanical Properties of Chromite Ore Briquettes and Subsequent Reduction

In order to optimize the binder percentage and briquetting pressure, two sets of briquettes will be made using chromite concentrate obtained from optimized tabling parameters. To make briquettes, a stoichiometric proportion of coke dust will be combined with binders and chromite particles. Molasses, water, and bentonite will be used as a binder. The briquette's ingredients will all be evenly combined and left to stand for the whole night. After that, the mixture will be formed into cylindrical briquettes by pressing it with a mechanical dye. There will be production of cylindrical briquettes with an average height of 1 cm and diameter of 2.5 cm.

The briquette will be made with various binder proportions under a fixed 450 kg briquetting pressure in order to obtain an optimal binder percentage. The preparation and reduction of briquettes for the optimization of binder percentages are shown in Figure 3.3. Stands for the chromite concentrate combined with a stoichiometric amount of coke, 1% bentonite, 1% molasses, and 1% water. In a similar vein, B, C, D, E, and F stand for 2%, 3%, 4%, 5%, and 6%, respectively, of bentonite, molasses, and water (each percentage), maintaining the same other parameters.

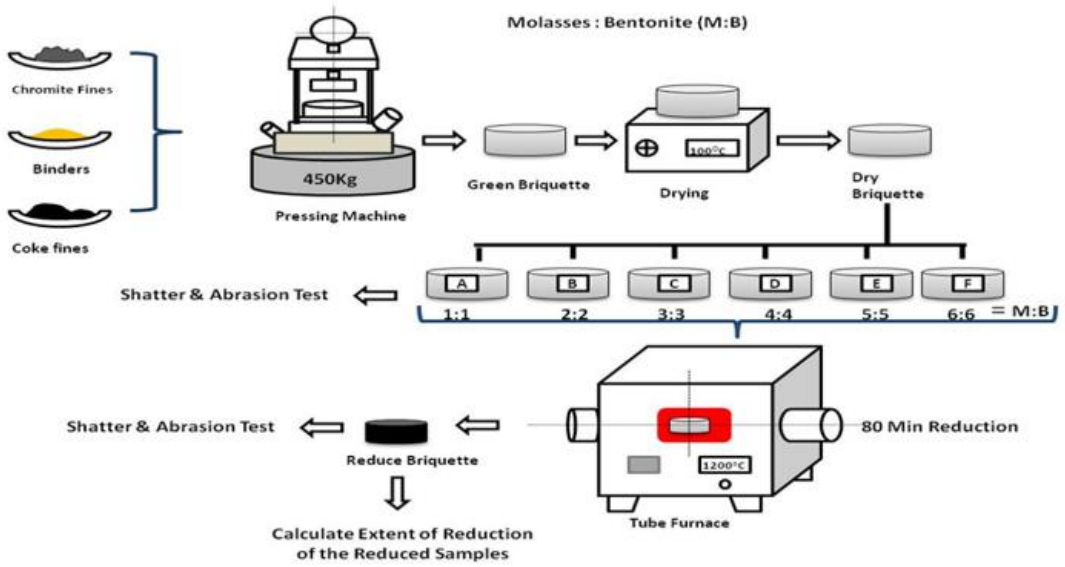

Figure 3.3: Simplified Processing Diagram of Briquette Preparation and the Reduction Process.

To obtain the optimum briquetting pressure, another set of briquettes will be prepared at five different pressures (350, 400, 450, 500, and 550 kg). Each briquette contains chromite concentrate, an optimal percentage of binder (in this case, 3% for each binder), and a stoichiometric amount of coke dust. All the green briquettes will be dried to provide mechanical strength.

The reduction of briquette will be carried out in the PID control tube furnace at 1200 ^{0}C for 80 minutes. The extent of reduction (EOR) will be computed following reduction. To determine the briquettes' mechanical properties, the shatter and abrasion indices will be measured both before and after reduction. Identify the best briquetting pressure and the binder percentage will be calculated for the reduction. The preparation of briquettes is shown in Fig. 3.3.

3.4 Isothermal Reduction and Smelting of Optimized Chromite Ore Briquettes

Briquettes will undergo both high- and low-temperature isothermal direct reduction following the optimization of the briquetting pressure and binder %. The raising hearth furnace (creating a reducing atmosphere) will be used for high-temperature reduction, with different temperatures of 1573K, 1623K, 1673, and 1723K and reduction times of 15, 30, 60, 90, and 120 minutes. On the other hand, low-temperature reduction will be done in a PID-controlled tube furnace that is electrically heated to four distinct temperatures: 1373K, 1423K, 11473K, and 1523K. Each temperature will be maintained for five different time intervals: 15, 30, 60, 90, and 120 minutes. Comparative isothermal reduction kinetics will be studied. Calculations will be made to determine the reduced briquettes' extent of reduction and degree of metallization. XRD and SEM studies will be used to characterize the reduced briquettes.

The reduced sample with the highest degree of metallization will be smelted for six hours at 1923K in a rising hearth furnace. AAS, XRD, SEM, EDX, and microstructure analysis will be used to characterize the metal and slag.

3.5 Low-Carbon Iron-Chromium Alloy Preparation by Aluminothermic Smelting Followed by Reduction of Chromite Pellets Using Syn Gas

Chromite ore fines will be homogeneously mixed with a stoichiometric ratio of appropriate binder (bentonite and molasses) and will placed into a dram pelletizer for the preparation of green pellets.

The pellets will be fired at a temperature of 1200 degrees Celsius to give them the appropriate strength. A flow diagram is given below that illustrates the process of making chromite pellets.

Synthetic gas will be used to reduce pellets in a gasification reactor. After crushing the reduced pellets and using magnetic separation, the chromite enrich fraction will be extracted. Subsequently, reduced materials will be introduced for characterization by AAS, XRD, and SEM analysis.

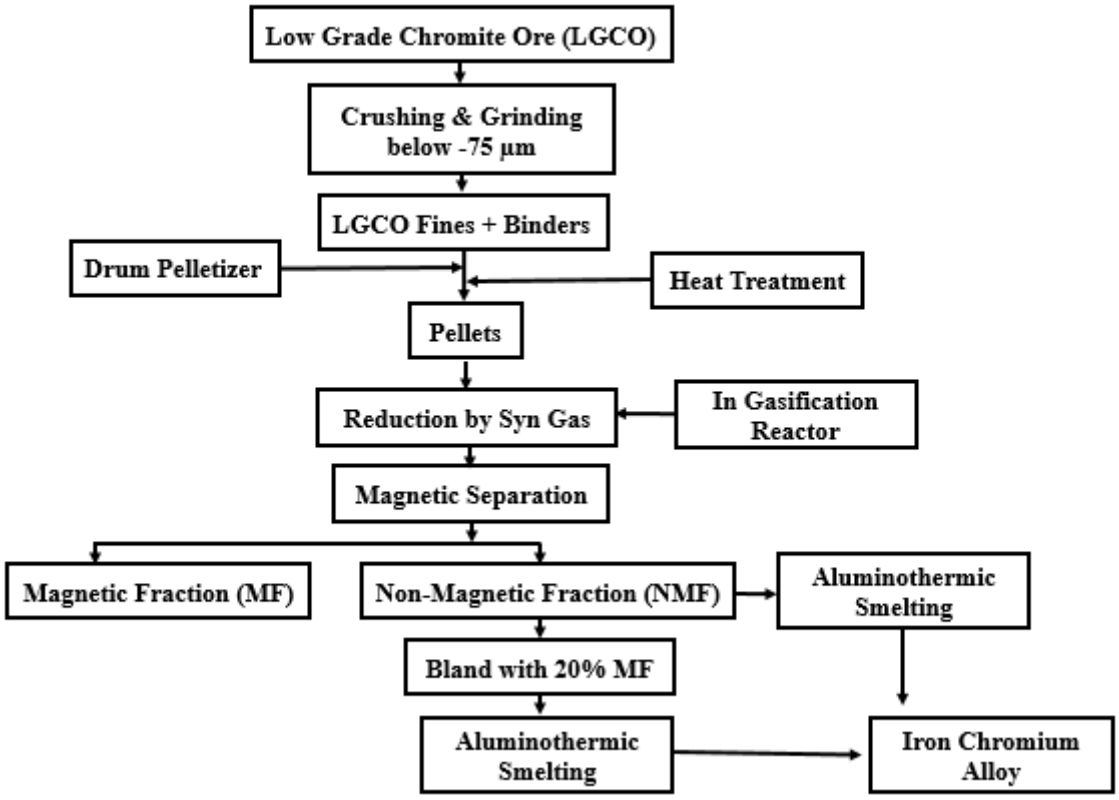

Figure 3.4: Flow Diagram of Iron-Chromium Alloy Preparation.

After the reduction of chromite pellets, the separated nonmagnetic component will be melted using an aluminothermic method to make iron-chromium alloy using magnesium ribbon. Furthermore, an additional fraction of the non-magnetic fraction will be mixed with 20% magnetic fraction and subjected to testing using identical methods. The quality of the final product will be characterized by AAS, XRD, SEM, and microscopic analysis. A flow diagram of the process is shown in Figure 3.4.

3.6 Oxidative Salt Roasting of Chromite Ore

A fixed amount of chromite fines (less than 75 µm) will be taken and combined evenly with nitrate in a platinum crucible. The crucible will be heated in an isothermal oxidative roasting furnace at 623 K. A predetermined amount of sodium hydroxide will be introduced into the crucible, and the mixture will then be roasted isothermally under atmospheric air conditions at

a constant temperature. For this experiment, three distinct temperatures 973 K, 1023 K, and 1073 K will be selected. To maintain each temperature, five different time intervals will be used: 15, 30, 60, 90, and 120 minutes. The roasted sample will then be leached in water for 1 hour at 60°C with stirring by a magnetic stirrer. The leachate will be agitated, filtered, and then transferred to a 500 ml volumetric flask for chemical analysis by atomic absorption spectroscopy (AAS). The leaching residue will be characterized by XRD and SEM-EDX. The filtrate will be neutralized first to precipitate aluminium hydroxide.

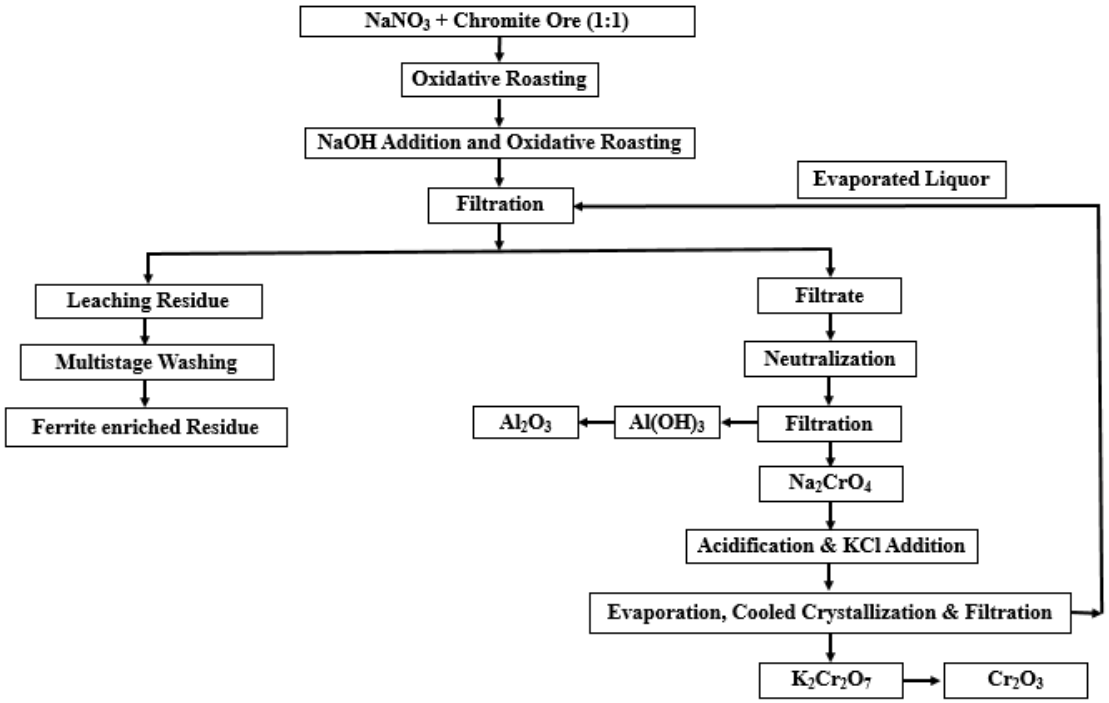

Figure 3.5: Flow Diagram of Oxidative Salt Roasting of Low-Grade Chromite Ore.

Whatman 41 filter paper will be used to filter the precipitation. Then the filtrate will be acidified with sulfuric acid. This acidic solution will be treated with solid potassium chloride (KCl) for the formation of potassium dichromate ($K_2Cr_2O_7$). The solution will then be concentrated by evaporation and cooled to obtain crystalline potassium dichromate. This crystalline potassium dichromate is then reduced with metallurgical-grade coke at 1173 K for 30 minutes to make chromium oxide. An outline of the process is shown in Fig. 3.5.

3.7 Bioleaching of Chromite Ore

Pseudomonas putida will be collected from ATCC Pune and used in the bioleaching process. In this process, a microbial culture solution will be prepared in a Luria broth medium (succinate medium). A total of 11 experimental setups will be prepared to investigate the leaching

behavior of low-grade chromite ore, where the variable parameters are pulp density and culture volume. In the 11 experimental setups, two blank experiments will be present to understand the leachability of chromite ore in the media. For each set of 11 sets of experiments, 100ml of Luria broth (LB) medium will be taken in 250ml of conical flask, and the pH of the media will be 7 using 0.1 N HCl or NaOH. Then the flasks will be autoclaved at 121°C for 15 minutes for sterilization. After that 48-hour-old Pseudomonas Putida culture will be inoculated into the media and incubated in a BOD shaker at 37°C and 110 rpm for bioleaching. Samples will be collected after a time interval of 1, 5, 10, 15, 20, 25, and 30 days for analysis. The pH of the leaching solutions will be measured and recorded. The concentrations of chromium, iron, and aluminum in the leached solutions will be determined using atomic absorption spectroscopy (AAS).

3.8 Overall Experimental Flow Diagram

The following schematic block diagram (Fig. 3.6) can be used to visualize the entire set of experimental works that are covered in the thesis.

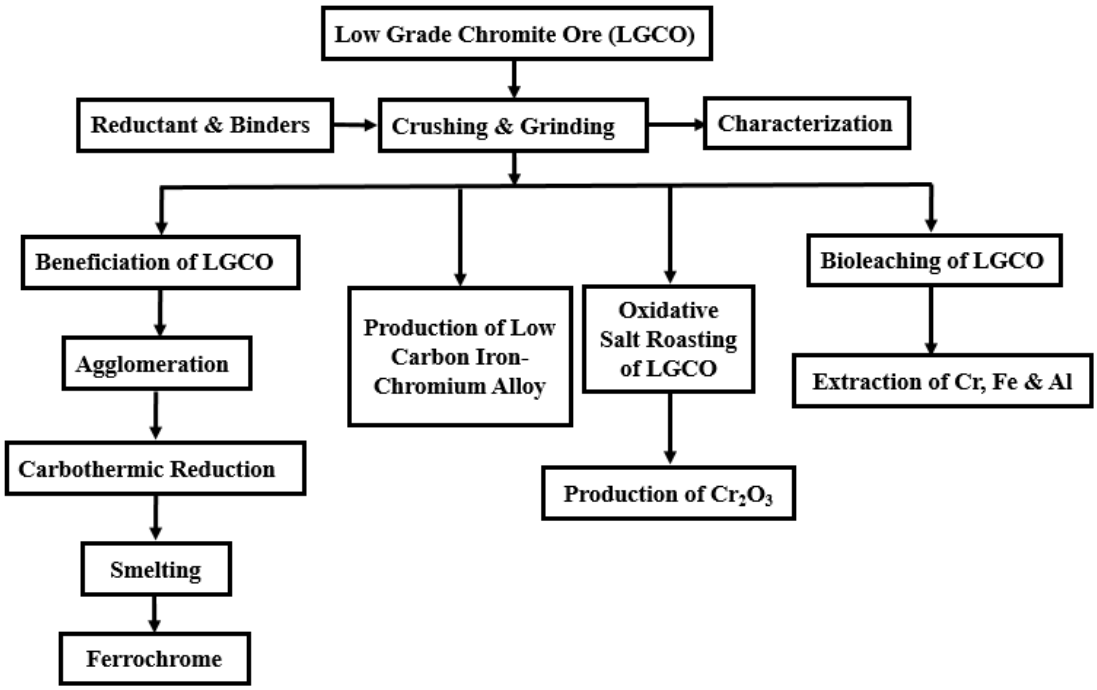

Figure 3.6: Schematic Block Diagram of the Overall Experiment.

Chapter-4

Equipment's Used

4. Introduction

The preparation of raw materials is essential for characterization and various experimental setups. Understanding the functionality of different types of equipment is crucial for designing experiments effectively. This chapter highlights the information concerning the various types of equipment utilized in this research project.

4.1 Sample Preparation Units

In the initial stage of ore processing, primary and secondary crushers play a crucial role in the crushing and grinding process. Specifically, jaw crushers serve as primary crushers, while roll crushers are employed as secondary crushers in the research project. These crushers yield heterogeneous ore fines with diverse particle size fractions. Subsequently, the BBS standard sieve, operated with a sieve shaker, is utilized to separate these fractions based on particle size. Detailed descriptions of the mentioned equipment are provided below.

4.1.1 Jaw Crusher

The initial reduction of lumpy chromite ore occurs in a jaw crusher, serving as the primary crusher in the process. This apparatus features two crushing jaws positioned at an inclination: one mobile and the other fixed to the equipment. The spacing between the two crushing jaws can be adjusted to accommodate varying productivity and particle size demands. Furthermore, the shape of the jaw can be customized depending on the ore's characteristics. The motion of the moving jaw applies crushing and compressive force to the feed material, facilitating its breakage. Fig. 4.1 illustrates a visual depiction of the jaw crusher.

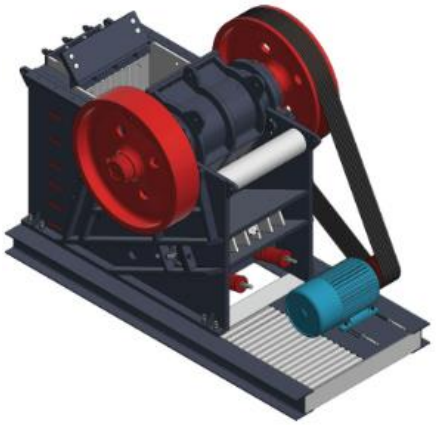

Figure 4.1: Jaw Crusher.

4.1.2 Roll Crusher

Following the initial processing of lumpy ore in the jaw crusher, chromite ore undergoes further crushing in a roll crusher. This apparatus consists of two rolls positioned head-on, rotating in

opposite directions. The location where the material is fed is adjustable, allowing for a gap between the two rollers. As the material passes between the rolls, the pressure exerted crushes it. The size of the feed material can vary, with the roll crusher's capacity accommodating dimensions ranging from 500mm to 2000mm. Fig. 4.2 provides a visual representation of the roll crusher.

Figure 4.2: Roll Crusher.

4.1.3 Disc Pulveriser

Disc pulverizers are extensively employed in the mining industry to generate ore fines. Consisting of two discs or plates, this apparatus features one rotating plate and another fixed in place. These plates are commonly constructed from cast iron. During grinding operations, ore with small particle sizes (6–15 mm) is placed between the two plates. The spacing between the plates can be adjusted externally, influencing the fineness of the feed material. Fig. 4.3 illustrates the typical configuration of a disc pulverizer.

Figure 4.3: Disc Pulveriser.

4.1.4 Sieve Shaker

After the chromite ore has undergone crushing and grinding, the various size fractions are separated using a sieve shaker. In this apparatus, BBS standard sieves are arranged in ascending order of sieve size, with the coarsest sieve positioned at the top and the smallest at the bottom. Each sieve is secured in place by two vertical rods and a top cover. The feed sample, consisting of chromite fines, is processed using the coarsest sieve. As the feed material undergoes agitation and vibration in the sieve shaker (Fig. 4.4), it moves either vertically or horizontally, resulting in the separation of particles.

Figure 4.4: A Set of Sieves with a Sieve Shaker.

4.1.5 Weighing Balance

A weighing balance is used to precisely measure the weight of any material. It is a fairly standard piece of equipment in any lab. The substance's weight was determined by placing it in a balance pan with two glass doors covering it. Glass doors block various environmental influences that could arise. A 1000 g capacity weighing balance with 0.001 g readability is used in this work. Fig. 4.5 illustrates a weighing balance.

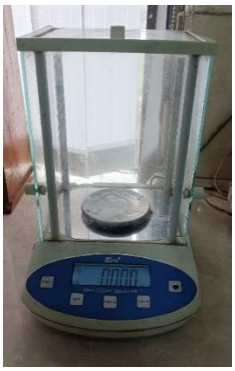

Figure 4.5: High-Precision Weighing Balance.

4.2 Characterization Units

Numerous pieces of equipment have been employed in the characterization of ore. A comprehensive understanding of these tools is essential for effectively concluding any research project. Critical characterizations, including the determination of chemical composition, phase analysis, and morphological examination of the ore, play a pivotal role in defining the experimental pathway. The following section provides a detailed description of the operation of such equipment.

4.2.1 X-Ray Diffractometer (XRD)

The X-ray powder diffraction method, commonly referred to as XRD serves to identify the phases present in an unknown sample. X-rays, owing to their wavelength's similarity to atomic distances, are utilized in this technique. These X-rays can penetrate the crystal lattice, providing valuable crystallographic data. Each crystal lattice possesses a unique intermolecular distance (d). In this method, a high-energy electron beam strikes a rotating heavy metal, typically copper, generating X-rays alongside other radiation. After passing through a quartz crystal monochromator, which filters only CuKα radiation with a wavelength of 0.15418 nm, the radiation is directed at the powder sample. The detector records diffracted radiation occurring at an angle of 2θ. According to Bragg's Law, diffraction follows the equation $n\lambda=2d\sin\theta$, where n, λ, d, and θ represent the X-ray's wavelength, diffraction angle, order of diffraction, and interplanar spacing, respectively. Notably, the interplanar spacing (d) is inversely proportional to θ, indicating that sinθ decreases with increasing interplanar spacing. Upon obtaining XRD data, plotting intensity against 2θ is feasible. The intensity of peaks is determined by the atoms'

arrangement within the crystal lattice, leading to constructive and destructive interference phenomena. The collected data is compared with the standard PDF database (utilizing software such as PCPDF-WIN or JCPDS from the International Center for Diffraction Data) to identify the unknown phase in the sample. In this study, we used a Rigaku Ultima III X-ray diffractometer, manufactured in Japan. An image of the XRD equipment is shown in Fig. 4.6.

Figure 4.6: X-Ray Diffractometer (XRD).

4.2.2 Wavelength Dispersive X-Ray Fluorescence Spectrometer (WDXRF)

The X-ray fluorescence Spectrometer (XRF) serves as a valuable tool for determining the elemental composition of unknown materials. Ionization occurs when a material is exposed to high-energy radiation, such as gamma or X-rays, causing atoms to lose their inner electron shells (K and L). Consequently, the atoms develop vacancies in these inner shells. Higher-energy electrons then fill these vacancies, leading to the emission of X-ray fluorescence. Each element exhibits a unique fluorescence property, enabling the identification of elements present in the sample based on the wavelength of fluorescence. Moreover, the quantity of each element can be determined by measuring the intensity of the fluorescence signal. In this study, Wavelength Dispersive X-ray Fluorescence (WDXRF) analysis is conducted using the Magi X 2424 model manufactured by PANalytical (refer to Fig A). The apparatus is controlled by an external computer running "Super Q" software. The sample is charged into the XRF spectrometer after being formed into briquettes. To create the briquettes, a mixture of 10% methyl acrylate in acetone is combined with 2.5g of fine chromite ore (finer than 200 mesh),

where methyl acrylate acts as a binder. This mixture is then compressed using a hydraulic press along with 5g of boric acid, ensuring thorough mixing. The resulting briquettes are pressed at a pressure of 200kN. Additionally, the XRF spectrometer utilizes a rhodium anode as a target to generate X-rays for analysis. Figure 4.7 shows an image of the WDXRF equipment.

Figure 4.7: WD-X-Ray Fluorescence Spectrometer.

4.2.3 Scanning Electron Microscope (SEM) and Field Emission Scanning Electron Microscope (FESEM)

The scanning electron microscope (SEM) stands as an indispensable tool for characterizing the surface morphology of both raw and treated materials. In this method, positively charged metals like tungsten are heated to produce an electron beam. This electron beam interacts with the sample through a scan coil and condenser, allowing for detailed examination. Electrons scatter across the sample's surface based on its morphology upon collision. The detector, coupled with a sensor, collects diffracted electrons to generate a three-dimensional image of the sample. In this research, morphological studies are conducted using a JEOL JSM-8360 scanning electron microscope from Japan. Initially, a fine chromite sample (finer than 200 mesh) is secured in a sample holder lined with carbon tape. To enhance imaging accuracy and mitigate electrostatic charge build-up, the sample is coated with a conductive substance, such as palladium. The coating process is facilitated by the JEOL JFC-1600 Auto Fine Coater. Additionally, energy-dispersive X-ray spectroscopy (EDX) is employed to qualitatively

analyze the elements present on the sample surface. The elemental composition is determined through EDX by measuring the x-ray wavelengths emitted from the sample surface during SEM analysis. Refer to Figure A for a SEM-EDX image. Furthermore, the field emission scanning electron microscope (FESEM) presents an advanced technique for obtaining high-resolution surface images. Operating under high vacuum conditions, FESEM emits electrons via a field emission mechanism, offering superior resolution compared to SEM. In this study, FESEM analysis is conducted using the Hitachi model S 4800. Fig. 4.8 shows an image of the FESEM.

Figure 4.8: Field Emission Scanning Electron Microscope.

4.2.4 Thermo Gravimetric-Differential Thermal Analyser (TG/DTA)

Temperature-induced changes can significantly impact a material's physical and chemical properties, leading to phenomena such as vaporization, sublimation, absorption, adsorption, and desorption. These alterations are detectable through Thermogravimetric Analysis (TGA), where the material's mass may fluctuate under heating conditions. In TGA, the sample undergoes heating within an inert atmosphere. Differential Thermal Analysis (DTA), meanwhile, monitors temperature and heat flow during the material's thermal transitions. By recording mass loss as temperature increases, DTA provides crucial insights into the material's behavior. In this study, Pyris Diamond Thermogravimetric/Differential Thermal Analysis (TG/DTA) equipment from PerkinElmer, Singapore, is utilized for TGA investigations. The

investigating temperature range is 0 to 1000°C and the heating rate is 10°C/min. The Thermo gravimetric-Differential Thermal Analyser is shown in Fig. 4.9.

Figure 4.9: Thermogravimetric-Differential Thermal Analyzer.

4.2.5 Flame-Atomic Absorption Spectrophotometer (AAS)

The atomic absorption spectrophotometer (AAS) is a valuable tool for identifying elements within a material. This technique often employs a hollow cathode lamp as the radiation source. The lamp, filled with inert gas, features a cathode tailored to the metal of interest. When a high voltage is applied between the cathode and anode, the inert gas becomes ionized and strikes the cathode. This process atomizes the atoms present on the cathode surface, elevating them to higher energy levels. Subsequently, as these atoms return to their ground energy state, they release energy in the form of radiation with a specific wavelength unique to each element. The emitted radiation traverses through the solvent and sample-containing flame. The detector then registers a decrease in incident radiation intensity and absorption of radiation energy if the atoms present in the cathode are also present in the sample. Utilizing concentration-versus-absorption curves based on the Beer-Lambert Law, it becomes possible to quantitatively estimate the concentration of atoms within the material. In this study, a mixture of 5.0g of sodium peroxide and fine chromite ore is fused for an hour at 900°C in a platinum crucible. The resulting mixture is transferred into a beaker (250 ml) which contains 60% perchloric acid and 25% distilled water. After thorough shaking and overnight standing for complete dissolution, the solution is taken into a 250 ml volumetric flask and made up the volume with

distilled water. The resultant solution undergoes analysis for chromium, iron, aluminum, and magnesium using the PinAAcle900F atomic absorption spectrophotometer from Perkin Elmer, Singapore, with the assistance of PC-based Syngistix software for AAS analysis (refer to Fig. 4.10).

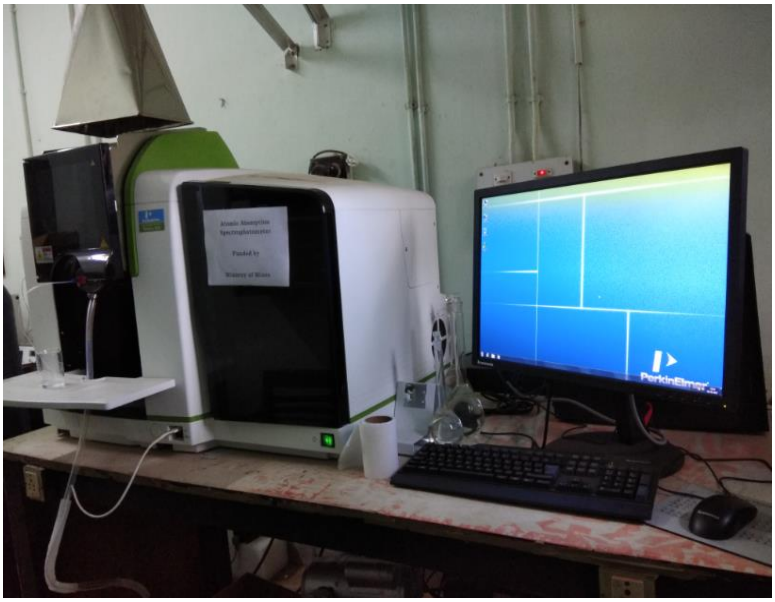

Figure 4.10: Flame-Atomic Absorption Spectrophotometer.

4.3 Experimental Unit

To understand the characteristics of chromite ore, samples undergo a series of processes including beneficiation, agglomeration, reduction, and smelting, each utilizing different equipment. Here's a summary of the equipment employed in this research project:

4.3.1 Wilfley Table

The wilfley table is a gravity concentration device widely employed in mineral processing plants for the recovery of valuable minerals from ores and concentrates. Its operation relies on separating minerals based on their specific gravity and particle size distribution. The table deck, featuring riffles or grooves, forms a concentrating bed for the mineral feed, creating a turbulent flow that aids in stratifying the material. A shaking motion, typically induced by an eccentric drive or motor-driven cam, agitates the feed material, enhancing the separation process. Water flow assists in carrying lighter particles away, while heavier mineral concentrate remains. Adjustable parameters such as shaking intensity, water flow rate, and table inclination angle

can be optimized to suit specific feed material characteristics and separation efficiency requirements. The separated mineral concentrate, enriched with desired minerals, is collected from one end of the table, while tailings containing lighter gangue minerals are discharged from the opposite end.

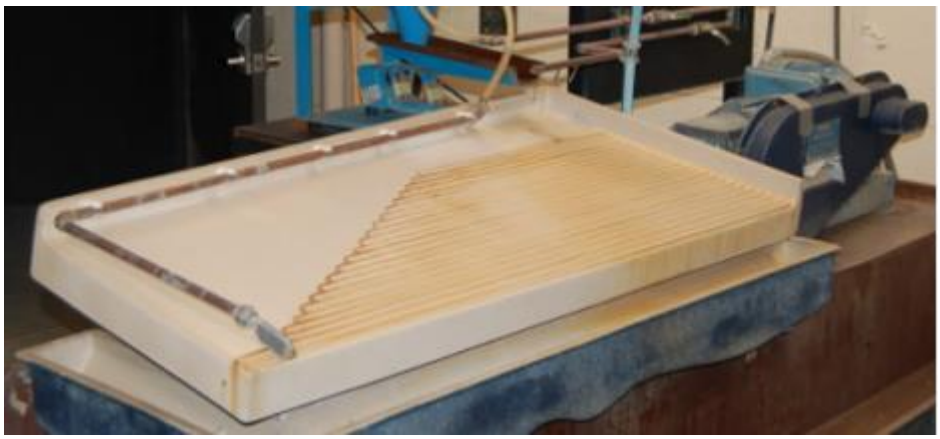

Figure 4.11: Wilfley Table.

In the laboratory-scale experiment, a wilfley table measuring 37 cm x 100 cm is used for the enrichment of chromite ore. The table features riffles with an approximate height of 2 mm, and the distance between riffles is approximately 14 mm. Throughout the experiment, the table vibrates at a fixed rate of 250 rpm. Refer to Fig. 4.11 for a visual representation of the wilfley table configuration.

4.3.2 Tube Furnace

Chromite ore is subjected to reduction in a standard tube furnace with a maximum temperature of 1350°C. The heating element used in the furnace is silicon carbide, with temperature control managed by a Proportional-Integral-Derivative (PID) controller. The furnace setup includes a horizontal alumina tube measuring 700 mm in length, with inner and outer diameters of 40 mm and 50 mm, respectively. The chromite sample is contained within a holder made of Inconel, a superalloy composed of austenitic nickel and chromium. The Inconel holder section measures 82 mm in length, with outer and inner diameters of 38 mm and 33 mm, respectively. This section is threaded onto a 210 mm hollow pipe. Positioned within the heating zone of the furnace, which extends 10 cm, the sample holder facilitates the reduction of chromite ore. For visualization, refer to Fig. 4.12, which illustrates the configuration of the tube furnace.

Figure 4.12: Tube Furnace.

4.3.3 Raising Hearth Furnace

Both the reduction smelting and pre-heat treatment of chromite ore are conducted in raising hearth furnaces capable of reaching a maximum temperature of 1650°C. The sample undergoes treatment on a platform constructed from alumina base bricks, which are adjustable in height within the furnace. Temperature control of the furnace is managed by a dedicated PC program. The sample is placed in a separate crucible based on specific requirements and positioned within the hearth for proximate analysis, preheating, and reduction smelting of both coke and chromite ore. For visualization, refer to Fig. 4.13, depicting the configuration of a raising hearth furnace.

Figure 4.13: Raising Hearth Furnace.

4.3.4 Coal Devolatilization Furnace:

In a devolatilization furnace, low-temperature reduction of chromite ore briquettes using boiler-grade coal is carried out, contributing to the production of synthesis gas. Synthetic gas comprises hydrogen, carbon monoxide, methane, and water vapor. The furnace comprises two distinct temperature zones: the reduction zone (1200°C) and the coal devolatization zone (550-600°C). The reduction zone, situated in the upper part of the furnace, accommodates the chromite sample for reduction. Meanwhile, the devolatization zone, located in the lower part, houses the coal. To optimize energy consumption, the devolatilization zone is positioned in the furnace such that coal undergoes devolatilization through reflected heat from the reduction zone. Temperature monitoring during the reduction process is facilitated by a PID-controlled display installed within the furnace, with silicon carbide rods employed for temperature detection. For visual reference, see Fig.4.14 illustrating a coal devolatilization furnace.

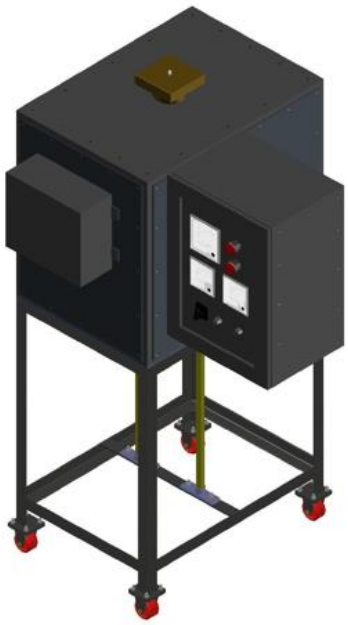

Figure 4.14: Coal Devolatilization Furnace.

Chapter-5

Geological Investigation of Chromite Source and Characterization of Raw Materials

5.1 Introduction

Characterizing the raw materials is a crucial step before creating an experimental route plan. The parameters involved in the process are influenced by the composition of ore, reductant and binder. Atomic absorption spectrophotometer (AAS), Thermo gravimetric-differential thermal analyzer (TG-DTA), Wavelength dispersive X-ray fluorescence spectrometer (WDXRF), X-ray diffraction (XRD), and Scanning electron microscope (SEM) are the instruments used in this study to characterize chromite ore. The following is a summary of the raw material characterization details found in this chapter.

5.2 Chromite Ore Geology

The East India Shield's greenstone-granite terrain is to be found between 21´ to 25º N latitude and 85º to 88º E longitude. It covers parts of Bihar, Jharkhand, Uttar Pradesh, Odisha, and West Bengal. This region exhibits chromite mineralization in conjunction with ultramafic iron ore group.

In Odisha, the Sukinda Valley in the Jajpur district is the source of chromite ore in the present research work. The predominant component of the chromite ore in the Sukinda Valley is chromite, with minor amounts of secondary silicates such as talc, serpentine, tremolite, uvarovite, and kammererite, along with ferrichromite, magnetite, and ilmenite. The world's biggest open-cast chromite ore mines are found in the valley, which has an abundance of chromite deposits.

The Tomka-Daitari range to the north and the Mahagiri range to the south encircle this valley, which has a general slope of 18 to 20 degrees towards the southwest and is dotted with lone mountains and ridges. The region experiences 90–194 cm of rainy fall each year, with winter temperatures ranging from 8 to 9 °C and summer temperatures from 46 to 47 °C. The Sukinda ultramafic complex, which is made up of occasionally occurring fragmented chromiferous ultramafic bodies, is located in a region of the metamorphosed Pre-Cambrians of Peninsular India and is bordered by latitudes 20°53' and 21°05' and longitudes 85°40' and 85°53'. The lopolith spans a zone 2 to 5 km wide, extending from Kansa in the east to Maruabil and further west, along the direction of ENE-WNW. This lopolith represents an interference of chromite-

rich ultramafic rocks from the Sukinda area into the Precambrian metamorphic formations. Chromite bands are found in this region.

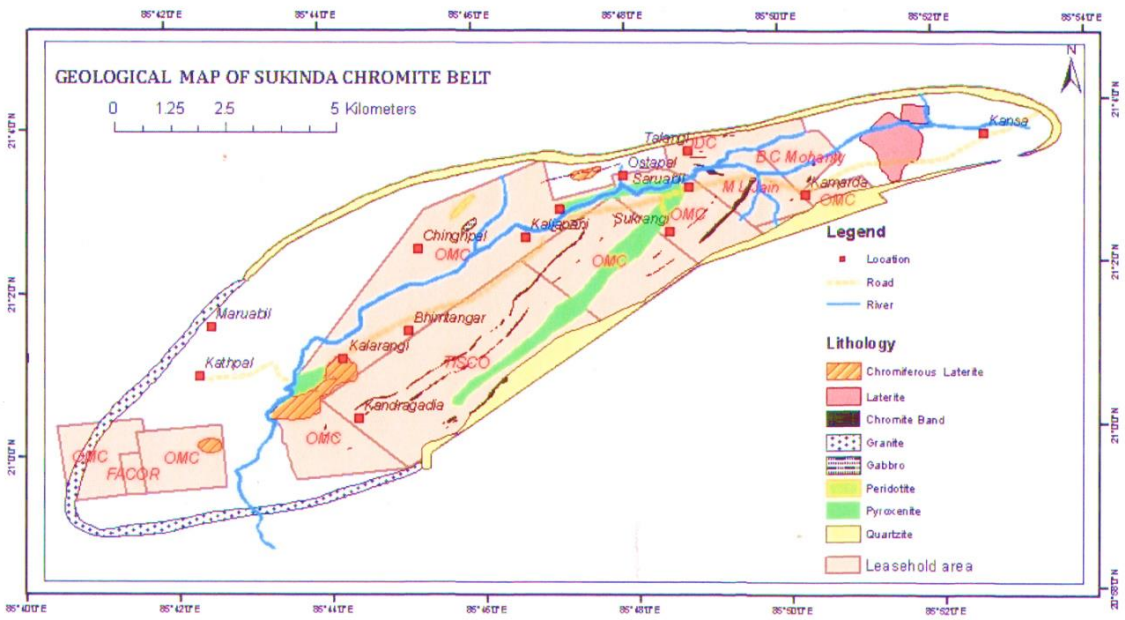

Figure 5.1: Geological Map of the Sukinda Chromite Belt.

There are primarily three bands of chrome ore where low-grade ores are collected for beneficiation. The geological map is displayed in Figure 5.1. The bands have an NE-SW trend and range in thickness. The nature of the ore bodies is sub-vertical. The southern band is identified by its grey color, hardness, and siliceous composition. Whereas, the middle and northern bands show brown color, iron-rich, and physically fragile or friable. The longest friable band in this region is the northern friable chrome ore band. Its strike length is roughly two kilometers from west to east. This band has a sharp dip of 85° to 90° towards the N-NNW and strikes in an ENE-WSW direction. It shows structures of widening and narrowing along both the horizontal and inclined directions of the rock layers. The ore body's width ranges from 4 to 20 meters. Chromite ore in this band has a tentative composition of 38 to 58 percent Cr_2O_3, 9.5 to 24.5 percent Fe, and 0.88 to 9.08 percent SiO_2. Between the northern and orthopyroxenite bands, the middle friable ore band is parallel to the former at a lateral distance of 200–250 meters. High iron content chrome ore is present in this band. The ore body is 3–8 meters wide. This band's chromite is composed of 1.2-13% SiO_2, 9-28% Fe, and 25-44% Cr_2O_3. The northern foothill of the Magagiri hill range is the location of the southern Lumpy ore band. This band's ore is siliceous, lumpy, hard, and grey in color. The body's width ranges from 0.75

meters to 8 meters. 23.42-47% Cr_2O_3, 10.29-11% Fe, and 8.88-24.61% SiO_2 are the major constituents of chromite.

5.3 Chromite Ore Analysis

The collected chromite ore is subjected to several characterization techniques in order to ascertain the composition of the ore body. A summary of the detailed analysis reports is given below.

5.3.1 WDXRF Analysis Report of Chromite Ore

The collected chromite ore is crushed and ground using a jaw crusher, roll crusher, and pulverizer to get the fine particle size. Wavelength dispersive x-ray fluorescence (WDXRF; PAN analytical) is used to analyze chromite fines (below 75 μm). Table 5.1 displays the analysis report and shows that the major constituents of the ore are Cr_2O_3 (26.88%), Fe_2O_3 (33.88%), and Al_2O_3 (21.075), with smaller amounts of oxides of silicon, magnesium, and titanium.

Table 5.1: WD-XRF Analysis Report of Low-Grade Chromite Ore.

Cr_2O_3	Fe	Mn	Al_2O_3	SiO_2	TiO_2	K_2O	Ni	P	S	V_2O_5	CaO	MgO	LOI
26.88	23.72	0.55	21.07	0.92	0.29	0.004	0.1	0.02	ND	0.172	0.02	5.1	8.99

5.3.2 AAS Analysis Report of Chromite Ore

The quantitative analysis for chromium, iron, and aluminium present in chromite ore is carried out by atomic absorption spectrophotometers (AAS). The fine chromite ore (0.5g) is fused with 5.0g Na_2O_2 and leached with 60% perchloric acid for the dissolution of ore. Then the solution is subjected to PinAAcle900F (Perkin Elmer, Singapore) for elemental analysis. The hollow cathode lamps (HCL) composed of iron, chromium, and aluminum are commonly used in AAS to quantify the concentration of each element in the ore. The primary wavelengths chosen are 357.9 nm for aluminum, 248.3 nm for chromium, and 309.3 nm for iron. The analysis report is given in Table 5.2.

Table 5.2: AAS Analysis Report of Chromite Ore.

Chromium (%)	Iron (%)	Aluminium (%)
18.06	23.88	11.4

5.3.3 XRD Analysis of Chromite Ore

Cu Kα is used by X-ray diffractometers (XRD; Rigaku Ultima III) to analyze the various phases in the ore. Fig. 5.2 displays the raw ore samples' XRD pattern. The figure indicates that berezovskite (Mg, Fe)(Al, $Cr)_2O_4$ is the main peak, with minor peaks consisting of quartz, hematite (Fe_2O_3), and aluminum hydroxide $Al(OH)_3$. An X-ray scene is executed at a constant speed of 2°/min, covering an angle range of 10° to 80°. The phase d values correspond to the typical JCPDS d values. [JCPDS – 85-0987, 84-1435, 86-1630, 86-1410].

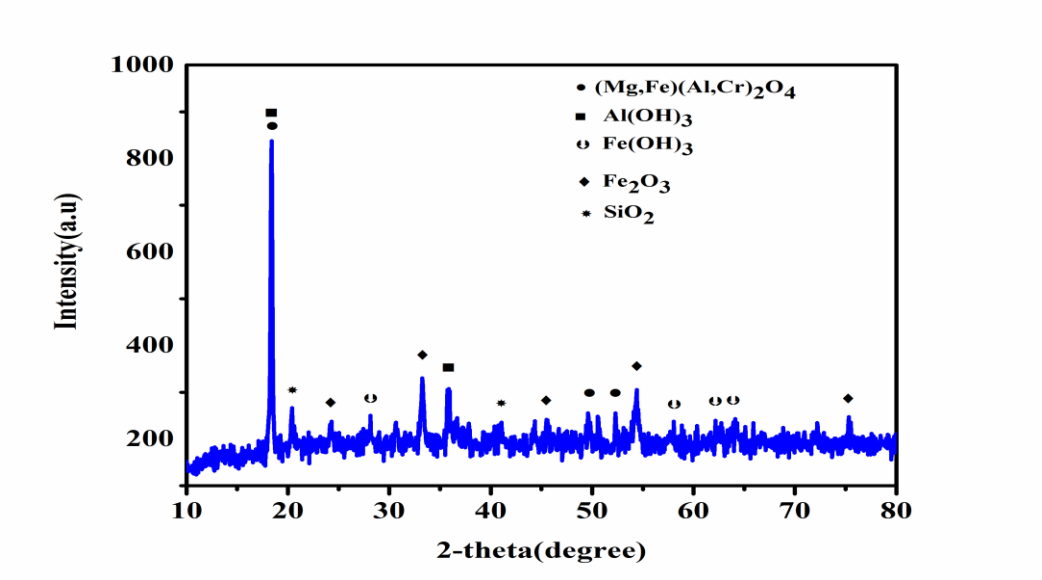

Figure 5.2: XRD Analysis of Chromite Ore.

5.3.4 SEM Analysis of Chromite Ore

Fig. 5.3 displays a micrograph image obtained using scanning electron microscopy (SEM) at various resolutions. The morphology of the chromite ore surface is displayed in the images. Images show that chromite grains have an uneven shape due to irregular particle size. The surfaces of chromite grains are associated with various gangues minerals.

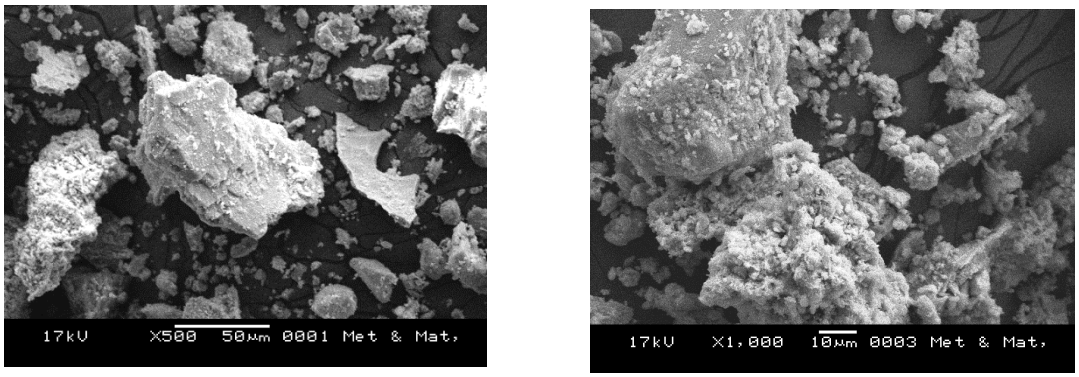

Figure 5.3: SEM Image of Chromite Ore at Different Resolutions.

5.3.5 Microstructure Analysis of Chromite Ore

In Fig. 5.4, the micrographs show the polished surface of chromite ore under a microscope at 200x magnification. The brighter colors indicate the grains of chromite, while gangue minerals surround darker regions. In both images, the shape of chromite grains is angular and varies in size, with some grains closely associated with gangue minerals. The grain sizes look like they range between 50 to 150 µm. Based on these observations, the predicted liberation size of chromite grains could be around 75 to 100 µm, ensuring effective separation during mineral processing.

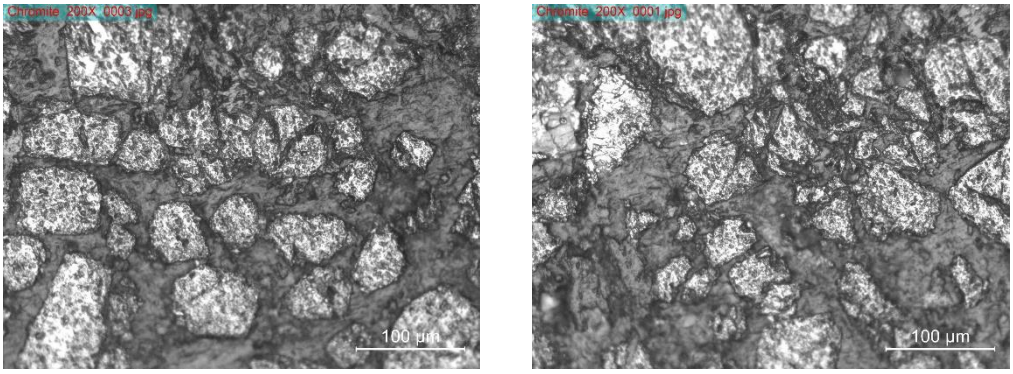

Figure 5.4: Microstructural Analysis of Chromite Ore at Various Surface Locations.

5.3.6 EDX Analysis of Chromite Ore

EDX spectrum and elemental composition of ore are shown in Fig. 5.5 and Table 5.3. The results showed that the leading elements found in the mineral are iron, aluminium, chromium, & oxygen. A high oxygen content suggests that the ore contains oxides of various elements. Fe to Mg and Cr to Al have respective α value ratios of 2.84 and 0.50. The results showed that iron and aluminum enrichment are present in the raw material.

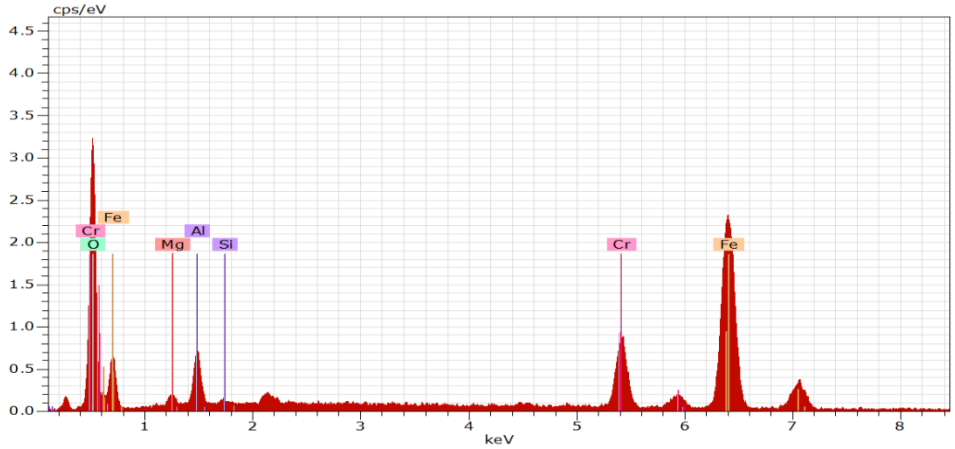

Figure 5.5: EDX Spectrum of Elements in Chromite Ore.

Table 5.3: EDX Result for the Chromite Ore.

Element	Weight%	Atomic% (α)
O K	36.89	57.43
Al K	12.65	13.95
Si K	2.23	2.70
Cr K	15.62	6.98
Fe k	28.64	14.01
Mg K	3.97	4.93

5.3.7 Distribution of Elements in Chromite Ore

The distribution of the various elements found in the ore is displayed in Fig. 5.6. In EDX mapping, a bright color points out the presence of that element in five distinct images. Comparable distribution patterns have been identified for Cr, Al, and Fe. Dark color is predominant in the case of Si and Mg, indicating a lower fraction present in the ore.

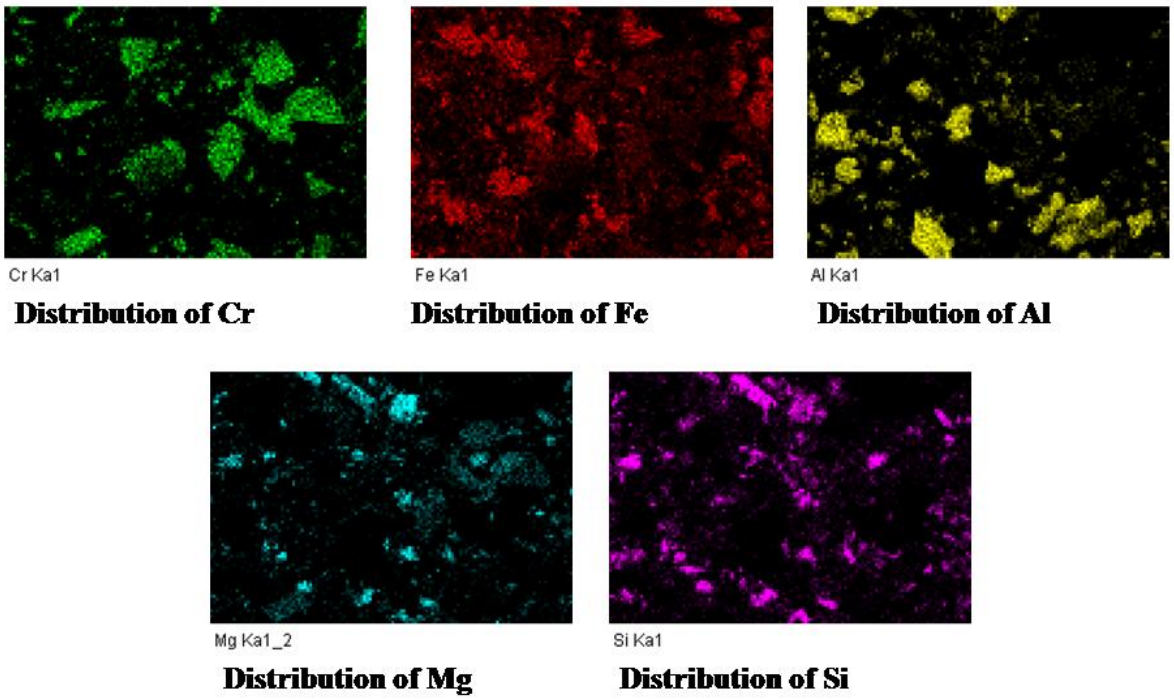

Figure 5.6: Elemental Analysis of Chromite Ore.

5.3.8 TGA-DSC Analysis of Chromite Ore

The temperature range for thermal analysis of chromite ore is 0-1000°C. Fig. 5.7 shows the graphical representation of heat flow and weight loss as temperature rises. The temperature range where a sharp weight loss is observed is between 300 and 350°C. At higher temperatures, the weight loss is only marginally decreased.

.

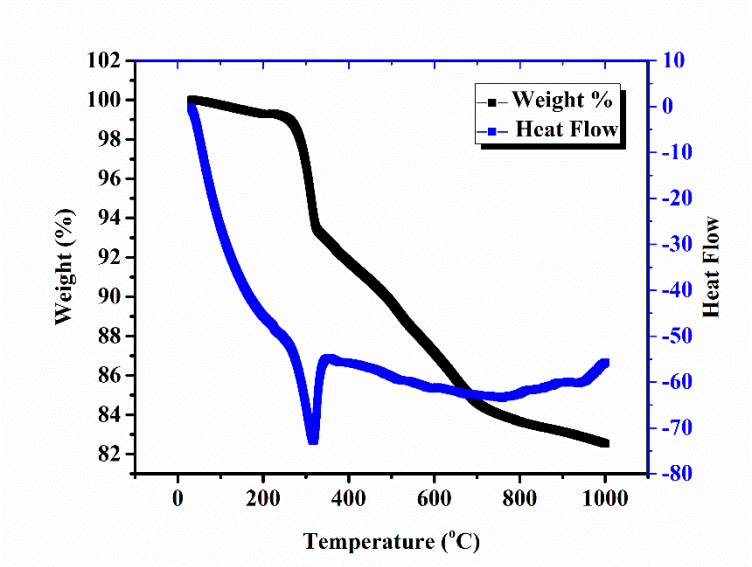

Figure 5.7: TGA-DSC Analysis of Chromite Ore.

5.3.9 Bulk Density

The collected ore is hard and dark brown in color and contains a high iron percentage. The bulk density of ore is found to be 3.665g/cc which is shown in Table 5.4 [**IS: 5842-1986**].

Table 5.4: Bulk Density of Raw Ore.

Physical properties	Unit
Bulk Density	3.665 g/cc

5.4 Analysis of Reductant

In this work, enriched chromite ore is carbothermally reduced primarily using coke. For the indirect reduction of chromite ore in the gasification furnace, boiler-grade coal is utilized. Before characterization, both reductants are crushed to a size smaller than 75 µm. Details about the characterization are provided below. Both coke and coal dust are collected from the Vizag Steel Plant.

5.4.1 Coke Dust

5.4.1.1 Proximate Analysis and Ultimate Analysis of Coke Dust

In the reduction process, the actual reductant composition is computed based on the stoichiometric calculation of coke dust and chromite ore. Table 5.5 lists the contents of the used coke sample, which contains 1% moisture, 0.4% volatile matter, 1.64% ash, and 84.96% fixed carbon. For one hour, the sample is dried at 105° C to determine the moisture percentage. To determine the volatile matter content, the dried sample is heated to 550° C. The sample is burned at 1000° C after the volatile matter has been removed, and the remaining portion is considered as the ash content. The ultimate analysis, which is also included in Table 5.5, is used to validate the proximate analysis report. The calorific value (air dry basis) of the coke is found to be 7910.86 cal/g.

Table 5.5: Proximate and Ultimate Analysis of Coke Dust.

Sl. No.	Parameters	Proximate Analysis Result (%)	Ultimate Analysis(ASTM D 5373.02)
1	Analytical Moisture	1.0	• % Carbon = 87.5 • % Nitrogen =1.351 • % Hydrogen = 0.065
2	Volatile Matter	0.4	
3	Ash Content	13.64	
4	Fixed Carbon	84.96	

5.4.1.2 TGA-DSC Analysis of Coke Dust

Room temperature to 1000°C is the temperature range for TGA-DSC analysis, which is conducted in an inert atmosphere. In this analysis, the nitrogen of UHP grade 99.99% is used. Fig. 5.8 shows how marginal weight loss up to 600°C can be caused by moisture loss and volatile matter from the coke dust. Coke started to burn at 700°C. Burning requires oxygen, which is obtained from the nitrogen source and the sample. The coke sample in the TGA-DSC is not stiff; air is present between the coke fines, which triggers the coke to burn at high temperatures. Nitrogen is also a source of oxygen and contains a trace amount of oxygen. At the temperature range 737 to 1000ºC the maximum loss of weight occurs, where a sharp exothermic peak is observed due to the burning of fixed carbon present in coke.

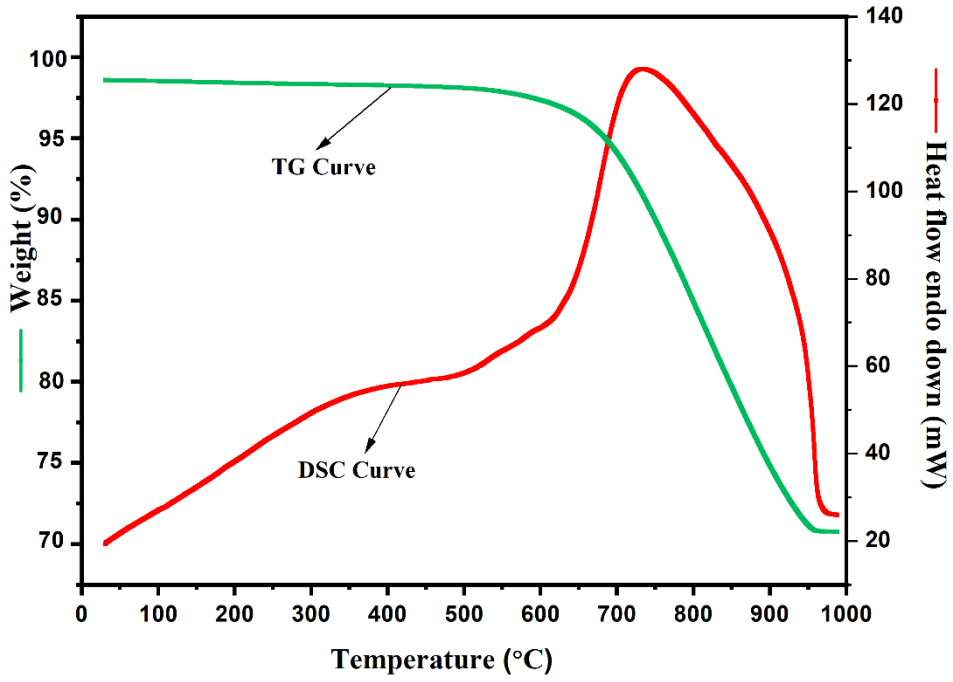

Figure 5.8: TGA-DSC Analysis of Coke.

5.4.1.3 SEM-EDX Analysis

The SEM microphotograph in Fig. 5.9 shows that there are irregularly sized particles in the coke dust. The picture displays the glossy cocaine particles. Carbon is the main peak visible in the EDX image, with smaller peaks for silicon, aluminum, and sulfur. According to the EDX analysis report in Table 5.6, the sample's weight-based carbon content is 83.26%, which is almost similar to the fixed carbon measured through proximate analysis.

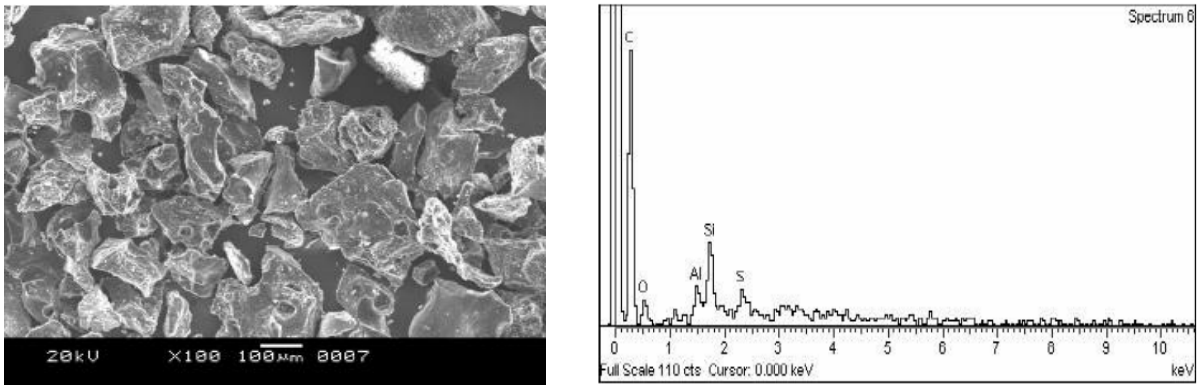

Figure 5.9: SEM-EDX Image of Coke Dust.

Table 5.6: EDX Analysis Report of Coke Dust.

Element	C K	O K	Al K	Si K	S K	Total
Weight %	83.26	11.97	1.32	2.38	1.07	100.0
Atomic %	88.05	9.58	0.79	1.05	0.53	100.0

5.4.2 Boiler Grade Coal

5.4.2.1 Proximate Analysis and Ultimate Analysis of Boiler Grade Coal

Proximate and ultimate analysis are used to determine the chemical composition of boiler-grade coal and help to identify the behavior of coal during reaction. Table 5.7 provides the ultimate and proximate analysis of coal. The coal sample has a high percentage of ash and volatile matter. 30.52% of it is fixed carbon. In other words, boiler grade produces less energy than coke. The gross calorific value is found to be 3038.92cal/g.

Table 5.7: Proximate and Ultimate Analysis of Boiler Grade Coal.

Sl. No.	Parameters	Proximate Analysis Result (%)	Ultimate Analysis
1	Analytical Moisture	7.3	• % Carbon = 50.9 • % Nitrogen =0.803 • % Hydrogen = 3.4
2	Volatile Matter	29.13	
3	Ash Content	33.05	
4	Fixed Carbon	30.52	

5.4.2.2 TGA-DSC Analysis of Boiler Grade Coal

In an inert atmosphere, boiler-grade coal is subjected to TGA-DSC analysis between room temperature and 1000°C. In this analysis, an inert atmosphere is produced using nitrogen of UHP grade 99.99%. A significant decrease in weight is noted in the temperature range of 350 to 500°C. Weight loss begins at 100°C because of moisture, but at that specific temperature range, weight loss happens because of volatile matter present in the coal. Coal started to burn at 700°C. Fig. 5.10 displays the TGA-DSC curve of boiler-grade coal.

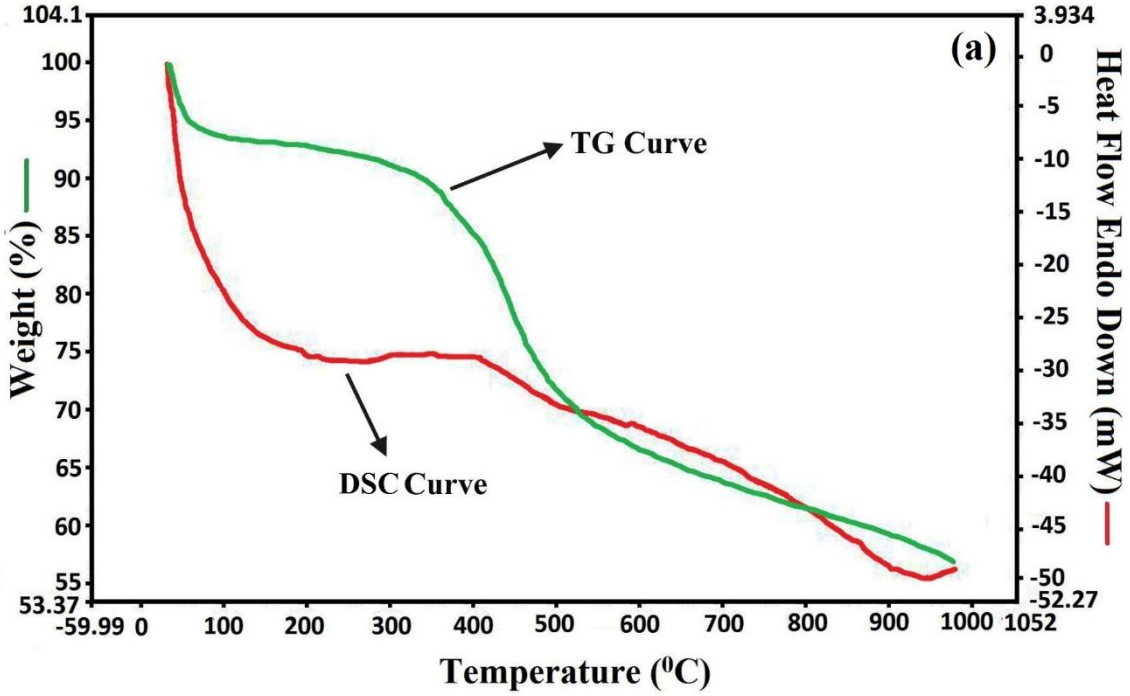

Figure 5.10: TGA-DSC Analysis of Boiler-Grade Coal.

5.5 Characterization of Binders

Binders are crucial to for agglomeration process because they provide durability and mechanical strength. Lime is used as a flux during smelting in the current study, while bentonite and molasses are utilized as binders during agglomeration. Molasses and bentonite are both collected from Tata Steel in Jamshedpur, Jharkhand, India.

5.5.1 Analysis of Bentonite

In the metallurgical field, bentonite is widely used as a binder in agglomeration processes. It is a common swelling clay that can be found in the crust of the earth. It is used as a purifier and absorbent because of its good swelling properties [1]. Bentonite causes swelling because of its capacity to absorb and retain water. Typically, two types of bentonite are widely accessible: sodium montmorillonite and calcium montmorillonite. Because sodium bentonite has a higher

retention capacity than calcium bentonite, its swelling capacity is higher [2]. Bentonite provides both mechanical strength and compactness to the agglomerate. The bentonite composition used in this research work is provided in Table 5.8.

Table 5.8: Composition of Bentonite (Provided by Tata Steel, India).

Typical constituents	**Contents**
SiO_2	59.10%
Al_2O_3	18.60%
Fe_2O_3	4.40%
CaO	1.90%
MgO	4.00%
K_2O	0.30%
Na_2O	2.50%
Moisture	6-12%
Swelling Index	22-26 (ml/2g)
Loss on Ignition	8.90%
Water absorption rate	>580%
PH	10-10.5
Cation Exchange Capacity	75-85 meq/100g

Proximate analysis is done at various temperatures for 60 60-minute period to determine the weight loss caused by bentonite during the reduction; the results are displayed in Table 5.9.

Table 5.9: Proximate Analysis of Bentonite.

Temperature	**1000 °C**	**1100°C**	**1200°C**	**1300°C**	**1400°C**	**1500°C**
Weight Loss	14.62%	17.22%	18.00%	18.44%	18.90%	19.28%

5.5.2 Analysis of Molasses

Molasses is combined with chromite or as a binder and reductant to prepare chromite ore briquettes. In briquettes, provides good green strength. Molasses function as a good binder in terms of economic viability when compared to glycerol, lignin, and starch [3]. It is a silica-free organic binder. A significant amount of inverted sugar is present in molasses, which aids in material combustion during reduction and raises the intermolecular force of attraction within the molecule. Molasses also boost porosity and reducibility during reduction. These days, it is widely employed as a binder in the agglomeration process because of its good mechanical strength and combustion properties [4]. The composition of molasses used in this work is given

in Table 5.11. The weight loss resulting from the reduction of molasses is calculated at different temperatures over 60 minutes using proximate analysis; the results are shown in Table 5.10.

Table 5.10: Proximate Analysis of Molasses.

Temperature	**1000 °C**	**1100°C**	**1200°C**	**1300°C**	**1400°C**	**1500°C**
Weight Loss	90.82%	92.30%	94.88%	95.60%	96.12%	97.0%

Table 5.11: Chemical Composition of Molasses (Provided by Tata Steel, India).

		75% D. M. Basis
Typical constituents	**Unit**	**Contents**
Refractometer Brix	.	79.5
Sucrose		29.50%
Fructose		7.10%
Glucose		5.20%
Total Sugars		41.80%
Total Sugars as invert		43.40%
Moisture	(g/kg)	250
Ash	(g/kg)	100
Total Organic Matter	(g/kg)	650
Non-sugar Organic Matter	(g/kg)	170
Crude Protein	(g/kg)	42
Crude Fibre	(g/kg)	0
Ether Extract	(g/kg)	Trace
Calcium	(g/kg)	8.0
Phosphorus	(g/kg)	0.7
Sodium	(g/kg)	1.6
Chlorine	(g/kg)	21.1
Magnesium	(g/kg)	5.4
Potassium	(g/kg)	33.3
Sulphur	(g/kg)	6.8
Copper	(mg/kg)	2.2
Zinc	(mg/kg)	2.7
Iron	(mg/kg)	101.0
Cobalt	(mg/kg)	3.8
Manganese	(mg/kg)	91.0

5.5.3 Analysis of Lime

Lime is mostly used as a flux during the smelting process in metallurgical operations. Lime is widely used in the steel-making process to remove impurities [5]. Lime combined with the

impurity to improve the slag metal's separation. In addition, it finds application in the construction, chemical, and environmental sectors. Lime helps to stabilize the soil so that it can be used to build roads. It also serves as a foundation for buildings [6]. The chemical composition of lime is calcium oxide (CaO), which is typically made by heating calcium carbonate ($CaCO_3$). In the current work, proper slag metal separation is achieved through the use of lime during the smelting of reduced chromite ore. The Tata Steel plant in Jamshedpur, Jharkhand, India, is the source of lime. Table 5.12 provides the composition of lime.

Table 5.12: Chemical Composition of Lime (Provided by Tata Steel, India).

Typical constituents	**Contents**
Acid Insoluble Matter	2.00%
SiO_2	1.00%
Alumina	0.10%
Fe	0.25%
CaO	74.00% (Available lime as Calcium Oxide – 70%
MgO	0.60%
Carbon Dioxide	0.80%
Mn	0.01%
Moisture	0.30%
Calcium Carbonate ($CaCO_3$)	1.8%
Calcium Hydroxide [$Ca(OH)_2$]	95.00%
Sieve Analysis:	
Minus 300 to Plus 212	0.00%
Minus 212 to Plus 150	0.80%
Minus 150 to Plus 75	1.90%
Minus 75 to Plus 45	2.00%
Minus 45	95.30%

5.6 Conclusion

It can be seen from WD-XRD, EDX, and chemical analysis (AAS) reports that the collected chromite ore has a 0.78 Cr/Fe ratio. The mineralogical investigation shows that the tested sample is low-grade chromite ore and ferruginous in nature. Microscopic analysis of chromite ore shows that the liberation size range of the chromite grain is 75-200μm. The primary phase found in the ore is berezovskite $(Mg, Fe)(Al, Cr)_2O_4$, according to the XRD pattern. Therefore, the ore body has a spinel structure and is complex in nature. The SEM image illustrates that chromite ore has an irregular shape and particle size. The distribution of alumnium throughout the cross-section of chromite particles is higher than any other element present in the

sample. TGA-DSC analysis reveals a significant weight loss between 300°C and 350°C, which indicates that the ore body has undergone some kind of chemical dissociation occur at that specific temperature. In the characterization of reductants, TGA-DSC analyses support the proximate coal and coke analyses. It is evident that when boiler-grade coal is heated to 550°C, a considerable amount of weight is lost as a result of volatile matter. In this study, two types of binder are used: bentonite, which is an inorganic binder, and molasses, which is an organic binder. The binders' composition reveals that while molasses has good adhesive properties, bentonite has a good capacity for swelling.

5.7 Reference

[1] H. H. Murray, “Chapter 6 Bentonite Applications,” 2006. doi: 10.1016/S1572-4352(06)02006-X.

[2] N. Muhammad and S. Siddiqua, “Calcium bentonite vs sodium bentonite: The potential of calcium bentonite for soil foundation,” in Materials Today: Proceedings, Elsevier Ltd, 2021, pp. 822–827. doi: 10.1016/j.matpr.2021.02.386.

[3] O. F. Obi, R. Pecenka, and M. J. Clifford, “A Review of Biomass Briquette Binders and Quality Parameters,” Apr. 01, 2022, MDPI. doi: 10.3390/en15072426.

[4] R. C. Uwaoma, C. N. Henning, J. R. Bunt, N. T. Leokaoke, and H. W. J. P. Neomagus, “Comparison of industrial wastes as a binder in the agglomeration of coal fines,” Results in Engineering, vol. 16, Dec. 2022, doi: 10.1016/j.rineng.2022.100729.

[5] S. Manocha and F. Ponchon, “Management of lime in steel,” Sep. 01, 2018, MDPI AG. doi: 10.3390/met8090686.

[6] I. T. Jawad, M. R. Taha, Z. H. Majeed, and T. A. Khan, “Soil stabilization using lime: Advantages, disadvantages and proposing a potential alternative,” Research Journal of Applied Sciences, Engineering and Technology, vol. 8, no. 4, pp. 510–520, 2014, doi: 10.19026/rjaset.8.1000.

Chapter-6

Processing Methods of Low-Grade Chromite Ore and Utilization

Characterization of collected chromite ore, reductants, and binders are summarized in Chapter 5. Four methods have been carried out for the utilization of the low-grade chromite ore. All four methods are explained in Chapter 6, which is subdivided into 6A, 6B, 6C, and 6D. Pyrometallurgical, hydrometallurgical, and bio-hydrometallurgical processes are used to treat chromite ore. The hydro-metallurgical and bio-hydro-metallurgical processes are covered in Chapters 6C and 6D, respectively. The pyro-metallurgical approach is covered in Chapters 6A and 6B.

The processing and subsequent analysis of low-grade chromite ore and products throughout the thesis are described in chapter 6 and the content of the chapter (sub-divided) is given as under:

Chapter 6A describes the processes of chromite ore beneficiation, agglomeration, reduction, and smelting.

- 6A.1 - Particle Size Distribution and Beneficiation of Low-Grade Chromite Ore.
- 6A.2 - Optimization of Briquetting Parameters of Chromite Fines to Produce Ferrochrome.
- 6A.3 – Smelting of Pre-heated Chromite Briquettes after the Reduction of Briquettes using Coke at Different Temperatures and its Kinetic Study.

In Chapter 6B, carbon-free iron-chromium alloy is produced by reducing low-grade chromite ore in a gasification reactor with the help of synergetic gas. The leaching behavior of salt-roasted low-grade chromite ore is examined in Chapter 6C to get chromium-based products. In Chapter 6D, a bio-hydro-metallurgical process is used to extract metal from chromite ore.

Chapter-6A.1

Particle Size Distribution and Beneficiation of Low-Grade Chromite Ore

6A.1.1 Introduction

Chromite ore is the primary source of chromium. India has large reserves of chromite which is about 344.016 million tons. Orissa alone accounts for 330.714 million tons and most of it is located in the Sukinda region [1]. Chromite has various applications in the steel industry, automobile industry, rails, refractory industry (owing to its high corrosion resistance and high melting properties), cement industry, non-ferrous alloy industry, chemical industry as ferrochrome chemical and chromium plating solution, etc.

Chromium exists as chromium spinel in chromite ores along with magnesium, aluminium, and iron in different proportions depending upon the deposits. Chromite is chemically represented as $FeO.Cr_2O_3$, where Fe is replaceable by Mg and Cr is replaceable by Al or Fe [2]. Chromite ore can be divided into three types: high-grade ore with a Cr_2O_3 content of 50%, subgrade ore containing 35–40% Cr_2O_3, and low-grade ore with 20–25% Cr_2O_3. High-grade chromite ore is directly transferred to the market for ferroalloy production. Beneficiation of ore is required in the case of subgrade and low-grade chromite ores to make them marketable.

6A.1.2 Literature Review

The comminution process is used for the liberation of gangue particles like serpentine, olivine, quartz, etc. from chromite ore. Two basic comminution processes are crushing and grinding. Different crushing equipment like jaw crusher, cone crusher, and roll crusher are used for crushing whereas ball mill and roll mill are generally used for grinding purposes. Different beneficiation processes have been used to increase the concentration of low-grade chromite ore. The processes commonly used are gravity separation, froth-flotation, electrostatic separation, magnetic separation, and selective flocculation. Beneficiation of chromite ore has been done by many researchers to improve the Cr/Fe ratio using different beneficiation techniques [3-7].

G. P. Gallios and colleagues investigated the behavior of chromite ore and its separation from serpentine through the flotation process. Their experimental results showed that sodium oleate, used as a collector in an alkaline medium, is vital for the flotation of low-grade chromite ore [8]. Flotation has proven to be an effective beneficiation technique, yielding substantial results for upgrading chromite ore. The problem arises since different chemicals are used which are not environment friendly. Apart from that, the process completely depends upon the nature of the gangue minerals. Chromite ore containing serpentine as

gangue minerals is very difficult to separate by this process due to the similar surface phenomena of both minerals [9]. The choice of collector is important in this process, which is controlled by the pH of the investigated media. For example, anionic collectors below pH 6 cannot be used in this process. In this process dimerization, miscellization, and precipitation-like phenomenons are involved [4]. This process is a good alternative method for chromite ore beneficiation.

For the beneficiation of low-grade chromite fines smaller than 150 μm, the selective flocculation process is another effective method. The basic principle of this technique is the adsorption of different flocculants on the selective mineral particles and helping them settle down faster than the rest of the minerals present in the ore body. The impure minerals are present in the solution as suspension after the adsorption of flocculant. Starch and various polyacrylamides show a stronger attraction to chromite than serpentine at pH levels above 11. This method is applicable for the recovery of chromite when there is a low amount of serpentine present in the ore as gangue material. [10-11]. However, when higher amounts of serpentine are present, some problems arise in the separation of chromite from the gangue.

The heavy media separation (HMS) technique is commonly applied for the separation of sand, coal, and high-density minerals from their ores. Lithium, manganese, and chromium-bearing ores are beneficiated by HMS. Optimizing the particle size of the feed sample is very important before processing it through HMS. The mixture of bromoform and carbon tetrachloride produces densities ranging from 1.58 to 2.89 g/cm3. In industrial mineral processing, this mixture is mainly used as a heavy medium. Alloys like ferrosilicon, which has a specific gravity range of 6.7–6.7, are used as heavy media for the upgradation of Ingassana low-grade chromite ore [12]. Recycling media is crucial in this process because it is costly. The wastage of heavy media increases the operational cost.

A high-intensity induced roll magnetic separator is also used for the chromite ore up-gradation process. Nevzat Aslan et al. used a multi-gravity separator and a high-intensity induced roll magnetic roll separator for chromite beneficiation, and optimization of process parameters has been carried out by the Taguchi method. It is observed that the grade and recovery improved up to 47.74% and 73.31% from 42.38% and 65.34%, respectively [4]. The influence of particle size present in the feed, speed of the drum, and flow rate of washing water are critical for chromite recovery in a multi-gravity separator. [13]. Using a basic magnetic separator, the Cr/Fe ratio can be increased from 1.49 to 2.42. [14]. S. K. Tripathy

and his team investigated the upgrading of chromite ore by utilizing four distinct types of magnetic separators. The investigation report shows that wet high-intensity magnetic separators and induced roll magnetic separators give better product quality with chromium oxide recovery. It is also observed that to obtain better product quality and recovery, two-stage operations are required at higher and lower magnetic field intensities [15]. However, the application of this process is suitable for ferruginous chromite ores, otherwise, it is a very costly process due to the expensive electrical energy involved in the process. The recovery percentage of chromium oxide is also not significant in the magnetic separation process. The reason behind that may be due to the chromite particles being coated with magnetic particles and during magnetic separation, it goes to the magnetic fraction which is treated as a waste product in that case.

Nowadays gravity separation technique is widely used for chromite ore beneficiation. Gravity separation is primarily carried out using methods such as wilfley tables, spiral gravity separators, heavy liquid separation, and jigging. Many researchers have reported that gravity separation technology is highly effective for chromite beneficiation [16-21]. Seifelnasr et al 2012 suggested a method for processing low-grade chromite ore containing 20-35% Cr_2O_3 using these techniques. The Cr_2O_3 content of raw chromite ore is only 34.2%, the chromium oxide content is up to 49%, and the recovery rate is 63%. The authors concluded that breaking the material into smaller pieces without refining is better than refining the product. [4]. Sunil Kumar Tripathy et al. used the wilfley table for gravity separation of lean-grade chromite, which contained 40.8% Cr_2O_3 with a Cr/Fe ratio of 1.7. After separation, the concentrate fraction contained 48.9% Cr_2O_3 with a Cr/Fe ratio of 2.31 [5]. The behavior of low-grade chromite ores for ferrochrome production using a shaking table and wet high-intensity magnetic stirring (WHIMS) is also studied by A.K. Das et al. in 2020. It is found that low-grade chromite ore could be upgraded from 16% to 42.5% using wet shakers and WHIMS [22]. It is clear from the above discussion that gravity separation offers several advantages over other mineral processing techniques, particularly for chromite ores. When properly executed, gravity separation using a wilfley table provides a high concentration ratio along with excellent selectivity. Additionally, it is easy to operate, involves low operating costs, requires minimal testing to achieve optimal separation, and allows for upfront alteration of key parameters [23].

6A.1.3 Methodology

However, in the present scenario, the availability of high-grade chromite ore is declining due to its huge demand and consumption in the alloy steel industry. Besides this, huge chromite fines are generated during chromite mining. Discarding these fines or using the fines in less important areas is equivalent to the loss/inappropriate uses of chromium and other valuable metals present in the fines. The detailed optimization study of low-grade chromite ore is limited and not many references are available. In the present investigation, an attempt has been made to provide a noble technique of heating followed by air quenching to generate a lot of physical defects like fissures, for easy subsequent processing. This is the main feature of the study to see the effect on the beneficiation of chromite ore by initiating cracks & fissures for the liberation of valuable minerals. The objective of the present study is to utilize the lean grade ore by beneficiation and generation of cracks & fissures in the raw materials leading to a probable increase of reducibility of upgraded materials. Laboratory scale wilfley table has been used for beneficiation of low-grade chromite. Three different parameters have been selected for the experiment. The impact of tilt angle, water flow rate, and pre-heating treatment on chromite ore before charging on the wilfley table have been investigated. The optimization of parameters is performed utilizing the Box-Behnken statistical design (BBD)

6A.1.4 Particle Size Distribution

WD-XRF analysis shows raw chromite ore contained 26.88% of Cr_2O_3 and 33.89% of Fe_2O_3 along with a Cr/Fe 0.78 [chapter 5, Table 5.1]. Chromite ore is crushed and ground by jaw crusher, roll crusher, and pulverizer to get the particle size distribution. Fine chromite samples are subjected to a set of BBD standard sieves containing seven different sieves having different sieve openings. The whole set of sieves is placed in a sieve shaker for the separation of different particle sizes. The chemical analysis of different size fractions is evaluated by AAS which is shown in Table 6A.1.1. It is observed that within particle size 0.152 to 0.104 mm, the concentration of chromium oxide content is increased up to 36.49%. At the intermediate region of particle size, iron content is minimum but with decreasing particle size, the percentage of iron is increasing in order. Besides this, the chromite fines retained on different sieves during the sieves analysis have been shown in the size distribution curve Fig. 6A.l.1.

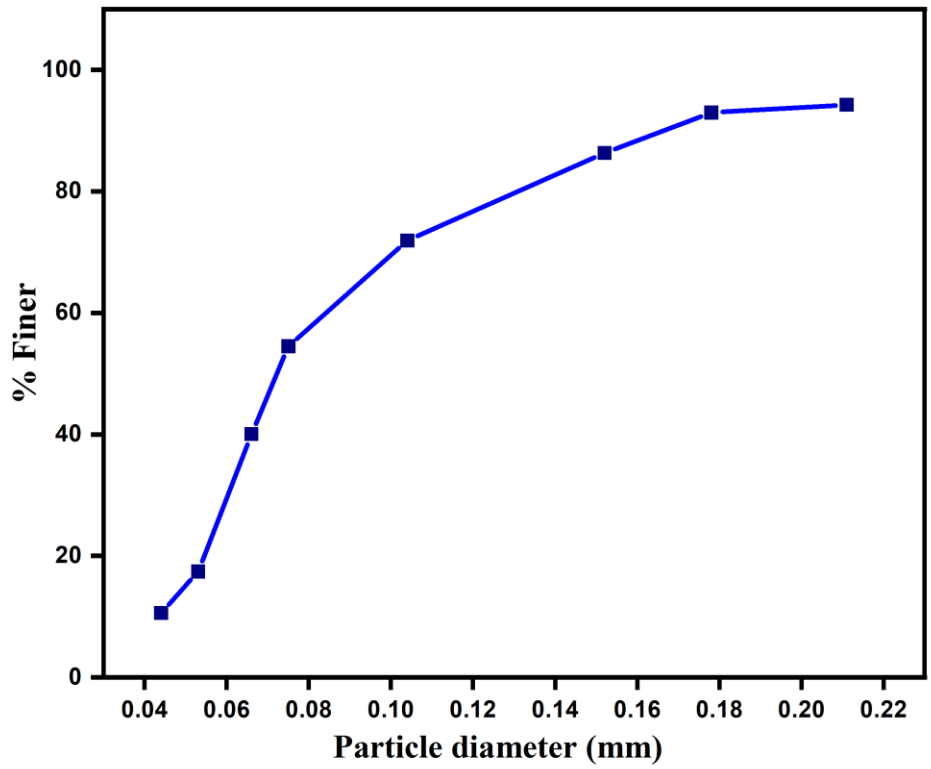

Figure 6A.1.1: Size Distribution Curve of Raw Chromite Sample.

Table 6A.1.1: Chemical Analysis of Different Size Fractions of Raw Chromite Ore.

Sieve Opening (mm)	Mass Retained (%)	Cr_2O_3 %	Fe_2O_3%	Cr/Fe
0.211	5.76	20.27	27.98	0.71
0.178	1.27	25.85	26.30	0.96
0.152	6.66	33.45	25.51	1.28
0.104	14.40	36.49	23.91	1.49
0.075	17.40	33.705	26.30	1.25
0.066	14.44	25.60	35.87	0.67
0.053	22.64	22.046	43.04	0.50
0.044	6.83	20.519	46.23	0.43
Rest	10.84	19.26	47.026	0.40

6A.1.5 Experimental Methods

6A.1.5.1 Beneficiation Procedure

Due to a low Cr/Fe ratio, 50% (w/w) of chromite fines in India are considered low grade and are disposed of into the tailing stream during the beneficiation process. There is a significant amount of chromite value in those fine and ultra-fine ore [24]. According to R. K. Rath et al., 68% (w/w) of the particles in the chromite tailing sample have a particle size of less than 11 microns [25]. The present investigation not only focuses on the upgradation of low-grade chromite ore but also the utilization of chromite fines which are generated during mining as well as chromite ore processing. Because of this, chromite samples that are crushed and ground smaller than 75 μm are considered feed samples for tabling operation, even though the particle size distribution shows that the highest free chromite particle sizes are found between -178 and +75 μm. The feed samples are mixed homogeneously for further analysis and testing. After mineralogical studies, the samples are divided into three parts and subjected to pre-heat treatment for 30 minutes in an oxidizing atmosphere at 28°C, 514°C, and 1000°C respectively in a raising hearth furnace. The choice of temperatures has been carried out with the help of thermogravimetric analysis and differential scanning calorimetry (TGA-DSC). Three different samples are homogeneously mixed and subjected to gravity separation using the set of combinations of parameters suggested by the box-Behnken statistical design (BBD) model. In that experiment laboratory scale wilfley table of 37 cm x 100 cm is used for the enrichment of the low-grade chromite ore. The variable parameters are the pre-heating of raw chromite ore, tilt angle, and water flow rate. The other parameters which are fixed for every experiment are given below:

Feed rate: 100 g/min where the solid-liquid ratio is 1:6

Particle size fraction of feed: 100% below 75 μm

Vibration rate: 250 rpm

Riffles height: not fixed but approximately 2 mm

Distance between riffles: not fixed but approximately 14 mm

For all the experiments the position of collection containers has been fixed for concentrate, middling, and tailing products. After each experiment, samples are collected from their fixed positions for further analysis. The overall process flow sheet of the experimental setup is shown in Fig. 6A.1.2.

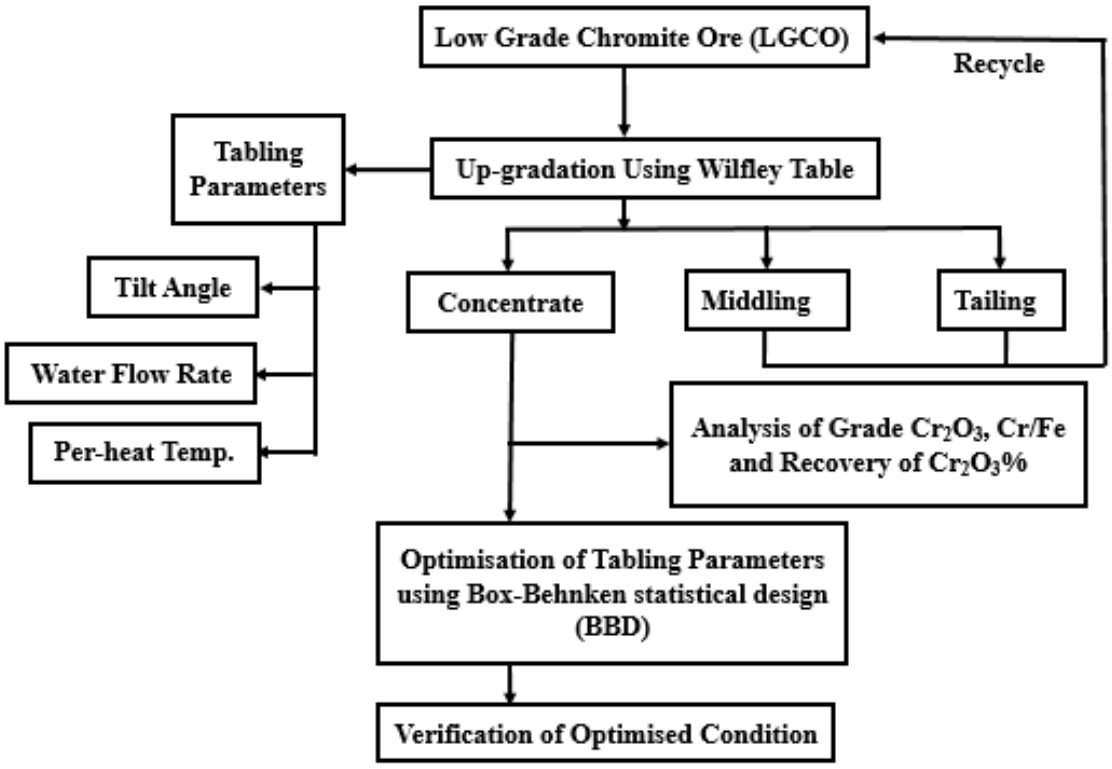

Figure 6A.1.2: Schematic Representation of the Experimental Setup.

6A.1.5.2 Application of the Box–Behnken Design

To minimize the number of experiments box-Behnken statistical design has been selected with 3 factors and 3 levels which gives a set of 17 runs for the optimization study. The set of experiments (N) provided by BBD is calculated by the equation; $N = 2K (K-1) + C$, where K represents the number of factors and C is the number of central points. The Design Expert 8.0.7.1 software has been used for this purpose.

In this work, tabling of chromite ore has been carried out to understand the important effect of the control factors on the three responses i.e. Cr/Fe ratio, grade (%), and recovery (%) of Cr_2O_3 in the concentrate fraction. The response is generated in the form of a second-order polynomial equation with the interaction among the influencing factors which is given in the following equation:

$$X\ (response) = Y + a_1A + a_2B + a_3C + a_4\,AB + a_5\,AC + a_6\,BC + a_7\,A^2 + a_8\,B^2 + a_9\,C^2$$

[Y is constant, a_i is the regression coefficient, and A, B, and C are independent variables [26-31].

Table 6A.l.2 represents the input parameters where each factor has three levels. Using BBD three factors and three levels of experiments have been carried out. The optimization of process parameters has been done by examining 17 sets of experiments instead of 27. With the help of mathematical modeling, a relation between the parameters and the response has been established. The interaction effects of input parameters on the response have been shown in response surface plots. The statistical and correlation analysis of different input parameters on the response has been performed by the analysis of variance (ANOVA).

Table 6A.1.2: Assignment of the Levels to the Factors.

		Levels	
Control factors	**Unit**	**Lower**	**Upper**
A: Tilt angle	°	2	8
B: Water flow rate	**l/min**	4	8
C: Quenching temperature	**°C**	28	1000

6A.1.6 Results and Discussion

6A.1.6.1 Pre-Heat Treatment of Chromite Ore

The composition of chromite ore obtained from the earth's crust is very complex in nature where main compound (chromium oxide) is physically and chemically combined with different types of gangue materials. Due to such complex mineralogy, it is very difficult to separate gangue materials from chromite ore. It is observed that pre-heat treatment is effective in inducing thermal shock which might lead to change in the structure of ore mineralogy. Heating at a particular temperature followed by air cooling generates fissures in ore body which may help in separation of gangue from the ore body. In Figure 6.3, the pattern of cracks & fissures present in chromite ore particles is shown at different magnification of before and after heat treatment of chromite ore at different temperatures. In Fig. 6A.1.3 (a), 6A.1.3 (b), and 6A.1.3 (c); the SEM images of raw chromite ore at 100X, 500X, and 1000X magnifications have been shown, respectively. Similarly Fig. 6A.1.3 (d), 6A.1.3 (e), and 6A.1.3 (f); the SEM images of pre-heated chromite ore at 514°C have been shown at different magnifications. The SEM images of pre-heated chromite ore at 1000°C have been shown at different magnifications as shown in Fig. 6A.1.3 (g), 6A.1.3 (h), and 6A.1.3 (i). It can be seen from the SEM images of the raw (after crushing) and pre-heat treated sample that cracks & fissures are predominantly present in the pre-heated sample

whereas the raw sample (after crushing) has no such significant cracks & fissures. The selection of heating temperature is very crucial because at high temperature fusion of low melting phases might take place which in turn will increase the density of the sample.

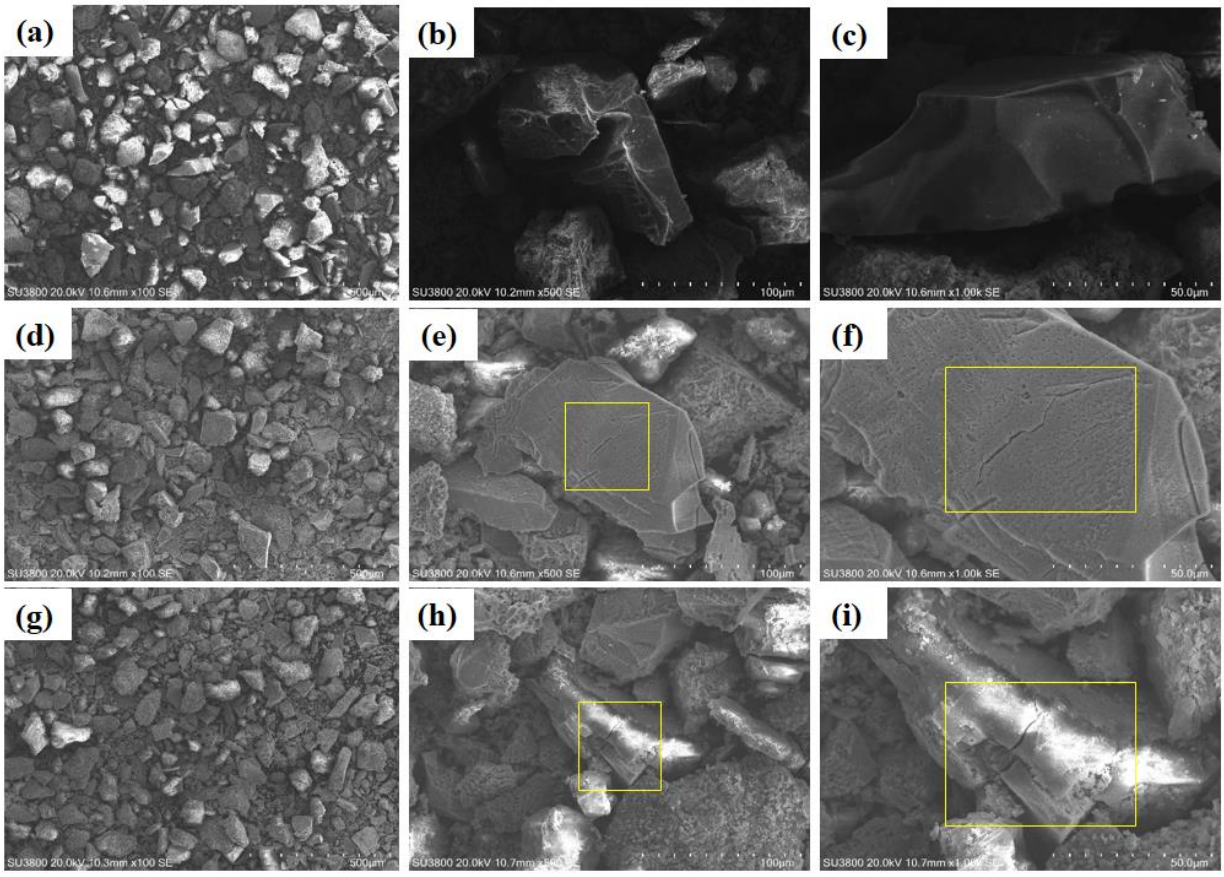

Figure 6A.1.3: SEM Image of Chromite Ore Fines at Different Magnifications: Before Heat Treatment (a, b, c), After Heat Treatment at 514ºC (d, e, f), and at 1000ºC (g, h, i).

In this investigation, the pre-heat treatment of low-grade chromite ore has been carried out under three conditions of temperature i.e. at room temperature (28°C), 514°C, and 1000°C in a raising hearth furnace. Samples are then subjected to tabling maintaining all the other parameters (tilt angle and water flow) as suggested by the BBD model for upgradation.

6A.1.6.2 Statistical Analysis

Maintaining all the conditions given by box-behnken design, 17 sets of experiments have been carried out in laboratory scale wilfley table. Cr: Fe, percentage Cr_2O_3 present in concentrate (grade Cr_2O_3%), and percentage Cr_2O_3 recovery have been calculated for each experiment which is shown in Table 6A.l.3. It is observed that the maximum Cr_2O_3 found in concentrate is 48.50% with the recovery of 38.42% and 39.62%. On the other hand, the

maximum Cr_2O_3 recovery percentage is 70.08% with the grade of Cr_2O_3 being 44.33%. Besides this maximum Cr: Fe ratio is found to be 2.17 with a recovery of 38.42%.The grade (g) and recovery (r) of Cr_2O_3 are found to be increased when tabling is carried out by pre-heat treated chromite ore keeping all other experimental parameters the same. It is observed that at a 2° tilt angle, water flow rate 6 l/min, the grade and recovery of Cr_2O_3% at room temperature and 1000°C are 40.90 (g), 63.99 (r) and 46.09 (g), 68.00 (r); respectively. So, tabling of pre-heat treated samples under the same conditions has shown better grades and recovery.

Table 6A.1.3: Box-Behnken Experimental Designs.

Sl. No.	Control factors			Experimental results		
	Tilt angle (°)	Water flow rate (l/min)	Pre-heat temp. (°C)	Cr: Fe	Grade Cr_2O_3 (%)	Total Cr_2O_3 recovery (%)
1	5	6	514	1.88	44.15	52.38
2	2	4	514	1.67	41.92	68.21
3	5	8	28	1.89	44.71	47.36
4	8	6	28	2.09	47.67	42.00
5	2	6	1000	1.76	46.09	68.00
6	5	8	1000	1.82	44.12	46.44
7	8	4	514	1.98	46.09	68.00
8	5	6	514	1.89	44.10	53.22
9	8	8	514	2.17	48.50	38.42
10	5	6	514	1.87	44.13	51.23
11	5	4	28	1.75	42.93	59.07
12	8	6	1000	2.13	48.50	39.62
13	5	6	514	1.88	44.13	51.21
14	5	4	1000	1.91	42.43	55.17
15	2	8	514	1.77	44.33	70.08
16	5	6	514	1.88	44.19	51.20
17	2	6	28	1.56	40.9	63.99

6A.1.6.3 Analysis of Variance (ANOVA)

The ANOVA of the quadratic model for Cr/Fe ratio, grade Cr_2O_3%, and Cr_2O_3 recovery percentage is shown in Table 6A.l.4. The model F-values for Cr/Fe ratio, grade Cr_2O_3%, and Cr_2O_3 recovery % are 20.10, 7.89, 21.60 respectively, which implies the model is adequate. There is only a 0.63% chance that a "Model F-value" this large could occur due to noise. Values of "Prob > F" less than 0.05 indicate model terms are significant. The coefficient of variation (C.V.) of 2.44%, 2.18%, and 5.31% indicates the dependability of the experiment is goodAn R-squared value greater than 0.90 indicates a strong alignment between the models and the experimental data. R^2 values for Cr/Fe grade Cr_2O_3 % and Cr_2O_3 recovery % are 0.9627, 0.9103, and 0.9652 respectively.

Table 6A.1.4: Statistical Results of the ANOVA.

Statistical results	**Response**		
	Cr/Fe	**Grade Cr_2O_3 %**	**Cr_2O_3 recovery %**
Model F-value	20.10	7.89	21.60
Model prob>F	0.0003	0.006	0.0003
C.V. %	2.44	2.18	5.31
R-squared	0.9627	0.9103	0.9652
R^2-adjusted	0.9131	0.7949	0.9219
Sum of square	0.38	67.40	1629.51
Degree of freedom	9	9	9
Standard deviation	0.046	0.97	2.90

The relationship between grade of Cr_2O_3 (%) and Cr_2O_3 Recovery % with the input parameters as genarated by BBD has been shown in terms of second order polynomial equation as given below.

Cr:Fe = + 0.98077 + 0.032841* Tilt angle + 0.086556 * water flow rate + 7.43588E-004 * pre-heat temp + 3.75000E-003 * tilt angle * water flow rate - $2.74348e^{-005}$ * tilt angle * pre-heat temp - $5.91564e^{-005}$ * water flow rate * pre-heat temp + $3.33333e^{-003}$ * tilt angle^2 - $3.12500e^{-003}$ * water flow rate^2 - $1.05844e^{-007}$ * pre-heat temp.^{2}.

Grade Cr_2O_3 = + 32.67748 - 0.52525 * angle + 2.28609 * water flow rate + $5.16655e^{-003}$ * pre-heat temp. + 0.000000 * angle * water flow rate - $7.47599e^{-004}$ * angle * pre-heat temp. -

$2.31481e^{-005}$ * water flow rate * pre-heat temp. + 0.18436 * angle^2 - 0.14581 * water flow rate ^{2} - $1.37598e^{-008}$ * pre-heat temp.^{2}.

Cr_2O_3 Recovery = + 85.83743 - 0.43742 * angle- 8.36900 * water flow rate + 0.026752 * pre-heat temp. - 1.31042 * angle * water flow rate - $1.09568e^{-003}$ * angle * pre-heat temp. + $7.66461e^{-004}$ * water flow rate * pre-heat temp. + 0.57356 * angle^2 + 0.94238 * water flow rate^2 - $1.69584e^{-005}$ * pre-heat temp.^{2}

6A.1.6.4 Verification Test

Figures 6A.1.4 (a), 6A.1.4 (b), and 6A.1.4 (c) show the plot of predicted versus actual Cr/Fe ratio, grade (%) of Cr_2O_3 in the concentrate, and Cr_2O_3 recovery percentage; respectively. Experimental data points present in the figures are very close to the predicted data points provided by BBD. The figures clearly show that there are no such serious violations of the assumptions that underlie the analysis [32]. The errors are distributed in a very significant manner, which is marginal. Thus, the outcomes predicted by the BBD closely match the experimental results.

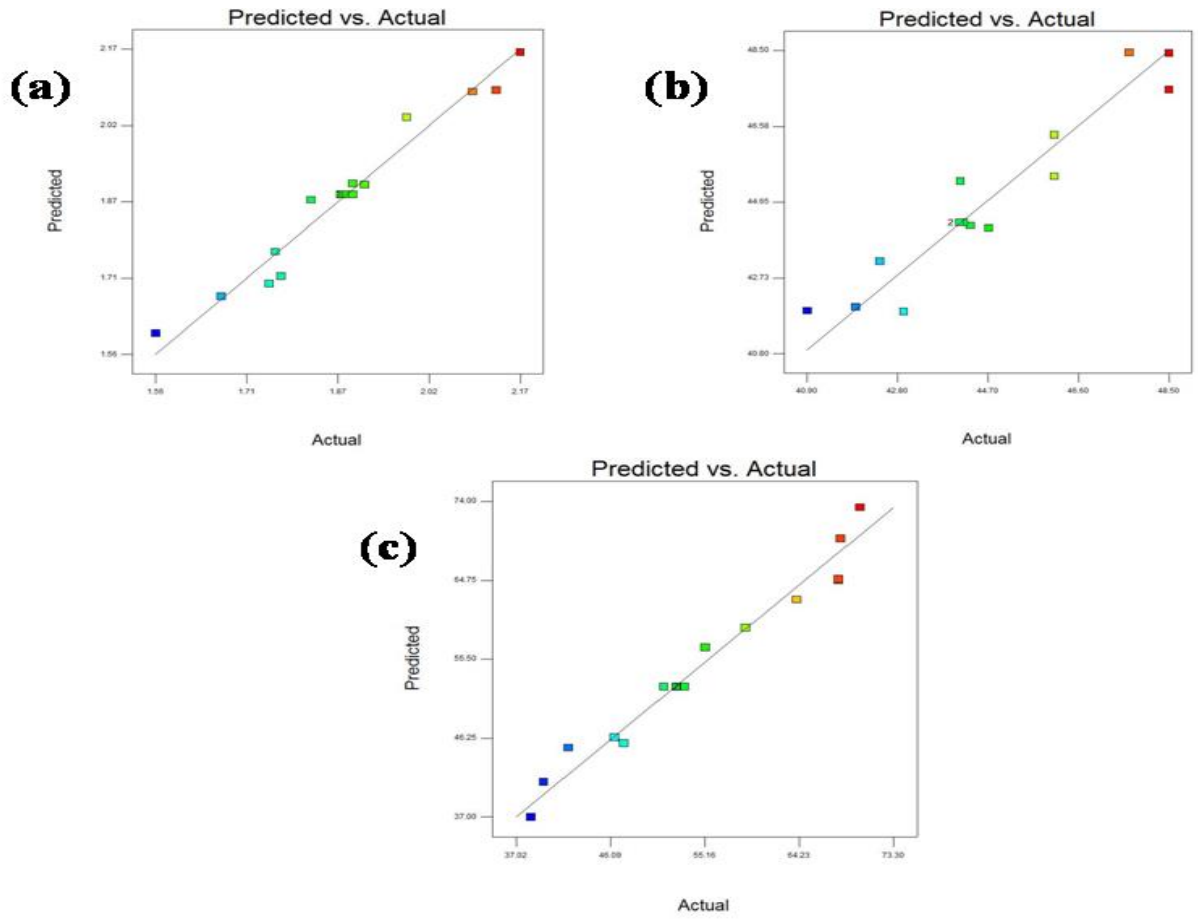

Figure 6A.1.4: Actual vs. Predicted Plots for (a) Cr/Fe Ratio, (b) Grade (%) of Cr_2O_3, and (c) Cr_2O_3 Recovery Percentage in the Concentrate.

Response surface plots give a better understanding of interactions between two independent variables and the other variable is located at center level. From Fig. 6A.1.5 (a), and 6A.1.5 (b) it is observed that with an increase in water flow rate and tilt angle, the Cr/Fe ratio and grade Cr_2O_3 in concentrate fraction increased but the Cr_2O_3 recovery decreased as shown in Figure 6A.1.5 (c). The gangue materials are pushed up by water when the tilt angle and water flow rate levels are high hence, gangue materials are increased in the tailing fraction, resulting in higher Cr_2O_3% in the concentrate fraction. As weight percentage decreases in concentrate fraction at a higher level of tilt angle and water flow rate, the percentage of Cr_2O_3 recovery is decreased in concentrate fraction.

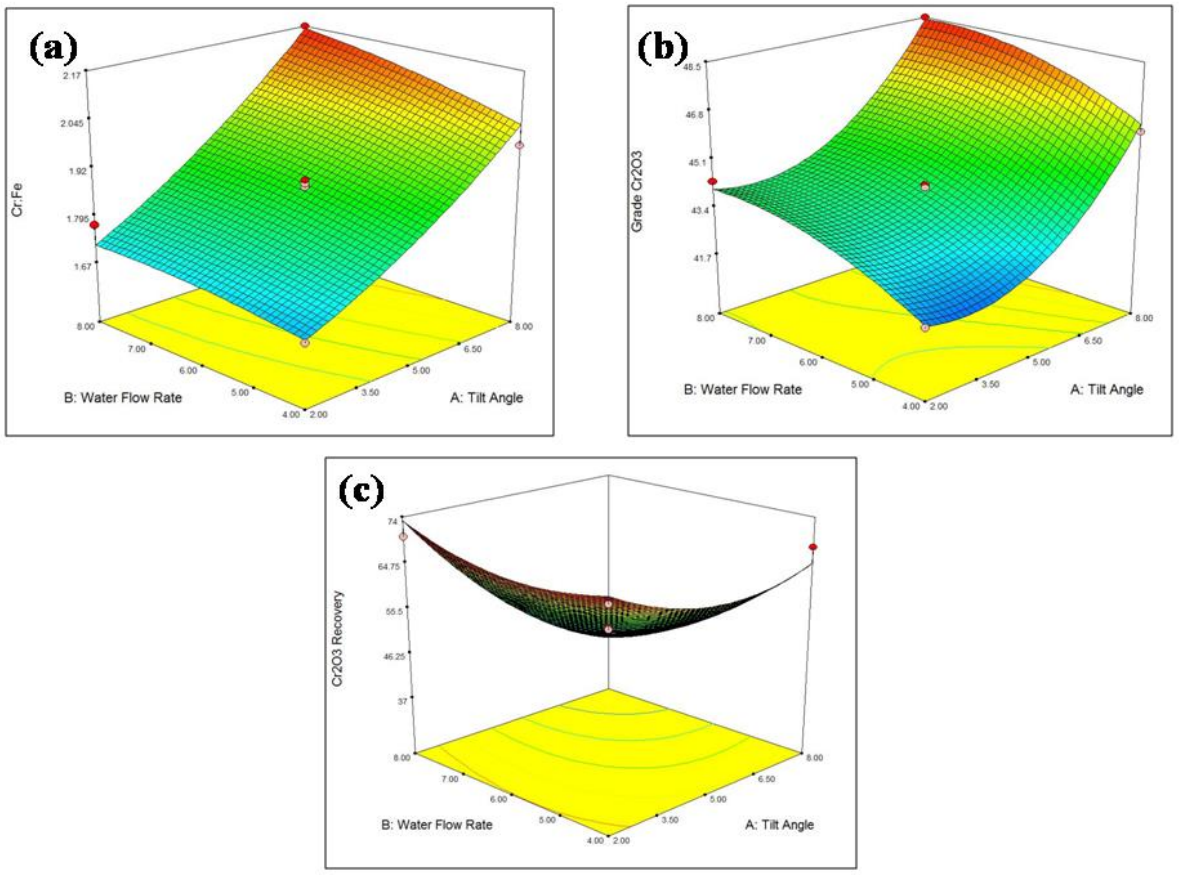

Figure 6A.1.5: Response Surface Plots Showing the Effect of Tilt Angle vs. Water Flow Rate on (a) Cr/Fe Ratio, (b) Grade (%) of Cr_2O_3, and (c) Cr_2O_3 Recovery Percentage in the Concentrate.

The effects of water flow and chromite preheating on the Cr/Fe ratio, Cr_2O_3 level (%) in the concentrate, and Cr_2O_3 recovery rate are shown in Fig. 6A.1.6. (a), 6A.1.6 (b), and 6A.1.6 (c); respectively. Maximum Cr_2O_3 recovery in concentrate fraction is found at an intermediate level of pre-heat treatment of chromite ore and water flow rate. Pre-heat treatment also increases the Cr/Fe and grade Cr_2O_3 in the concentrate fraction. This happens due to the thermal shock induced by the pre-heat treatment followed by air cooling which leads to a change in the structure of ore mineralogy which is responsible for the good separation of gangue materials from chromite ore.

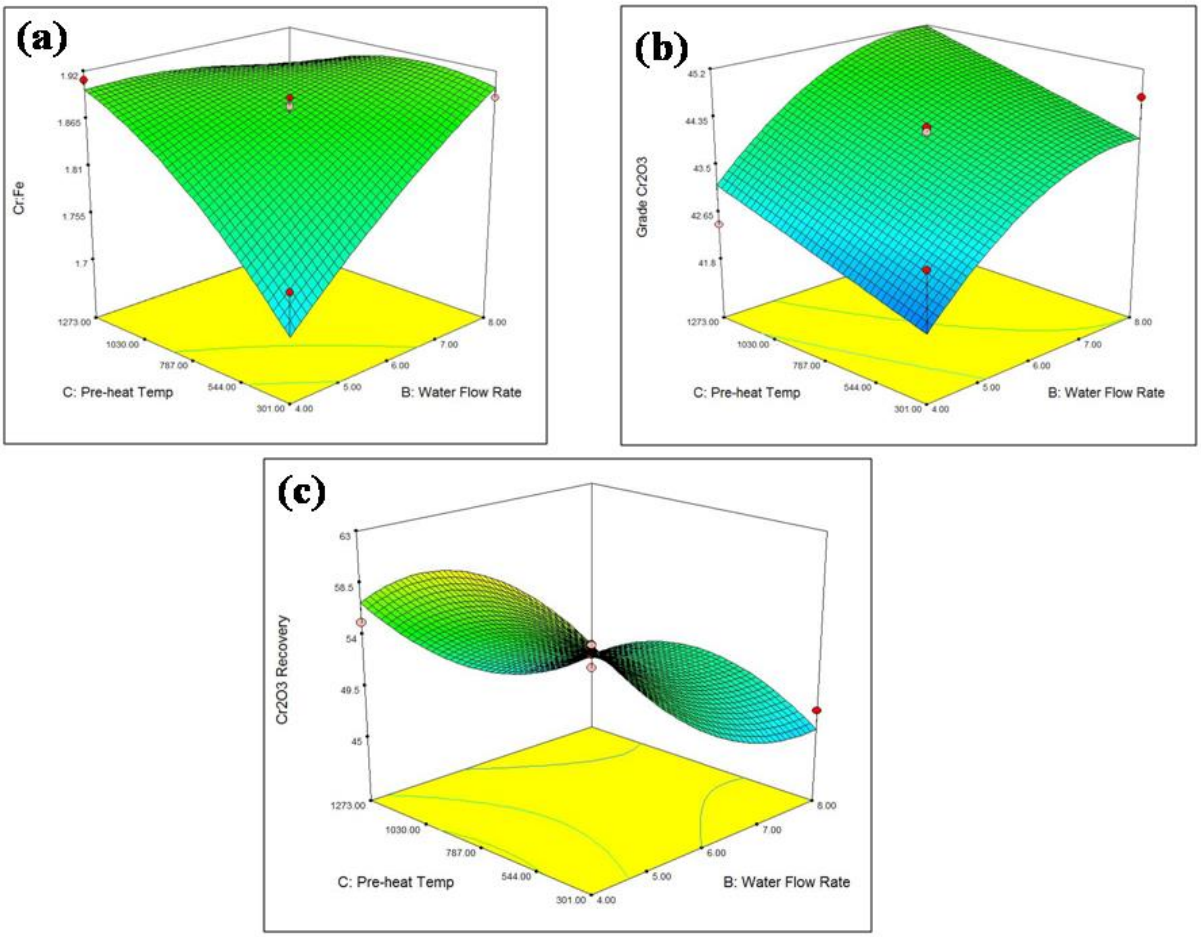

Figure 6A.1.6: Response Surface Plots Showing the Effect of Pre-Heat Temperature vs. Water Flow Rate on (a) Cr/Fe Ratio, (b) Grade (%) of Cr_2O_3, and (c) Cr_2O_3 Recovery Percentage in the Concentrate.

Similarly, Fig. 6A.1.7 (a), 6A.1.7 7(b), and 6A.1.7 (c) represent the effect of tilt angle and pre-heat treatment of chromite ore on Cr/Fe ratio, grade (%) of Cr_2O_3 in the concentrate & Cr_2O_3 recovery percentage; respectively. Maximum Cr/Fe ratio is found to be at the highest level of tilt angle and intermediate level of pre-heat temperature but in the case of grade Cr_2O_3 percentage, it is maximum at the highest level of tilt angle and the lowest level of pre-heat temperature. But Cr_2O_3 recovery is maximum in intermediate levels.

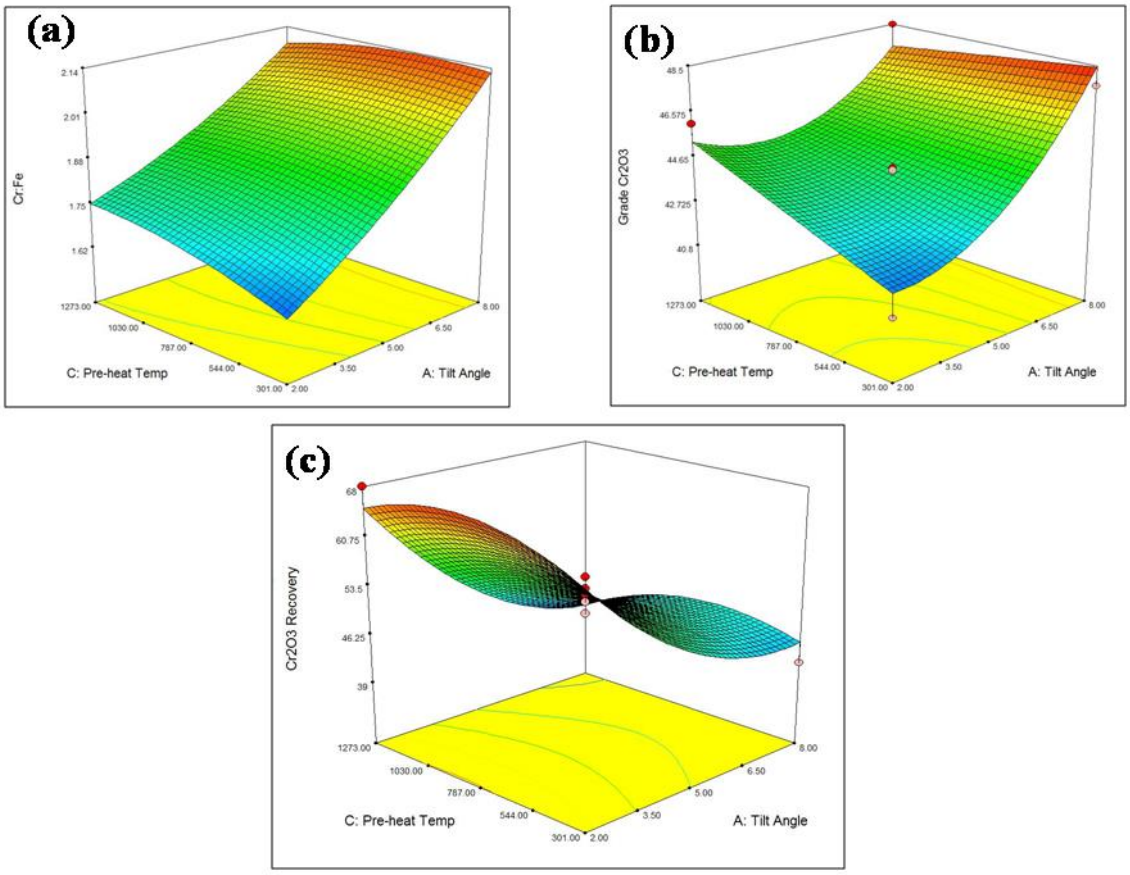

Figure 6A.1.7: Response Surface Plots Showing the Effect of Pre-Heat Temperature vs. Tilt Angle on (a) Cr/Fe Ratio, (b) Grade (%) of Cr_2O_3, and (c) Cr_2O_3 Recovery Percentage in the Concentrate.

From the above discussions, it can concluded that quite similar effects of input parameters are shown for the Cr/Fe ratio and grade Cr_2O_3% in concentrate fraction. However opposite results are observed for the Cr_2O_3 recovery percentage. This is because the recovery percentage depends upon the weight percentage of the concentrate fraction along with Cr_2O_3%. The corresponding values of input parameters for optimizing each response are given by the BBD model, which is shown in Table 6.5. The result is generated by the model according to the desirability of the response. The predicted value of responses is also reflected in the relation between the Cr/Fe ratio, grade Cr_2O_3%, and Cr_2O_3 recovery percentage. The optimal result, with the highest desirability, is achieved at a tilt angle of 8°, a water flow rate of 4 L/min, and preheating the chromite ore to 443.72°C. The chromite sample is subjected to the wilfley table maintaining the above-predicted input parameters for verification of the predicted response. The experimental results match reasonably to the predicted results which are given in Table 6A.l.5**.**

Table 6A.1.5: Predicted and Experimental Results of Chromite Concentrate at Predicted Input Parameters Given by BBD.

Sl. No.	Predicted input parameters			Predicted responses		
	Tilt angle(°)	Water flow rate(l/min)	Pre-heat temp.(°C)	Cr/Fe ratio	Grade Cr_2O_3 (%)	Cr_2O_3 recovery (%)
Predicted	**8.00**	**4.00**	**443.72**	**2.02**	**46.43**	**65.09**
Experiment	**8.00**	**4.00**	**443.72**	**1.91**	**46.02**	**65.95**

6A.1.6.5 XRD Analysis of Chromite Concentrate

The XRD analysis report of chromite ore concentrate after tabling is shown in Fig. 6A.1.8. The major peak is found to be aluminian chromite $Fe(Al, Cr)_2O_4$ along with hematite and aluminum oxide. It is clearly observed that the intensity of the $Fe(Al, Cr)_2O_4$ peak is much higher in chromite concentrate compared to raw chromite ore indicating the higher grade of concentrates.

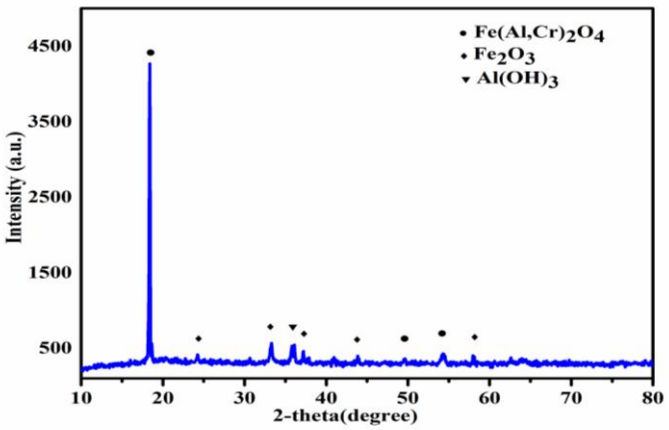

Figure 6A.1.8: XRD Analysis of Chromite Ore Concentrate.

6A.1.6.6 SEM-EDX Analysis of Chromite Concentrate

It is observed from Table 6A.l.6 that the weight percentage of chromium has significantly increased in the concentrate fraction. The EDX spectrum is shown in Fig. 6A.1.9, which reflects that the peak intensity of chromium is highest among all elements present in the chromite ore. The α value ratio of Cr to Al in raw chromite ore and chromite concentrate is

0.50 and 2.0, respectively. The values indicate that the raw material is enriched with aluminium whereas chromite concentrate is enriched with chromium.

Table 6A.1.6: EDX Result of Chromite Concentrate.

Element	Weight%	Atomic% (α)
O K	32.97	57.27
Al K	7.81	8.38
Si K	1.42	1.94
Cr K	35.96	16.75
Fe K	16.83	8.60
Mg K	5.01	7.06

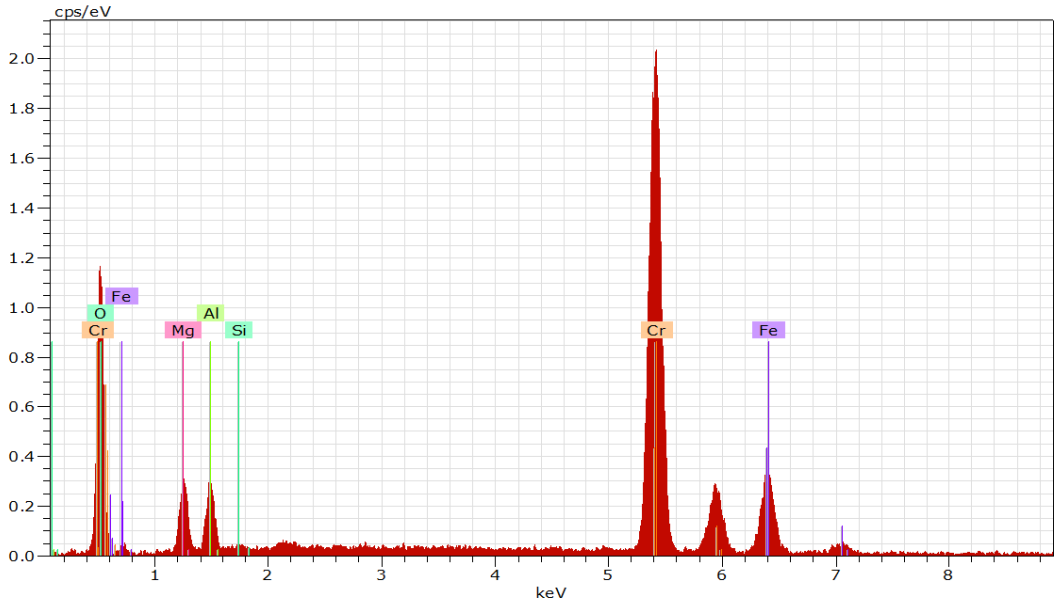

Figure 6A.1.9: EDX Spectrum Analysis of Elements in the Chromite Concentrate.

The distribution of different elements present in the chromite concentrate is shown in Fig. 6A.1.10. From the EDX elemental mapping, it can be seen that chromium is distributed homogeneously along with iron in the crystal grain. The concentration of silicon and aluminum in the concentrate fraction is lower than the raw chromite ore.

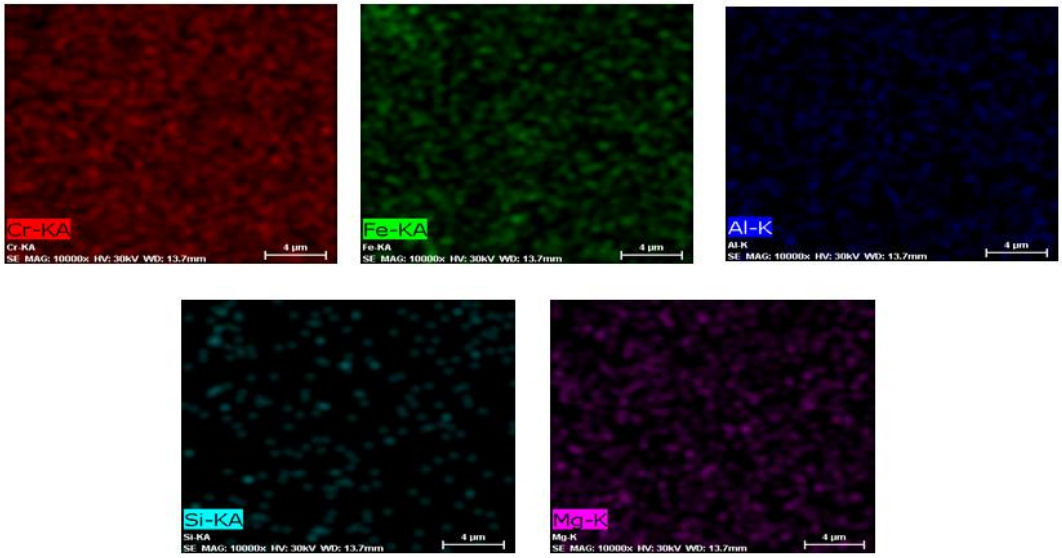

Figure 6A.1.10: Elemental Analysis of Chromite Ore Concentrate.

The SEM image of the beneficiated chromite concentrate at different magnifications has been given in Fig. 6A.1.11 (a) and 6A.1.11 (b). Cracks & fissures are present in the crystal grain. Pre-heat treatment changes the surface morphology of the upgraded material which may in turn increase the reducibility.

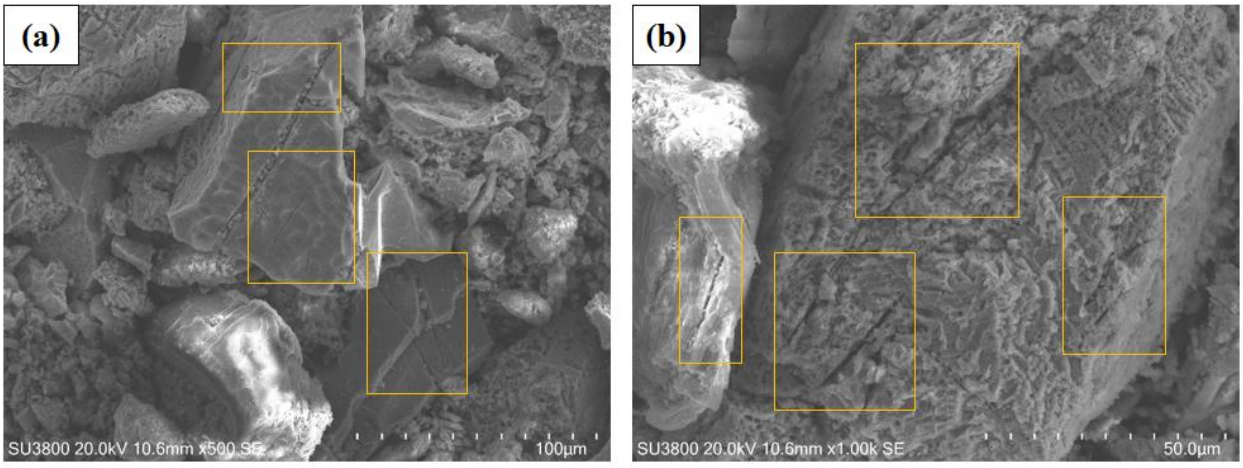

Figure 6A.1.11: SEM Image of Chromite Ore Concentrate.

6A.1.7 Conclusion

There is a clear effect of particle size on the chromium-iron ratio and its distribution. The chromium iron ratio can be improved from 0.78 to 0.91 along with the Cr_2O_3 recovery of 86.90% by simple particle distribution. The gravity separation by the means of wilfley table (lab scale) is found to be very effective for upgradation. The present work represents the

optimization of tabling process parameters with the help of the BBD model. Amongst all the input parameters, tilt angle is the dominant parameter as compared to the other two parameters. Preheating significantly impacts the Cr_2O_3 recovery rate because air quenching causes cracks and fissures to form in the ore bodies. pre-heat treatment at a particular temperature helps the separation of gangue minerals from chromite ore. The experimental R^2 values for Cr/Fe ratio, grade of Cr_2O_3, and Cr_2O_3 recovery are found to be 0.96, 0.91, and 0.96 respectively which shows the experimental results closely align with the values predicted by the BBD model. The ANOVA results also depict the same observation for different values in the statistical model. 3D response surface plots show the relationship between various input parameters and the response. The maximum Cr/Fe ratio, grade Cr_2O_3%, and Cr_2O_3 recovery percentage achieved in the present experiment are 2.17, 48.50, and 70.08; respectively under different conditions keeping the response maximum. It is found that low-grade chromite ore can be upgraded to a Cr_2O_3 content of 46.02% with a Cr/Fe ratio of 1.91. The recovery rate in the concentrate fraction reached 65.95%. This is achieved under the following conditions recommended by the BBD model: a tilt angle of 8°, a water flow rate of 4 L/min, and a preheating temperature of 443.72°C. The study of the extent of reduction of the upgraded raw materials after being pre-heat treated can give a better understanding of the impact of pre-heat treatment on the reducibility of the upgraded material. If positive results can be achieved, scaling up of the test, for commercialization can be carried out in the future.

6A.1.8 References

[1] Indian Bureau of Mines, "Indian Minerals Yearbook 2019," *(Part-III) Miner. Rev.*, vol. 58th Edition, no. september, pp. 1–6, 2020.

[2] M. M. H. Al-tigani, A. A. Mohamed, A. Ahmed, and S. Seifelnasr, "Mineralogical and Chemical Characterization of Disseminated Low-Grade Sudanese Chromite Ore in Gedarif State at Umm Saq a ta-Qala Elnahal," *J. Envi. Anal.*, vol. 6, no. 3, pp. 1-5, 2019.

[3] T. Çiçek, H. Cengizler, and I. Cöcen, "An efficient process for the beneficiation of a low grade chromite ore," *Trans. Institutions Min. Metall. Sect. C Miner. Process. Extr. Metall.*, vol. 119, no. 3, pp. 142–146, 2010, doi: 10.1179/174328508X369996.

[4] A. A. Seifelnasr, T. Tammam, and A. Z. M. Abouzeid, "Gravity concentration of sudanese chromite ore using laboratory shaking table," *Physicochem. Probl. Miner. Process.*, vol. 48, no. 1, pp. 271–280, 2012.

[5] S. K. Tripathy, V. Singh, and Y. Ramamurthy, "Improvement in Cr:Fe Ratio of Indian Chromite Ore for Ferro Chrome Production," *Int. J. M ining Eng. M ineral Process.*, vol. 1, no. 3, pp. 101–106, 2012, doi: 10.5923/j.mining.20120103.01.

[6] N. Aslan, "Multi-objective optimization of some process parameters of a multi-gravity separator for chromite concentration," *Sep. Purif. Technol.*, vol. 64, no. 2, pp. 237–241, 2008, doi: 10.1016/j.seppur.2008.10.004.

[7] G. . Özkan and B. İpekoğlu, "Concentration Studies on Chromite Tailings by Multi Gravity Separator," in *International Mining Congress and Exhibition of Turkey*, 2001, pp. 765–768.

[8] G. P. Gallios, E. A. Deliyanni, E. N. Peleka, and K. A. Matis, "Flotation of chromite and serpentine," *Sep. Purif. Technol.*, vol. 55, no. 2, pp. 232–237, 2007, doi: 10.1016/j.seppur.2006.12.015.

[9] A. A. . S. Seifelnassr, and T. A. K. Tamam, "Flotation Behavior of Sudanese Chromite Ores," *JES. J. Eng. Sci.*, vol. 39, no. 3, pp. 649–661, 2011, doi: 10.21608/jesaun.2011.127667.

[10] B. Beklioglu and A. Arol, "Selective flocculation behavior of chromite and serpentine," *Sel. flocculation Behav. chromite serpentine*, vol. 38, no. 1, pp. 103–112, 2004.

[11] N. C. Karmakar, B. S. Sastry, and R. P. Singh, "Flocculation of chromite ore fines suspension using polysaccharide based graft copolymers," *Bull. Mater. Sci.*, vol. 25, no. 6, pp. 477–478, 2002, doi: 10.1007/BF02710531.

[12] M. M. H. Al-tigani, A. A. Mohamed, A. Abdullah, and S. Seifelnasr, "Beneficiation of Disseminated Low-Grade Sudanese Chromite Ore in Gedarif State at Umm Saqata-Qala Elnahal," *J. Envi. Anal.*, vol. 6, no. 4, pp. 1–7, 2019.

[13] A. M. Rao, R. K. Rath, M. K. Mohanta, B. Dey, M. Sahoo, and R. Singh, "Beneficiation Studies on Low Grade Chromite Ores using Multi Gravity Separator," pp. 76–81, 2017.

[14] S. Inal and I. Alp, "Beneficiation of Magnetite Rich Chromite Ore with Magnetic Separation," in *Proceedings of 14th International Mineral Processing Symposium*–

Kuşadası, Turkey, 2014, pp. 135-140.

[15] S. K. Tripathy, P. K. Banerjee, and N. Suresh, “Magnetic separation studies on ferruginous chromite fine to enhance Cr : Fe ratio Magnetic separation studies on ferruginous chromite fine to enhance Cr : Fe ratio,” *Int. J. Miner. Metall. Mater.*, vol. 22, no. March, p. 212, 2015, doi: 10.1007/s12613-015-1064-4.

[16] Y. R. Murthy, S. K. Tripathy, and C. R. Kumar, “Chrome ore beneficiation challenges & opportunities - A review,” *Miner. Eng.*, vol. 24, no. 5, pp. 375–380, 2011, doi: 10.1016/j.mineng.2010.12.001.

[17] O. Bayat, I. Cocen, and T. Cicek, "Concentration of Adana-Aladag Chromite Tailings by Gravitational Methods," in *VIII Balkan Mineral Processing Conference* , 1999, pp. 91–98.

[18] Y. R. Murthy and S. K. Tripathy, “Process optimization of a chrome ore gravity concentration plant for sustainable development,” *J. South. African Inst. Min. Metall.*, vol. 120, no. 4, pp. 261–268, 2020, doi: 10.17159/2411-9717/990/2020.

[19] I. B. Can, B. Özsoy, and L. Ergün, “Developing an optimum beneficiation route for a low-grade chromite ore,” *Physicochem. Probl. Miner. Process.*, vol. 55, no. 4, pp. 865–878, 2019, doi: 10.5277/ppmp19006.

[20] G. A. Sen, “Application of full factorial experimental design and response surface methodology for chromite beneficiation by Knelson concentrator,” *Minerals*, vol. 6, no. 1, 2016, doi: 10.3390/min6010005.

[21] S. K. Das, “Quantitative mineralogical characterization of chrome ore beneficiation plant tailing and its beneficiated products,” *Int. J. Miner. Metall. Mater.*, vol. 22, no. 4, pp. 335–345, 2015, doi: 10.1007/s12613-015-1078-y.

[22] A. K. Das *et al.*, “Processing of Low-Grade Chromite Ore for Ferroalloy Production: A Case Study from Ghutrigaon, Odisha, India,” *Trans. Indian Inst. Met.*, vol. 73, no. 9, pp. 2309–2320, 2020, doi: 10.1007/s12666-020-02032-5.

[23] A. Falconer, "Gravity Separation: Old Techmique/New Methords," *Phys. Sep. Sci. Engin.*, vol. 12, no. 1, pp. 31-48, 2003,doi: 10.1080/1478647031000104293

[24] B. K. Sarkar, M. G. Dastidar, R. Dey, G. C. Das, S. Chowdhury, and D. K. Mahata, “Optimization of Reduction Parameters of Quenched Titaniferous Magnetite Ore by Boiler Grade Coal Using Box–Behnken Design,” *J. Inst. Eng. Ser. D*, 2019, doi: 10.1007/s40033-019-00184-3.

[25] L. Wu, K. L. Yick, S. P. Ng, and J. Yip, “Application of the Box-Behnken design to the optimization of process parameters in foam cup molding,” *Expert Syst. Appl.*, vol. 39, no. 9, pp. 8059–8065, 2012, doi: 10.1016/j.eswa.2012.01.137.

[26] B. K. Sarkar, M. G. Dastidar, R. Dey, G. C. Das, S. Chowdhury, and D. K. Mahata, “Optimization of Reduction Parameters of Quenched Titaniferous Magnetite Ore by Boiler Grade Coal Using Box–Behnken Design,” *J. Inst. Eng. Ser. D*, 2019, doi: 10.1007/s40033-019-00184-3.

[27] L. Wu, K. L. Yick, S. P. Ng, and J. Yip, “Application of the Box-Behnken design to the optimization of process parameters in foam cup molding,” *Expert Syst. Appl.*, vol. 39, no. 9, pp. 8059–8065, 2012, doi: 10.1016/j.eswa.2012.01.137.

[28] M. I. Sabela, S. Kanchi, B. Ayyappa, and K. Bisetty, "A box-behnken design and response surface approach for the simultaneous determination of chromium (III) and (VI) using catalytic differential pulse polarography," *Int. J. Electrochem. Sci.*, vol. 9, no. 12, pp. 6751–6764, 2014.

[29] S. A. Pasma, R. Daik, M. Y. Maskat, and O. Hassan, "Application of box-behnken design in optimization of glucose production from oil palm empty fruit bunch cellulose," *Int. J. Polym. Sci.*, vol. 2013, 2013, doi: 10.1155/2013/104502.

[30] S. K. Tripathy, Y. Ramamurthy, and V. Singh, "Recovery of Chromite Values from Plant Tailings by Gravity Concentration," *J. Miner. Mater. Charact. Eng.*, vol. 10, no. 01, pp. 13–25, 2011, doi: 10.4236/jmmce.2011.101002.

[31] C. Biswas, S. Samanta, A. Bhattacharyya, M. G. Chaudhuri, and R. Dey, "Statistical optimisation parameter for lean grade self-reducing nuggets by surface response modelling to produce pig iron," *Trans. Institutions Min. Metall. Sect. C Miner. Process. Extr. Metall.*, vol. 126, no. 3, pp. 172–181, 2017, doi: 10.1080/03719553.2016.1204083.

[32] E. Kilickap, "Optimization of cutting parameters on delamination based on Taguchi method during drilling of GFRP composite," *Expert Syst. Appl.*, vol. 37, no. 8, pp. 6116–6122, 2010, doi: 10.1016/j.eswa.2010.02.023.

Chapter-6A.2

Optimization of Briquetting Parameters of Chromite Fines to Produce Ferrochrome

6A.2.1 Introduction

Chromite is a key raw material for the iron and steel industry, as ferrochrome (FeCr) is produced from this source. Typically, high-grade chromite ore is utilized to produce the various grades of FeCr. Low-grade and sub-grade chromite ore is mined, crushed, beneficiated, & transported to metallurgical and chemical industries for different types of applications. Since silicious chromites are fragile, this generates lots of fines. Those fines are not only responsible for environmental pollution but also influence the economy of industry. Utilization and up-gradation of those fines is a very challenging aspect. Therefore agglomeration of chromite fines is very crucial to utilize it further. Chromite ore deposits in India are found in Odisha, Maharashtra, Karnataka, Manipur, Nagaland, Tamil Nadu, and Andhra Pradesh states [1].

6A.2.2 Literature Review

India has an abundance of diverse mineral resources. India is ranked third in the world with regard to its chromite reserve. India produced 4.2 million MT of chromite ore in 2022, compared to only 2.5 million MT in 2020. The production of chromite will increase by 68% in 2022 compared to 2020. The availability of chromite ore and affordable electricity in India contribute to a rise in chromite production. India produced 199.9 GW of power in 2012; by 2023, that amount will have increased to 416.0 GW. India has a great deal of potential for growth in the global market by putting several green projects into action to lower the cost of electricity, which is the single biggest expense component in the production of FeCr. The price of electricity was 4.55 INR/kWh in 2012, but by 2022, it will have increased to 6.29 INR/kWh [2]. Processing chromite ore and producing ferrochrome require enormous amounts of electricity, which is one of the main factors driving up ferrochrome prices on the international market [3].

High-grade lumpy chromite ore is used for the production of ferrochrome. Lumps of ore are charged into submerged arc furnaces (SAFs) after being combined with an appropriate carbonaceous reducing agent. Nowadays, the utilization of chromite fines (generally <6mm) in this process is limited [4] because beneficiate fines are not directly charged into SAFs for smelting. Fines are creating many problems in SAFs, like:

- 1. In SAFs, fines create a surface layer that causes "bed turnover."
- 2. Fines lower furnace efficiency;
- 3. Fines raise the need for electrical energy;
- 4. Fines may have disastrous consequences in the furnace that compromise safety; and so on [5][6][7].

Before pre-reduction and smelting, agglomeration of beneficiate chromite fines is crucial. Generally, various agglomeration techniques namely pelletizing, sintering, and briquetting are being used to utilize these fines. Different research investigators indicated that pelletization, sintering, and briquetting are very useful for further processing of fines.

The pelletization process is more suitable for ultra-fines (below 75 microns) of chromite ore [8][9][10]. The energy-specific consumption of this process is low respective to the sintering process. Chromite ore fines are combined with the proper binder and fed into a drum pelletizer during the pelletization process. The green pellets produced by this process have a low mechanical strength. Green pellets are heated above 1300°C in a rotary kiln, to provide the required strength [8][11]. However, the strength gained in this way is insufficient. The pellets' low strength prevents them from charging the furnace to 100% capacity. For this reason, lumpy chromite ore and pellets are combined & fed into the furnace[12][13]. Binders are crucial to the pelletization process because they give the pellets their strength. In the industrial context, bentonite is frequently used as a binder. However, to improve the mechanical strength of pellets, researchers are currently looking for better adhesives, such as molasses, low melting silica, Na_2CO_3, hydrated lime, boron-containing flux, dextrin and carboxymethyl cellulose (CMC), etc [13][14][15][16]. The same adhesive hurts the smelting process. According to et. Al. B.W. Neizel $CaCO_3$ acts as a good adhesive but it is responsible for furnace damage and safety issues during the smelting process [17]. Et. Al. A. P. Zambrano reported that 4% sodium silicate as a binder provided better green as well as dried strength of chromite pellets than bentonite. [17][18]. While it has been shown that pelletizing chromite ore can produce high-quality agglomerates, the main drawback of this process is the necessary size reduction, which requires a significant amount of energy [19].

The sintering process involves combining fine limestone or dolomite, solid fuels such as coal or coke breeze, fine ore particles (-10mm to +1mm), and other plant-derived metallurgical wastes. The mixture is then ignited on a moving grate with air coming from the top. During the sintering process, ore fines fuse to form larger particles [20][21]. The tabling process generated a chromite concentrate with particles smaller than 2 mm. That’s why the sintering process is not suitable for the agglomeration of those chromite fines. However, more than 80% of high-grade chromite ores are fragile and tend to break down into fines when handled [19]. Oxides with high melting points, such as Cr_2O_3, MgO, and Al_2O_3, are present in concentrated chromite ore. These oxides are generally considered as refractory constituents [11]. Because chromite is refractory by nature, the sintering process must be done at a very high temperature in order to achieve high strength and metallurgical performance [19]. Iron ore is more conducive to the

sintering process than chromite ore. A temperature of 1300°C is needed to produce iron ore sinter. Low melting gangue materials fuse at this temperature, producing a 35-45% liquid phase [22]. Conversely, a temperature of 1400°C to 1600°C is needed to produce chromite ore sinter. The required temperature depends on the type of gangue material present in the ore [20][23]. Because of olivine, only 20% of the sinter exhibits a molten phase at these temperatures [24]. The composition (SiO_2, $A1_2O_3$, CaO, Na_2O) and firing temperatures of this molten phase determine its physical and chemical characteristics [10]. Some benefits of the sintering process are as follows:

- 1. It has a high mechanical strength;
- 2. It doesn't require grinding;
- 3. Sinter can provide pre-reducing performance because of its good conductivity;
- 4. Sinter with a uniform size distribution in SAF bed can improve metallurgical performance during smelting [19][25].

However, the sintering process is not as practical as the chromite agglomeration technique because of the complex structure of chromite ore.

The concentrate of chromite obtained through flotation, multi-gravity separation, and tabling is extremely fine (less than 1%). These fines cannot be agglomerated using the sintering process. Briquetting is appropriate for those fines as long as the proper parameters are maintained [26]. First, chromite ore is combined with a stoichiometric amount of reductant, flux, and suitable binders in the briquetting process. The mixture is put through a hydraulic press to create green briquettes. It is dried to add strength to the briquettes [27]. In this method, the choice of binders and briquetting pressure are very important. The briquetting process uses a variety of inorganic and organic binders. During that process, inorganic binders like gypsum, lime, clay, and water glass as well as organic binders like tar, dextrin, and molasses are frequently used. [28]. Different types of resin are also excellent binders. However, it is not economically feasible to use resin. Cement and bentonite boost strength at high temperatures, while molasses provides good compressive strength at low temperatures. In order to achieve good slag metal separation and a high Cr recovery rate, lime is added while the chromite ore is being melted. When molasses and lime combine, calcium saccharate is created. This substance has good mechanical stability at low temperatures but also breaks down readily at high ones. High temperatures are needed for the sintering process, but not for the briquetting process. Palletization requires a similar high cost of grinding since it is effective well with ultra-fine particles. Sintering and pelletization are more complex and expensive than briquetting [29][30].

In this study, beneficiation is carried out using the wilfley table and the effect of feed rate on percentage recovery of Cr_2O_3 has been investigated. Besides this, chromite concentrate is agglomerated using briquetting process. Bentonite, molasses, and water are used as binders. The objective of this work is to agglomerate the beneficiated chromite ore in the form of briquettes. Optimization of briquetting parameters is carried out using shatter and abrasion index.

6A.2.3 Materials and Methods

Chapter 5A.1 shows that optimization of the Cr_2O_3 recovery percentage and grade percentage with a tilt angle of 8°, a water flow rate of 4.0 L/min, and chromite ore per heated temperature of 443.72°C is achievable. So the sample is subjected to pre-heat treatment at 443.72 °C. Pre-heat treated chromite ore is then subjected to a lab-scale wilfley table of 37 cm × 100 cm at different feed rates, maintaining a 4.0 l/min water flow rate and an 8° tilt angle. After getting the optimized feed rate overall preheated sample is subjected to tabling to get the chromite concentrate. The briquetting technique is then used to agglomerate the chromite concentrate. The chromite concentrate is used to prepare two sets of briquettes. The main constituents of briquettes are chromite concentrate and a stoichiometric amount of coke dust as a reductant. Bentonite, molasses, and water are added as a binder. To get an optimized binder percentage the briquettes are produced with different binder proportions under fixed briquetting pressure of 450 kg. The flow diagram of the briquetting and reduction process is given in Fig. 6A.2.1, where A represents that chromite concentrate mixed with a stoichiometric amount of coke, 1 % bentonite, 1% molasses, and 1% water. Similarly, B, C, D, E, and F represent 2%, 3%, 4%, 5%, and 6% bentonite, molasses, and water (each percentage) respectively keeping the other parameters the same (Table 6A.2.1).

Table 6A.2.1: Preparation of Briquettes with Different Binder Percentages.

Sample ID	Bentonite (%)	Molasses (%)	Water (%)
A	1	1	1
B	2	2	2
C	3	3	3
D	4	4	4
E	5	5	5
F	6	6	6

Another set of briquettes is made at five different pressures (350 kg, 400 kg, 450 kg, 500 kg, 550 kg) to get the optimized briquetting pressure where each briquette contains chromite

concentrate, optimized amount of binder percentage (here 3% binder), and a stoichiometric amount of coke dust. The reduction of briquette is carried out in the PID control tube furnace at 1200 ^{0}C for 80 minutes. After reduction, the extent of reduction (EOR) is calculated.

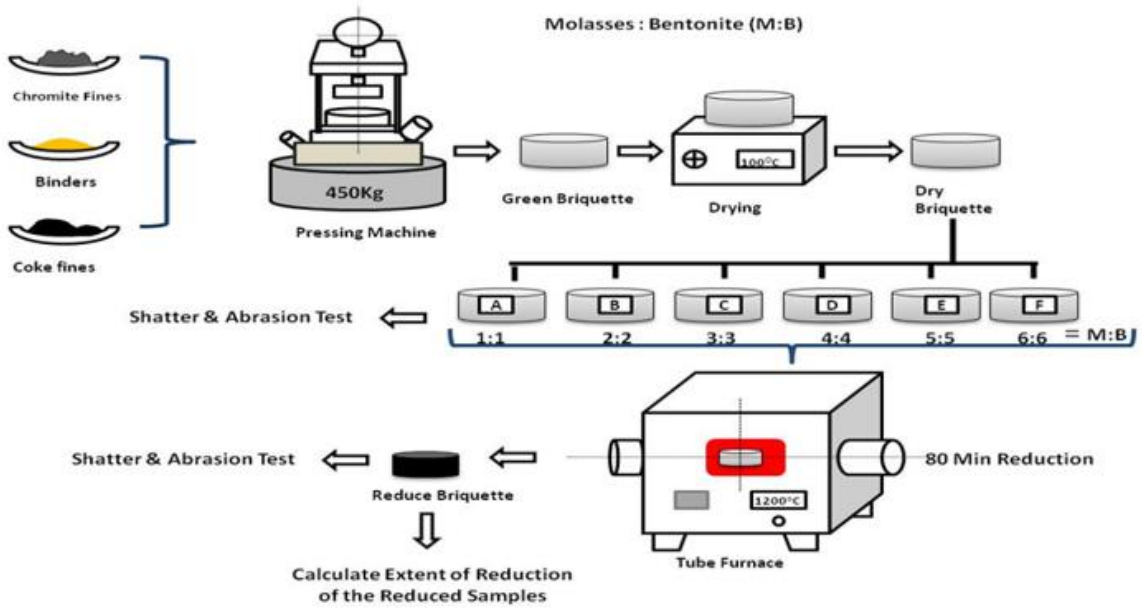

Figure 6A.2.1: Simplified Processing Diagram of the Reduction Process.

6A.2.4 Results and Discussion

6A.2.4.1 Effect of Feed Rate

The sample is fed at three different feed rates i.e. 50g/min, 100g/min, and 150g/min maintaining the same all other parameters. The other parameters are given below:

Particle size fraction of feed: 100% below 75 μm

Tilt angle: 8°

Water flow rate: 4.0 l/min

Pre-heat temperature of ore: 443.72°C

Amplitude of the table: 250 rpm

Solid-liquid ratio: 1:4

Riffles height: not fixed but approximately 2 mm

Distance between riffles: not fixed but approximately 14 mm.

The complete summary of the experimental analysis is shown in Table 6A.2. Three zones are created after tabling which are called concentrate, middling, and tailing. The concentrate side has a chromium oxide percentage higher than 40.92% for each of the three sets of experiments. As a result, tabling might produce an important development suitable for metallurgical

processing. The concentrate portion contains a higher percentage of chromium oxide than the middling and tailing portions. The highest weight percentage at the concentrate fraction is found to be 40.98% maintaining a 50 g/min feed rate. If the feed rate is increased to 150 g/min, only 29.04% weight has been recovered at the concentrate portion. The downward pushing force generated by the wash water is the same for all three experimental sets because the water flow rate and angle are fixed. Increasing the feed rate could therefore increase the concentration of solids in the system and increase the downward pressure that the wash water applies to the solid particles. In that case, the solid particles that overflow from the riffles are absorbed by the middling and tailing section. This decreases the weight percentage in the concentrate fraction at high feed rates.

Table 6A.2.2: Effect of the Feed Rate of the Wilfley Table on the Concentration of the Low-Grade Chromite Ore.

Feed Rate (g/min)	**Products**	**Weight (%)**	**Cr_2O_3 Recovery (%)**	**Grade Cr_2O_3 (%)**
50	Concentrate	40.98	62.26	40.93
	Middling	26.36	28.84	29.47
	Tailing	15.32	0.933	1.64
	Total	82.66	92.03	
100	Concentrate	38.60	65.95	46.03
	Middling	28.24	25.37	24.20
	Tailing	16.08	1.54	2.58
	Total	82.92	92.86	
150	Concentrate	29.04	52.28	48.51
	Middling	30.93	33.82	29.48
	Tailing	22.42	3.98	4.722
	Total	82.39	90.04	

The highest grade of Cr_2O_3 percentage is found to be 48.51%, at a feed rate of 150g/min, but recovery is less in that case. The relation between feed rate vs grade Cr_2O_3 and Cr_2O_3 recovery is shown in Fig. 6A.2.2. The maximum recovery of chromium oxide in the concentrate has been determined to be 65.95% with 46.035% grade Cr_2O_3 at 100g/min. At that condition, the grade of Cr_2O_3 in the middle and tailing portion is found to be 24.20% and 1.54% respectively.

So 100 g/min feed rate is very suitable for industrial applications. Appendix I contains the calculations for the grade of Cr_2O_3 and the corresponding recovery percentage.

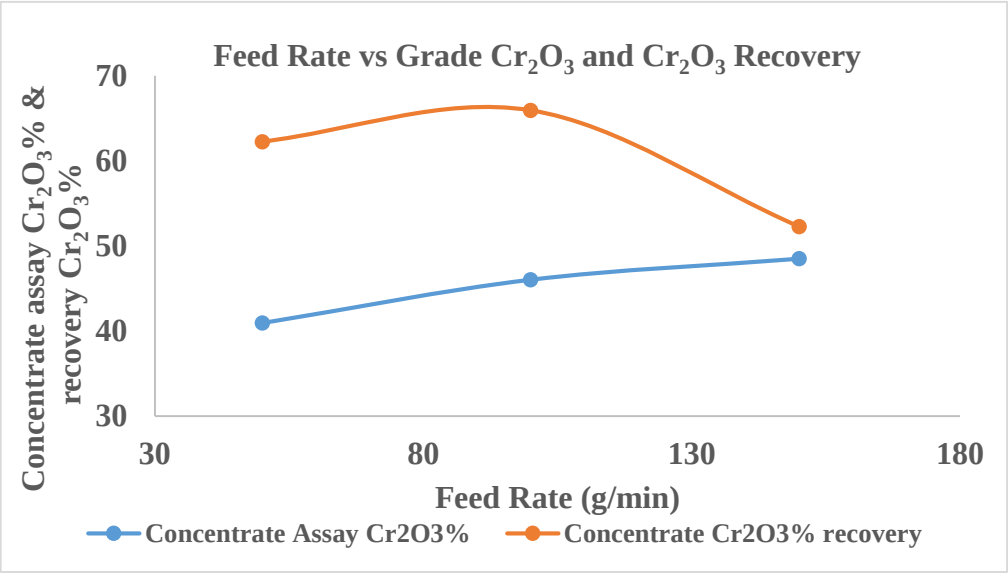

Figure 6A.2.2: Feed Rate vs. Grade Cr_2O_3 and Cr_2O_3 Recovery Curve in the Concentrate Fraction.

6A.2.4.2 XRD Analysis

The XRD analysis of concentrate, middling, and tailing is represented in Fig. 6A.2.3. It is observed that iron aluminium chromium oxide is the major phase along with hematite. The peak intensity of the $Fe(Al, Cr)_2O_4$ phase is very significant for the concentrate, compared to middling and tailing. This result indicates the feasibility of the up-gradation of low-grade chromite ore by gravity separation technique is very effective for this kind of raw material.

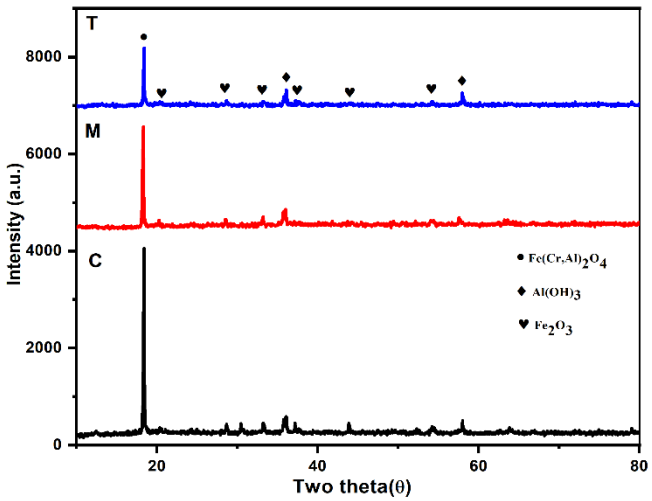

Figure 6A.2.3: XRD Analysis Report of the Chromite Fraction Generated During Tabling Under Optimized Conditions.

6A.2.4.3 SEM Analysis

SEM image of different chromite fractions obtained in concentrate, middling, & tailing at optimized conditions is shown in Fig. 6A.2.4. The images are taken at the same magnification.

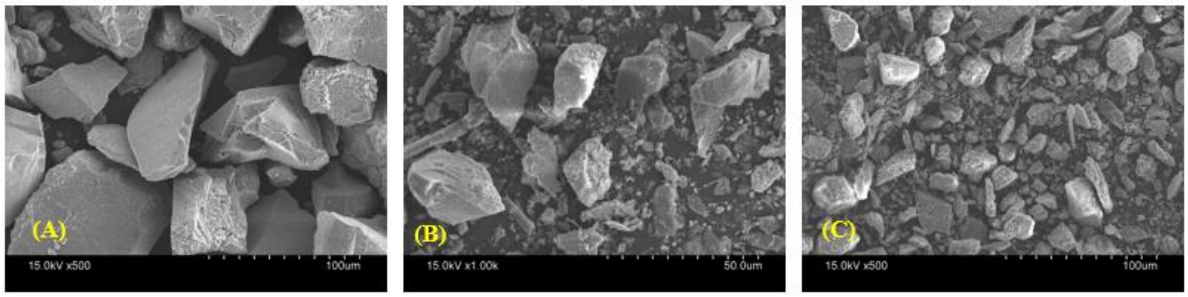

Figure 6A.2.4: SEM Image of the Chromite Fraction Generated During Tabling Under Optimized Conditions: (A) Concentrate, (B) Middling, (C) Tailing.

It is observed in the tailing sample that, the chromite grain has an irregular shape and size. The chromite grain size in the tailing sample is smaller compared to concentrate and middling. This is due to the presence of a lighter matrix in chromite ore which is enriched in the tailing portion during tabling. But in concentrate fraction which is shown in Fig. 6A.2.4 (A), chromite grains are irregular in shape but the distribution of grains is much organised manner. The surface morphology of the concentrate fraction is smooth concerning middling and tailing.

6A.2.4.4 Effects of Binder Percentage

Concentrate, obtained from tabling at optimized conditions, is agglomerated in the form of briquettes, and briquetting parameters are optimized using shatter & abrasion tests.

6A.2.4.4.1 Mechanical Properties of the Briquette Samples

The strength of briquettes is investigated using shatter and abrasion index to optimize the binder percentage. Briquettes are dropped four times onto a steel plate from a height of two meters to evaluate the shatter index. On the other hand to calculate the abrasion index the dry briquette sample is put into a tumbler and rotated for 300 revolutions where the rotation amplitude is 30rpm. The fines generated for both cases are collected and sieved using 0.5mm sieves. The shatter index (SI) and the abrasion index (AI) are calculated as follows:

$SI = (W_R/W_t)*100$

$AI = (W_p/W_t)*100$

Where; W_t = total weight of briquette.

W_R = Weight retained on the 0.5mm sieve.

W_P = Weight passing through the 0.5mm sieve.

The mechanical stability of agglomerated chromite ore briquettes, both before and after reduction, is evaluated with various binder percentages, as shown in Fig. 6A.2.5. Mechanical stability is directly proportional to binder percentage before and after reduction but the effect of binder percentage after the reduction is prominent compared to before reduction. During the reduction, cracks and pores are generated in the briquettes which reduce the mechanical stability of briquettes. Besides this the reduction of briquettes at lower binder percentage, the swelling is more along with cracking of the sample. The maximum mechanical stability is observed when a briquette is produced by using 6% of each binder before and after reduction.

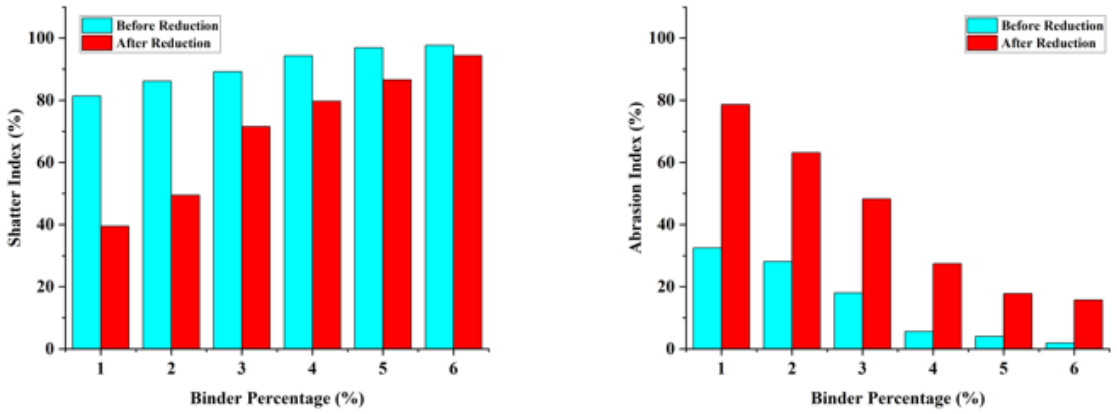

Figure 6A.2.5: Mechanical Properties of Chromite Ore Briquettes with Different Binder Percentages before and After Reduction.

6A.2.4.4.2 Extent of Reduction of the Reduced Samples

The extent of reduction is calculated by weight loss which occurs during the reduction of chromite ore briquettes. The stoichiometric carbon required for the reduction process is shown in Appendix II. The extent of reduction is graphically represented in Fig. 6A.2.6. The reactions that occur during direct reduction may be expressed as follows:

$3Fe_2O_3 + C \rightarrow 2Fe_3O_4 + CO$ [1]

$Fe_3O_4 + C \rightarrow 3FeO + CO$ [2]

$FeO + C \rightarrow Fe + CO$ [3]

$Cr_2O_3 + 3C = 2Cr + 3CO$ [4]

$Cr_2O_3 + 3CO = 2Cr + 3CO_2$ [5]

The reactions are heterogeneous, happening at phase boundaries, with mass and heat transfer between the reaction interface and the bulk phase. The weight loss during the reduction decreases as the binder percentage in briquettes increases. Weight loss occurs due to the removal of oxygen from chromium oxides, iron oxide, bentonite, molasses, and coke dust

(generally from volatile matter and fixed carbon). From Fig. 6A.2.6, it is observed that the extent of reduction decreases with increasing binder percentage. Briquettes produced at low binder percentages are more porous. So diffusion of reducing gas from the surface to the bulk of the briquette occurs more consequence manner during the reduction at a lower binder percentage. The briquette produced at 3% of each binder gives a reasonable amount of mechanical stability along with acceptable EOR.

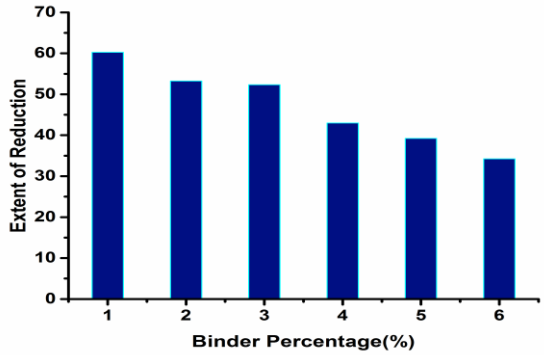

Figure 6A.2.6: Extent of Reduction of the Reduced Samples at 1200°C for 80 Minutes with Different Binder Percentages.

6A.2.4.5 Effects of Pressure

6A.2.4.5.1 Mechanical Properties of the Briquette Samples

The stability of agglomerated chromite ore briquettes prepared at different pressures is measured before and after the reduction of briquettes which is given in Fig. 6A.2.7. It is observed that the stability of agglomerated chromite ore briquettes increased with higher briquetting pressure. At high pressure inter particle space shrunk which increased the compactness of the briquettes.

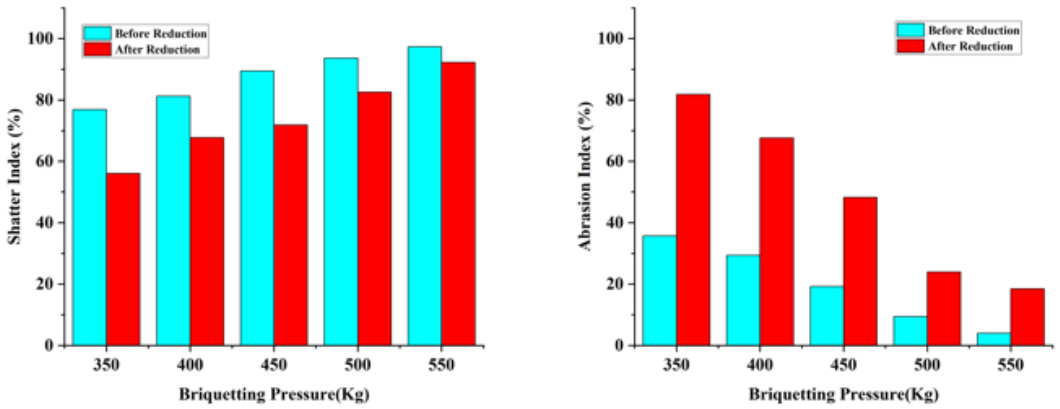

Figure 6A.2.7: Mechanical Properties of Chromite Ore Briquettes with Different Briquetting Pressures before and After Reduction.

6A.2.4.5.2 Extent of Reduction of the Reduced Samples

The carbothermic reduction has been carried out for chromite ore briquettes at different briquetting pressure and the extent of reduction obtained is shown in Fig. 6A.2.8. The weight loss is found to decrease with a rise in the briquetting pressure. Briquettes produced at low pressure are more porous so that diffusion of reducing gas increases leading to a good extent of reduction. The maximum EOR of 58.66% is achieved at 350kg pressure but the stability of the briquettes is very poor. However, the briquettes produced at 450kg pressure are suitable for further processing for the production of ferrochrome.

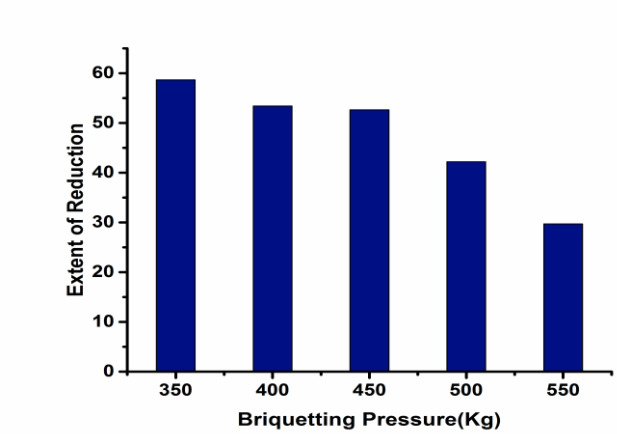

Figure 6A.2.8: Extent of Reduction of the Reduced Samples at 1200^{o}C for 80 Minutes with Different Briquetting Pressures.

6A.2.6 Conclusion

Gravity separation of low-grade chromite ore using the wilfley table is a very effective technique for up-gradation. In wilfley table pre-heated (443.72°C) chromite ore, at an 8° tilt angle, 4.0 l/min water flow rate, and 100 g/min feed rate results in 46.03% chromium oxide in concentrate, compared to 26.88% in the feed sample. Mechanical properties of the chromite ore briquettes before and after reduction improve on raising the percentages of bentonite and molasses. Reducing the binder percentage increases EOR and reducibility. The stability of agglomerated chromite ore briquettes is increased by an increase in briquetting pressure. EOR depends upon briquetting pressure and increases with a decrease in briquetting pressure. From the experimental observation, 3% bentonite and 3% molasses as a binder gives better mechanical strength and optimum reducibility. The optimized briquetting pressure is found to be 450Kg. So, 3% bentonite, 3% molasses, 3% water, and 450 Kg pressure are chosen as the optimum experimental parameters which can provide good mechanical strength and

reducibility. Moreover, this condition is suitable for charging the chromite ore briquettes into SEAF for high or medium-carbon ferrochrome production.

6A.2.7 References

[1] M. O. F. Mines, I. Bureau, and O. F. Mines, “Yearbook 2018 MINISTRY OF MINES INDIAN BUREAU OF MINES,” vol. 2018, no. 0712, 2019.

[2] M. O. F. Power. Govt. of India, "Annual Report 2023-2024," pp. 1-214.

[3] R. K. Mohapatra, “Energy Consumption and Conservation Measures in Ferro Chrome – A Step towards Green Manufacturing,” vol. 4, no. 1, pp. 393–396.

[4] B. W. Neizel, J. P. Beukes, P. G. Van Zyl, and N. F. Dawson, “Why is $CaCO_3$ not used as an additive in the pelletised chromite pre-reduction process?,” *Miner. Eng.*, vol. 45, pp. 115–120, 2013, doi: 10.1016/j.mineng.2013.02.015.

[5] E. L. J. Kleynhans, B. W. Neizel, J. P. Beukes, and P. G. Van Zyl, “Utilisation of pre-oxidised ore in the pelletised chromite pre-reduction process,” *Miner. Eng.*, vol. 92, pp. 114–124, 2016, doi: 10.1016/j.mineng.2016.03.005.

[6] E. L. J. Kleynhans, J. P. Beukes, P. G. Van Zyl, P. H. I. Kestens, and J. M. Langa, “Unique challenges of clay binders in a pelletised chromite pre-reduction process,” *Miner. Eng.*, vol. 34, no. 2012, pp. 55–62, 2012, doi: 10.1016/j.mineng.2012.03.021.

[7] P. V. T. Rao, “Agglomeration and Prereduction of Ores,” *4th Refresh. Course Ferro Alloy.*, pp. 1–15, 1994, [Online]. Available: http://eprints.nmlindia.org/5783

[8] V. Singh and S. M. Rao, “Study the effect of chromite ore properties on pelletisation process,” *Int. J. Miner. Process.*, vol. 88, no. 1–2, pp. 13–17, 2008, doi: 10.1016/j.minpro.2008.04.003.

[9] J. Pal, “Innovative Development on Agglomeration of Iron Ore Fines and Iron Oxide Wastes,” *Miner. Process. Extr. Metall. Rev.*, vol. 40, no. 4, pp. 248–264, 2019, doi: 10.1080/08827508.2018.1518222.

[10] V. Tathavadkar, V. Singh, and S. M. Rao, “Study of liquid phase formation during the sintering of chromite pellets and its effect on the properties of pellets,” *Proc. Int. Semin. Miner. Process. Technol.*, no. 1995, pp. 431–435, 2006.

[11] B. Nandy, M. K. Chaudhury, J. Paul, and D. Bhattacharjee, “Sintering characteristics of indian chrome ore fines,” *Metall. Mater. Trans. B Process Metall. Mater. Process. Sci.*, vol. 40, no. 5, pp. 662–675, 2009, doi: 10.1007/s11663-009-9268-5.

[12] U. Atalay and G. Zbayoglu, "Beneficiation and Agglomeration of Chromite Its Application in Turkey," *Miner. Process. Extr. Metall. Rev.*, vol. 9, no. 1–4, pp. 185–194, 1992, doi: 10.1080/08827509208952703.

[13] P. V. T. RAO and A. K. DAS, "Agglomeration of Chrome Ore Fines for Ferrochrome Making - A Step Towards Increased Competitiveness," *Ferro Alloy Ind. Lib. Econ.*, pp. 51–58, 1997.

[14] I. Bondarenko, E. Kuldeyev, S. Temirova, A. Tastanova, and N. Sadykov, "Obtaining of strong chromium pellets with the use of a ferrosilicon-calcium binder," *Metalurgija*, vol. 61, no. 2, pp. 359–362, 2022.

[15] A. A. Akberdin, A. S. Kim, and R. A. Akberdin, "AGGLOMERATION OF REFRACTORY CHROMITE ORE A.A. Akberdin, A. S.," *The thirteenth International Ferroalloys Congress Efficient technologies in ferroalloy industry, pp. 1-4*, 2013.

[16] S. Dwarapudi, V. Tathavadkar, B. Chennarao, T. K. S. Kumar, and T. K. Ghosh, "Development of cold bonded chromite pellets for ferrochrome production in submerged arc furnace," *26th Int. Miner. Process. Congr. IMPC 2012 Innov. Process. Sustain. Growth - Conf. Proc.*, vol. 53, no. 1, pp. 1279–1288, 2012.

[17] S. P. Du Preez, Z. Maree, and J. P. Beukes, "Sodium silicate cold-bonded chromite pellets for the ferrochromium industry-identifying a suitable process," *Mater. Res.*, vol. 23, no. 4, 2020, doi: 10.1590/1980-5373-MR-2020-0246.

[18] A. P. Zambrano, C. Takano, M. B. Mourao, and S. Y. Tagusagawa, "Binder behavior on chromite-carbon composite pellets," *Mater. Res.*, vol. 19, no. 6, pp. 1344–1350, 2016, doi: 10.1590/1980-5373-MR-2016-0264.

[19] S. Agarwal, J. Pal, and D. Ghosh, "Development of chromite sinter from ultra-fine chromite ore by direct sintering," *ISIJ Int.*, vol. 54, no. 3, pp. 559–566, 2014, doi: 10.2355/isijinternational.54.559.

[20] M. G. Rocha, A. S. Da Silva, M. B. Mourao, M. N. Kurauchi, and C. Takano, "Fundamental aspects of sintering of chromites concentrates," *Trans. Institutions Min. Metall. Sect. C Miner. Process. Extr. Metall.*, vol. 123, no. 4, pp. 251–256, 2014, doi: 10.1179/1743285514Y.0000000080.

[21] T. Umadevi, A. Brahmacharyulu, A. K. Roy, P. C. Mahapatra, M. Prabhu, and M. Ranjan, "Influence of iron ore fines feed size on microstructure, productivity and quality of iron ore sinter," *ISIJ Int.*, vol. 51, no. 6, pp. 922–929, 2011, doi: 10.2355/isijinternational.51.922.

[22] M. Zhou, Z. Yu, P. Wang, H. Xie, Y. Wen, and J. Li, "Thermodynamic analysis of iron ore sintering process based on biomass carbon," *Energies*, vol. 13, no. 22, pp. 1–14, 2020, doi: 10.3390/en13225988.

[23] Z. Deqing, L. Jian, P. Jian, and H. Aoping, "Sintering behaviours of chromite fines and the consolidation mechanism," *Int. J. Miner. Process.*, vol. 86, no. 1–4, pp. 58–67, 2008, doi: 10.1016/j.minpro.2007.11.002.

[24] S. Agarwal, J. Pal, and D. Ghosh, "Smelting characteristics of fluxed chromite sinter and its performance assessment in electric arc furnace to produce high carbon ferrochrome," *Ironmak. Steelmak.*, vol. 43, no. 2, pp. 97–111, 2016, doi: 10.1179/1743281215Y.0000000054.

[25] Q. Fangming and Z. Lin, "A Preliminary Study on Pellet-Sintering of Chromite Fines," *The proceedings of INFACON 8*, pp. 184–188, 2017.

[26] T. Çiçek, H. Cengizler, and İ. Cöcen, "Briquetting Fine Chromite Concentrates," *Proc. XIIIth Int. Miner. Process. Symp.*, pp. 1–9, 2012.

[27] V. Singh, T. K. Ghosh, Y. Ramamurthy, and V. Tathavadkar, "Beneficiation and agglomeration process to utilize low-grade ferruginous manganese ore fines," *Int. J. Miner. Process.*, vol. 99, no. 1–4, pp. 84–86, 2011, doi: 10.1016/j.minpro.2011.03.003.

[28] E. S. Olson, "30. Binder modification and devalopment..pdf," 1998, *Energy & Enviranmental Research Center, University of North Dakota*.

[29] N. R. Shoko and N. N. Malila, "Briquetted Chrome Ore Fines Utilisation in Ferrochrome Production At Zimbabwe Alloys," *Tenth Int. Ferroalloys Congr.*, no. February, pp. 291–299, 2004.

[30] C. R. Ray, P. K. Sahoo, and S. S. Rao, “Strength of chromite briquettes and its effect on smelting of charge chrome / ferro chrome,” *Innov. Ferro Alloy Ind. - Proc. XI Int. Conf. Innov. Ferro Alloy Ind. Infacon XI*, pp. 63–66, 2007.

Chapter-6A.3

Smelting of Pre-heated Chromite Briquettes after the Reduction of Briquettes using Coke at Different Temperatures and its Kinetic Study

6A.3.1 Introduction

Chromite is the main raw material used to make ferroalloy and stainless steel. Pre-reducing chromite is required to obtain a higher degree of reduction and less energy consumption during the smelting process. It has been reported that pre-reducing chromite ore before smelting could save between 45% and 50% of electrical energy [1]. Ore, coke, and flux are charged in the furnace during reduction. This ore is typically lumpy, ranging in size from 10 to 75 mm. Furthermore, different-sized coke is charged into the furnace; typically, the coke has a size range of 30 to 50 mm. The fines are agglomerated to produced pellets or briquettes and then subjected to furnace for reduction [2]. The pre-reduced ore undergoes smelting in a submerged electric arc furnace, resulting in the production of various types of ferrochrome.

6A.3.2 Literature Review

The type of ore, the reductant, and the experimental parameters (temperature, particle size, etc.) affect the chromite ore reduction process. Ellingham diagram indicates that in the reduction temperature range of 1373-1523 K, none of the oxides in chromite other than Fe_2O_3 will be chemically affected [3]. When chromite ore is reduced with coal at 1473 K, Neuschutz [4] reported that iron oxide is reduced faster than chromium oxide, and the reduction products contained only 5% Cr. High temperatures are required for the reduction of silicon oxides. The reduction of chromite ore with graphite showed that iron oxide is completely reduced first, then the reduction of chromium oxide starts [5]. Reddy et al. [6] additionally observed that when various chromite ores are reduced in the temperature range of 973-1373 K, only the iron oxide is reduced which is present in the ore. The reduction follows the nucleation growth kinetic model with an activation energy varying between 23 and 55.8 kJ/mol. Iron's catalytic action is the cause of the low activation energy. Chakraborty et al. studied the reduction of two varieties of chromite ores using carbon within a temperature range of 1173-1573 K. [7]. The reduction of chromium starts only after the completion of iron oxide reduction. The reduction of iron is determined to be controlled by diffusion, with an activation energy of 135 kJ/mol, according to the Ginstling and Brounsthein (GB) equation. Either a chemical reaction or nucleation with an activation energy of 130 kJ/mol controls the chromium reduction. Lekatou et al. [8] noticed that above 1573 K, a fast reduction of chromite-carbon pellet could be achieved because, at this condition, reduction of iron oxide is easier than chromium oxide. Cheng et al. [9] also noted that when the reducing agents are present in optimized amounts at 1373 K, the chromium oxide remains unreacted, but the majority of the iron oxide is reduced.

Sundar Murti et al. [10] found that during the reduction of synthetic chromite with carbon in the temperature range of 1423-1573 K, the process is controlled by oxygen diffusion in the chromite, following the Ginstling–Brounsthein equation. The same authors [11] also observed that oxygen diffuses from the ore to the gas-solid interface with an activation energy of 238 kJ/mol, controlling the reduction of chromite ore at 1513-1583. In both experiments, carbide formation is not detected during reduction.

Nafzieger et al. [12] investigated the carbothermic reduction of chromite ore using various reducing agents. There it is found that the reaction is initially nucleation-controlled. However, no single kinetic equation can sufficiently explain the overall reduction. In the presence of solid carbon, chromite is reduced more effectively than CO gas, as reported by Van Vuuren et al. [13]. They concluded that a diffusion-controlled mechanism (Jander equation) sufficiently described the reduction. In addition, the Greek and Cypriot ores are not reduced by pure carbon monoxide gas, as reported by Vazarlis and Lekatou [14]. Reduction with carbon followed the GB equation. The main factor controlling the rate is the movement of carbon into the chromite pellets, possibly via the reaction products. The reduction kinetics of transvaal chromite ores are satisfactorily explained by the GB equation [11]. The range of the activation energy is 145-300 kJ/mol, dependent upon the type of ore. Early on, carbon diffuses primarily through volume, but later on, intermetallic carbide formation plays a major role in transferring carbon. According to Kikkonen et al. [15], the diffusion of the product gas (CO) through the product layer regulates the rate at which chromite pellets are reduced with carbon. According to Lekatou and Walker [8][16], the formation of metallic particles at the chromite/carbon interfaces initiates chromite reduction, and the subsequent reaction is controlled by the movement of iron and chromium from within the grain.

According to Ding and Warner [17], the reduction of chromite pellets by graphite in the solid state follows both nucleation and a chemical control mechanism requiring 114 kJ/mol of activation energy. During the final stages, the control mechanism is the diffusion of gas through the product layer, requiring an activation energy of 221 kJ/mol. The activation energy in the early stage of reduction composite pellets of carbon-chromite is calculated by the same authors [18] to be 118 kJ/mol. The reaction seems to be controlled by either nucleation or a chemical reaction. The initial stage of chromite pellet reduction by carbon in the presence of lime is found to have an observed activation energy of 92 kJ/mol, with heat transfer and nucleation or chemical reactions controlling the reduction up to 50% [11]. Surface-contracting interfacial reaction is determined to be the rate-determining step in the initial stage of the reduction of

Fe_2O_3-Cr_2O_3-NiO by graphite at 1623-1823 K, while two-dimensional diffusion controls the reaction during the final stage [19]. The observed activation energies are 174.54 kJ/mol and 55.43 kJ/mol, respectively. Carbothermal reduction of $Fe_2Cr_2O_4$ using graphite at 1623-1823 K showed that the reaction's products are significantly affected by temperature and initial carbon content [20].

In a study on the reduction of pellets containing iron ore and carbon, the process below 1173 K is controlled by three-dimensional diffusion (Jander equation). At 1373 K, the reduction is governed by a three-dimensional phase-boundary controlled model involving interfacial reactions. [21]. The activation energy is determined to be 198.66 kJ/mol, 207.66 kJ/mol, and 227.35 kJ/mol when the degree of reduction is 0.0-0.4, 0.4-0.7, and 0.7-1.0, respectively, using a three-dimensional phase-boundary controlled model. The activation energy required to reduce pellets containing iron ore and carbon is calculated by kinetic study [22]. For the initial reduction stage, the activation energy ranges from 0.86 to 8.82 kJ/mol. In the final stages, it ranges from 12.37 to 38.32 kJ/mol. The authors noted that the initial stage of reduction is controlled by the mechanism of gaseous diffusion. In the final stage, the reduction is controlled by a mixed mechanism involving both chemical reactions and gaseous diffusion. According to Gupta et al. [23], an interfacial chemical reaction with an activation energy of 134.56 kJ/mol is responsible for controlling the reduction of Fe_2O_3-coke fine nuggets. Hematite reduction in the presence of coke has been investigated both isothermally and non-isothermally at 1423-1573 K [24]. The results indicated that the reduction process followed the Avrami-Erofeev model (n = 2/3), which has an activation energy of 171.25 kJ/mol. The reduction of iron ore nuggets by the devolatilization of lean-grade coal is studied by Biswas et al. [25] and is found to be regulated by 2-D diffusion (Valensi equation).

Sarkar et al. conducted an investigation into the kinetics of reducing titaniferous magnetite ore with low-grade coal.[26] found that diffusion (Jander equation) followed by contracting geometry (interfacial chemical reaction) is rate-controlling in the early stages. It is found that the corresponding activation energy is 179.80 KJ/mol and 93.42 KJ/mol, respectively. Thermogravimetric analysis of the reduction kinetics of titanomagnetite concentrate-coal briquettes in an argon atmosphere is carried out [27]. The study found that different mechanisms control the reaction at various stages. For a reduction extent of less than 0.2, the phase boundary chemical reaction is dominant, with an apparent activation energy of 68 kJ/mol. At a reduction extent greater than 0.75, the process is controlled by three-dimensional diffusion, requiring an activation energy of 134 kJ/mol. When the reduction progressed, the

activation energy increased, and the reaction is under mixed control for the extent of reduction in the range of 0.2-0.75. The reduction of high Cr-V titanomagnetite pellets by the H_2-CO-CO_2 gas mixture is found to be controlled by mixed internal diffusion and interfacial reaction initially and only by internal diffusion subsequently [28].

Ferrochrome, a chromium-iron alloy, is produced by the smelting of pre-reduced chromite briquettes. A critical alloy called ferrochrome is mainly formed from chromium and iron, containing minor traces of carbon & other elements [16]. In many industrial processes, particularly for producing stainless steel and other specialty alloys, it is of great significance. Ferrochrome usually consists of silicon, carbon, and other alloying elements in addition to 50-70% chromium and 15-30% iron [29]. The exact composition varies depending on the application. Ferrochrome exhibits high corrosion resistance, hardness, and temperature resistance, making it ideal for use in environments where these properties are crucial, such as in stainless steel production. Ferrochrome is predominantly employed in stainless steel manufacturing. In stainless steel alloys, chromium serves an essential function in boosting the steel's resistance to corrosion and giving it a bright, glossy sheen. During the manufacturing process, ferrochrome can be added to molten steel to modify the alloy's characteristics to suit the needs of various applications, including construction materials, appliances, automotive parts, and cutlery. Ferrochrome serves as an alloying component in creating various specialty steels and alloys, in addition to stainless steel. To increase the hardness, toughness, and resistance to wear & corrosion of nickel-based alloys, tool steels, and high-strength low-alloy (HSLA) steels, it is frequently added [30][31]. Ferrochrome is utilized in the refractory industry to make refractory bricks and linings for industrial kilns and high-temperature furnaces. Chromium increases the refractory material's resistance to heat shock and chemical corrosion, extending its useful life under demanding operating circumstances. Ferrochrome is used in the chemical industry to make a variety of chemicals, such as catalysts, pigments, and chromium salts. Surface coating, textile dyeing, leather tanning, and electroplating all use chromium compounds that come from ferrochrome. Ferrochrome is used in defense and aerospace applications that call for high-performance materials. Its outstanding resistance to heat and corrosion makes it suitable for manufacturing missile casings, jet engine components, and turbine blades. In the energy industry, ferrochrome is used to fabricate parts like turbine shafts, valves, and fittings that are used in power generation and transmission systems. It is commonly used in steam and gas turbines because of its stability at high temperatures and oxidation resistance. Ferrochrome is an adaptable alloy with a broad range of industrial uses,

especially in the steelmaking sector, where its special qualities help to produce strong, long-lasting materials that are necessary for contemporary manufacturing techniques and infrastructure [32][33].

Chromite ore is smelted to produce the ferrochrome alloy, which generates ferrochrome slag as a byproduct. It is produced when high temperatures are applied to chromite ore in a smelting furnace. The ore is primarily composed of chromium oxide (Cr_2O_3), iron oxide (FeO), and other impurities [20]. Ferrochrome slag's composition and characteristics are influenced by several variables, including the raw materials utilized, the method of smelting, and the cooling & solidification processes. When chromite ore is reduced in a submerged arc furnace (SAF) or other smelting reactors, ferrochrome slag is produced. The ferrochromium industry generates around 1-1.2 kg of solid waste material per kilogram of ferrochrome produced. This waste predominantly consists of ferrochrome ash, along with air-cooled and water-cooled ferrochrome slag [34]. Chromium ore is smelted at temperatures exceeding 1873K while being combined with fluxes and carbonaceous reducing agents. Smelting produces ferrochrome alloys by reducing iron and chromium oxides, while non-metallic substances and impurities condense into a molten slag phase. The composition of ferrochrome slag varies depending on factors such as the composition of the chromite ore, the smelting process parameters, and the presence of additional fluxes or additives [35][36]. However, typical compositions of ferrochrome slag are listed in Table 6A.3.1.

Table 6A.3.1: Composition of Ferrochrome Slag Found in Other Studies [34][35][36][37].

Constituent	**Mahamaya et al.**	**Jena et al.**	**Islam et al.**	**Dash et al.**
Al_2O_3	21.58	23.6	18.47	23.69
SiO_2	21.28	27.8	36.35	26.98
MgO	24.94	23.7	27.24	24.06
CaO	4.07	3.51	5.38	4.75
Cr_2O_3	19.46	9.16	8.51	13.68
Fe_2O_3	5.89	3.60	5.21	5.63

The physical and chemical properties of the slag are determined by the ratio of these constituents. Ferrochrome slag typically has a granular-to-amorphous texture, a dark color, and a glassy look [37]. Its specific gravity and density, which can vary from 2.5 to 3.5 g/cm³, are determined by its chemical composition. Depending on the chemical composition and cooling rates, the slag may contain silicate minerals and crystalline phases like spinel ($FeCr_2O_4$). Because it contains both magnesium oxide and calcium oxide, ferrochrome slag has a pH between 9 and 11, making it extremely basic. There's a chance that it contains residual chromium compounds containing Cr^{6+} ions, which could be hazardous to the environment [38].

The mechanical properties of ferrochrome slag vary depending on its chemical composition and rate of cooling. It can range from brittle to relatively durable, influencing its suitability for different applications, such as aggregate in construction materials. Improper disposal of ferrochrome slag can result in environmental contamination. The Cr^{6+} ion present in ferrochrome slag can lead to land and water contamination due to the leaching of potentially toxic elements such as chromium, iron, and other heavy metals. This contamination can harm ecosystems and pose risks to human health. The handling and processing of ferrochrome slag has the potential to produce particulate matter and dust, which may contribute to local air pollution. Inhalation of airborne particles can pose respiratory health risks to workers and nearby communities. Ferrochrome slag can have beneficial applications, such as in construction materials and road infrastructure [39].

In the present chapter, the reduction behavior of beneficiated pre-heated chromite ore is investigated. Besides this, the kinetics associated with the reduction process of chromite ore by coke fines at high temperatures are investigated. Finally, ferrochrome is produced by smelting pre-reduced chromite ore.

6A.3.3 Materials & Methods

6A.3.3.1 Briquette Preparation

Chromite concentrate found in the tabling process (given in chapter 6A.1) is fed material for the reduction and smelting process. A stoichiometric mixture of coke dust, 3% molasses, bentonite, & water as a binder is mixed with chromite concentrate to create chromite briquettes. After all ingredients are mixed homogeneously, 450 kg of briquetting pressure is used to form a cylindrical briquette. Every briquette has dimensions of 12 mm in vertical height and 25 mm across in diameter. The approximate weight of each briquette is 10 grams.

6A.3.3.2 Reduction Method

Low-temperature chromite reduction is conducted in a tubular furnace with a PID control system. The temperature accuracy of the furnace is within ±5°C. The dried briquette's initial weight has been recorded for every reduction using an electronic balance before being put in an inconel. The inconel has a cylindrical shape and is attached to an exhaust tube. An additional 1.5 grams of coke dust are added to the inconel along with chromite briquettes to create a reducing atmosphere. Inconel is heated to a specific temperature and then left in the furnace for a specific time length. The mixed gas produced during the reduction process can escape through the exhaust tube. The exhaust tube's outlet is sealed after a specified time, and Inconel

is removed from the furnace to cool in the open air. Finally, the reduced briquettes are weighed on an electronic balance, and the weight loss is recorded to determine the extent of reduction.

High-temperature reduction is carried out by raising hearth furnace producing a reduced atmosphere. The dried briquette is weighed using an electronic balance before putting it in a zirconium crucible. The zirconium crucible is arranged inside a square brick framework and covered with lump coke. After it reaches the specified temperature, the entire setup is put inside the furnace for reduction. Lump coke is periodically subjected in the furnace every 15 minutes to maintain a reducing atmosphere. The mixed gas produced during reduction is extracted using the exhaust tube of the furnace. After the completion of the reduction time, the briquette is cooled down in atmospheric conditions and takes the final weight to get the weight loss of the briquette due to reduction. Reduced samples are characterized by XRD and SEM analysis.

6A.3.3.3 Extent of Reduction (EOR)

The extent of reduction is defined by the following method:

EOR = (Oxygen removed/theoretical oxygen removed for the 100 percent reduction of Cr_2O_3 & Fe_2O_3 which is present in the chromite ore) × 100.

6A.3.3.4 Metallization Test

The metallic chromium present in the sample after reduction is estimated by the chemical method. In this process, reduced chromite ore is crushed and ground below 75 µm for better dissolution. Take a 0.1-gram fine sample in a round bottom flask and add 100 ml acid mixture. The acid mixture contains 10% ortho-phosphoric acid and 40% sulfuric acid. Reflux it for 2 hours with a reflux condenser. After that, allow the solution to cool to room temperature, then transfer it by filtration into a 250-ml volumetric flask (VF). Whatman 42 filter paper is used for filtration. The residue present in the filter paper is washed with hot distilled water at least five to six times. Take a 1.0-ml aliquot from 250 ml VF transfer it to a 50-ml volumetric flask and fill to the mark. This sample is subjected to an atomic absorption spectrophotometer for the analysis of chromium concentration [923]. Similarly, metallic iron is determined by the chemical titration method. A 0.2-gram reduced chromite sample is taken and placed in a dry comical flask. 100 milliliters of freshly made 10% ferric chloride solution is then added to the sample to estimate the amount of metallic iron. After that, the mixture is stirred for half an hour. On the other hand, 50 ml of a 1:1 orthophosphoric and hydrochloric acid mixture is made in a beaker and transferred into the conical flask. After that, the mixture is cooled and titrated

using a BDS indicator against a 0.1N $K_2Cr_2O_7$ solution. The following calculation is used to determine metallic iron:

Fe= (ml of $K_2Cr_2O_7$ * normality of $K_2Cr_2O_7$ * 0.01862 *100) / Sample weight

The degree of metallization (DOM) is calculated by the following method:

$DOM = (M_R/T) \times 100$

Where M_R represents the metallic chromium or iron formation during reduction and T represents the total metallic chromium or iron present in the ore.

6A.3.3.5 Isothermal Kinetic Study of Chromite Briquettes

Isothermal kinetic studies of chromite reduction at high temperatures have been carried out in the present investigation. High-temperature reduction is investigated at 1573, 1623, 1673, and 1723 K. Each set of temperature reductions is done at five specific times: 15, 30, 60, 90, and 120 minutes. Experimental data are tested by different isothermal kinetic models, which are given in Chapter 1, Section 1.11.

6A.3.3.6 Smelting Process

The reduced sample with the highest degree of metallization is mixed with 3% lime and subjected to a raising hearth furnace for smelting. The smelting process is carried out at 1873K for six hours. The characterization of the product is carried out by AAS, XRD, SEM, and EDX analysis.

6A.3.4 Results and Discussions

6A.3.4.1 Effect of Time and Temperature on Chromite Briquettes

In the reduction process, the weight loss of the sample during the reduction is influenced by both the reduction temperature and duration. The weight loss and reduction time relationship at low temperatures (1373K-1573K) is shown in Fig. 6A.3.1A, while the weight loss and reduction time relationship at high temperatures (1573-1726K) is represented by Fig. 6A.3.1B. The percentage weight loss is computed according to the equation below:

Weight Loss (%) = $(M_o - M_t)*100/ M_o$

Where M_o and M_t stand for the weight of the briquettes of chromite ore at a reduction time of t minutes, before and after the reduction process.

It has been observed that as temperature and time increase, chromite ore reduction increases. The total weight loss of the chromite briquettes during reduction must be calculated to evaluate the degree of reduction (DOR) or extent of reduction (EOR). This weight loss occurs due to reductants (coke), binders (molasses, bentonite), and the removable oxygen present in the ore. The weight loss at 1373 K is found to be 16.52% and 21.73% for reductions of 15 and 120 minutes, respectively. In contrast, weight loss at 1723 K is found to be 27.49% and 33.96% for reductions of 15 and 120 minutes, respectively.

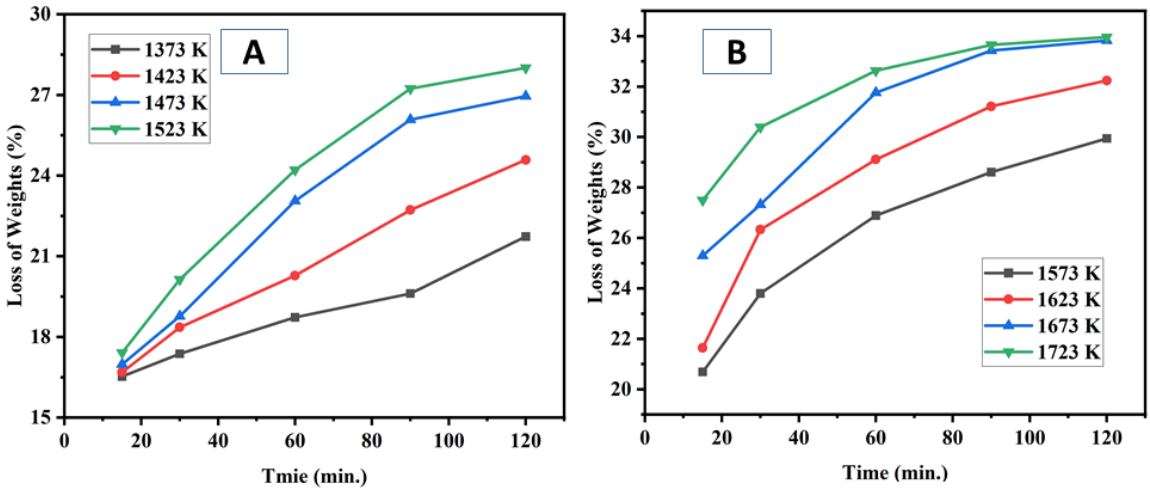

Figure 6A.3.1: Loss of Weight vs. Time Plot for Reduced Chromite Briquettes at Various Times and Temperatures [(A) for Low Temperature and (B) for High Temperature].

6A.3.4.2 XRD Analysis of Reduced Briquettes

Fig. 6A.3.2 displays the XRD analyses of the reduced samples after 120 minutes at low temperatures. The different reduction temperatures are 1373 K, 1423 K, 1473 K, 1523 K, and 1673 K. From Fig. 6A.3.2 (a, b), it can be seen that the XRD of reduced chromite ore at 1373 and 1423 K does not significantly differ from that of the raw materials shown in Chapter 5, Section 5.3.3. The fact that there is no new phase visible in the XRD pattern suggests that the degree of reduction at that temperature is very nominal. When chromite ore is reduced to a temperature of 1473 and 1523 K, the spectrum shows that the spinel peaks shift to a higher diffraction angle (2θ) which is shown in Fig. 6A.3.2 (c, d). The possible spinel phases in the reduced ore are (Mg, Fe)(Al, Cr)$_2$O$_4$, FeCr$_2$O$_4$, MgCr$_2$O$_4$, MgAl$_2$O$_4$, Fe$_3$O$_4$, and FeAl$_2$O$_4$. Two theta values for all those phases are much closer to each other. It seems that iron began to reduce at this temperature range, but chromium oxide reduction did not start. Iron oxide in the chromite ore undergoes reduction to form iron carbide and wustite (FeO). Since the

temperature is below 1573 K, there is no significant phase present in the XRD image which provides evidence of chromium reduction.

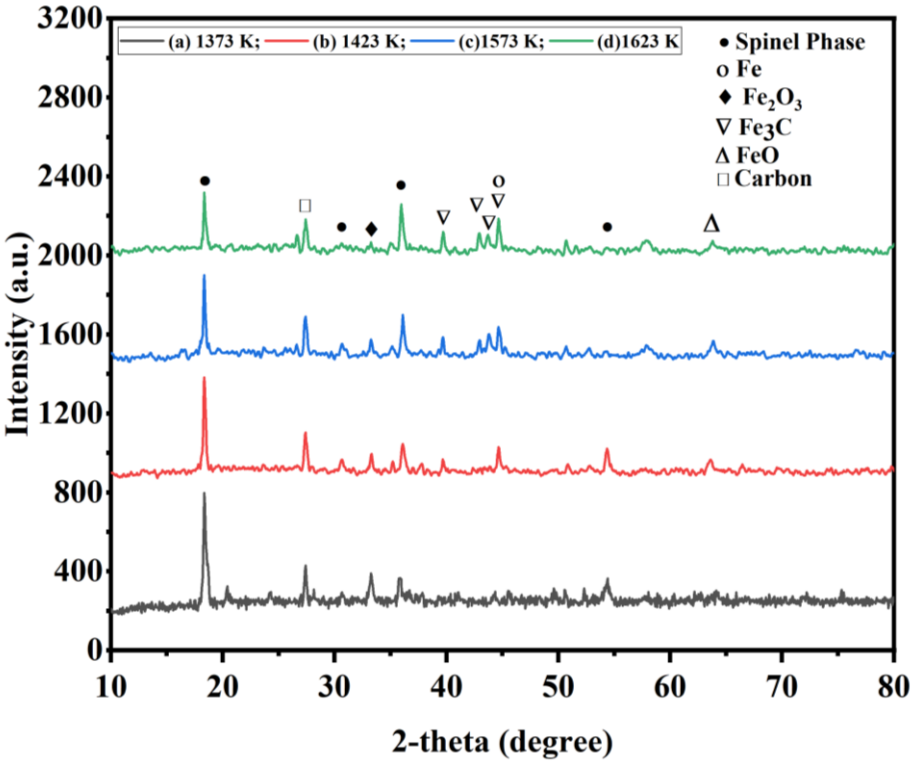

Figure 6A.3.2: XRD Analyses of Reduced Samples at (a) 1373 K, (b) 1423 K, (c) 1473 K, and (d) 1523 K for 2 Hours.

The iron carbide phase and metallic phase appeared in the XRD spectrum at 1523 and 1573 K, respectively. At that temperature, the formation of metallic iron takes place, which shows the metallic phase in the XRD pattern. Fig. 6A.3.3 shows the reduction of chromite briquettes at 1573, 1623, 1673, and 1723 K. A metallic phase is detected in the XRD spectrum at 1573 K as a new phase. As the reduction increases, increases the intensity of this phase. The chromium iron carbide $(Cr, Fe)_7C_3$ phase is observed in the sample, which is reduced at 1623 K. Thus, it can be concluded that chromium oxide began to reduce after 1573 K. As the temperature increases, the metallic and chromium-iron carbide phases appear in the XRD spectrum. The carbide phase is seen to decrease at higher temperatures, indicating that it represents the intermediate phase created in the process of chromite reduction. Temperature higher than 1673 K, $(Cr, Fe)_7C_3$ may act as a reducing agent so it converts to metallic phase. As the temperature increases, the area of the unreacted spinel phase decreases. At high temperatures, the metallic phase dominates the XRD pattern. The phases that appeared at different reducing temperatures are summarized in Table 6A.3.2.

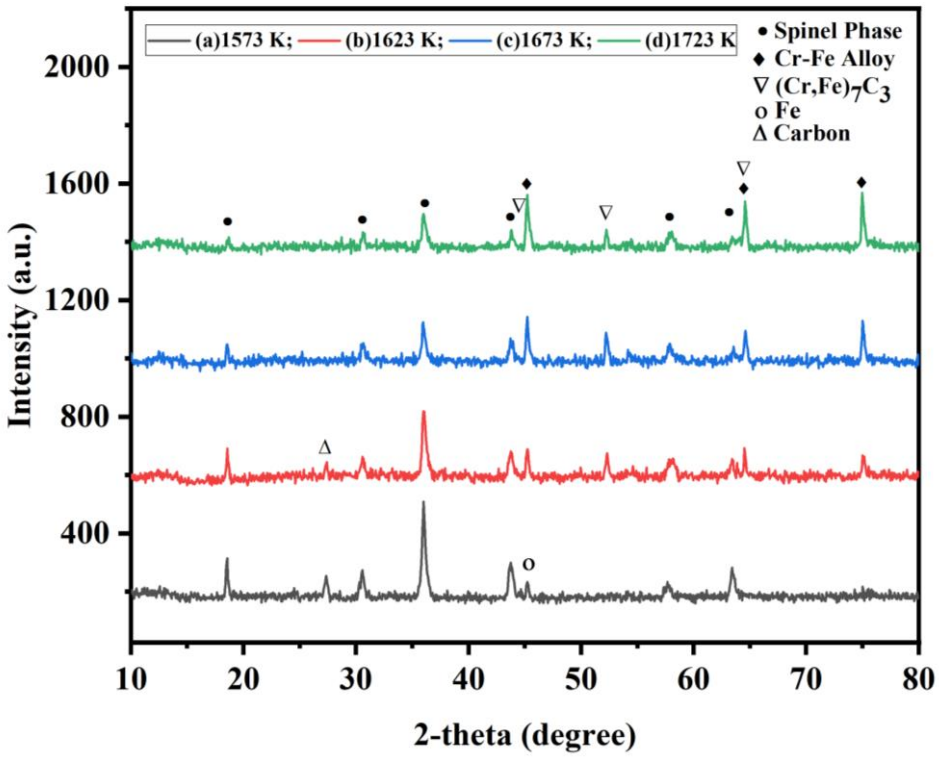

Figure 6A.3.3: XRD Analyses of Reduced Samples at (a) 1573 K, (b) 1623 K, (c) 1673 K, and (d) 1723 K for 2 Hours.

Table 6A.3.2: Phases Appeared in Reduced Briquettes after 120 Minutes of Reduction Time at Different Temperatures.

Temperature (K)	Reduction Time (min.)	Identified Phase
1373	120	Spinel Phase, Carbon, Fe_2O_3
1423	120	Spinel Phase, Carbon, Fe, Fe_2O_3,Fe_3C, FeO
1473	120	Spinel Phase, Carbon, Fe, Fe_2O_3,Fe_3C, FeO
1523	120	Spinel Phase, Carbon, Fe,Fe_3C, FeO
1573	120	Spinel Phase, Carbon, Fe
1623	120	Spinel Phase, Carbon, Cr-Fe Alloy, $(Cr,Fe)_7C_3$
1673	120	Spinel Phase, Cr-Fe Alloy, $(Cr,Fe)_7C_3$
1723	120	Spinel Phase, Cr-Fe Alloy, $(Cr,Fe)_7C_3$

6A.3.4.3 SEM Analysis of Reduced Briquettes

Fig. 6A.3.4 shows the SEM images of the reduced samples at 1373, 1423, 1473, and 1523 K after 120 minutes. At 1373 K, the reduced sample contained a mixture of carbon and chromite.

The morphology of reduced chromite ore changes from raw chromite ore, as shown in Chapter 5, Section 5.3.4. Fig. 6A.3.4 (B) shows the formation of a small, spherical-shaped metallic phase on the surface of chromite ore at 1423 K. These spherical morphologies indicate that at that temperature, metallic iron starts to form. Small, spherical metallic irons are agglomerated and become depleted from the chromite ore at 1473 K. The formation of metallic iron is observed in the chromite briquettes reduced at 1523 K, which is shown in Fig. 6A.3.4 (D). The formation of iron in chromite surface depends upon reducing temperature.

.

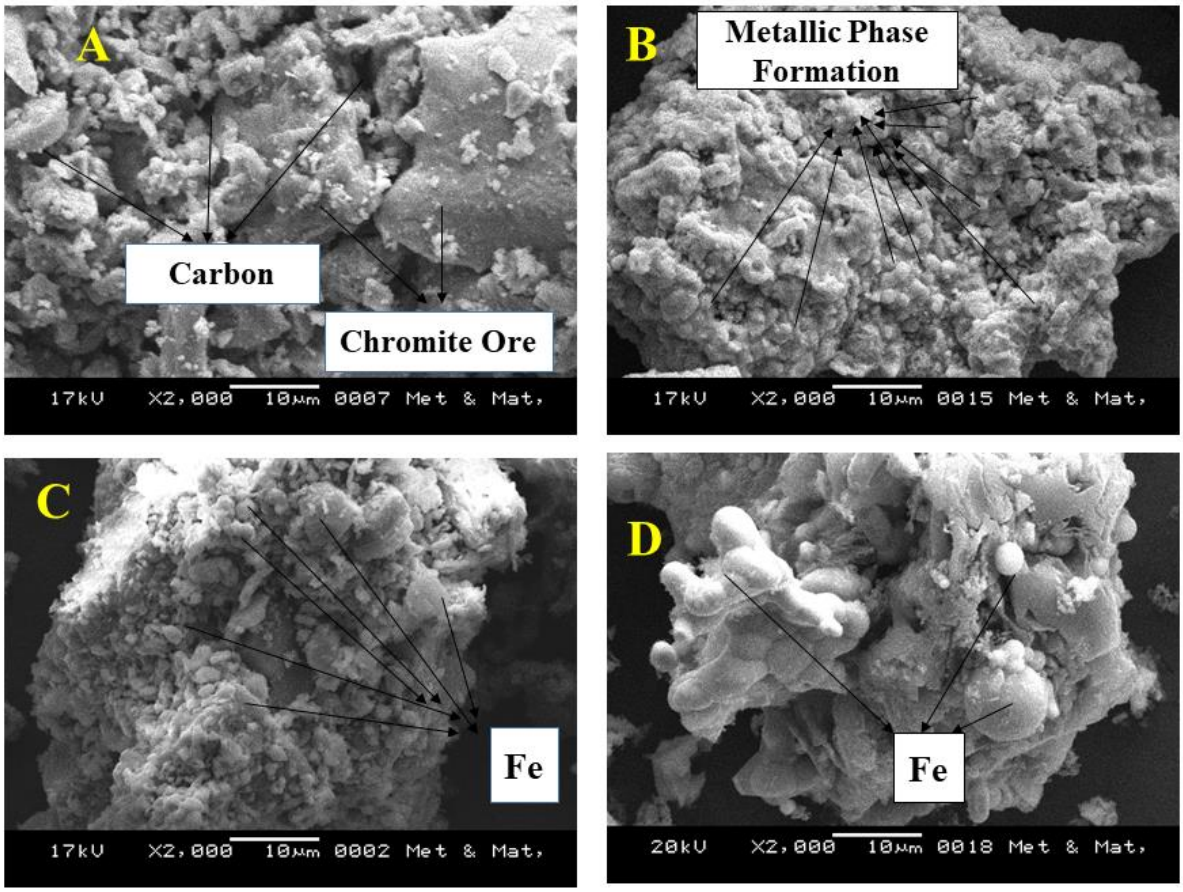

Figure 6A.3.4: SEM Image of Reduced Chromite Briquettes After 120 Minutes at (A) 1373 K, (B) 1423 K, (C) 1473 K, and (D) 1523 K.

Fig. 6A.3.5 shows the SEM picture of the reduced chromite ore at 1723 K for 120 minutes. The images have been taken at various magnifications, denoted by the numbers 6A.3.5A to 6A.3.5F. Porous surface structure can be observed at lower magnifications (6A.3.5A, 6A.3.5B, and 6A.3.5C). In high-temperature reduction, structural rearrangement or gas evolution prompts the development of pores during reduction. At 1723K, the reduced

briquettes' surface morphology is different from that of the original ore. The surface morphology shown in Figs. 6A.3.5D, 6.A.3.5E, and 6A.3.5F is at a higher magnification. The image shows the major metallic phase's association with the chromite surface. Agglomeration of iron and chromium during the reduction process causes the formation of the metallic phase.

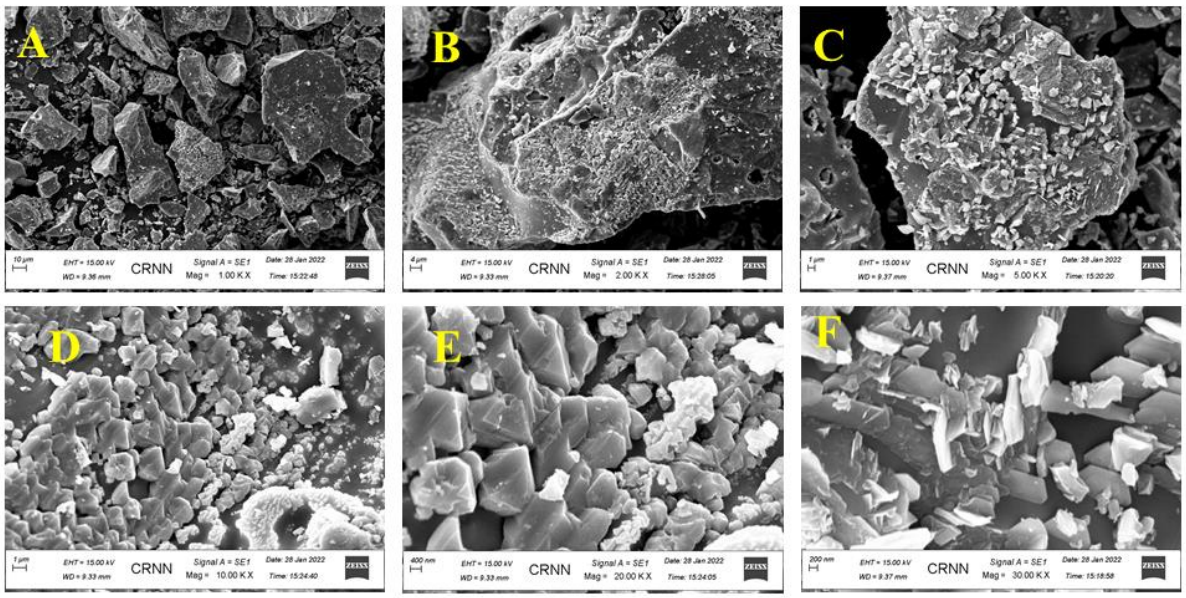

Figure 6A.3.5: FESEM Image at Different Magnifications of Reduced Chromite Briquettes after 120 Minutes at 1723 K.

6A.3.4.4 Phase Transformation during the Reduction of Chromite Briquettes

It is clear from the study of the XRD pattern of reduced chromite ore at different temperatures, that the iron oxide in the ore is initially reduced during carbothermic reduction. Iron carbide intermediate occurs as a result of the reduction of iron oxide. Table 6A.3.2 shows the chromite briquettes' observed carbothermic reduction phase. The table indicates the formation of metallic iron and iron carbide begins at 1423 K. The peak of Fe_2O_3 gradually decreases to produce iron as the reduction temperature rises. At 1573 K, the iron carbide phase is not present in the XRD pattern, but a predominant metallic phase is observed. This indicates that a significant portion of the iron in the ore is reduced at that temperature. The mechanism of iron oxide reduction in chromite ore at 1573 K is represented by equations 1 through 9. Magnetite is formed during the reduction process, which subsequently reduces to wustite and iron.

$$3Fe_2O_3 + C = 2Fe_3O_4 + CO \quad (1)$$

$$Fe_3O_4 + C = 3FeO + CO \quad (2)$$

$Fe_2O_3 + C = 2FeO + CO$ 3

$Fe_2O_3 + 3CO = 2Fe + 3CO_2$ 4

$Fe_3O_4 + 4CO = 3Fe + 4CO_2$ 5

$Fe_3O_4 + C = Fe_3C + 4CO$ 6

$FeO + C = Fe + CO$ 7

$FeO + CO = Fe + CO_2$ 8

$Fe_3C + FeO = 4Fe + CO$ 9

The XRD spectrum shows the first peak for chromium iron carbide, which corresponds to the reduction of chromite briquettes at 1623 K. It indicates that chromium reduction begins after 1573 K. At high temperatures, chromite undergoes a phase transformation, forming a solid solution containing both iron oxide and chromium oxide. The solid solution is then reduced by carbon and carbon monoxide. Carbides are formed during the chromite reduction process and can function as a reduction agent at high temperatures. The carbon present in the carbides can react with oxides, such as those in chromite ore, to facilitate the reduction process. It is observed that the $(Cr,Fe)_7C_3$ phase exhibits a very high peak intensity at 1673 K, but that intensity decreases at 1723 K. However, compared to 1673 K, the alloying phase's intensity is higher at 1723 K. Thus, it can be concluded that at high temperatures, chromium-iron carbide acts as a reducing agent. Equations 10 to 19 provide a summary of the probable reactions involved in the reduction of chromite at high temperatures.

$2(Mg,Fe)(Al,Cr)_2O_4 + C = Cr_2O_3 + 2MgAl_2O_4 + Fe_2O_3 + CO$ 10

$3FeCr_2O_4 + 17C = Fe_3C + 2Cr_3C_2(s) + 12CO$ 11

$7Cr_2O_3 + 27C = 2Cr_7C_3(s) + 21CO$ 12

$21FeCr_2O_4 + 109C = 7Fe_3C + 6Cr_7C_3(s) + 84CO$ 13

$3FeCr_2O_4 + 16Fe_3C = 2Cr_3C_2 + 51\ Fe + 12CO$ 14

$Cr_2O_3 + Cr_7C_3 = 9Cr + 3CO$ 15

$Cr_7C_3 + 3\ CO_2 = 7Cr + 6CO$ 16

$Cr_2O_3 + 3CO = 2Cr + 3\ CO_2$ 17

$FeCr_2O_4 + 4Fe_3C = 13Fe + 2Cr + 4CO$ 18

$FeCr_2O_4 + 4CO = Fe + 2Cr + 4CO_2$ 19

6A.3.4.5 Degree of Metallization at Different Time & Temperature

In the reduction of chromite ore, the degree of metallization (DOM) is crucial because it shows how much of the ore has been converted into metallic iron and chromium. This DOM is crucial for determining the efficiency of the reduction process and the resulting product quality. In the processing of chromite ore, higher metallization levels typically result in a higher recovery rate of valuable metals like iron and chromium, which improves the economy and product quality. The effect of both temperature and time on the degree of iron metallization is shown in Fig. 6A.3.6. Iron metallization is seen to begin at 1373 K, but the yield is only 3.38%. The iron metallization increases with temperature. It is found that the reduced sample contains 40.68% metallic iron at 1523K for a 120-minute reduction. Fig. 6A.3.6 (B) shows the maximum metallic iron content of 75.71%, which is achieved in the reduced sample at a temperature of 1723K.

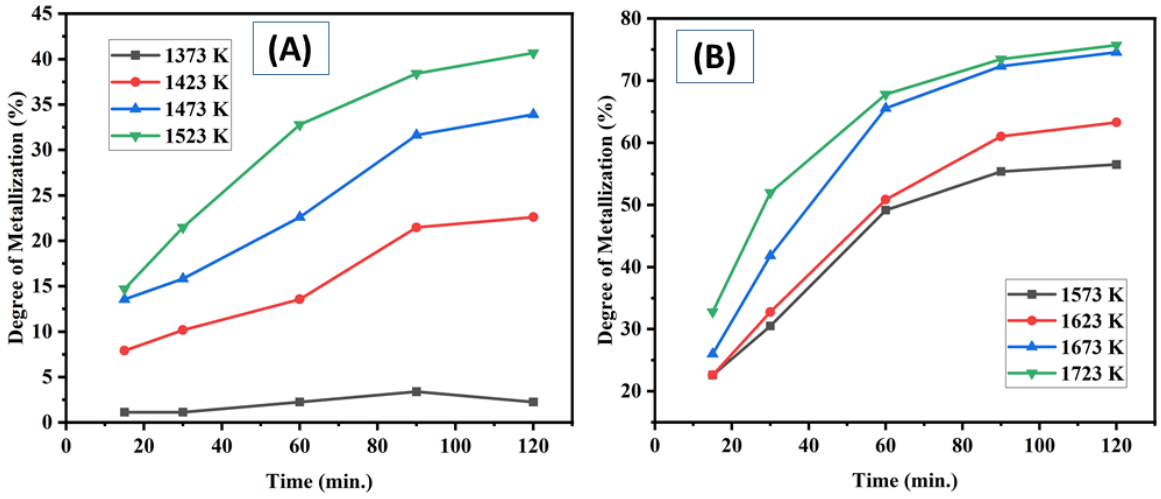

Figure 6A.3.6: Effect of Time and Temperature on the Degree of Metallization of Iron [(A) at Low Temperature and (B) at High Temperature].

However, up to 1523 K, metallic chromium is not detected. Since the sample is reduced to 1573K, metallic chromium is found in it. The effect of temperature and duration on the degree of chromium metallization is shown in Fig. 6A.3.7. At a temperature of 1723K, a maximum metallization percentage of 75.50 is achieved.

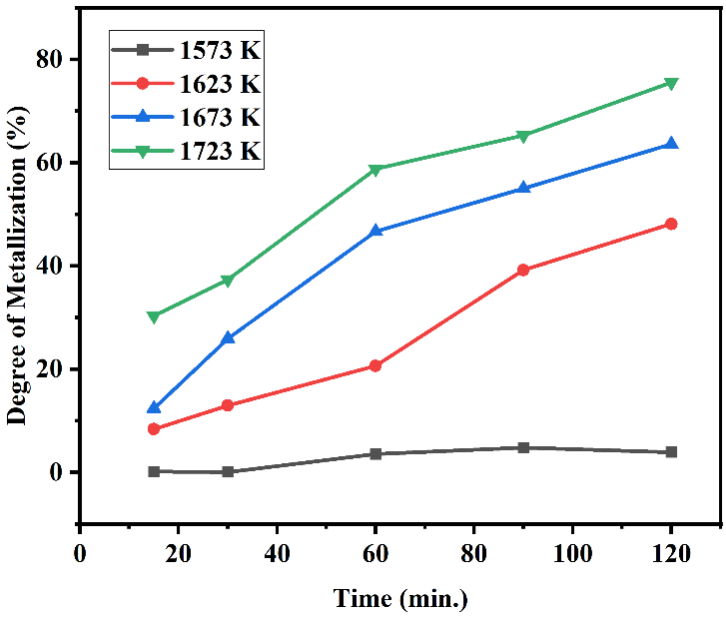

Figure 6A.3.7: Effect of Time and Temperature on the Degree of Metallization of Chromium.

6A.3.4.6 Isothermal Kinetic Study for Reduction of Chromite Briquettes

Reduction kinetic studies are crucial for metallurgy, materials science, chemical engineering, and other industries to improve process efficiency, product quality, safety, and environmental sustainability. That is why the kinetic study of chromite ore reduction has attracted lots of interest. In the present isothermal kinetic study, the term "α" refers to the degree of reduction (DOR) or extent of reduction (EOR).-

$$\alpha = W_t / W_T \qquad 20$$

Where W_T is the theoretical oxygen removed for the 100% reduction of Cr_2O_3 and Fe_2O_3, which are present in the chromite ore, and W_t is the weight loss due to oxygen removal during the reduction of chromite briquettes. Equation 20 represents α as a function of time. Fig. 6A.3.8 shows the experimentally obtained temporal variation of the extent of reduction. It is observed that as the reduction temperature increases, α increases. For a reduction time of 120 minutes, the extent of reduction up to 0.997 is obtained at 1723K. The extent of the reduction calculation is given in Appendix III.

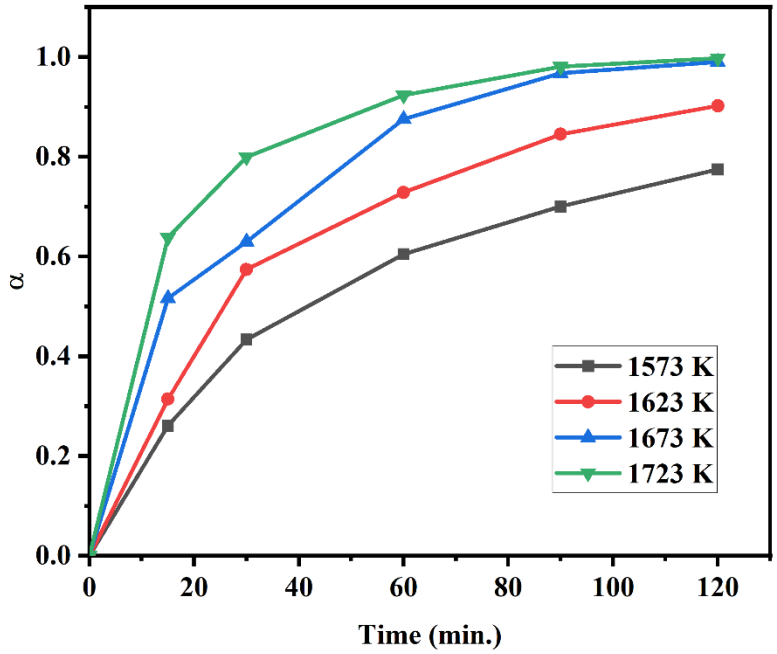

Figure 6A.3.8: Effect of Time and Temperature on the Extent of Reduction.

The functional relationship between the extent of reduction α and t for a particular mechanism is given as:

$$g(\alpha) = k \cdot t \qquad 21$$

where k and t stand for the apparent rate constant and reduction time, respectively. According to Arrhenius' equation, the apparent rate depends on temperature and varies with the rate-controlling regime. In Chapter 1, Section 1.11, g(α) for different rate-controlling regimes is shown. α is a fractional quantity that varies from 0 to 1. The rate-control mechanism is identified through reduced-time analysis of the reaction that takes place during the reduction process.

When α = 0.5, equation 21 is represented as

$$g(\alpha = 0.5) = k \cdot t_{0.5} \qquad 22$$

Where $t_{0.5}$ is the period of time required to achieve a 50% reduction in the experiment. Now divide Eq. 21 by Eq. 22.

$$g(\alpha)/g(\alpha = 0.5) = t/t_{0.5} \qquad 23$$

The term "θ_{model}" refers to the left side of equation 23, while "θ_{expt}" refers to the right side. The dimensionless quantities θ_{model} and θ_{expt} are commonly referred to as reduced times. It is represented as:

$$\theta_{model} = g(\alpha)/g(\alpha = 0.5) \quad 24$$

$$\theta_{expt} = t/t_{0.5} \quad 25$$

From equation 23, it is concluded that

$$\theta_{expt} = \theta_{model} \quad 26$$

θ_{model} is estimated from $g(\alpha)$ and $g(\alpha = 0.5)$, using the equations associated with different rate-controlling mechanisms. θ_{expt} is Obtained from experimental t values for different α and $t_{0.5}$ values.. Based on the experimental results, the computed points (α, θ_{expt}t) should fall on the theoretically calculated α versus θ_{model} plot to have an appropriate rate-controlling regime that operates throughout the entire temperature range.

Thirteen different model predictions are compared with the experimental results. It is observed that at the initial time of reduction, diffusion control models (D1–D6) show a larger deviation from experimental results. The D3 model value lets a good deal with the value obtained experimentally at the final stage of reduction. On the other hand, the nucleation growth model (NG1) and the rate-controlling models (R1-R3) show a reasonable degree of performance during the early stages of conversion, but a deviation is observed later on. The cylindrical contracting geometic (CG2) model predicts the best fit during the initial period. Fig. 6A.3.9 (A) to (D) shows the reduced time plots for the CG2 and D3 models. The figures show that all experimental points (α, θ) at a given isothermal temperature are very close to the theoretical curves of CG2 and D3 at the first and last stages of reduction, respectively. The θexpt versus θmodel curve also confirms the D3 and CG2 models, as represented in Fig. 6A.3.10. The majority of the points are found to fall around the $\theta_{expt} = \theta_{model}$ line. Plots of $g(\alpha)$ against time are investigated for twelve rate-controlling regimes at each temperature to confirm this

mechanism further. Table 6A.3.3 and Table 6A.3.4 show the regression coefficient (R^2) values for the twelve rate-controlling regimes.

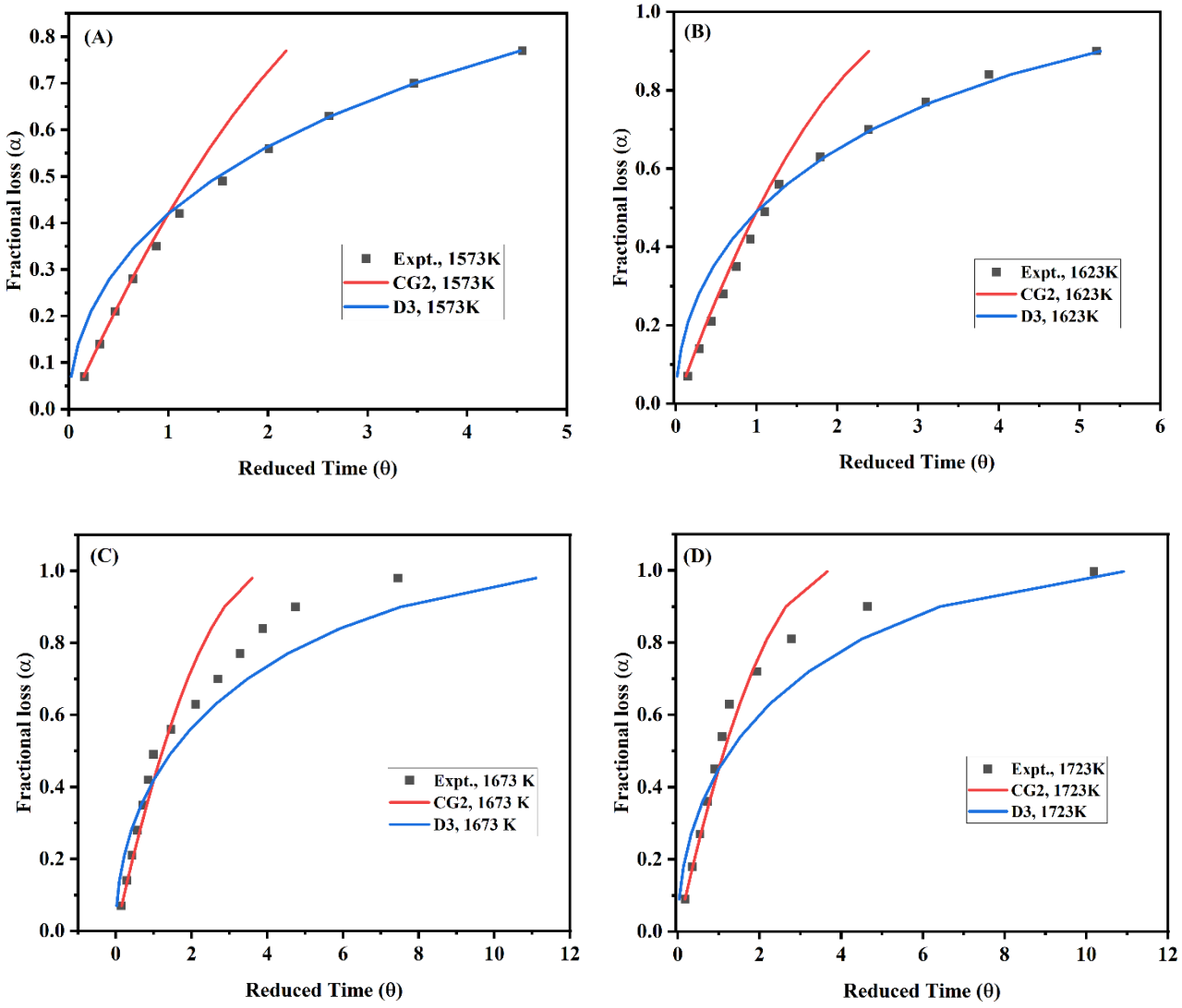

Figure 6A.3.9: Reduced Time Plot at Different Reduction Temperatures Along with Theoretical α vs θ for CG2 and D3 Models at (A) 1573 K, (B) 1623 K, (C) 1673 K, and (D) 1723 K.

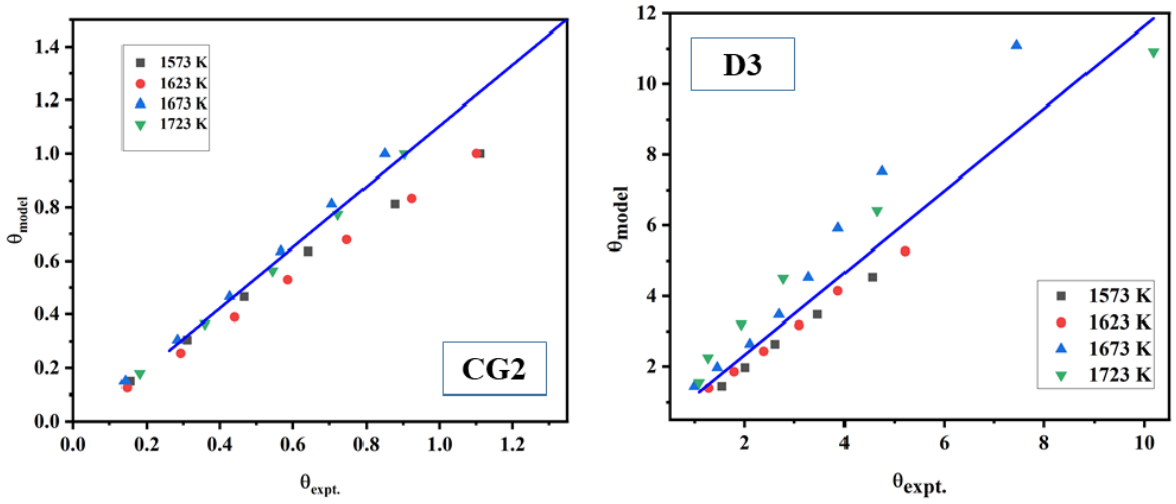

Figure 6A.3.10: θ_{expt} vs θ_{model} Plot for CG2 and D3 Models.

Table 6A.3.3: Regression Coefficient (R^2) for Different Kinetic Models at the Initial Stage g(α)=k.t.

G (α) =k.t.	Model	Temperature				Average
		1573 K	1623 K	1673 K	1723 K	
$[1-(1-\alpha)^{1/2}] = kt$	CG2	0.99782	0.99995	0.9994	0.99921	0.9990
$[1-(1-\alpha)^{1/3}] = kt$	CG3	0.99847	0.9976	0.99892	0.99856	0.9983
$\alpha^2 = kt$	D1	0.99372	0.99315	0.96884	0.96921	0.9812
$\alpha + (1-\alpha)\ln(1-\alpha) = kt$	D2	0.99043	0.98959	0.96118	0.96037	0.9753
$1-2/3\alpha - (1-\alpha)^{2/3} = kt$	D3	0.98909	0.98804	0.95821	0.95687	0.9730
$[1-(1-\alpha)^{1/3}]^2 = kt$	D4	0.98615	0.98455	0.95195	0.94944	0.9680
$[(1+\alpha)^{1/3}-1]^2 = kt$	D5	0.99679	0.99602	0.97694	0.97787	0.9869
$[(1-\alpha)^{1/3}-1]^2 = kt$	D6	0.98615	0.98455	0.95195	0.94944	0.9680
$[-\ln(1-\alpha)]^{2/3} = kt$	NG1	0.99292	0.9923	0.99737	0.99789	0.9951
$[-\ln(1-\alpha)] = kt$	R1	0.99937	0.99879	0.99749	0.99663	0.9980
$[(1-\alpha)^{-1/2}-1] = kt$	R2	0.99973	0.99905	0.9941	0.99199	0.9962
$[(1-\alpha)^{-1}-1] = kt$	R3	0.99889	0.99748	0.98908	0.98507	0.9926

Table 6A.3.2 and Table 6A.3.3 shows that the CG2 and D3 models have the highest R^2 values throughout the beginning and final stages of the reduction process, which are extremely close to 1. At high temperatures, the reduction of chromite briquettes follows a mixed mechanism. Fig. 6A.3.11 shows the $[1-(1-\alpha)^{1/2}]$ vs time plot for the CG2 model at four distinct temperatures during the initial reduction period. On the other hand, Fig. 6A.3.12 shows the D4 mechanism's

$1\text{-}2/3\alpha - (1\text{-}\alpha)^{2/3}$ vs time plot for a later stage of reduction at different temperatures. The slope of the linear fit curve at four distinct temperatures for the CG2 and D3 models can be used for calculating the apparent rate constant (k). Table 3 summarizes the slope of this individual straight line as well as the regression coefficient (R^2).

Table 6A.3.4: Regression Coefficient (R^2) for Different Kinetic Models at the Final Stage g(α)=k.t.

G (α) =k.t.	Model	Temperature				Average
		1573 K	1623 K	1673 K	1723 K	
$[1-(1-\alpha)^{1/2}] = kt$	CG2	0.9940	0.9819	0.9839	0.93567	0.9739
$[1-(1-\alpha)^{1/3}] = kt$	CG3	0.9959	0.9875	0.9921	0.9637	0.9848
$\alpha^2 = kt$	D1	0.9948	0.9915	0.9863	0.9252	0.9744
$\alpha + (1-\alpha)\ln(1-\alpha) = kt$	D2	0.9985	0.9986	0.9976	0.9675	0.9905
$1\text{-}2/3\alpha - (1-\alpha)^{2/3} = kt$	D3	0.9993	0.9997	0.9982	0.9870	0.9961
$[1-(1-\alpha)^{1/3}]^2 = kt$	D4	0.9999	0.9972	0.9827	0.9982	0.9945
$[(1+\alpha)^{1/3}-1]^2 = kt$	D5	0.9918	0.9852	0.9784	0.9080	0.9588
$[(1-\alpha)^{1/3}-1]^2 = kt$	D6	0.9999	0.9972	0.9827	0.9982	0.9945
$[-\ln(1-\alpha)]^{2/3} = kt$	NG1	0.9960	0.9816	0.9917	0.9754	0.9862
$[-\ln(1-\alpha)] = kt$	R1	0.9986	0.9963	0.9980	0.9974	0.9976
$[(1-\alpha)^{-1/2}-1] = kt$	R2	0.9998	0.9975	0.9373	0.9338	0.9671
$[(1-\alpha)^{-1}-1] = kt$	R3	0.9975	0.9772	0.8263	0.8810	0.9205

Table 6A.3.5 shows that at the beginning and final stages of the reaction, the R^2 values for CG2 and D3 are 0.99. Each constituent comes into contact with the others when chromite ore, binders, and coke are combined to make chromite briquettes. During the initial stages of reduction, carbon reduces the oxide in the ore, producing carbon monoxide, carbon dioxide, and metal carbide. The surface chromite molecules in the briquettes are reduced first. In the final stage of reduction, the carbon monoxide produced in the initial stage acts as a reducing gas. Reductant molecules are absorbed and react on the surface of chromite ore in the CG2 mechanism. This proximity lowers the activation energy and decreases the distance between the reacting molecules, which speeds up the reaction in the CG2 mechanism. In a cylindrical, contracting geometry, the reduction process frequently occurs via a diffusion-controlled mechanism. In the D3 mechanism, the reducing gas molecules diffuse from the surface of

briquettes through the gas phase to reach the core of the briquettes, where the cross-section area decreases along the flow direction. This diffusion process allows the reductant molecules to collide with the ore body more frequently, increasing the chances of a successful reaction.

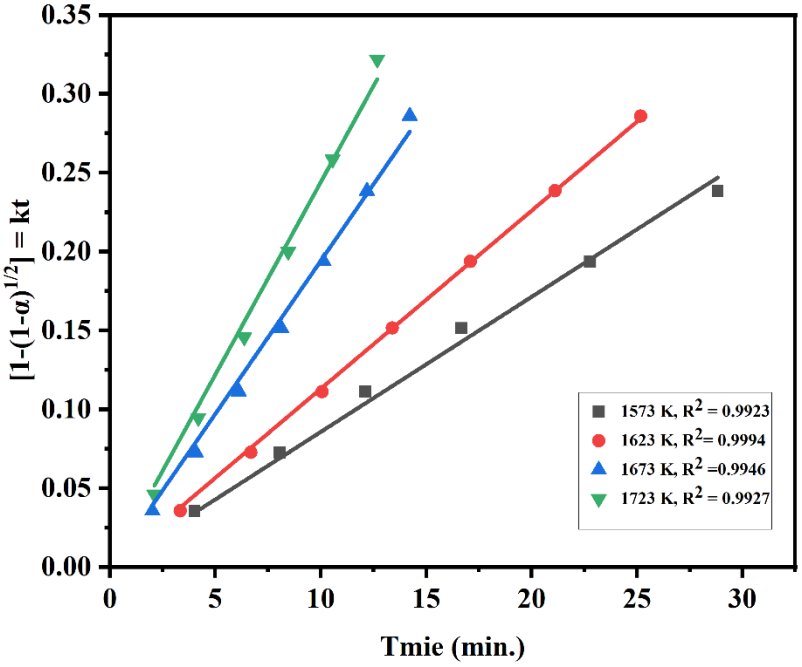

Figure 6A.3.11: [1 - (1 - α)$^{1/2}$] vs Time Plot for the CG2 Model at Different Reduction Temperatures.

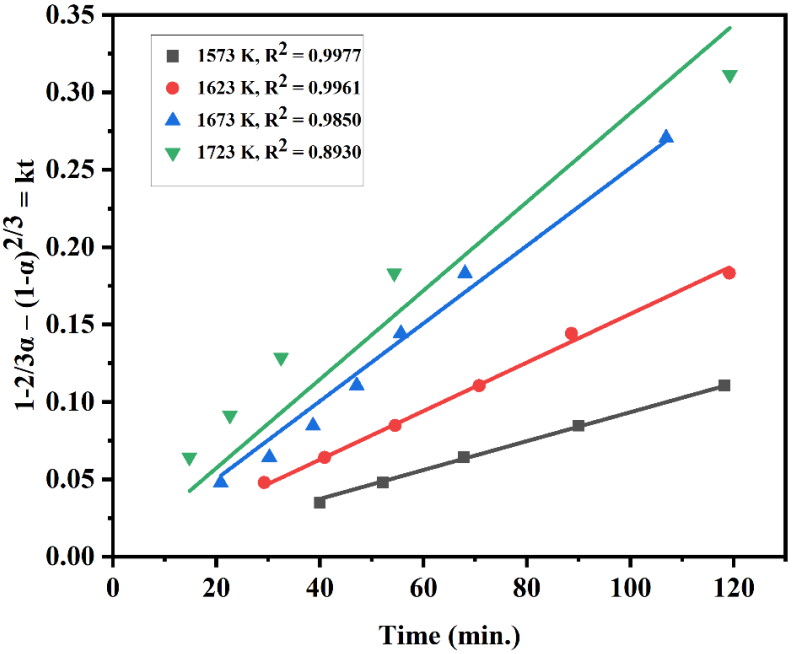

Figure 6A.3.12: [1 - 2/3α – (1 - α)$^{2/3}$] vs Time Plot for the D3 Model at Different Reduction Temperatures.

Table 6A.3.5: Apparent Rate Constant & Regression Coefficient Obtained from Different Plots.

Temperature (K)	Slope(k) (min^{-1}) $[1-(1-\alpha)^{1/2}]$	Regression coefficient (R^2)	Slope(k) (min^{-1}) $[1-2/3\alpha-(1-\alpha)^{2/3}]$	Regression coefficient (R^2)
1573	0.0086	0.9923	0.0009	0.9977
1623	0.0113	0.9994	0.0016	0.9961
1673	0.0194	0.9946	0.0025	0.9850
1723	0.0244	0.9927	0.0029	0.8930

6A.3.4.7 Activation Energy

The activation energy is calculated using the Arrhenius equation. The equation is given below:

$$k = A \exp. -(E_a/RT) \quad (27)$$

Here, k denotes the apparent rate constant, in this equation, A symbolizes the pre-exponential factor, Ea is the activation energy (KJ/mol), R represents the universal gas constant, and T is the reduction temperature. For the CG2 and D3 mechanisms, the ln k vs 1/T plot is shown in Fig. 6A.3.13A & Fig. 6A.3.13B, respectively. The slope of the straight line is used to calculate the activation energy obtained from the Arrhenius plot. For the initial phase of reduction, the calculated activation energy is 165.357 KJ/mol, and for the next phase of reduction, it is 179.36 KJ/mol. Compared to the CG2 mechanism, the diffusion mechanism requires more energy because the reducing gas or molecules must diffuse through the gas phase to reach the solid surface. As a result, in the D3 mechanism, the activation energy is higher compared to the CG2 mechanism.

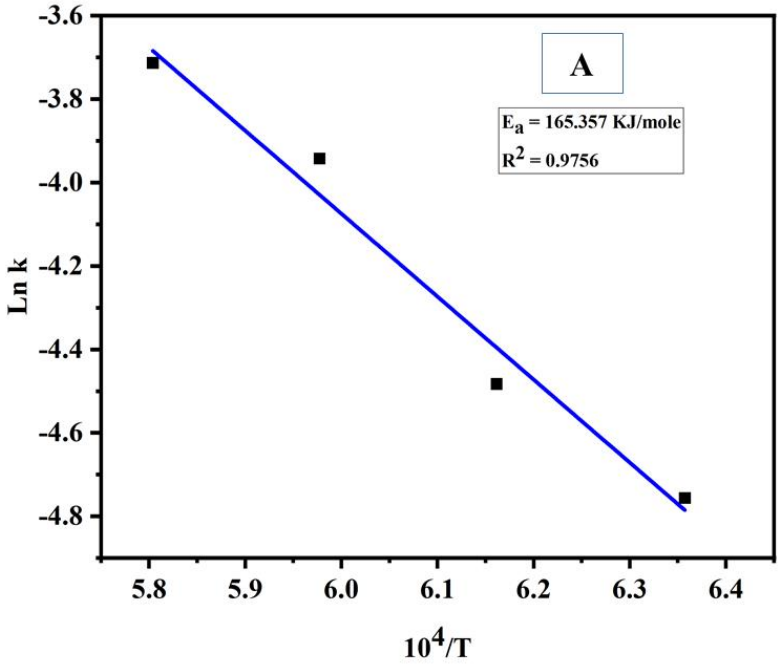

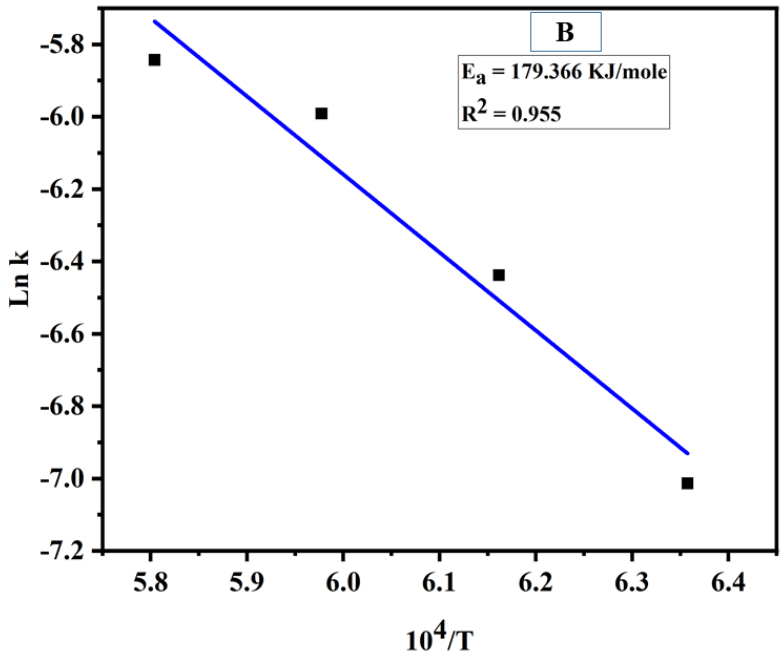

Figure 6A.3.13: Arrhenius Plot for Two Different Parts of the Kinetic Model [(A) for CG2 and (B) for D3].

6A.3.4.8 Smelting of Reduced Chromite Briquettes

The maximum degree of reduction is shown by chromite briquettes reduced for 120 minutes at 1723 K. The level of metallization in the reduced iron briquettes and chromium at that condition is found to be 75.71% and 75.50%, respectively. In a raising hearth furnace, this reduced sample is combined with 3% lime (CaO) and melted at 1873 K. The smelting procedure is carried out in a graphite crucible. The metal and slag generated by this process are analyzed to determine the quality of the final product.

6A.3.4.8.1 XRD Analysis of Ferrochrome

Metallic yield obtained from the smelting process is characterized by XRD which is shown in Fig. 6A.3.14. Metallic chromium and iron phases are the predominant phases present in the XRD pattern along with carbon. The presence of chromium and iron in their metallic form suggests that the ferrochrome is produced during the smelting process. The presence of carbon indicates the possibility of carbon-containing phases, such as carbides, in the ferrochrome.

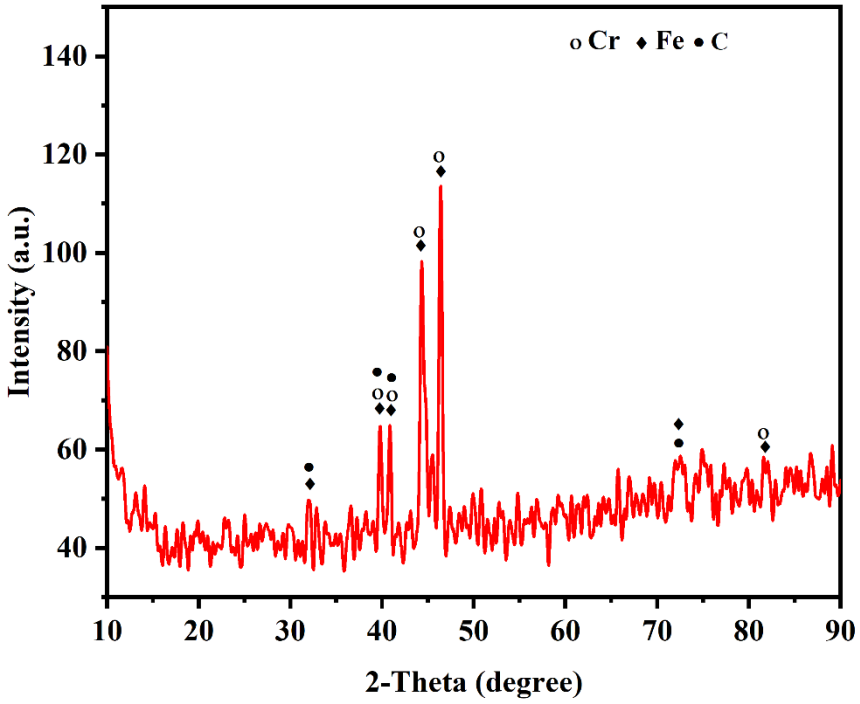

Figure 6A.3.14: XRD Image of Ferrochrome.

6A.3.4.8.2 SEM Analysis of Ferrochrome

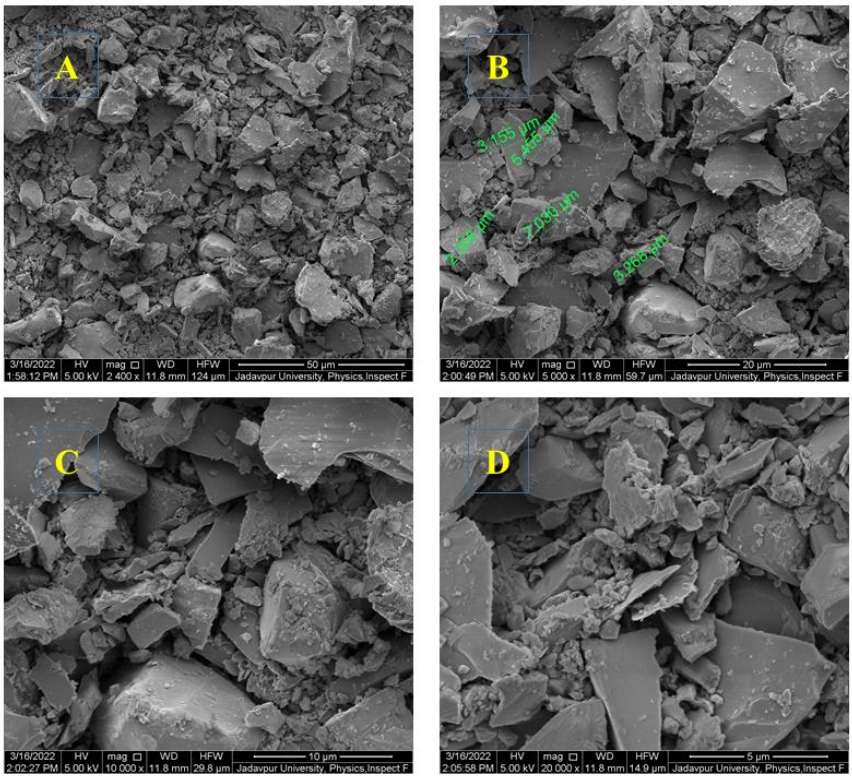

Figure 6A.3.15: SEM Image of Ferrochrome at Different Magnifications: (A) 2400x, (B) 5000x, (C) 1000x, and (D) 20000x.

The SEM image of ferrochrome is depicted in Fig. 6A.3.15. Upon observation, it is evident that there are no pores or cracks present within the structure. The surface of the crystal grain appears smooth, with the shape and size of the grains displaying a highly irregular nature.

6A.3.4.8.3 EDS Analysis of Ferrochrome

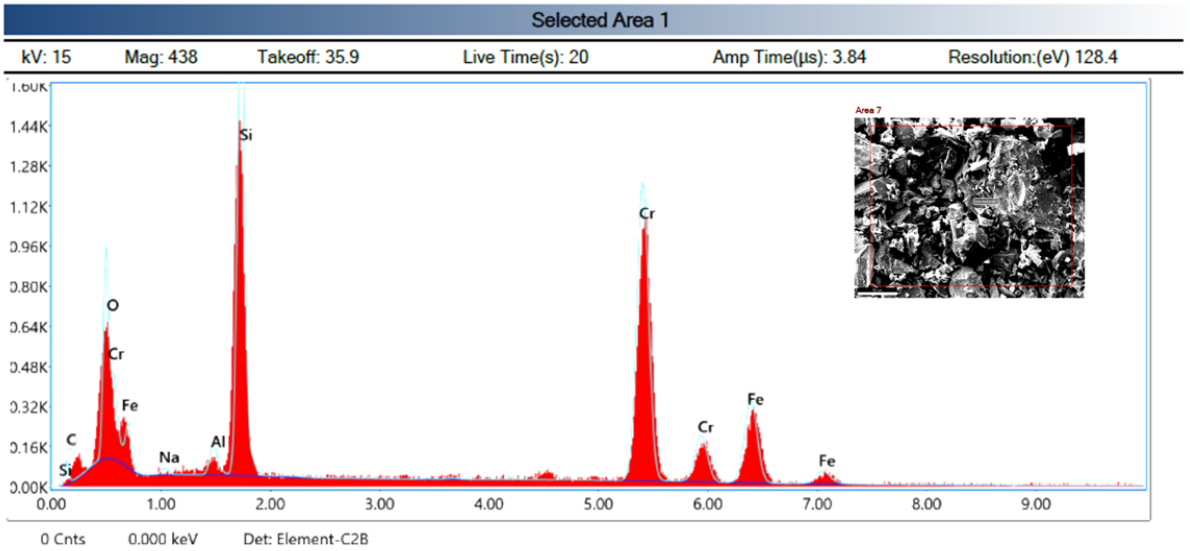

Figure 6A.3.16: EDS Image of Ferrochrome.

Table 6A.3.6: Elemental Composition of Ferrochrome.

Element	Weight %	Atomic %
O K	1.02	2.28
CK	3.96	4.83
NaK	0.47	0.89
AlK	0.82	1.32
SiK	9.63	17.98
CrK	54.06	49.18
FeK	30.03	23.52

EDS image is shown in Fig. 6A.3.16 and the elemental analysis is shown in Table 6A.3.6. EDS analysis reveals that chromium (54.06%) and iron (30.03%) are the primary components in the alloy. This also suggests that the alloy obtained during smelting is ferrochrome, which may contain impurities such as carbon, silicon, and trace amounts of sodium and aluminum. This finding is further supported by ICP-OES analysis, as detailed in Table 6A.3.7, which shows that the produced ferrochrome comprises 52.96% chromium, 28.72% iron, 10.59% silica, and 4.88% carbon.

Table 6A.3.7: ICP-OES Analysis of Ferrochrome.

Element	Cr	Fe	Al	Si	C	S	P
Concentration (%)	52.96	28.72	1.87	10.59	4.88	0.082	0.010

6A.3.4.8.4 XRD Analysis of Ferrochrome Slag (FCS)

The different oxides found in the ore and flux combine to form the molten slag phase in the process of reducing the chromite ore. The principal constituents of the slag are silica (SiO_2), alumina (Al_2O_3), lime (CaO), magnesia (MgO), iron, and chromium oxide. These components are present in the slag in an extremely complex manner. The complex structure is also caused by the chromium and iron's varying oxidation states, which are present in the slag. Fig. 6A.3.17 shows the XRD analysis of slag obtained during the smelting process. Spinel, forsterite, gehlenite, clinopyroxene, and quartz are the main phases visible in the image. The chemical representations of spinel, forsterite, and gehlenite are (Fe, Mg), (Cr, Al, Fe)$_2O_4$, (Fe, Mg)$_2SiO_4$, and $Ca_2Al_2SiO_7$. The general formula of clinopyroxenes is (Ca, Mg, Fe, Na)(Mg, Fe, Al)(Si, Al)$_2O_6$. In the slag phase, the dominance of various silica phase types is visible. The reason behind it is that silicon forms a very stable compound with aluminium, magnesium, calcium, iron, and chromium.

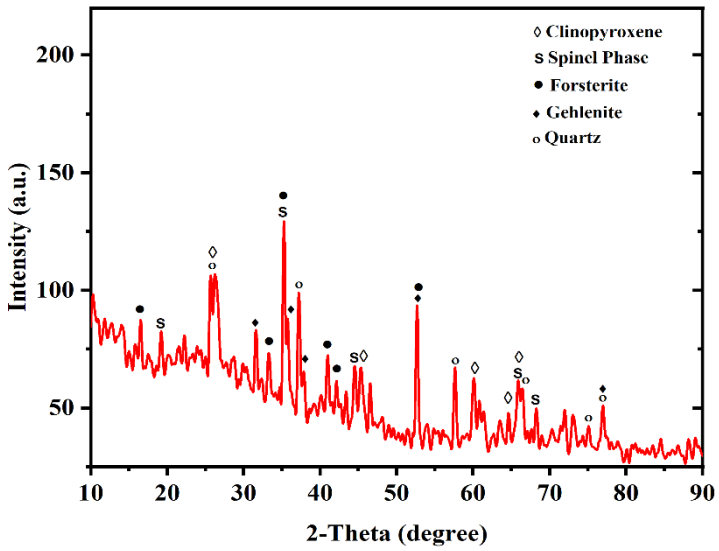

Figure 6A.3.17: XRD Image of Ferrochrome Slag.

6A.3.4.8.5 SEM Analysis of Ferrochrome Slag

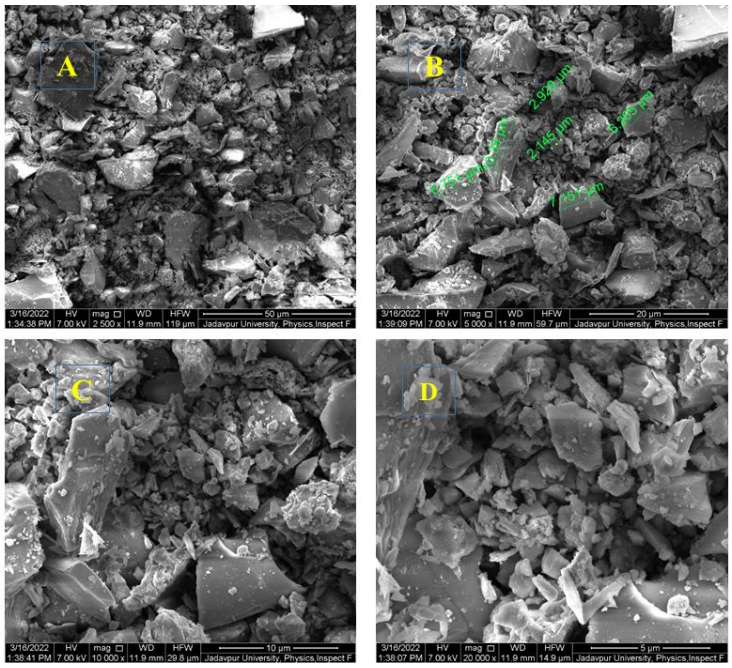

Figure 6A.3.18: SEM Image of Ferrochrome Slag at Different Magnifications: (A) 2500x, (B) 5000x, (C) 1000x, and (D) 20000x.

Fig. 6A.3.18 (A-D) has a SEM image of ferrochrome slag at various magnifications. It is observed that, along with crystalline grains, the image contains a smooth, glassy surface matrix. The shape of the particles is irregular in nature, and some elongated particles are observed in the image. Crystal grains having different diameters are shown in Fig. 6A.3.18 (B).

6A.3.4.8.6 EDS Analysis of Ferrochrome Slag

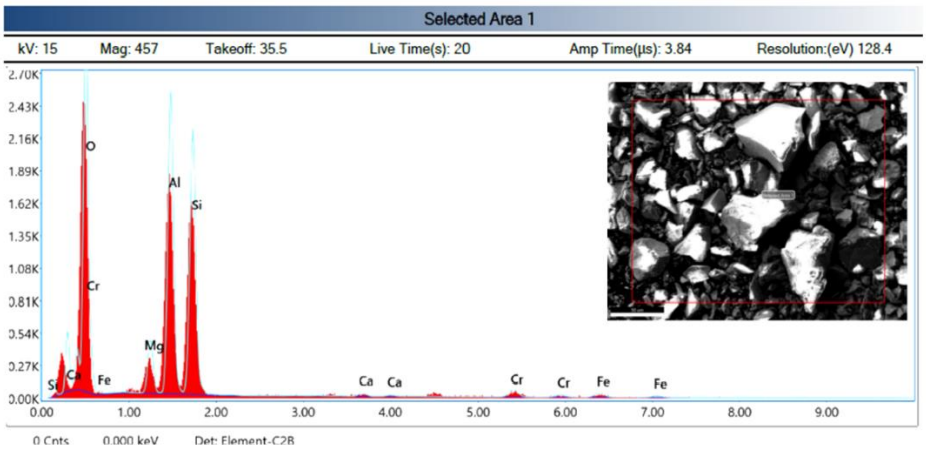

Figure 6A.3.19: EDS Image of Ferrochrome Slag.

Table 6A.3.8: Elemental Composition of Ferrochrome Slag.

Element	Weight %	Atomic %
O K	40.3	54.84
MgK	9.21	7.76
AlK	18.9	16.04
SiK	21.2	16.68
CaK	2.85	1.57
CrK	4.54	1.92
FeK	2.99	1.18

The EDS image and elemental composition of ferrochrome slag are shown in Fig. 6A.3.19 and Table 6A.3.8, respectively. The EDS analysis indicates that silicon (21.2%), aluminum (18.9%), magnesium (9.21%), 4.54% chromium, and 2.99% iron are the principal elements present in the slag. The EDS analysis and XRD analysis both show that silicon (Si) and aluminum (Al) are the main constituents in ferrochrome slag. The spatial visualization of elemental distributions across the surface of the slag sample is shown in Fig. 6A.3.20 (A-I). The SEM image is represented in image 6A.3.20A, the overall elemental mapping is represented in image 6A.3.17B, and the mapping of each element present in the slag is represented by 6A.3.20 (C-I). Each map is associated with a particular element that is found during analysis (e.g., O, Si, Al, Mg, Cr, and Fe). The relative abundance of each element at various locations on the sample surface is represented by the intensity of the colors or shades in the maps. It can be concluded that the distribution of elements within the ferrochrome slag is irregular in nature. ICP-OES analysis of FCS is shown in Table 6A.3.9. According to the results obtained from the ICP-OES analysis, the composition of the alloy is as follows: chromium (Cr) comprises 3.97%, iron (Fe) 1.84%, silicon (Si) 23.35%, aluminum (Al) 21.26%, magnesium (Mg) 4.98%, and calcium (Ca) 3.42%. These findings provide a comprehensive insight into the elemental distribution within the alloy, elucidating its chemical makeup concerning each constituent element.

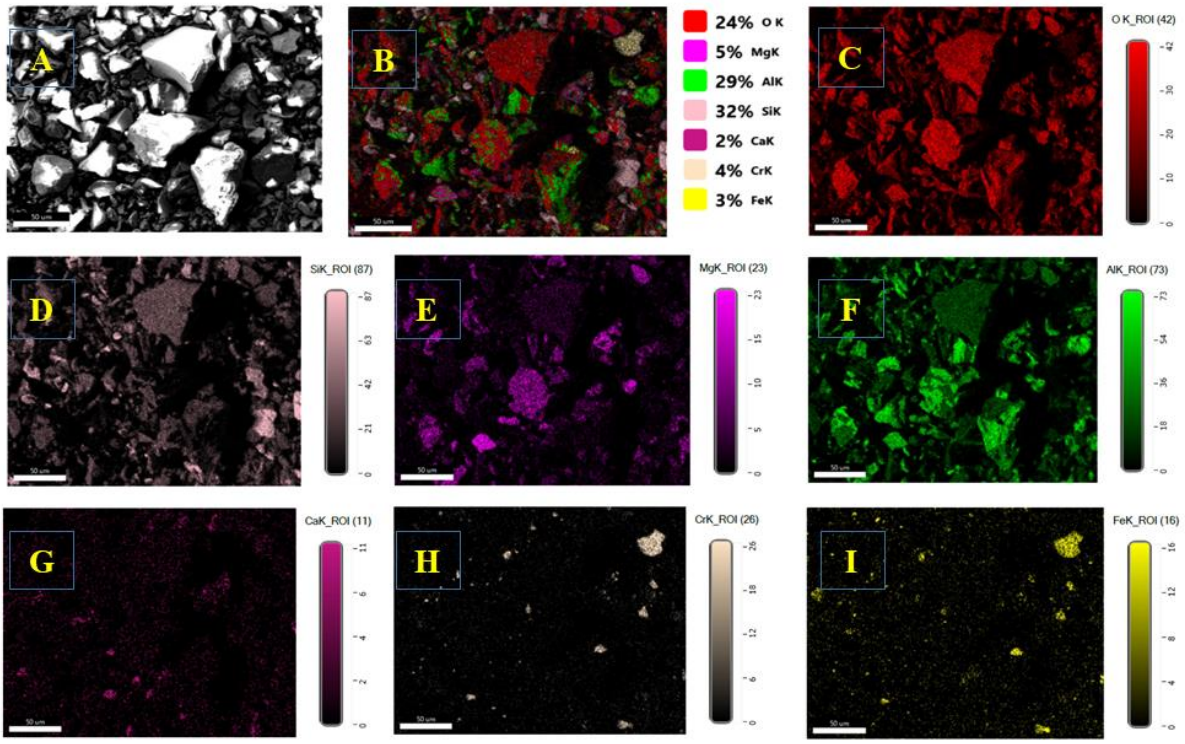

Figure 6A.3.20: Elemental Mapping of Ferrochrome Slag.

Table 6A.3.9: ICP-OES Analysis of Ferrochrome Slag.

Element	Cr	Fe	Si	Al	Mg	Ca
Concentration (%)	3.97	1.84	23.35	21.26	4.98	3.42

6A.3.5 Conclusion

In the isothermal reduction of chromite ore, both reduction time and temperature play very important roles. It can be seen that the extent of reduction is directly proportional to both reduction time and temperature. Chromium reduction initiates at temperatures exceeding 1573K. The initial occurrence of the chromium carbide phase is detected in the reduced chromite ore via X-ray diffraction (XRD) analysis at 1623K. Thus, it is evident that chromium reduction commences after the completion of iron reduction. The degree of metallization indicates that below 1573K, metallic chromium is not present in the reduced sample, whereas the metallization of iron initiates from 1373K. As time and temperature rise, the degree of metallization progressively increases. At 1723K, the maximum degree of metallization for chromium and iron is achieved after 120 minutes of reduction time, reaching 75.50 % and 75.71%, respectively. The presence of metallic fractions in the reduced ore not only enhances

process efficiency but also ensures economic viability in the smelting process. At high temperatures, the reduction initially follows the CG2 mechanism, facilitated by favorable conditions for the carbothermic reduction of chromite to metallic iron and chromium. However, with prolonged reduction time, the thermodynamic stability of Cr_2O_3 increases in comparison to chromite, prompting a transition to the D3 mechanism. This mechanism involves the reduction of Cr_2O_3 by carbon and CO. As the reduction progresses, the kinetic favorability of the CG2 mechanism diminishes due to increased activation energy or alterations in reaction rates. In contrast, the D3 mechanism becomes predominant at these stages. The activation energy obtained for the CG2 and D3 mechanisms is 165.357 KJ/mol and 179.36 KJ/mol, respectively. Ferrochrome is achieved by the smelting of pre-reduced chromite briquettes. As per ICP-OES analysis, the resulting ferrochrome comprises 52.96% chromium and 28.72% iron, accompanied by trace amounts of carbon, silicon, sulfur, and phosphorus. The slag obtained in the smelting process contains significant amounts of silica, alumina, and iron oxides, it can be classified as a siliceous aggregate. The major mineral phases in FCS are silicate and aluminate, with forsterite ($MgSi_2O_4$) found in the olivine group and magnesium aluminate ($MgAl_2O_4$) in the Spinel group. Despite the achievement of the desired chromium and iron content, the obtained ferrochrome remains a crude product requiring further refinement to meet stringent industrial specifications. Further purification processes are necessary to eliminate impurities and fine-tune the alloy composition to meet the precise requirements of stainless steel manufacturers. These refining steps may involve decarburization, desulfurization, and deoxidation techniques to enhance the purity and quality of the ferrochrome.

6A.3.6 Reference

[1] D. M. A. Khan, "Reduction kinetics of chromite pellets," *Mater. Sci. Forum*, vol. 760, pp. 85–94, 2013, doi: 10.4028/www.scientific.net/MSF.760.85.

[2] S. Ranganathan, K. M. Godiwalla, and D. Chakraborty, "Investigation of the kinetics of reduction of chromite ore lumps with large particles of coke," *Trans. Institutions Min. Metall. Sect. C Miner. Process. Extr. Metall.*, vol. 120, no. 2, pp. 71–78, 2011, doi: 10.1179/037195510X12816242170690.

[3] D. Chakraborty, S. Ranganathan, and S. N. Sinha, "Influence of temperature and particle size on reduction of chromite ore," *Innov. Ferro Alloy Ind. - Proc. XI Int. Conf. Innov. Ferro Alloy Ind. Infacon XI*, no. March, pp. 145–152, 2007.

[4] D. Neuschütz, "Kinetic Aspects of Chromite Ore Reduction with Coal at 1200 to 1550°C," *Int. Ferroalloys Congr. Infacon 6*, vol. I, pp. 65–70, 1992.

[5] P. Weber and R. H. Eric, "The reduction of chromite in the presence of silica flux," *Miner. Eng.*, vol. 19, no. 3 SPEC. ISS., pp. 318–324, 2006, doi: 10.1016/j.mineng.2005.07.010.

[6] R. G. Reddy and R. B. Inturi, "Reduction of roast Movat chromite ore with carbon," *Miner. Metall. Process.*, vol. 16, no. 2, pp. 46–50, 1999, doi: 10.1007/bf03402808.

[7] D. Chakraborty, S. Ranganathan, and S. N. Sinha, "Investigations on the carbothermic reduction of chromite ores," *Metall. Mater. Trans. B Process Metall. Mater. Process. Sci.*, vol. 36, no. 4, pp. 437–444, 2005, doi: 10.1007/s11663-005-0034-z.

[8] A. Lekatou and R. D. Walker, "Mechanism of solid state reduction of chromite concentrate," *Ironmak. Steelmak.*, vol. 22, no. 5, pp. 393–404, 1995.

[9] N. LI, J. CHEN, H. YAN, X. mei FENG, H. jun CUI, and J. ying LIU, "Temperature Rise Characteristics of Carbon-Containing Chromite Ore Fines in Microwave Field," *J. Iron Steel Res. Int.*, vol. 15, no. 1, pp. 1–5, 2008, doi: 10.1016/S1006-706X(08)60001-1.

[10] N. S. Sundar Murti and V. Seshadri, "Kinetics of Reduction of Synthetic Chromite With Carbon.," *Trans. Iron Steel Inst. Japan*, vol. 22, no. 12, pp. 925–933, 1982, doi: 10.2355/isijinternational1966.22.925.

[11] P. Gupta, A. K. Bhandary, M. G. Chaudhuri, S. Mukherjee, and R. Dey, "Kinetic Studies on the Reduction of Iron Oxides in Low-Grade Chromite Ore by Coke Fines for Its Beneficiation," *Arab. J. Sci. Eng.*, vol. 43, no. 11, pp. 6143–6154, 2018, doi: 10.1007/s13369-018-3324-x.

[12] R. H. Nafziger, J. E. Tress, and J. I. Paige, "Carbothermic reduction of domestic chromites," *Metall. Trans. B*, vol. 10, no. 1, pp. 5–14, 1979, doi: 10.1007/BF02653965.

[13] C. P. J. Van Vuuren, J. J. Bodenstein, M. Sciarone, and P. Kestens, "The Reduction of Synthetic Iron Chromite in the Presence of Various Metal Oxides - a Thermo-analytical Study ," *Infacon 6*, vol. 1, pp. 51–55, 1992, [Online]. Available: http://md1.csa.com/partners/viewrecord.php?requester=gs&collection=TRD&recid=19 9210420857MD

[14] H. G. Vazarlis and A. Lekatou, "Pelletising-sintering, prereduction, and smelting of Greek chromite ores and concentrates," *Ironmak. Steelmak.*, vol. 20, no. 1, pp. 42–53,

1993.

[15] M. Kekkonen, Y. Xiao, and L. Holappa, "Kinetic study on solid state reduction of chromite pellets," *Int. Ferroalloys Congr. Infacon 7*, no. June, pp. 351–360, 1995.

[16] A. Lekatou and R. D. Walker, "Solid state reduction of chromite concentrate: melting of prereduced chromite," *Ironmak. Steelmak.*, vol. 22, no. 5, pp. 378–392, 1995.

[17] Y. L. Ding and N. A. Warner, "Catalytic reduction of carbon-chromite composite pellets by lime," *Thermochim. Acta*, vol. 292, no. 1–2, pp. 85–94, 1997, doi: 10.1016/s0040-6031(97)00050-6.

[18] Y. L. Ding and A. J. Merchant, "Kinetics and mechanism of smelting reduction of fluxed chromite. Part 1: Carbon-chromite-flux composite pellets in Fe-Cr-C-Si melts," *Ironmak. Steelmak.*, vol. 26, no. 4, pp. 247–253, 1999, doi: 10.1179/030192399677103.

[19] P. Ma, B. Lindblom, B. Björkman, and B. Björkman, "SCANDINAVIAN JOURNAL OF METALLURGY Mechanism study on solid-state reduction in the Fe 2 O 3-NiO-Cr 2 O 3-C system using thermal analyses," *Scand. J. Metall.*, vol. 34, pp. 22–30, 2005.

[20] Y. L. Zhang, Y. Liu, and W. J. Wei, "Carbothermal reduction process of the Fe-Cr-O system," *Int. J. Miner. Metall. Mater.*, vol. 20, no. 10, pp. 931–940, 2013, doi: 10.1007/s12613-013-0817-1.

[21] Y. Man, J. X. Feng, F. J. Li, Q. Ge, Y. M. Chen, and J. Z. Zhou, "Influence of temperature and time on reduction behavior in iron ore-coal composite pellets," *Powder Technol.*, vol. 256, pp. 361–366, 2014, doi: 10.1016/j.powtec.2014.02.039.

[22] R. Sah and S. K. Dutta, "Kinetic studies of iron ore-coal composite pellet reduction by TG-DTA," *Trans. Indian Inst. Met.*, vol. 64, no. 6, pp. 583–591, 2011, doi: 10.1007/s12666-011-0065-x.

[23] P. Gupta, A. De, and C. Biswas, "The Effect of Presence of SiO2, Al2O3 and P2O5 on the Reduction Behaviour of Fe2O3 Nuggets with Coke Fines," *Arab. J. Sci. Eng.*, vol. 41, no. 12, pp. 4743–4752, 2016, doi: 10.1007/s13369-016-2212-5.

[24] Z. hong Wang, G. feng Li, Y. sheng Sun, and M. zhao He, "Reduction behavior of hematite in the presence of coke," *Int. J. Miner. Metall. Mater.*, vol. 23, no. 11, pp. 1244–1251, 2016, doi: 10.1007/s12613-016-1345-6.

[25] C. Biswas, P. Gupta, A. De, M. G. Chaudhuri, and R. Dey, "Kinetic studies on the reduction of iron ore nuggets by devolatilization of lean-grade coal," *Int. J. Miner. Metall. Mater.*, vol. 23, no. 12, pp. 1360–1368, 2016, doi: 10.1007/s12613-016-1359-0.

[26] B. K. Sarkar, S. Samanta, R. Dey, and G. C. Das, "A study on reduction kinetics of titaniferous magnetite ore using lean grade coal," *Int. J. Miner. Process.*, vol. 152, no. February 2018, pp. 36–45, 2016, doi: 10.1016/j.minpro.2016.05.011.

[27] T. Hu, X. W. Lü, C. G. Bai, and G. B. Qiu, "Isothermal reduction of titanomagnetite concentrates containing coal," *Int. J. Miner. Metall. Mater.*, vol. 21, no. 2, pp. 131–137, 2014, doi: 10.1007/s12613-014-0875-z.

[28] J. Tang, M. sheng Chu, F. Li, Y. ting Tang, Z. gen Liu, and X. xin Xue, "Reduction mechanism of high-chromium vanadium–titanium magnetite pellets by H2–CO–CO2 gas mixtures," *Int. J. Miner. Metall. Mater.*, vol. 22, no. 6, pp. 562–572, 2015, doi: 10.1007/s12613-015-1108-9.

[29] D. Yu and D. Paktunc, "Direct production of ferrochrome by segregation reduction of chromite in the presence of calcium chloride," *Metals (Basel).*, vol. 8, no. 1, 2018, doi: 10.3390/met8010069.

[30] X. Hu, *Studies on Carbothermic Reduction of Chromite in the Presence of FeOx*. 2016.

[31] J. Basson and J. Daavittila, *High Carbon Ferrochrome Technology*, Twelfth Edition. Elsevier, 2013. doi: 10.1016/B978-0-08-097753-9.00009-5.

[32] Y. E. Lee, "Ferroalloys: Production and use in Steel-making," *Encycl. Mater. Sci. Technol.*, pp. 3039–3044, 2001, doi: 10.1016/b0-08-043152-6/00544-1.

[33] M. I. Gasik, *Technology of Chromium and Its Ferroalloys*, Twelfth Edition. Elsevier, 2013. doi: 10.1016/B978-0-08-097753-9.00008-3.

[34] M. K. Dash and S. K. Patro, "Effects of water cooled ferrochrome slag as fine aggregate on the properties of concrete," *Constr. Build. Mater.*, vol. 177, pp. 457–466, 2018, doi: 10.1016/j.conbuildmat.2018.05.079.

[35] S. Jena and R. Panigrahi, "Performance assessment of geopolymer concrete with partial replacement of ferrochrome slag as coarse aggregate," *Constr. Build. Mater.*, vol. 220, pp. 525–537, 2019, doi: 10.1016/j.conbuildmat.2019.06.045.

[36] M. Z. Islam, K. M. A. Sohel, K. Al-Jabri, and A. Al Harthy, "Properties of concrete with ferrochrome slag as a fine aggregate at elevated temperatures," *Case Stud. Constr. Mater.*, vol. 15, no. February, p. e00599, 2021, doi: 10.1016/j.cscm.2021.e00599.

[37] M. Mahamaya and S. K. Das, "Characterization of ferrochrome slag as a controlled low-strength structural fill material," *Int. J. Geotech. Eng.*, vol. 14, no. 3, pp. 312–321, 2020, doi: 10.1080/19386362.2018.1448527.

[38] P. N. Ojha, A. Singb, B. Singh, and V. Patel, "Experimental investigation on use of ferrochrome slag as an alternative to natural aggregates in concrete structures," *Res. Eng. Struct. Mater.*, vol. 7, no. 2, pp. 225–244, 2021, doi: 10.17515/resm2021.255ma0202.

[39] O. Gencel, M. Sutcu, E. Erdogmus, V. Koc, V. V. Cay, and M. S. Gok, "Properties of bricks with waste ferrochromium slag and zeolite," *J. Clean. Prod.*, vol. 59, no. November, pp. 111–119, 2013, doi: 10.1016/j.jclepro.2013.06.055.

Chapter-6B

Utilisation of Low Grade Chromite Ore for the Production of Low Carbon Chromium Iron Alloy

6B.1 Introduction

High-chromium alloy steel boasts exceptional metallurgical properties, including enhanced hardenability, corrosion resistance, and strength. The presence of chromium renders the steel self-hardening, augmenting both its hardenability and hardness. When coupled with low carbon content, chromium levels exceeding 12% confer impressive corrosion resistance upon the steel. Conversely, elevated carbon content, when combined with chromium, heightens abrasion and wear resistance. Furthermore, chromium reinforces the steel's strength, particularly at high temperatures. Consequently, ferrochrome, owing to its valuable attributes, finds widespread application in alloy steel production. Such alloy steel varieties are extensively utilized across various sectors for the manufacture of stainless steel, tool steel, high-temperature alloy steel, and super alloys. The conventional metallurgical process utilized in the production of ferrochrome involves the Submerged Electrical Arc Furnace (SEAF), where high-grade chromite ore (containing over 40% Cr_2O_3) undergoes reduction with metallurgical grade petroleum coke. However, following the carbothermic reduction of chromite ore using coke, the residual carbon proves challenging to eliminate without resorting to a second-stage smelting process employing Fe-Si. Consequently, the resulting product from ferrochrome preparation tends to be saturated with carbon (typically ranging between 6-8% w/w), leading to a host of complications in low-carbon alloy production.

6B.2 Literature Review

The majority, over 80%, of global ferrochrome production is allocated to stainless steel manufacturing. Commercially, four primary grades of ferrochromium are produced. These grades are categorized based on their carbon and chromium content, as outlined in Table 6B.1.

Table 6B.1: Types of Ferrochrome.

Sl. No.	**Type**	**Carbon Content (%)**	**Chromium Content (%)**
1	High Carbon Ferrochrome or Charge Chrome	6-9	>60
3	Medium Carbon Ferrochrome	1-4	56-70
4	Low Carbon Ferrochrome	0.015-1	56-70

Chromite and magnesiochromite serve as primary chromium ores, undergoing initial smelting for ferrochrome production. Besides iron and chromium, chromite also contains trace amounts of cobalt and nickel. Leaching techniques have been devised to efficiently extract cobalt and nickel from chromite ore. Additionally, chromite constitutes a significant component in the production of natural refractory materials, ceramics, and electrodes. High-aluminum chromites, in particular, are pivotal in manufacturing chrome-magnesite bricks, a key natural refractory material.

Chromite exhibits a spinel structure wherein the divalent atoms typically comprise iron or magnesium, while the trivalent atom is predominantly chromium. Through carbothermic reduction, chromite is converted into high-carbon ferrochrome. Presently, high-carbon ferrochrome is predominantly manufactured via the submerged electrical arc process. In the current procedure of ferrochrome production employing the submerged electrical arc (SEAF) method, carbon-chromite composite agglomerates are utilized. These agglomerates undergo pre-reduction through a rotary kiln process before being introduced into the SEAF furnace [3-4]. The utilization of pre-reduced chromite ore has demonstrated several significant advantages. Among these benefits are:

(i) Reduction in energy requirements.

(ii) Enhanced utilization of fines through the agglomeration of chromite fines and reductants.

(iii) Improved operational control of the submerged electrical arc furnace (SEAF) [4].

It has been observed that energy consumption inversely correlates with the percentage of chromite pre-reduction. Pre-reduction processes are typically conducted at temperatures around 1623 K, with South African ore samples achieving pre-reduction levels of approximately 90% iron and 50% chromium. According to S. McCullough et al. [5], the incorporation of pre-reduced chromite ore can potentially reduce electrical energy consumption in the submerged arc process by up to 40%. Additionally, research suggests that the rate constant for the reduction reaction experiences an increase as the particle size of both the ore and the suitable reductant reduces. Notably, raw coke demonstrates greater efficacy as a reducing agent compared to devolatilized coke [6].

In a study conducted by Nafziger et al., various reductants including petroleum coke, devolatilized coke (DVC), and graphite are employed for reduction. Results indicated that the highest degree of reduction occurred within the initial 15 minutes at 1623K. Similarly, findings

by D. Chakraborty et al. [6-7] proposed the existence of an optimal time frame and carbon addition, beyond which no further enhancement in reduction is observed.

At elevated temperatures, the reduction of chromium oxide is thermodynamically favored, succeeded by the complete reduction of iron within the chromite spinel structure. Research by O. Soykan et al. [8-9] has indicated that up to 40% reduction, the reduction rate is predominantly influenced by the interfacial area shared between the reduced and unreduced components. The reducibility of chromite ore exhibits an inverse relationship with the Cr/Fe ratio. Iron plays a catalytic role in this process, facilitating chromium reduction by forming iron carbide (Fe_3C). Furthermore, variations in the Cr/Fe ratio lead to discrepancies in crystal structures and gangue materials within the ore; ores with higher and lower Cr/Fe ratios tend to exhibit distinct crystal structures [10].

Previous studies have highlighted several fundamental methods for reducing chromite ore. Among these methods, the carbothermic reaction stands out as the most commonly employed. This can be achieved through:

(i) Solid chromite reduction using either solid or gaseous reactants.

(ii) The direct reaction occurs within the slag or metal phase, where carbon dissolved in the metal phase reduces the dissolved chromite in the slag.

(iii) The dissolved chromite in the slag directly reacts with carbon particles suspended within it. [11-12].

Various additives, including CaO, MgO, Na_2O_2, Al_2O_3, and K_2CO_3, have been found to influence the reduction kinetics of chromite ore by positively impacting the Boudouard reaction. However, in the chromite ore reduction process, MgO and SiO_2 hinder the reduction process. MgO impedes the carbothermic reduction process by forming a more stable phase, $MgCr_2O_4$. Similarly, the presence of SiO_2 results in a decrease in the reduction rate during the metallic chromium process, because of the creation of a liquid phase of $CrO\text{-}SiO_2$. Conversely, the presence of CaO has been observed to enhance reduction kinetics with a decrease in the size of chromite ore particles [3,13]. Considering the catalytic effects of additives, lime has been observed to facilitate the catalytic reduction of carbon-chromite composite pellets. This phenomenon is attributed to lime's incorporation into the spinel structure of chromite, leading to the release of FeO and thereby enhancing the reducibility of the chromite. Additionally, during the reduction of chromite ore, Al_2O_3 accelerates the rate of reduction through the

diffusion of Cr^{3+} ions in the solid phase [13]. M.H. Farjadi and S. McCllough further note that the MgO/Al_2O_3 ratio directly correlates with the Cr_2O_3 content in the slag. A higher MgO/Al_2O_3 ratio in the deposit necessitates higher operating temperatures than those typically employed in the smelting of chromite ores [5,14].

Applying a stoichiometric ionic framework to analyze the spinel, Energy Dispersive X-ray Analysis (EDAX) unveiled a distinct diffusion pattern: Fe^{2+} and Cr^{3+} ions diffused outward from the outer core, whereas Cr^{2+}, Al^{3+}, and Mg^{2+} ions moved inward. Fe^{3+} and Fe^{2+} ions present on the chromite particle surface at the beginning transformed into their metallic state through reduction. Subsequently, Cr^{3+} ions are promptly converted to the +2 oxidation state. Cr^{2+} ions, migrating inward to the particle's core, promoted the reduction of Fe^{3+} ions within the spinel beneath the surface to Fe^{2+} ions present at the junction of the inner and outer cores. Fe^{2+} ions subsequently migrated toward the surface, in this area, they are reduced to the metallic state of iron. Upon complete reduction of iron, Cr^{3+} ions, along with any remaining Cr^{2+}, are reduced to their metallic form, yielding a spinel, $MgAl_2O_4$, free from iron and chromium. After metalization, the iron and chromium subsequently underwent Carburization in the reduction stage, which produces $(Fe, Cr)_7C_3$ [6,15,16].

However, despite the advantages discussed above regarding the use of Submerged Electrical Arc Furnaces (SEAF), it's important to acknowledge that they still contribute to the overall electricity demand. With the ever-increasing demand for electricity, its cost has surged significantly. Additionally, the pre-reduction process, which involves pelletizing and determining the level of pre-reduction, must also be considered from an operational perspective for SEAFs. These factors, including the level of pre-reduction, residual carbon content, and temperature of the feed, have a profound impact on SEAF operations [17].

In our current endeavor, our primary focus is to minimize the reliance on electricity or any other fuels, thus ensuring a low-cost production of ferrochrome. Additionally, we utilize low-grade ores to capitalize on ore availability and reduce production costs. However, it's important to acknowledge that the application of different types of furnaces and production methods for ferrochrome may introduce various factors that need careful consideration.

6B.3 Materials and Methods

Low-grade chromite ores, sourced from Sukinda mines in Jajpur district, Orissa, with a chromium oxide content of less than 30%, are employed in the preparation of ferrochrome. This low-grade ore undergoes crushing to produce fines with a particle size below +75μm for

characterization purposes. The detailed characterization of the raw ore is provided in Chapter 5, Section 5.3. Composite pellets are then created by homogenously mixing the fine chromite ore with bentonite, molasses, and water. A sample mixture weighing 12.5 g is placed into a drum pelletizer to form green pellets. Subsequently, these green pellets are fired at 1473K to enhance their strength. A flow diagram illustrating the process of chromite pellet preparation is presented in Fig. B.1.

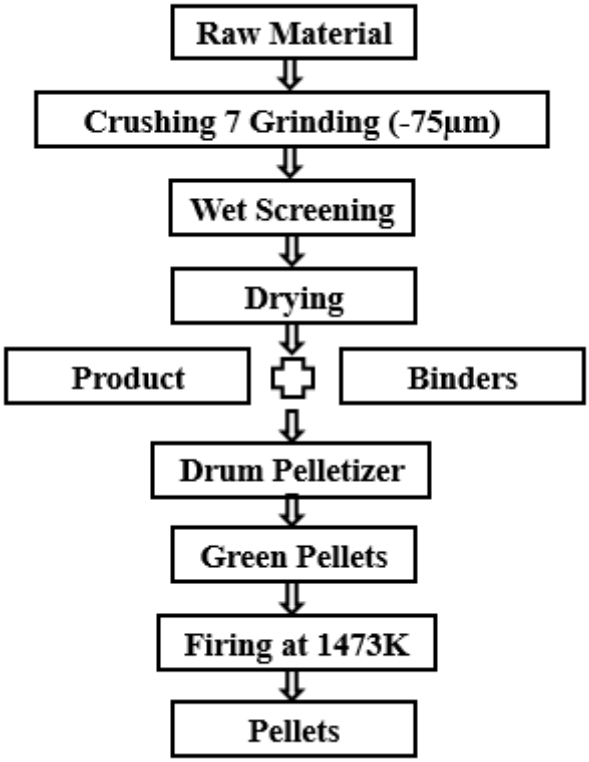

Figure 6B.1: Flow Diagram of Pellet-Making.

Subsequently, these pellets undergo a reduction in a gasification reactor utilizing synergetic gas. The reduced pellets are then crushed and subjected to magnetic separation to isolate the chromite-enriched fraction. All enriched raw materials undergo characterization using Atomic Absorption Spectroscopy (AAS), X-ray Diffraction (XRD), and Scanning Electron Microscopy (SEM).

The segregated non-magnetic portion resulting from the reduction of chromite pellets is further processed through aluminothermic reduction melting to produce ferrochrome, employing magnesium ribbon. At the same time, a portion of 20% of the magnetic fraction is blended with the non-magnetic fraction and undergoes an identical experimental procedure to observe the

separation between slag and metal. The quality analysis of ferrochrome is evaluated based on the extent of reduction of the material.

6B.4 Results and Discussion

6B.4.1 Extent of Reduction of Chromite

The reduction process is conducted in a PID-controlled gasification furnace. Pelletized chromite ore underwent reduction at three distinct temperatures over four different durations. Specifically, four samples are treated at 1373K for durations of 30 mins, 60 mins, 90 mins, and 120 mins, respectively. Similarly, four samples are subjected to treatment at 1423K and another four at 1473K. The maximum extent of reduction is observed at 1473K, with the pellets exposed to the reducing environment for 2 hours. The degree of reduction is summarized in Table 6B.2.

Table 6B.2: Extent of Reduction of the Chromite Ore.

Temperature (K)	Time(mins)	Initial Wt.(gm)	Final Wt.(wt)	Weight loss(gm)	Extent of reduction (%)
1373K	30	7.580	7.287	0.293	3.79
	60	7.624	7.279	0.345	7.54
	90	7.742	7.314	0.428	13.24
	120	7.597	7.108	0.489	18.40
1423K	30	8.178	7.831	0.347	5.94
	60	7.689	7.301	0.388	10.50
	90	6.576	6.108	0.468	22.27
	120	6.067	5.579	0.488	27.53
1473K	30	7.722	7.332	0.390	10.53
	60	7.523	7.054	0.469	17.25
	90	6.826	6.289	0.537	26.53
	120	7.620	6.975	0.645	29.93

From Fig. 6B.2, it is evident that the extent of reduction demonstrates an upward trend, both (i) with rising temperatures and (ii) as duration increases. It's noteworthy that when all experimental parameters are held constant, the extent of reduction exhibits a direct correlation with time and temperature. Notably, reduction at 1473K for two hours yields the highest extent of reduction, thus establishing it as the optimal condition.

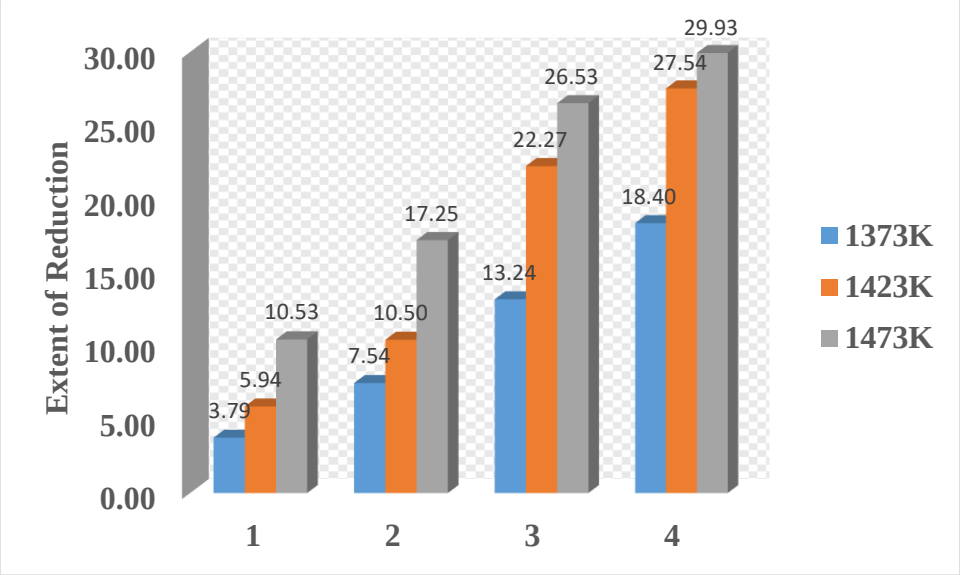

Figure 6B.2: Bar Graph Showing the Extent of Reduction at Different Time Durations: (1) 30 Minutes, (2) 60 Minutes, (3) 90 Minutes, and (4) 120 Minutes.

6B.4.2 Characterization of Reduced Chromite Ore

6B.4.2.1 XRD Analysis of the Reduced Chromite Ore

The X-ray diffraction (XRD) analysis of reduced chromite ore conducted at temperatures of 1373K, 1423K, and 1473K for 120 minutes is shown in Fig. 6B.3. The major phases detected in the reduced sample include spinel, gibbsite, magnetite, wustite, and metallic iron. It is observed that spinel emerges as the predominant phase in the XRD pattern. The presence of metallic iron indicates the initiation of iron oxide reduction at 1373K, with its intensity escalating as the temperature rises. However, within the temperature range of 1373K to 1473K, there is no substantial evidence in the XRD pattern suggesting the reduction of chromium oxide.

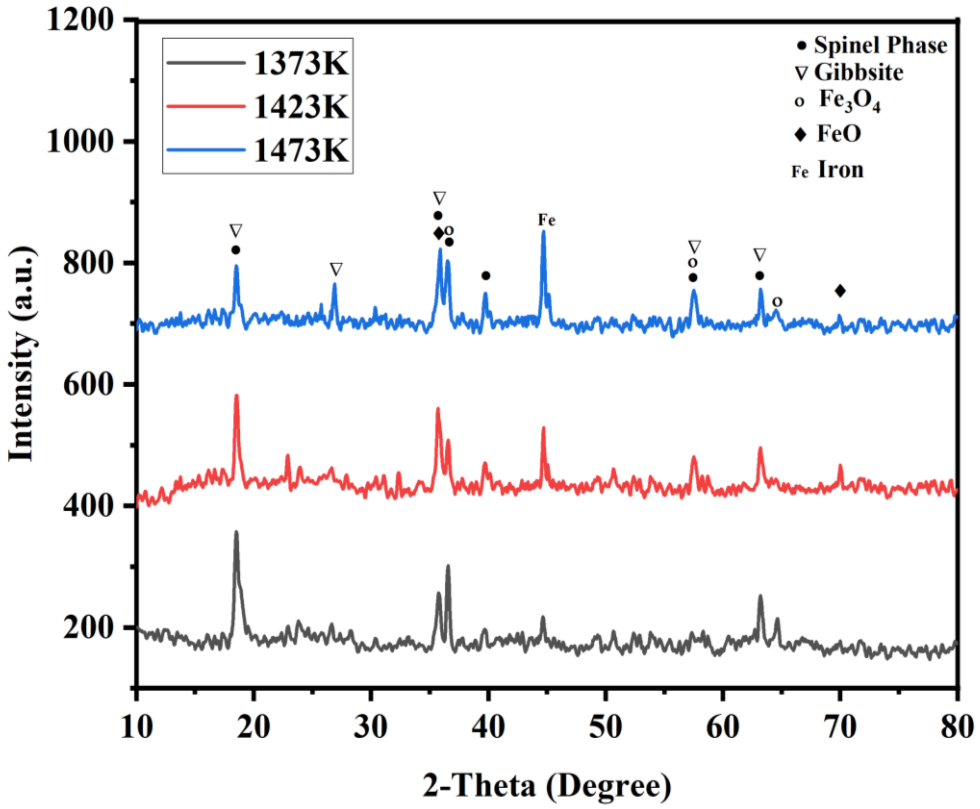

Figure 6B.3: XRD Analysis of Reduced Chromite Ore at 1373 K, 1423 K, and 1473 K for 120 Minutes of Reduction.

6B.4.2.2 SEM Analysis of the Reduced Chromite Ore

The SEM image of reduced chromite ore is shown in Fig. 6B.4. At the image **A** porous structure of the surface is observed. Image B reveals the granular dispersion indicative of oxygen removal from the ore during the reduction process. At a higher magnification image **C** shows that the porous structure is spheroidal and granular in shape.

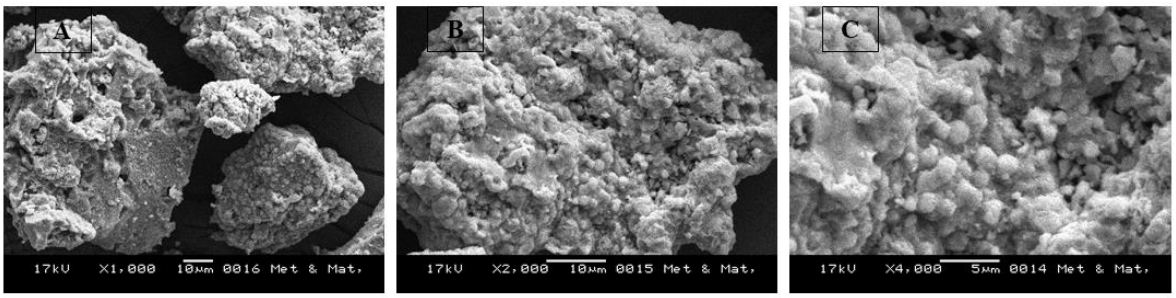

Figure 6B.4: SEM Image of Reduced Chromite Ore at Different Magnifications: (A) 1000x, (B) 2000x, and (C) 4000x.

6B.4.3 Chemical Analysis of Non-Magnetic Fraction by AAS

The optimum reduced chromite ore undergoes magnetic separation using a magnetic separator with a strength of 0.02 Tesla. Following this step, a quantitative analysis of the non-magnetic fraction sample is conducted using Atomic Absorption Spectroscopy (AAS) to determine the percentages of chromium and iron. The fuel utilized for this analysis is a mixture of air and acetylene. The analysis reveals that the chromium and iron percentages in the sample are 25.18% and 21.20% respectively. In raw chromite ore Cr: Fe is 0.775 which has enhanced up to 1.18 after magnetic separation.

6B.4.4 XRD Analysis of Magnetic and Non-Magnetic Fractions

The X-ray diffraction (XRD) patterns of the magnetic and non-magnetic fractions are illustrated in Fig. 6B.5. Analysis reveals distinct mineralogical compositions for each fraction. In the non-magnetic fraction, the predominant phase identified is the spinel phase, while the magnetic fraction exhibits a predominance of metallic phase, accompanied by spinel, gibbsite, and magnetite phases. This suggests a selective enrichment of certain minerals during the magnetic separation process. Specifically, magnetic minerals such as magnetite (Fe_3O_4) or strongly iron and chromium oxides in their magnetic forms are enriched in the magnetic fraction. contributing to its distinctive mineralogical composition.

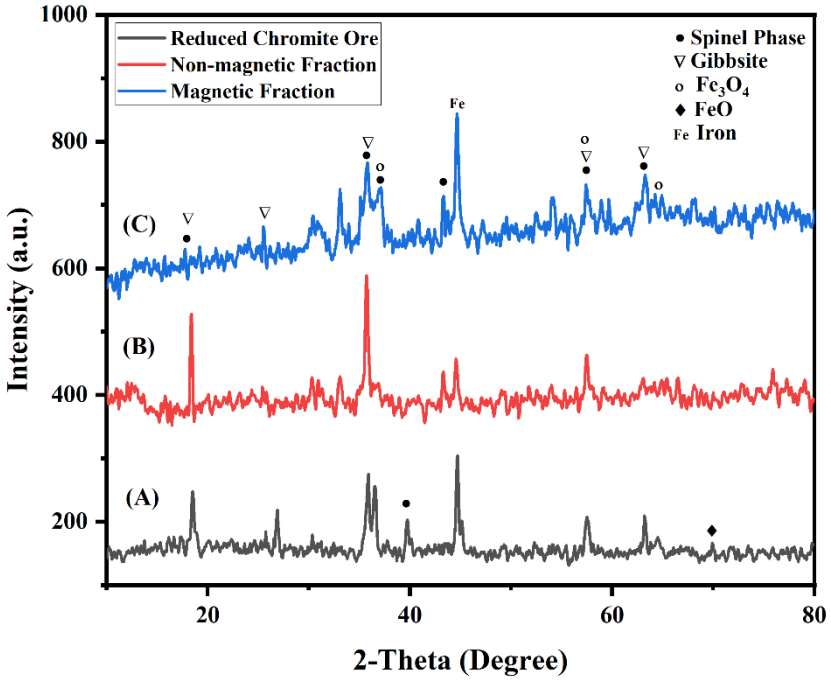

Figure 6B.5: XRD Analysis of (A) Reduced Chromite Ore, (B) Non-Magnetic Fraction, and (C) Magnetic Fraction.

6B.4.5 Product Analysis of Aluminothermic Reduction

The chemical compositions of the products wield significant influence over chromite ore smelting. This influence becomes evident during the smelting process, where it's observed that products obtained from blending 20% magnetic fraction with non-magnetic fraction yield superior metallic output alongside effective slag metal separation. From a thermodynamic standpoint, changes in chromium's activity within these products can profoundly affect the smelting process. Reduced chromium content translates to diminished chromium activity, thus enhancing the overall thermodynamic efficiency of chromite ore smelting.

6B.4.5.1 XRD Analysis of Product

The XRD analysis of the product obtained is shown in Fig. 6B.6. It shows that an iron-chromium alloy is produced. When only nonmagnetic fraction is charged in aluminothermic smelting, $Cr_{1.36}Fe_{0.52}$ is the major phase. However, after blending with a 20% magnetic fraction, $CrFe_4$ became the major phase. The chromium: iron ratio is decreased in the case of blended products. The addition of magnetic fraction increases the volume of the metallic fraction.

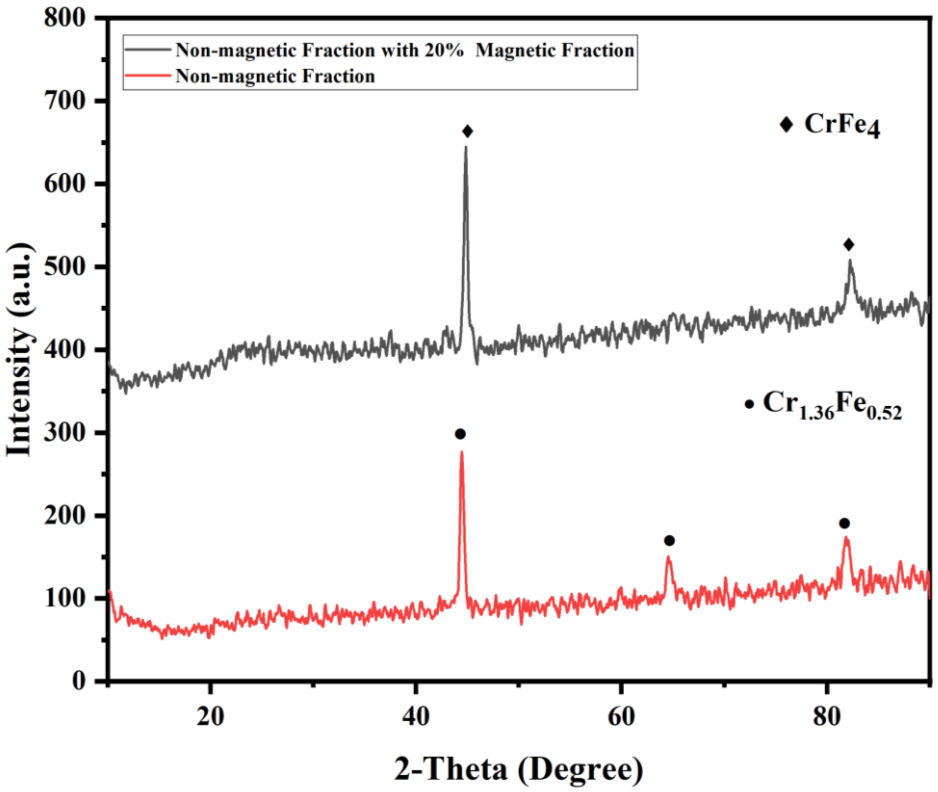

Figure 6B.6: XRD Analysis of Aluminothermic Smelting Product.

6B.4.5.2 SEM Analysis of Product

The SEM image of the smelting product at different magnifications is shown in Fig. 6B.7. The SEM image revealed the lamellar structure of chromium iron alloy. In image **A** the grains are irregular in shape with entrapment of various unreacted aluminium particulates. It is shown in images **B** & **C** as a clear-cut intergranular structure with a variation of lamellar structure. SEM image **D** shows the elongated lamellar structure of ferrochrome with dispersion of particulate within the lamellar structure, vermicular lamellar structure.

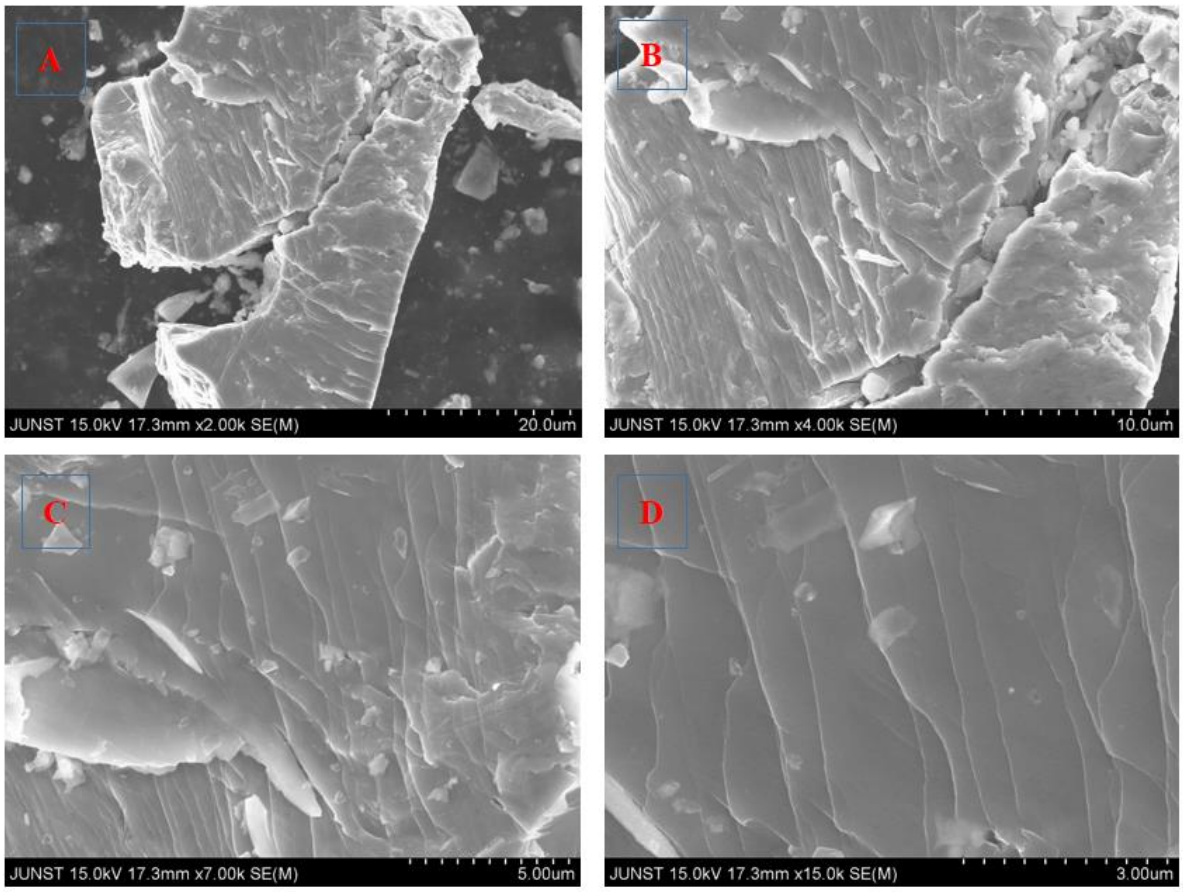

Figure 6B.7: SEM Image of the Chromium-Iron Alloy Obtained by Smelting the Non-Magnetic Fraction.

6B.4.5.3 EDX Analysis of Product

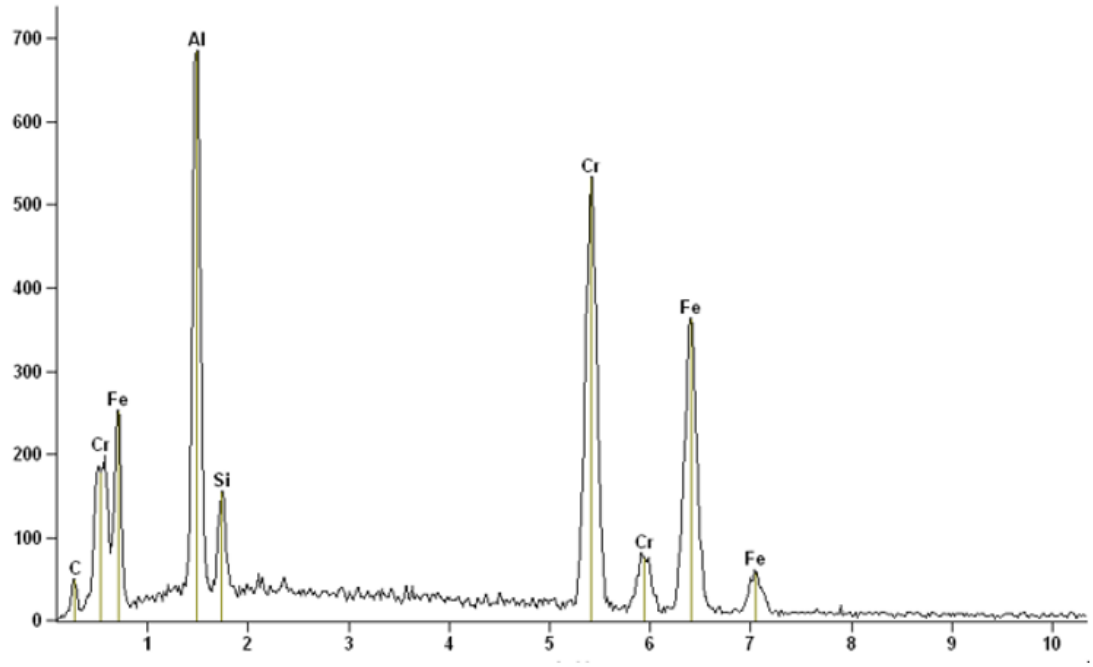

Figure 6B.8: EDX Image of the Smelting Product from the Non-Magnetic Fraction.

Table 6B.3: EDX Analysis of Smelting Product from Non-Magnetic Fraction.

Element	Weight (%)	Atom (%)
C K	3.88	16.58
Al K	11.94	18.13
Si K	1.94	2.82
Cr K	39.51	31.13
Fe K	42.73	31.34
Total	100.00	100.00

The EDX analysis report of the product resulting from the smelting of the non-magnetic fraction is depicted in Fig. 6B.8 and detailed in Table 6B.3. According to the table, the primary constituents of the product are iron (42.73%), chromium (37.51%), and aluminum (11.94%). This alloy, while formed through the smelting process, contains some impurities. Specifically, it is determined that the chromium-to-iron ratio in the crude product is 0.92.". Enhancing the raw material's quality through proper upgrading proves beneficial in reducing the aluminum content both in the charge and the resultant product. Furthermore, employing an appropriate

amount of flux in the charge has led to improved slag metal separation, thereby enhancing metal recovery.

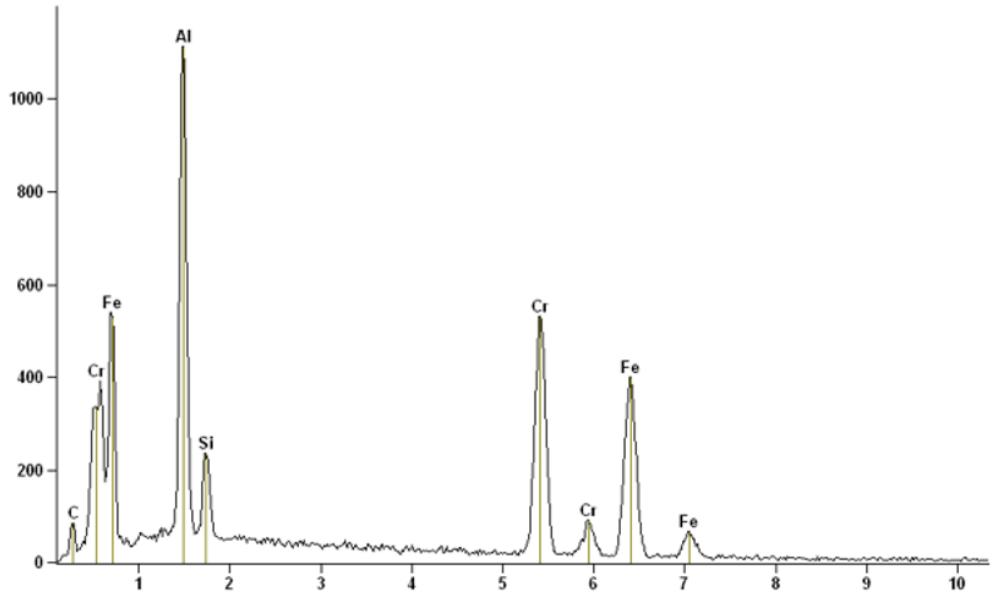

Figure 6B.9: EDX Image of the Smelting Product from the Non-Magnetic Fraction Blended with the Magnetic Fraction.

Table 6B.4: EDX Analysis of Smelting Product from Non-Magnetic Fraction Blended with Magnetic Fraction.

Element	Weight (%)	Atom (%)
C K	7.46	23.38
Al K	8.75	14.90
Si K	2.97	3.97
Cr K	33.95	23.85
Fe K	46.87	33.90
Total	100.00	100.00

The EDX analysis report of the product resulting from the smelting of the non-magnetic fraction (NMF) blended with 20% magnetic fraction (MF) is presented in Fig. 6B.9 and detailed in Table 6B.4. According to the table, the product comprises 46.87% iron, 33.95% chromium, and 8.75% aluminum. Notably, the chromium-to-iron ratio in the product is determined to be 0.72. It's worth noting from physical observations that chromite ore with a lower Cr/Fe ratio tends to yield a superior metallic output.

6B.4.5.4 AAS Analysis of Product

The quantitative analysis of products is conducted via AAS which is shown in Table 6B.5. Results indicate that the product obtained from the smelting of the non-magnetic fraction (NMF) contains 42.02% chromium, 45.32% iron, and 10.86% aluminum. Conversely, in the blended product, chromium comprises 36.64%, iron constitutes 52.06%, and aluminum accounts for 7.52%.

Table 6B.5: AAS Analysis of Smelting Products.

Product Obtained from/ Element	Chromium (%)	Iron (%)	Aluminium (%)	Cr/Fe
NMF	42.02	45.32	10.86	0.92
NMF blend with 20% MF	36.64	52.06	7.52	0.70

6B.4.5.5 Microstructure of smelting products

The microstructure of the smelting product is depicted in Fig. 6B.10. Upon examination, irregular shapes and sizes of grain boundaries are observed in both products. However, the blended product exhibits greater irregularity with its grain boundary. Additionally, the presence of inclusions is indicated by black spots. Image B reveals a two-phase distribution within the grain, featuring a bulk matrix phase and a dispersed phase.

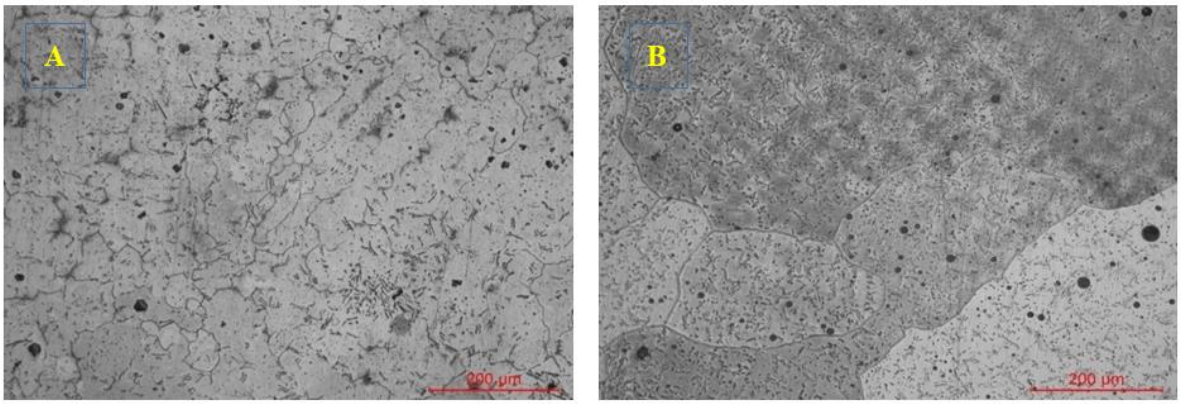

Figure 6B.10: Microstructure of Products: (A) Without Blending and (B) Blending with 20% Magnetic Fraction (MF).

6B.5 Conclusion

The pre-reduction of low-grade chromite ore is effectively achieved in a gasification furnace using lean-grade coal. Maximum extent of reduction (EOR) occurs at 1473K for a 2-hour reduction time. XRD analysis of the reduced chromite ore reveals the intensity of the metallic iron peak increases with higher reduction temperatures. Subsequent magnetic separation following chromite ore reduction enhances the Cr/Fe ratio from 0.775 to 1.18, as evidenced by XRD analysis of the magnetic and non-magnetic fractions. Analysis of the product confirms the production of an iron-chromium alloy. In the absence of blending, the $Cr_{1.36}Fe_{0.52}$ phase is observed, whereas, with 20% blending with the magnetic fraction, the $CrFe_4$ phase emerges. Higher blending ratios result in decreased Cr: Fe ratios. The addition of a magnetic fraction to the charge increases the volume of the metalized phase. SEM imaging reveals a distinct lamellar structure of the ferroalloy. The Cr/Fe ratios in the aluminothermic smelting products are 0.92 and 0.70 in the smelting of non-magnetic and magnetic fractions, respectively. Observations include a two-phase distribution within the grain and numerous inclusions in the product. Further upgrading of the obtained product is necessary, entailing the development of a proper slag phase and reducing aluminum in the charge by substitution with Fe-Si reducer.

6B.6 References

[1] P. J. Bhonde, A. M. Ghodgaonkar, and R. D. Angal, "Various techniques to produce low carbon ferrochrome," in *INFACON XI*, 2007, pp. 85-90.

[2] P. Weber and R. Hurman Eric, "The reduction of chromite in the presence of silica flux," *Minerals Engineering*, vol. 19, no. 3, pp. 318-324, 2006. DOI10.1016/j.mineng.2005.07.010.

[3] J. S. J. Van Deventer, "The effect of additives on the reduction of chromite by graphite: An isothermal kinetic study," Thermochimica Acta, vol. 127, pp. 25-35, 1988. https://doi.org/10.1016/0040-6031(88)87481-1.

[4] C. Takano, A. P. Zambrano, A. E. A. Nogueira, M. B. Mourao, and Y. Iguchi, "Chromite reduction reaction mechanisms in carbon-chromites composite agglomerates at 1773K," *ISIJ International*, vol. 47, no. 11, pp. 1585–1589, 2007.

[5] S. McCullough, S. Hockaday, C. Johnson, and N. A. Barcza, "Pre-reduction and smelting characteristics of Kazakhstan ore samples," *The Twelfth International Ferroalloys Congress Sustainable Future*, pp. 249-262, 2010.

[6] D. Chakraborty, S. Ranganathan, and S. N. Sinha, "Influence of temperature and particle size on reduction of chromite ore," *INFACON XI*, pp. 145-152, 2007.

[7] R. H. Nafziger, J. I. Paige, and J. E. Tress, "Carbothermic reduction of domestic chromites," *Metallurgical Transactions B*, vol. 10B, pp. 5-14, Mar. 1979. DOI https://doi.org/10.1007/BF02653965.

[8] O. Soykan, R. H. Eric, and R. P. King, "Kinetics of the reduction of bushveld complex chromite ore at 1416 °C," *Metallurgical Transactions B*, vol. 22B, pp. 801-810, 1991. DOI https://doi.org/10.1007/BF02651157.

[9] O. Soykan, R. H. Eric, and R. P. King, "The reduction mechanism of a natural chromite at 1416 °C," *Metallurgical Transactions B*, vol. 22B, pp. 53-63, 1991. DOI https://doi.org/10.1007/BF02672527.

[10] A. Atasoy and F. R. Sale, "An investigation on the solid state reduction of chromite concentrate," *Solid State Phenomena*, vol. 147-149, pp. 752-757, 2009. DOI: https://doi.org/10.4028/www.scientific.net/SSP.147-149.752.

[11] W. J. Rankin, "Reduction of chromite by graphite and carbon monoxide," *Trans. Inst. Min. Metall.*, vol. C88, pp. C107, 1979.

[12] S. Ueda, K. Yangiya, K. Watanabe, T. Murakami, R.Inoue and T Ariyama, "Reaction Model and Reduction Behavior of Carbon Iron Ore Composite in Blast Furnace," *ISIJ International*, vol. 49 , no. 6, pp. 827–836, 2009.

[13] Y. Wang, L. Wang, and K. C. Chou, "Effects of CaO, MgO, Al_2O_3, and SiO_2 on the carbothermic reduction of synthetic $FeCr_2O_4$," *Vol. 51*, no. 1, B, pp. 17-24, 2015.

[14] M. H. Farjadi and J. Azari, "Effect of chrome ore quality on ferrochrome production efficiency," *Proceedings: Tenth International Ferroalloys Congress: INFACON X: 'Transformation through Technology*, pp. 103-107, 2004.

[15] O. Soykan, R. H. Eric, and R. P. King, "The reduction mechanism of a natural chromite at 1416°C," *Metallurgical Transaction B*, vol. 22B, pp. 53-63, 1991.

[16] Y. L. Ding and N. A. Warner, "Catalytic reduction of carbon-chromite composite pellets by lime," *Thermochimica Acta*, vol. 292, pp. 85-94, 1997.

[17] Y. L. Ding and N. A. Warner, "Kinetics and mechanism of reduction of carbon-chromite composite pellets," *Iron Making and Steelmaking*, vol. 24, no. 3, pp. 224-229, 1997.

Chapter-6C

Synthesis of Chromium Oxide from Low-Grade Chromite Ore through Oxidative Roasting with Sodium Nitrate and Sodium Hydroxide

6C.1 Introduction

Chromium oxides are widely used in various ways, including as coloring agents in paints and coatings, as additives in concrete and other construction materials, and in situations where long-lasting color is important. In addition to their role in coloring, oxides of chromium find applications in various other fields [1]. They are used as catalysts to facilitate chemical reactions, abrasives for grinding and smoothing surfaces, polishing materials for achieving smooth finishes, and refractories because of their high-temperature tolerance & harsh conditions. In these applications, the focus is not solely on color but also on the specific chemical composition and physical characteristics of the oxides. The demand for chromium-containing salts has been steadily increasing due to their versatile applications [2]. Chromite, abundantly present in the earth's crust, emerges as a cost-effective source for obtaining chromium. It's classified based on the Cr_2O_3 content, with high-grade chromite ore having more than 40% Cr_2O_3 and low-grade chromite ore having less than 40% Cr_2O_3. High-grade chromite ore stands out as a crucial resource for ferrochromium production through pyro-metallurgical methods, predominantly contributing to stainless steel manufacturing. Currently, researchers are endeavoring to produce chromium salts from low-grade chromite ore owing to the escalating demand for high-grade chromite ore in the metallurgical sector.

6C.2 Literature Review

Chromite, an important source of chromium, has historically been processed using pyro-metallurgical methods, such as smelting, to extract chromium. However, the limitations of these processes, including high energy consumption, environmental pollution, and difficulties in treating low-grade ores, have prompted researchers to explore alternative approaches [3], [4]. The environmental impact of traditional pyro-metallurgical processes, characterized by emissions of greenhouse gases, particulate matter, and toxic by-products, has led to increased scrutiny and regulatory pressure. Hydrometallurgical methods offer a cleaner and more environmentally friendly alternative, minimizing air pollution and reducing the carbon footprint of chromium extraction. Hydrometallurgical processes, on the contrary, typically demand lesser energy inputs in contrast to pyro-metallurgical methods, thereby fostering energy conservation and cost-effectiveness [5]. Within this framework, the utilization of leaching agents stands out as a pivotal factor in augmenting process efficiency by facilitating the dissolution of chromite ore at

ambient or moderate temperatures, obviating the necessity for high-temperature smelting procedures. Notably, traditional pyro-metallurgical techniques often prove inadequate in treating low-grade chromite ores due to their refractory nature and suboptimal recovery rates. In contrast, hydrometallurgical processes exhibit superior leaching kinetics and enhanced extraction efficiencies, enabling economically viable recovery of chromium from hitherto untapped low-grade deposits [6]. Furthermore, hydrometallurgical methods afford greater control over reaction conditions, thereby ensuring the production of high-purity chromium compounds with minimal impurities. Consequently, the transition towards hydrometallurgical approaches in chromite ore treatment signifies a momentous paradigm shift propelled by environmental, economical, and technological imperatives. By surmounting the constraints associated with traditional pyro-metallurgical processes, these innovative methodologies promise to revolutionize the chromium extraction industry, heralding a more sustainable and environmentally conscientious future [7].

In the conventional chromate production process, three main steps are involved. First, chromite ore is heated in a process called roasting. During roasting, chromite is mixed with sodium carbonate, limestone, and dolomite additives, and heated to 1100°C in a rotating kiln [8], [9]. Then, it is soaked in water and evaporated to form crystals. Figure 6C.1 illustrates the conventional process for converting chromite ore into chromium oxide (Cr_2O_3). This process converts the chromite ore into sodium chromate (Na_2CrO_4), which is water-soluble, where limestone and dolomite act as both separators and reaction facilitators. Sodium chromate (Na_2CrO_4) transforms sodium dichromate ($Na_2Cr_2O_7$) through a reaction with sulfuric acid. Chemical reactions (1) through (3) outline the key transformations during oxidation roasting [10].

$$4FeO.CrO_3 + 8\ Na_2CO_3 + 7\ O_2 = 8\ Na_2CrO_4 + 2Fe_2O_3 + 8CO_2 \quad (1)$$

$$2MgO.Cr_2O_3 + 4Na_2CO_3 + 3O_2 = 4Na_2CrO_4 + 2MgO + 4CO_2 \quad (2)$$

$$4Na_2CrO_4 + H_2SO_4 = Na_2Cr_2O_7 + Na_2SO_4 + H_2O \quad (3)$$

$$2Na_2Cr_2O_7 + 4H_2SO_4 = 2Cr_2O_3 + 4NaHSO_4 + 2H_2O + 3O_2 \quad (4)$$

Sodium dichromate ($Na_2Cr_2O_7$) is then fused with concentrated sulfuric acid (H_2SO_4) to get Chromium oxide. The reaction involved in this step is shown in equation (4).

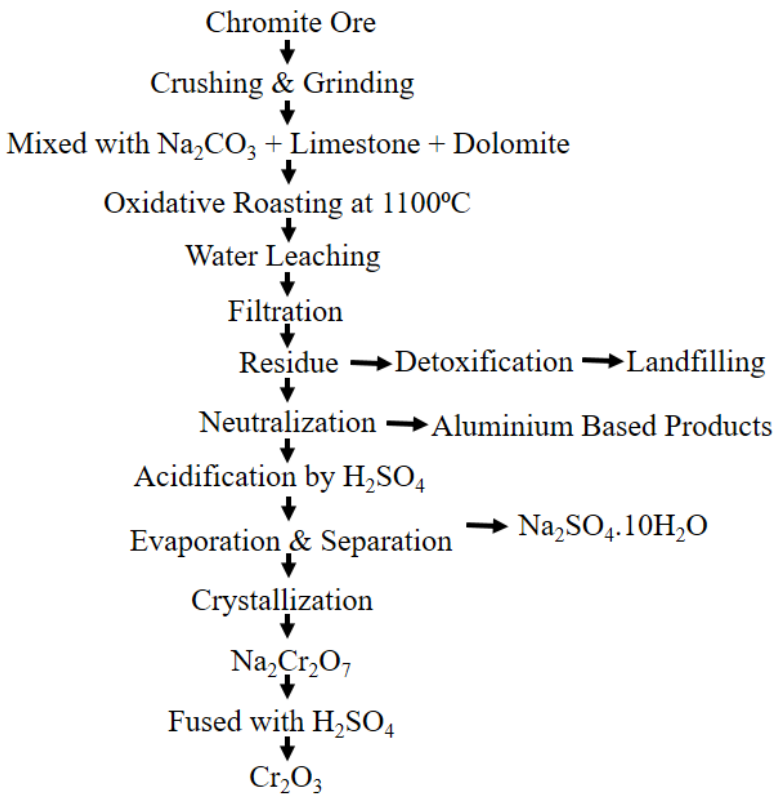

Figure 6C.1: Flow Diagram of the Conventional Process of Chromium Oxide Production [8].

In this methodology, chromate plants emit substantial volumes of chromium-laden residues, dust, and waste gases, precipitating severe pollution challenges. These emissions pose a grave threat to subterranean aquifers, river systems, marine ecosystems, and human well-being [11]. Regrettably, the process yields chromium recovery rates below 85%, with energy efficiency levels around 20% [9].

Several recent approaches have been documented, including techniques like acid and alkali leaching under atmospheric and elevated pressures, along with studies exploring soda-ash roasting [10], [12].In base leaching of chromite ore, sodium hydroxide (NaOH) and potassium hydroxide (KOH) are crucial agents. They facilitate the extraction of chromium from the ore matrix, contributing importantly to the efficiency of the extraction process. Numerous attempts have been undertaken to lower the reaction temperature, such as mechanically activating chromite ore using sodium hydroxide at temperatures below 240°C in an oxygen-pressurized environment (10 bar). This approach resulted in achieving 98% chromium extraction within 120

minutes [3]. Yang Zhang and colleagues studied the high-pressure leaching of chromite ore using NaOH in the presence of $NaNO_3$. Their findings showed that the reaction temperature could be reduced from over 500°C to approximately 400°C. Sodium nitrate ($NaNO_3$) is observed to not be consumed in the oxidation process, yet achieved a chromium yield exceeding 99%. In this method, chromite ore undergoes initial oxidation by $NaNO_3$, resulting in the formation of $NaNO_2$ as a reduction product, which is then re-oxidized to $NaNO_3$. $NaNO_3$ acts as an oxygen carrier, enhancing its efficiency by reducing oxygen mass transfer resistance. Gang Chen studied the leaching of chromite ore using 50% KOH under high oxygen pressure. It is observed that the extraction rate of chromium increased notably with rising temperature and oxygen partial pressure. The leaching process is found to be controlled by surface chemical reactions, according to kinetic analysis. Leaching chromite ore at 220°C for 5 hours under 2.0 MPa oxygen pressure resulted in a chromium recovery yield of 99% [13]. Stephen Parirenyatwaet al. found that at 400 °C, potassium hydroxide (KOH) effectively extracts chromium from chromite ore compared to sodium hydroxide (NaOH). At higher temperatures (700 °C and 1000 °C), similar chromium recovery rates are observed when roasting with either hydroxide. It is observed that at 1000 °C for 2 hours, roasting chromite with sodium and potassium hydroxides resulted in approximately 95% chromium extraction yield, followed by water leaching [14]. Currently, researchers are exploring the extraction of chromium salts using primary amines and ammonium sulfates alternatives to NaOH and KOH [15], [16].

Sulfuric acid is preferred over hydrochloric acid for acid leaching due to the latter's generation of harmful fumes and potential environmental hazards from HCl. Sulfuric acid's primary advantage in leaching processes is its avoidance of chromium(VI)-bearing substances. This process involves treating chromite ore with sulfuric acid in the presence of an oxidant, typically atmospheric oxygen or sodium chlorate, at elevated temperatures. Furthermore, optimizing parameters such as temperature, duration, pressure, acid dosage, and concentration consistently improves chromite leaching efficiency [17], [18], [19]. The temperature typically used in sulfuric acid leaching for chromite ore processing ranges from approximately 140°C to 210°C [20]. For instance, E. Vardar et al. demonstrated that at 210°C, 77% weight of sulfuric acid efficiently leached chromium over 6 hours, and the addition of perchloric acid reduced leaching time by 50% while maintaining the same chromium recovery [20]. The economic viability of the process is a concern due to the cost of perchloric acid. Chengjun Liu et al. studied the sulfuric acid

leaching of low iron content chromite ore, the best conditions are identified as 176°C, a dichromic acid/chromite mass ratio of 0.12, and an 81% concentration of sulfuric acid [21]. They found that the decomposition efficiency correlates strongly with chromite's Fe(II) content, highlighting its significant influence. Dichromic acid functions both as an oxidant and a catalyst in this leaching process. Qing Zhao et al. corroborated these findings, noting that chromite stability decreases notably with higher Fe(II) content in oxidizing solutions. One of the challenges in sulfuric acid leaching is managing the composition of the leachate, which typically includes dissolved iron, magnesium, and aluminum as impurities. These must be separated to obtain pure chromium compounds which is typically achieved through oxalic acid treatment followed by pH adjustment [22].

Chromite ore processing residue (COPR) is a solid waste generated during traditional chromate production using lime and soda ash. It's classified as hazardous due to the presence of compounds having a Cr^{6+} oxidation state, a recognized carcinogenic compound. [22], [23]. Remediation aims to convert Cr(VI) into less toxic trivalent chromium (Cr(III)). Despite this complexity, COPR presents challenges for complete Cr(VI) reduction due to its varying mineral compositions and high pH [24]. Currently, COPR is primarily disposed of, leading to two main issues: persistent leaching of Cr(VI) and uncontrolled expansion, posing significant environmental and geological risks in urban areas worldwide [25]. The process of detoxifying COPR includes using sulfuric acid to regulate its pH as part of the hydro-remediation procedure [26].

The complete removal of hexavalent chromium (Cr(VI)) cannot be achieved solely with sulfuric acid, prompting the need to explore alternative treatments for effective COPR remediation. Xiao-bin et al. found that hydrofluoric acid (HF) effectively disrupts Cr(VI)-bearing minerals, facilitating the release of Cr(VI) into the leachate. It is noted that particle size has a significant impact on the acid-leaching of Cr(VI) from COPR, followed by the duration of the leaching process, with HF concentration and temperature exerting minor effects, and stirring rate having negligible influence [27].

So far, there has been limited literature on the use of hydrofluoric acid (HF) for treating COPR, possibly due to its highly corrosive nature, capable of causing severe burns to human and animal skin & muscle, and even erosion of bones [28], [29]. The use of sulfuric acid typically achieves a

chromium extraction efficiency of around 90%, prompting researchers to explore alternative pathways for chromite extraction from ore [30]. Despite its effectiveness, the inability to achieve complete extraction necessitates innovation in process design and chemistry. This limitation underscores the ongoing efforts in the field to enhance extraction yields, optimize resource utilization, and develop sustainable practices in chromium production from chromite.

This study proposed an environmentally friendly method for producing potassium chromate through hydrometallurgy, aiming to reduce pollution from chromite ore processing residue. The research examines how $NaNO_3$ influences the oxidation of chromite with oxygen or air. Additionally, the study focuses on reaction rates, exploring the impact of variables like reaction time, temperature, and the proportion of ore to alkali.

6C.3 Experimental Procedure

The collected low-grade chromite ore undergoes crushing and grinding using a jaw crusher, ball mill, and pulverizer, and this processed ore is utilized for the entire experiment. A fine chromite sample (75 μm) is dried at 105°C for 24 hours in a hot air oven. For each experiment, 1.0 g of the ore is mixed with 1.0 g of sodium nitrate and placed into a platinum crucible. The crucible is subsequently positioned in a raising hearth furnace and maintained at 623K for 1 hour. After this period, the crucible is allowed to cool to atmospheric temperature. A predetermined amount of sodium hydroxide is introduced into the crucible, and the mixture is then roasted isothermally under atmospheric air conditions at a constant temperature. In the current study, roasting temperatures of 973K, 1023K, and 1073K are selected, with roasting times of 15 minutes, 30 minutes, 60 minutes, 90 minutes, and 120 minutes investigated which is shown in Table 6C.1.

Table 6C.1: Overview of Chromite Ore Roasting Using NaOH at Various Temperatures and Times.

Ore: $NaNO_3$	Roasting Time (min.) & Temperature (K)	Ore: NaOH	Roasting Temperature (K)	Roasting Time (min.)
1:1	60 & 623	1:3 (Explain in the result and discussion part)	973	15,30,60,90,120
			1023	
			1073	

The ratio of ore to sodium hydroxide is varied to investigate the dissolution process of chromite ore in NaOH, as summarized in Table 6C.2. All roasted samples are soaked in water at 60°C for one hour while being stirred continuously at 700 rpm using a magnetic stirrer. The resulting leachates collected during experiments conducted at various temperatures and durations are analyzed using atomic absorption spectroscopy (AAS). The residue obtained from this process is thoroughly washed and analyzed using X-ray diffraction (XRD) and scanning electron microscopy (SEM).

Table 6C.2: Summary of Chromite Ore Roasting at Different Ore to NaOH Ratio and Times.

Ore: $NaNO_3$	**Roasting Time (min.) & Temperature (K)**	**Ore: NaOH**	**Roasting Temperature (K)**	**Roasting Time (min.)**
1:1	60 & 623	1:1	1073 (Explain in the result and discussion part)	15,30,60,90,120
		1:2		
		1:3		
		1:4		

The leachates obtained under optimized conditions are first neutralized to precipitate aluminium hydroxide, which is filtered using Whatman 41 filter paper. The resulting filtrate is then acidified with sulfuric acid. This acidic solution is treated with solid potassium chloride (KCl) to form potassium dichromate ($K_2Cr_2O_7$). Evaporation is used to concentrate the solution and cooled to obtain crystalline potassium dichromate. The chromate crystals are carefully filtered and washed. The liquid wash is recycled for initial washing. Recycling the liquid waste is necessary because chromium in the residue can form hexavalent chromium compounds, which are carcinogenic. The potassium dichromate obtained in that process is further reduced with metallurgical-grade coke at 1173 K for 30 minutes to produce chromium oxide. The overall flowchart of the process is provided in Fig. 6C.2.

The recovery of chromium is calculated using equation (5).

$$\text{Chromium recovery \%} = ([Cr]_l / [Cr]_o) \times 100 \quad (5)$$

Where $[Cr]_l$ and $[Cr]_o$ denote the percentage of chromium present in leach liquor and the percentage of chromium present in chromite ore.

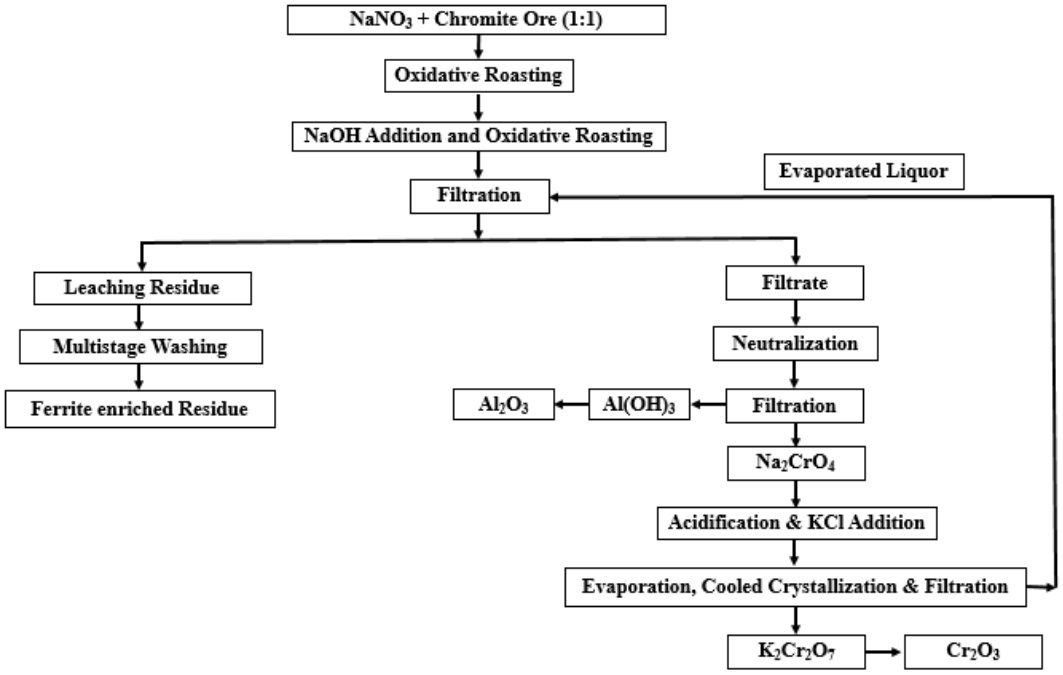

Figure 6C.2: Flow Chart for the Preparation of $K_2Cr_2O_7$ from Low-Grade Chromite Ore.

6C.3.1 Purity of Potassium Dichromate

Acidic ferrous ammonium sulfate (FAS) is employed to assess the purity of the resultant product. A known mass of potassium dichromate ($K_2Cr_2O_7$) is dissolved in distilled water to form a solution. To acidify the potassium dichromate solution, sulfuric acid (H_2SO_4) is added. The solution is titrated with a standard FAS solution until the endpoint is achieved. A color change from orange generally indicates the endpoint (due to dichromate ions) to green (due to the formation of chromium(III) ions). The reaction involved in this process is:

$$6Fe^{2+} + Cr_2O_7^{2-} + 14H^+ = 2Cr^{3+} + 6Fe^{3+} + 7H_2O \qquad 6$$

The concentration of potassium dichromate is determined by calculating the amount of FAS solution required and its known concentration. According to the balanced chemical reaction (6), it is established that 1 mole of $K_2Cr_2O_7$ reacts with 6 moles of Fe^{2+}. Therefore, the molarity of potassium dichromate (M_1) can be calculated using equation 7.

$M_1 = (M_2 \times V_2) / 6 \times V_1$ 7

In this context, M_2 stands for the concentration of ferrous ammonium sulfate (FAS), V_2 specifies the amount of FAS solution utilized during the titration (measured in liters), and V_1 indicates the volume of the potassium dichromate solution employed in the titration (also measured in liters)

The purity of $K_2Cr_2O_7$ is calculated by equation 8.

$$\text{Purity (\%)} = (M_p / M_t) \times 100 \quad (8)$$

Where M_p is the molarity obtained by the resultant product and M_t is the theoretical molarity of potassium dichromate in the sample, based on its molecular weight and the initial mass used.

6C.4 Results and Discussion

6C.4.1 Effect of Sodium Nitrate ($NaNO_3$) on Chromium Recovery from Low-Grade Chromite Ore

In the current study, each sample undergoes heating with sodium nitrate ($NaNO_3$) at 350°C for 1 hour before fusion with NaOH. Previous literature has demonstrated that chromite can be oxidized with $NaNO_3$. This process involves converting chromite, a chromium-containing mineral, using sodium nitrate as an oxidizing agent [34].

6C.4.1.1 Process

At temperatures below 380°C, the reaction between chromite ore and sodium nitrate primarily yields sodium chromate (Na_2CrO_4) and nitrogen dioxide gas (NO_2). Above 380°C, the reaction proceeds differently due to the higher temperature, resulting in more extensive decomposition and different products like Na_2O and O_2. The balanced chemical equations for these reactions are represented as equations 9 and 10 respectively:

$$4\ FeCr_2O_4 + 8\ NaNO_3 \rightarrow 4\ Na_2CrO_4 + 2\ Fe_2O_3 + 8\ NO_2 \quad (9)$$

$$4\ FeCr_2O_4 + 10\ NaNO_3 \rightarrow 2\ Na_2O + 4\ Na_2CrO_4 + 2\ Fe_2O_3 + 5\ NO_2 + O_2 \quad (10)$$

6C.4.1.2 Effect of Sodium Nitrate

Two sets of experiments are conducted to investigate the effect of sodium nitrate ($NaNO_3$) on chromium recovery from low-grade chromite ore.

- In the first experimental setup, the ore is subjected to roasting with $NaNO_3$ at 350°C for 1 hour, followed by further roasting with NaOH at 800°C, and finally leaching in water.
- The second setup omitted the initial $NaNO_3$ roasting step and directly roasted the chromite ore with NaOH at 800°C, followed by leaching in water.

The experiments are monitored for chromium recovery percentage over time, and the results are graphically represented in Fig. 6C.3. Initially (0-20 minutes), both setups demonstrated a rapid increase in chromium recovery, with nearly identical rates. During the intermediate phase (20-60 minutes), the setup including $NaNO_3$ exhibited a faster recovery rate compared to the setup without $NaNO_3$. By the 60-minute mark, chromium recovery reached approximately 80% with $NaNO_3$, while without $NaNO_3$, it is around 70%. In the final phase (60-120 minutes), chromium recovery continued to rise in both setups, but the setup with $NaNO_3$ achieved a notably higher final recovery percentage. After 120 minutes, chromium recovery with $NaNO_3$ reached approximately 99.52%, whereas without $NaNO_3$, it stabilized at around 80%. The inclusion of an initial roasting step with $NaNO_3$ at 350°C appeared to enhance the subsequent roasting process with NaOH at 800°C, resulting in improved chromium recovery. $NaNO_3$ likely acted as an oxidizing agent, facilitating the conversion of chromium into a more leachable form during the NaOH roasting step.

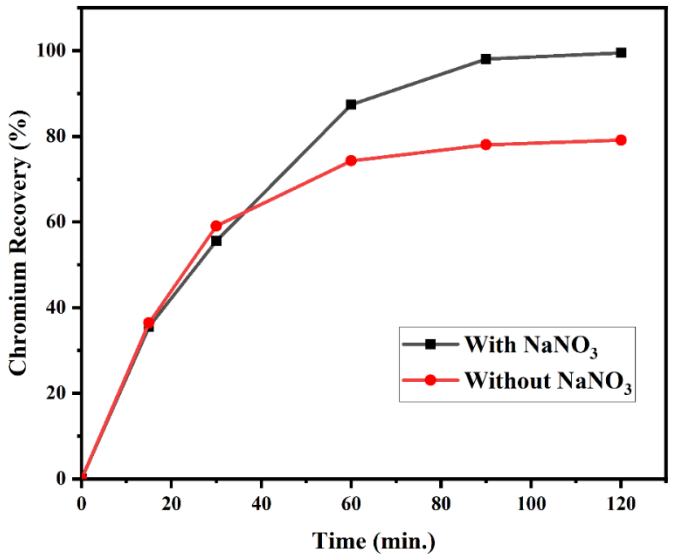

Figure 6C.3: Effect of Sodium Nitrate on Chromium Recovery from Low-Grade Chromite Ore.

6C.4.1.3 SEM Analysis of $NaNO_3$ Roasted Sample

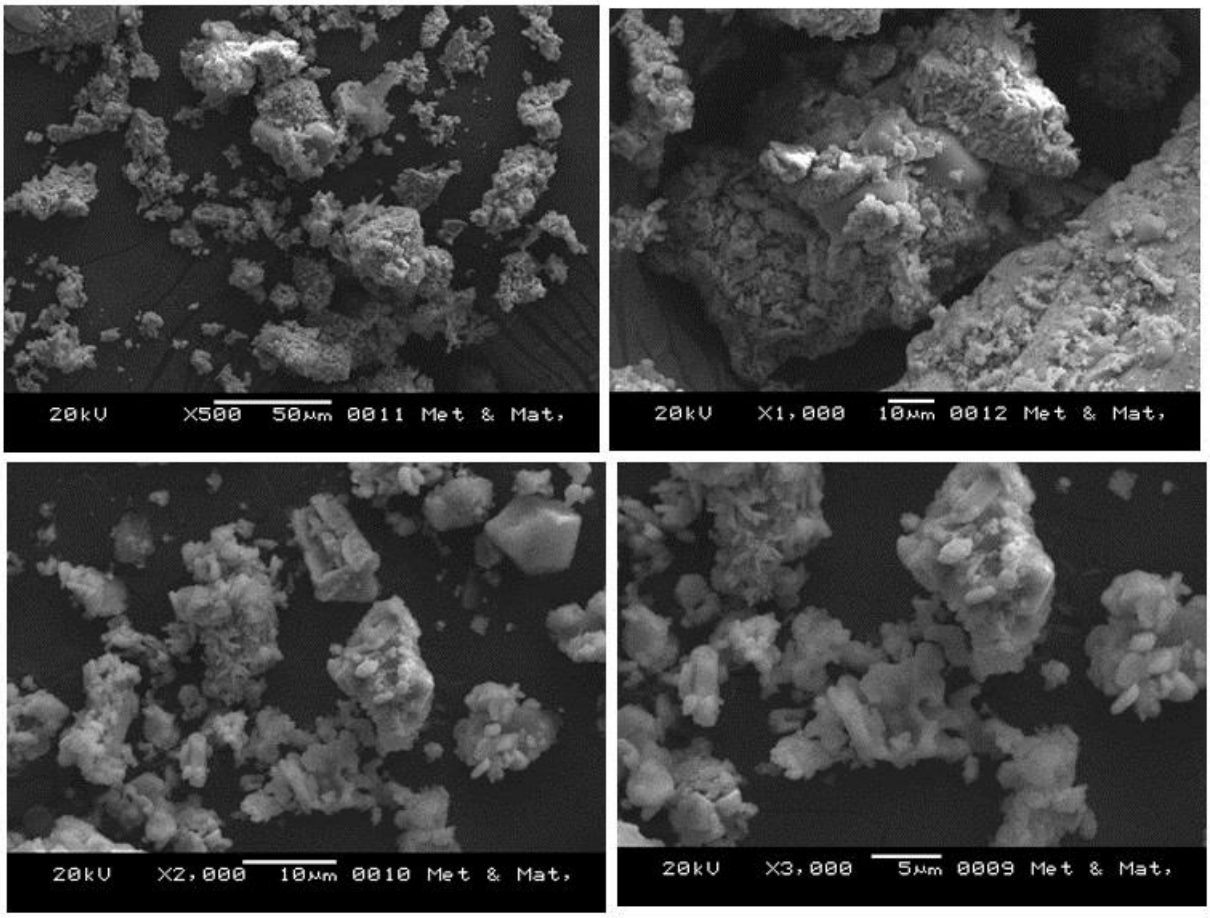

Figure 6C.4: SEM Images of Roasted Chromite Ore with $NaNO_3$ at Different Magnifications.

SEM images are presented in Chapter 5A, section 5.3.4, depicting raw chromite ore. The images reveal coarse particles with a heterogeneous morphology characterized by angular shapes. Fig. 6C.4 shows SEM images of chromite ore roasted with $NaNO_3$ at varying magnifications. These images illustrate the transformative effects of oxidative roasting on the ore's structure and composition. Post-roasting, there is a noticeable reduction in particle size, indicating fragmentation induced by the oxidative process. The particles exhibit a rougher, more porous surface post-roasting, suggesting enhanced reactivity facilitated by the oxidative environment.

Overall, the ore structure appears more granular and fragmented, underscoring the profound impact of oxidative roasting on chromite's physical properties. The extensive fragmentation and increased porosity are attributed to oxidative reactions between chromite and $NaNO_3$, resulting in the formation of new compounds and gases that disrupt the original ore structure.

6C.4.2 Effect of Different Parameters on Chromite Oxidation

The oxidation of chromite is affected by several important factors, such as temperature, the presence of oxidizing agents like sodium nitrate and sodium hydroxide, as well as the concentration of these agents.

6C.4.2.1 Effect of Sodium Hydroxide Concentration on Chromium Recovery

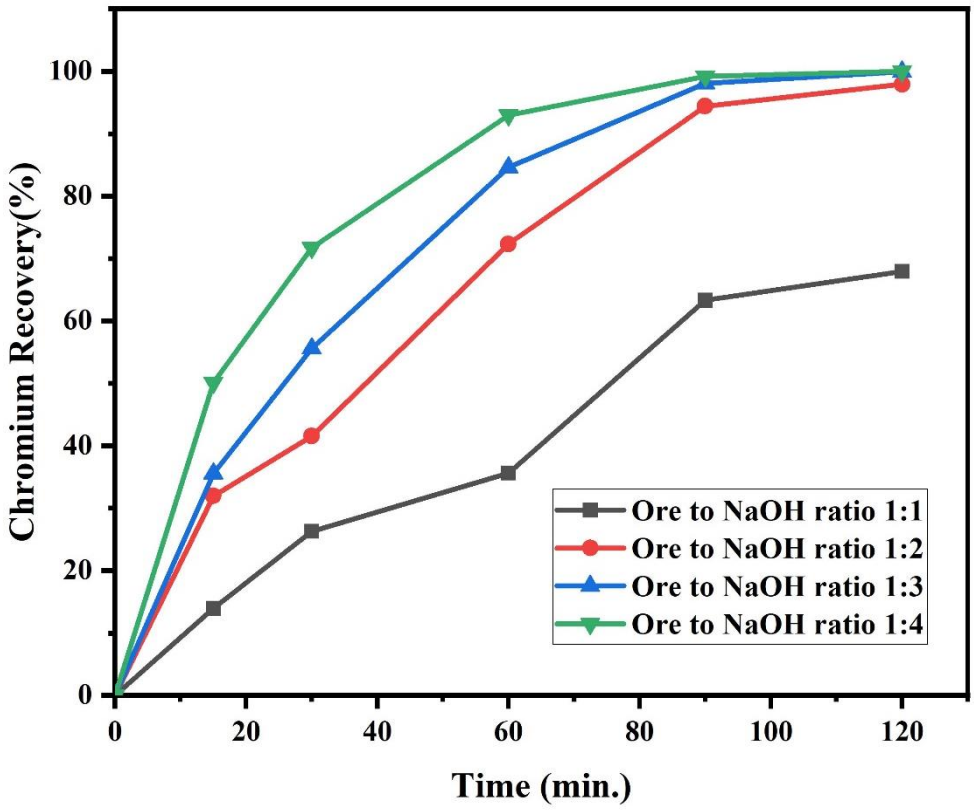

Figure 6C.5: Recovery of Chromium at Different Ore-to-Sodium Hydroxide Ratios at 1073K.

Fig. 6C.5 illustrates the chromium recovery percentage from chromite ore over time at varying ore-to-alkali (NaOH) ratios. The results demonstrate that higher NaOH concentrations (ratios 1:2, 1:3, and 1:4) markedly enhance chromium recovery rates compared to the 1:1 ratio. This

underscores the pivotal role of NaOH in the leaching efficiency of chromite ore. At the 60-minute mark, chromium recovery percentages are 35.64% (1:1 ratio), 72.33% (1:2 ratio), 84.59% (1:3 ratio), and 92.98% (1:4 ratio). By the 120-minute mark, the recovery percentages improve to 67.94% (1:1 ratio), 97.92% (1:2 ratio), 99.52% (1:3 ratio), and 99.71% (1:4 ratio). Notably, ratios of 1:3 and 1:4 yield similar high recovery rates, both reaching about 99% by 120 minutes. Consequently, increasing NaOH concentration beyond a 1:3 ratio may offer minimal additional benefits, suggesting 1:3 as potentially optimal considering cost and resource efficiency. Additionally, chromium recovery increases over time across all NaOH concentrations, with significant gains observed within the initial 60 minutes. Subsequently, the rate of increase levels off, indicating that most leaching occurs early in the process. In summary, higher NaOH concentrations enhance the efficiency of chromium recovery from chromite ore, with a 1:3 ratio potentially offering optimal efficiency in terms of both time and resource utilization.

6C.4.2.2 Effect of Temperature and Time on Chromium Recovery

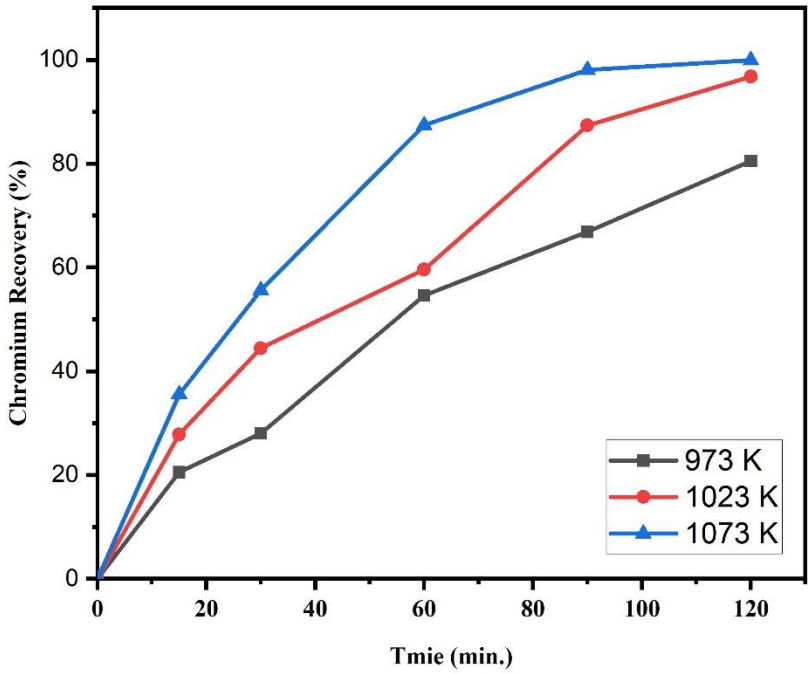

Figure 6C.6: Recovery of Chromium at Different Temperatures with a Constant Ore-to-NaOH Ratio of 1:3.

Figure 6C.6 illustrates the percentage chromium recovery over roasting time and temperature, with a constant ore to NaOH ratio of 1:3. The results indicate a significant improvement in

chromium recovery rate as temperature rises from 973 K to 1073 K. The highest recovery rate is observed at 1073 K, followed by 1023 K, with the lowest recovery rate at 973 K. Concurrently, chromium recovery increases over time at all temperatures, with initial rapid increases leveling off as the reaction progresses, suggesting near-complete leaching. By the 120-minute mark, chromium recovery percentages are 80.51% (973 K), 96.77% (1023 K), and 99.52% (1073 K). These findings suggest that higher temperatures notably enhance the efficiency of chromium leaching from chromite ore, achieving higher recovery rates in a shorter duration. The temperature-dependent increase in recovery rate implies an endothermic nature of the leaching reaction, benefiting from the additional energy provided at higher temperatures. Thus, roasting pre-oxidized chromite ore with NaOH at 1073K for 120 minutes is optimal for maximum chromium recovery of 99.52%.

6C.4.3 Isothermal Kinetic Study of Chromite Leaching with Sodium Hydroxide Following $NaNO_3$ Treatment

In this isothermal kinetic study, the term "α" represents the fractional recovery of chromium, defined as $\alpha = [Cr]_l / [Cr]_0$, where $[Cr]_0$ is the chromium percentage in the chromite ore and $[Cr]_l$ is the chromium percentage in the leach liquor. Equation 10 shows α as a function of time (t). The relationship between fractional chromium recovery α and time (t) for a specific mechanism is expressed as:

$$g(\alpha) = k \cdot t \qquad 11$$

Here, k signifies the apparent rate constant, with t indicating the roasting time. According to Arrhenius' equation, the apparent rate depends on temperature and varies with the rate-controlling regime. In Chapter 1, Section 1.11, g(α) expression is given in detail for different rate-controlling regimes. The value of α ranges from 0 to 1. Roasting time analysis identifies the rate-control mechanism during the leaching process. The relationship between θ_{model} and θ_{expt} is discussed in Chapter 6A, Section 6A.3.4. Based on experimental results, the computed points (α, θ_{expt}) should align with the theoretical α versus θ_{model} plot to determine the appropriate rate-controlling regime across the temperature range.

Thirteen different model predictions are compared with experimental results. Contracting geometry models (CG2-CG3) and rate-controlling models (R1-R3) showed significant deviations from the experimental results. In contrast, the nucleation growth model (NG1) performed

reasonably well throughout the conversion stages. The anti-Jander (D5) model provided the best fit for the overall leaching process. Fig. 6C.7 displays the roasting time plots for the D5 model at different temperatures, showing that all experimental points (α, θ) at a given isothermal temperature closely match the theoretical curves of the D5 model during the leaching process. At all temperatures, the fractional chromium recovery (α) increases with time (θ). At 973K, the fractional recovery of chromium is about 2.5 when θ is 0.9. This recovery increases to roughly 3.0 at 1023K with θ at 1.0 and further rises to approximately 4.0 at 1073K with θ remaining at 1.0. This indicates that higher temperatures enhance the leaching efficiency, resulting in higher chromium recovery rates. The increase in recovery with temperature is consistent with the Arrhenius equation, which states that reaction rates generally increase with temperature.

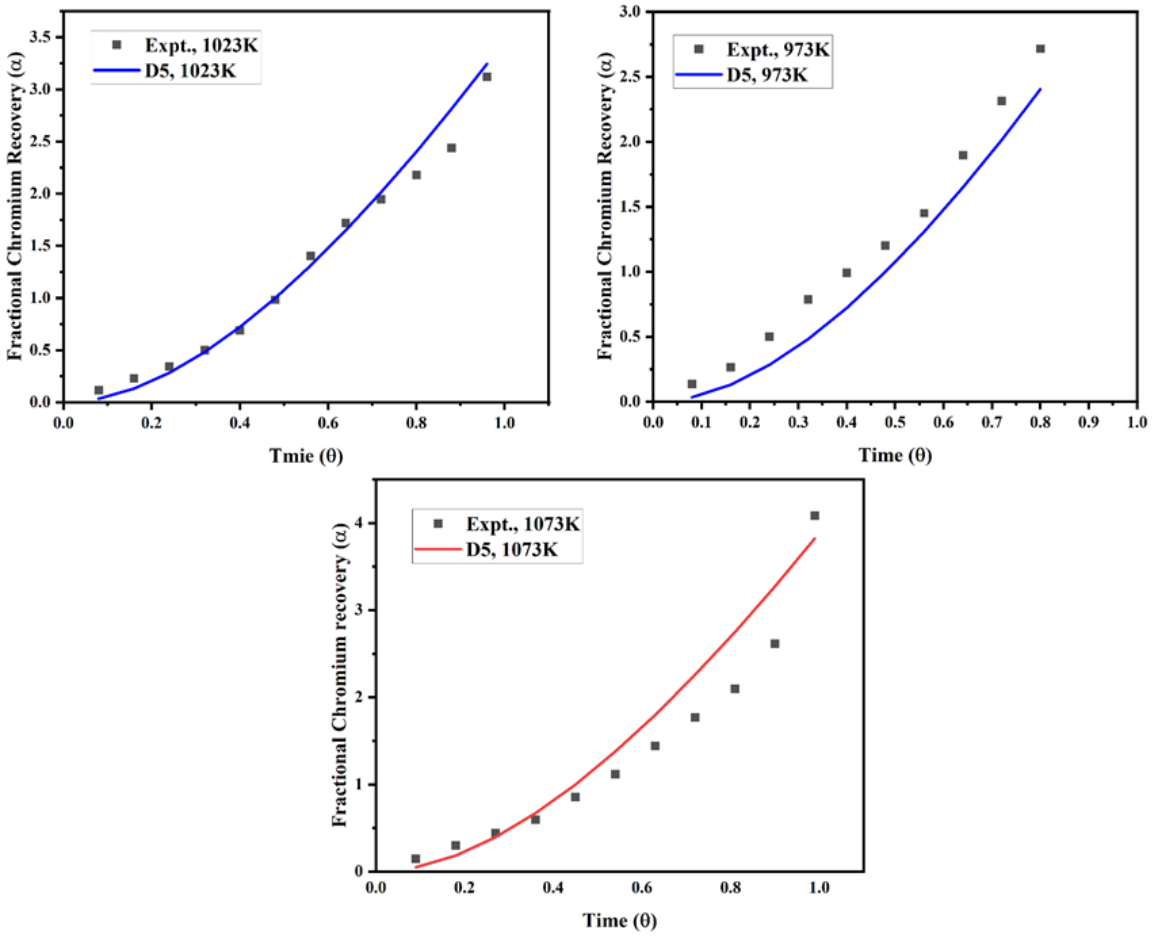

Figure 6C.7: Leaching Time Plot at Different Roasting Temperatures Along with Theoretical α vs θ for the D5 Model at (A) 973 K, (B) 1023 K, and (C) 1073 K.

Table 6C.3 shows the regression coefficient (R^2) values for the twelve rate-controlling regimes. From the table, it is observed that the CG2 and D5 models are the most reliable for describing the kinetics of the process across the temperature range studied, as indicated by their high R-squared values. The D1 and NG1 models also provide a good fit but are less consistent at higher temperatures. The D4, D6, R2, and R3 models show poor performance, particularly at elevated temperatures, making them less suitable for accurately describing the kinetics under these conditions. However D5 model has the highest R^2 values throughout the leaching process. Fig. 6C.8 displays the plot of $[(1+\alpha)^{1/3} -1]^2$ against time for the D5 model at three different temperatures during the roasting process. The slope of the linear fit at these temperatures for the D5 model is used to determine the apparent rate constant (k).

Table 6C.3: Regression Coefficient (R^2) for Different Kinetic Models g(α) = k.t.

G (α) =k.t.	Model	Temperature			Average
		973K	1023K	1073K	
$[1-(1-\alpha)^{1/2}] = kt$	CG2	0.9947	0.9833	0.9734	0.9838
$[1-(1-\alpha)^{1/3}] = kt$	CG3	0.9704	0.9678	0.9459	0.9614
$\alpha^2 = kt$	D1	0.9745	0.9735	0.9739	0.9740
$\alpha + (1-\alpha)\ln(1-\alpha) = kt$	D2	0.9550	0.9381	0.9311	0.9413
$1-2/3\alpha - (1-\alpha)^{2/3} = kt$	D3	0.9455	0.9152	0.8977	0.9194
$[1-(1-\alpha)^{1/3}]^2 = kt$	D4	0.9247	0.8599	0.8114	0.8653
$[(1+\alpha)^{1/3} -1]^2 = kt$	D5	0.9858	0.98636	0.9869	0.9897
$[(1-\alpha)^{1/3} -1]^2 = kt$	D6	0.9247	0.8599	0.8114	0.8653
$[-\ln(1-\alpha)]^{2/3} = kt$	NG1	0.9953	0.9651	0.9230	0.9611
$[-\ln(1-\alpha)] = kt$	R1	0.9778	0.9184	0.8522	0.9161
$[(1-\alpha)^{-1/2}-1] = kt$	R2	0.9491	0.8053	0.6724	0.8089
$[(1-\alpha)^{-1}-1] = kt$	R3	0.9105	0.6866	0.5613	0.7194

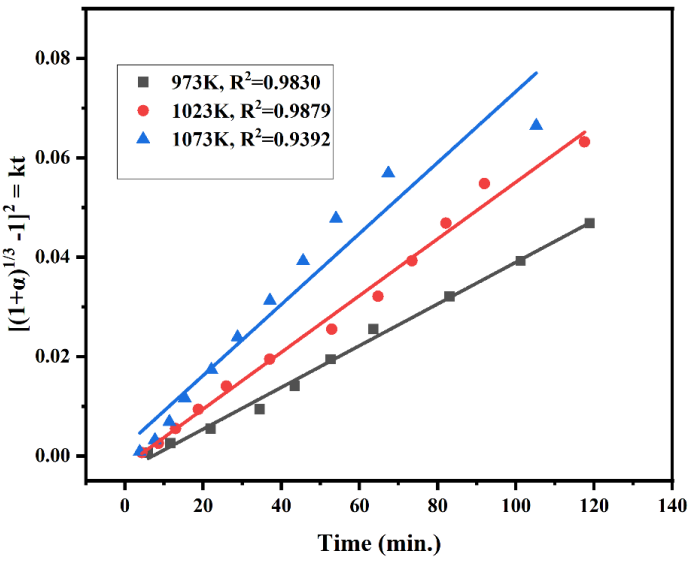

Figure 6C.8: $[(1 + \alpha)^{1/3} – 1]^2 = kt$ vs Time Plot for the D5 Model at Different Reduction Temperatures.

Table 6C.4 provides the slope of each linear fit of Fig. 6C.8 along with the corresponding regression coefficient (R^2). The regression coefficient (R^2) indicates the goodness of fit of the linear regression line to the data points. The slope (k) and R^2 of the $[(1+\alpha)^{1/3} -1]^2 = kt$ vs time plot increases with temperature which indicates higher temperatures result in an increased leaching rate. The high R^2 values confirm the validity of the D5 model in describing the kinetics of the leaching process across different temperatures.

The roasting of chromite with sodium nitrate and sodium hydroxide results in the oxidation of chromium, leading to the formation of sodium chromate, while the iron in chromite is converted to iron oxide (Fe_2O_3). During this process, a solid product layer forms on the surface of the chromite particles, comprising primarily iron oxide and potentially other reaction products. This product layer consists of iron oxide and possibly other reaction products. When the roasted ore is subjected to water leaching, the sodium chromate formed during roasting dissolves, releasing chromate ions into the solution. The anti-Jander model suggests that diffusion of reactants or products through the solid product layer controls the reaction rate. In chromite leaching, this means that the rate at which the chromate ions diffuse through the iron oxide layer (or any other solid product layer) to the solution determines the overall reaction rate. As chromite ore exhibits a spinel structure in its core, its surface is similarly dense. The surface density varies according to the ore's composition and the phases it contains. This dense nature hinders the diffusion of

chromate ions into the solution, thereby limiting the leaching process. Consequently, the leaching rate varies with the composition of different types of chromite ore.

Table 6C.4: Apparent Rate Constant and Regression Coefficient Derived from Various Plots.

Temperature (K)	Slope(k) (min^{-1}) $[(1+\alpha)^{1/3} -1]^2$	Regression coefficient (R^2)
973	0.00041	0.9830
1023	0.00050	0.9879
1073	0.00071	0.9392

6C.4.3.1 Activation Energy

The activation energy is determined using the Arrhenius equation, which is expressed as follows:

$$k = A \exp. - (E_a/RT) \qquad 12$$

In equation (1), k represents the apparent rate constant, A denotes the pre-exponential factor, Ea stands for the activation energy (in kJ/mol), R is the universal gas constant, and T signifies the roasting temperature. For the D5 mechanism, the natural logarithm of the rate constant (k) versus the inverse of temperature (1/T) is shown in Fig. 6C.9. The activation energy Ea is determined from the slope of the straight line obtained in the Arrhenius plot. The value of the calculated activation energy is 48.375 kJ/mol.

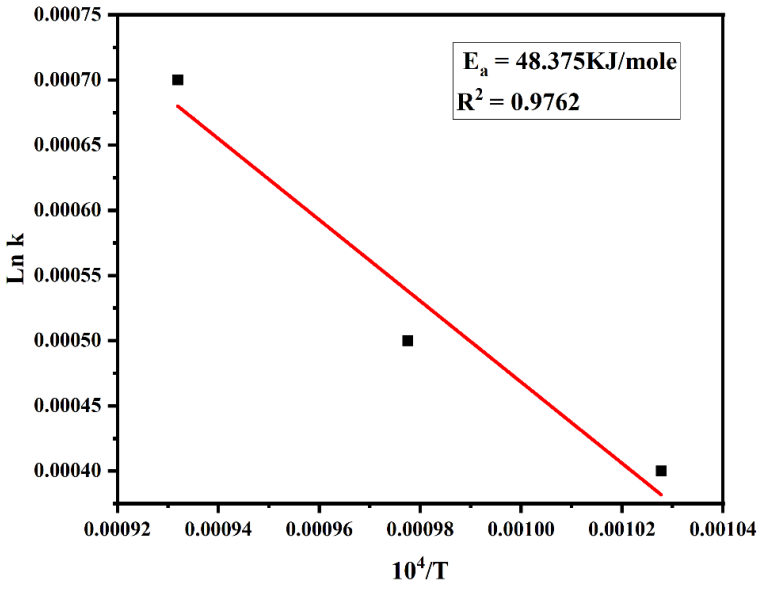

Figure 6C.9: Arrhenius Plot for the D5 Kinetic Model.

6C.4.4 Analysis of Leaching Residue (Roasted at 1073K for 120 min.)

The chromite ore is roasted under the optimized conditions and then leached in water. The leaching residue is characterized using chemical analysis, SEM, and XRD, as described below:

6C.4.4.1 Chemical Analysis of Leaching Residue

The WDXRF analysis of the chromite ore leaching residue is summarized in Table 6C.5. The high Fe_2O_3 content indicates iron constitutes the main component of the residue. The low Cr_2O_3 content (0.346%) suggests that most of the chromium has been successfully leached out, corroborating the high chromium recovery rate mentioned earlier. The presence of other oxides (MgO, Al_2O_3, SiO_2, Na_2O) and the LOI value provide additional information on the residue's composition and the efficiency of the leaching process.

Table 6C.5: WDXRF Analysis of Leaching Residue.

Fe_2O_3	Cr_2O_3	MgO	Al_2O_3	SiO_2	Na_2O	LOI
66.74	0.346	1.82	2.13	4.18	6.87	17.90

6C.4.4.2 XRD Analysis of Leaching Residue

The residue obtained by the leaching process is analyzed by XRD, which is shown in Fig. 6C.10. The leaching residue is found to contain spinel ((Mg, Fe)(Cr, $Al)_2O_4$), magnesiochromite ($MgCrAlO_4$), and hematite (Fe_2O_3) phases when chromite ore is roasted at 973K. At this temperature, the presence of the chromite spinel phase ((Mg, Fe)(Cr, $Al)_2O_4$) indicates incomplete decomposition of chromite ore. The formation of $MgCrAlO_4$ suggests initial decomposition and reformation of phases involving Cr and Al. When the roasting temperature is 1023K, the leaching residue contains prominent hematite and magnesioferrite ($MgFe_2O_4$) phases. The formation of $MgFe_2O_4$ suggests a phase transformation where Fe and Mg form new compounds as Cr and Al are leached out. Roasting at 1073K results in the residue containing hematite as the major phase. The absence of ((Mg, Fe)(Cr, $Al)_2O_4$) and $MgCrAlO_4$ suggests complete decomposition of the initial spinel structure. The high intensity of $MgFe_2O_4$ peaks indicates a stable phase at this temperature, likely due to the reorganization of Mg and Fe atoms.

Table 6C.6: Different Phases Present in the Leaching Residue at Different Roasting Temperatures.

Temperature (K)	Roasting Time (min.)	Identified Phase
973	120	Spinel Phase, $MgCrAlO_4$, Fe_2O_3, $MgFe_2O_4$
1023	120	Fe_2O_3,$MgCrAlO_4$, $MgFe_2O_4$
1073	120	Fe_2O_3, $MgFe_2O_4$

The XRD patterns depict the phase transitions and decomposition of chromite ore during roasting with NaOH at 1073K for varying durations [Fig. 6C.11]. The predominant phases identified are Fe_2O_3 and $MgFe_2O_4$, alongside intermediate phases such as (Mg, Fe)(Cr, Al)$_2O_4$, $MgCrAlO_4$, and $Al(OH)_3$, which evolve with increasing roasting time, indicating a stepwise breakdown and reformation of compounds. During the initial roasting period (15-30 minutes), the spinel structure ((Mg, Fe)(Cr, Al)$_2O_4$) and $Al(OH)_3$ are present, with partial formation of Fe_2O_3 and $MgCrAlO_4$. As the roasting time extends (60-90 minutes), significant decomposition of the spinel structure occurs, resulting in increased prominence of Fe_2O_3 and $MgFe_2O_4$, with $MgCrAlO_4$ persisting as an intermediate phase. By 120 minutes, complete decomposition of the initial spinel and $Al(OH)_3$ phases is observed, with Fe_2O_3 and $MgFe_2O_4$ becoming the dominant phases, indicating a stable composition after prolonged roasting.

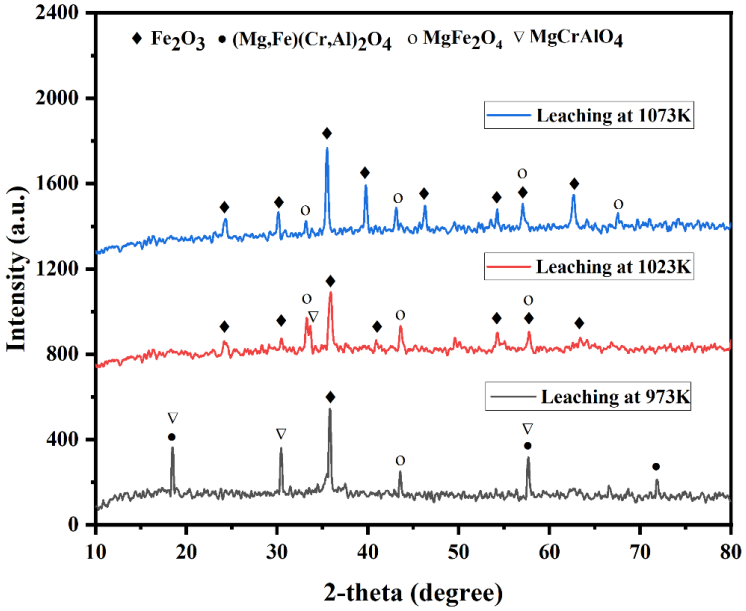

Figure 6C.10: XRD Analysis of Chromite Ore Leaching Residue After Roasting at Different Temperatures for 120 Minutes.

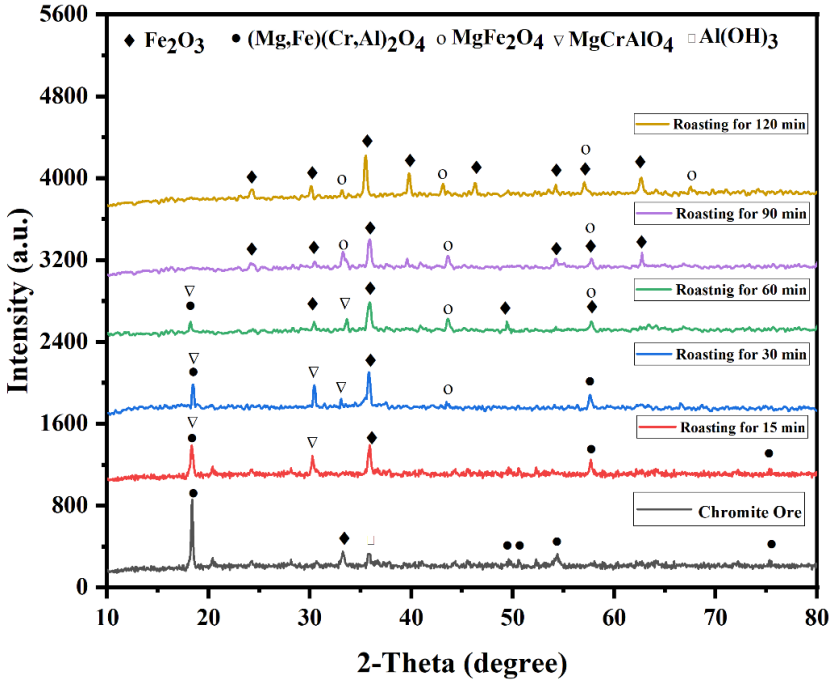

Figure 6C.11: XRD Analysis of Chromite Ore Leaching Residue After Roasting at 1073 K for Different Periods.

6C.4.4.3 SEM Analysis of Leaching Residue

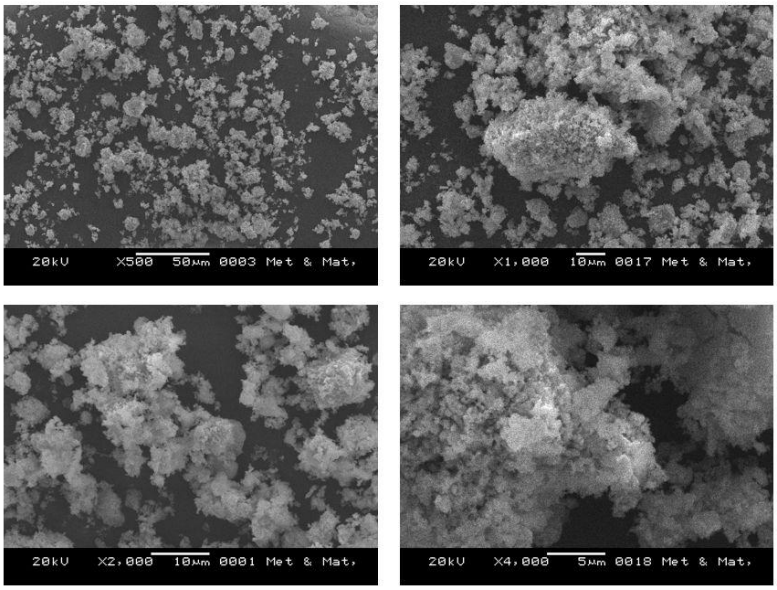

Figure 6C.12: SEM Image of Leaching Residue Obtained from Optimum Roasting Conditions at Different Magnifications.

Fig. 6C.12 presents the morphology of the leaching residue resulting from NaOH leaching of chromite ore. The image displays clusters of particles with varying sizes, visibly agglomerated into larger, irregularly shaped aggregates. Particle sizes appear to be in the micron scale, as confirmed by the scale bar (10 μm), and their irregular shapes suggest a heterogeneous composition of materials. The particles exhibit a rough and porous surface texture, indicating substantial chemical alteration during the leaching process. This rough and porous nature suggests an effective breakdown of the chromite ore. However, the presence of agglomerates suggests that residues may still contain some unreacted ore or secondary phases formed during leaching.

6C.4.5 Leaching Behavior of Chromium, Aluminium, and Iron

Table 6C.7 presents an analysis of the solubility of chromium, aluminum, and iron during the alkaline leaching process of low-grade chromite. The percentage extraction of chromium increases significantly with time, reaching 99.52% after 120 minutes, indicating that longer roasting time enhances the chromium extraction process. Probable reactions involved in that process are shown in Equations 13-16. From the table, it can be observed that aluminium recovery increases with time, starting from 29.19% at 15 minutes and reaching 97.76% at 120 minutes. This indicates that longer roasting times enhance the extraction of aluminium from the ore. The increasing percentage of aluminium recovery with longer roasting times shows that extended exposure to NaOH at 1073 K is effective in converting aluminum-containing minerals into soluble forms that can be leached out and recovered in water. During the roasting process, aluminium oxide (Al_2O_3) present in chromite ore reacts with sodium hydroxide (NaOH) to form sodium aluminate ($NaAlO_2$). The maximum aluminium recovery is found to be 97.76%. The reactions involved are shown in equation 17-19:

$$4FeCr_2O_4 + 8NaNO_3 \rightarrow 4Na_2CrO_4 + 2Fe_2O_3 + 8NO_2 \quad (13)$$

$$FeCr_2O_4 + 4NaOH + 2/7O_2 \rightarrow Fe_2O_3 + 2Na_2CrO_4 + 2H_2O \quad (14)$$

$$Fe_2O_3 + 2NaOH + 4Na_2CrO_4 \rightarrow 2NaFeO_2 + 4Na_2CrO_4 \quad (15)$$

$$Cr_2O_3 + 4NaOH + 2/3O_2 \rightarrow 2Na_2CrO_4 + 2H_2O \quad (16)$$

$Al_2O_3 + 2NaOH \rightarrow 2NaAlO_2 + H_2O$ 17

$NaAlO_2 + 2H_2O \rightarrow 2NaOH + Al(OH)_3$ 18

$2Al(OH)_3 + Heat \rightarrow Al_2O_3 + 3H_2O$ 19

On the other hand, iron oxide shows inertness towards sodium hydroxide and enters the residue phase. During roasting with NaOH, iron in the chromite ore forms compounds that are less soluble in water compared to aluminium compounds. These iron compounds, such as ferrites or iron oxides, are stable and do not dissolve easily during the leaching process. The ferrite-enriched residue is suitable for use as raw material in different industries. It can be utilized in the production of magnetic materials, such as ferrites, which are critical for electronic components and transformers. Additionally, this residue can be processed to recover valuable metals like chromium and iron, contributing to resource recycling and reducing waste. Furthermore, it can be incorporated into construction materials, such as concrete, to improve material properties or mitigate the environmental impact of raw material extraction.

Table 6C.7: Dissolution of Chromium, Aluminum, and Iron during Alkali Leaching of Low-Grade Chromite Ore.

Roasting Temperature (K)	Ore to NaOH Ratio	Time (Min)	Chromium (%)	Aluminium (%)	Iron (%)
1073	1:3	15	35.59	29.19	-
		30	55.60	66.37	-
		60	87.44	80.74	0.11
		90	98.04	94.64	0.53
		120	99.52	97.76	0.84

6C.4.6 Analysis of Aluminium Product

6C.4.6.1 XRD Analysis

The product obtained by the neutralization of the leachate is filtered out, and water is removed from the precipitate by heating it. The XRD analysis of the byproduct is shown in Fig. 6C.13. Based on the X-ray diffraction (XRD) analysis, the presence of only the aluminum oxide (Al_2O_3) phase in the sample indicates that the aluminum hydroxide ($Al(OH)_3$) has been completely

converted to aluminum oxide upon heating. This suggests that the thermal decomposition process is successful and that no other phases or impurities are present in the sample. Therefore, it can be concluded that the heating conditions are adequate to fully decompose $Al(OH)_3$ into Al_2O_3, resulting in a pure aluminum oxide phase as confirmed by the XRD pattern.

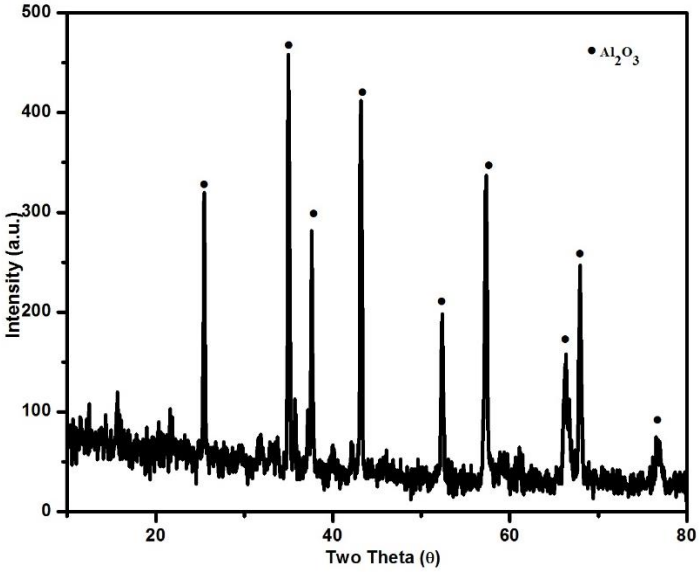

Figure 6C.13: XRD Analysis of By-Product Obtained by the Neutralization of the Leachate.

6C.4.6.2 SEM Analysis

The SEM images (Fig. 6C.14) show the morphology of Al_2O_3 obtained after roasting chromite ore with $NaNO_3$ and NaOH, followed by leaching, filtration, neutralization, and heating. The images are taken at different magnifications to provide a detailed understanding of the sample's morphology. The SEM analysis at various magnifications shows that the Al_2O_3 obtained has a rough and irregular morphology at lower magnifications. Higher magnifications reveal well-defined crystalline structures on the surface, indicating good crystallinity. The presence of crystalline features, such as plate-like or needle-like structures, at higher magnifications confirms the high crystallinity of the Al_2O_3 product. This is consistent with the XRD analysis (shown in Figure Y), which confirmed Al_2O_3 as the major phase.

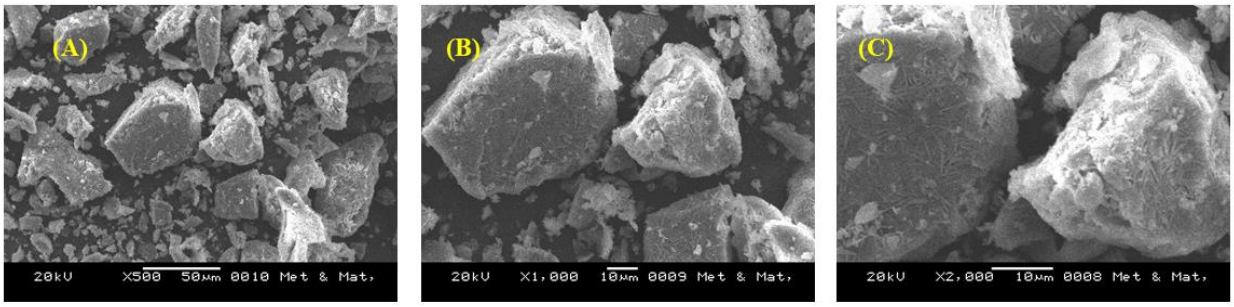

Figure 6C.14: SEM Image of Aluminium Oxide at Different Magnifications.

6C.4.7 Purity of the Potassium Dichromate

The purity of potassium dichromate obtained through optimized roasting conditions was determined using a chemical method. Using equation 8, the purity of the final $K_2Cr_2O_7$ is calculated to be 90.76%. This purity suggests that the product may not meet reagent grade standards. Possible reasons for this include inadequate control of acidity, incomplete transformation of Na_2CrO_4 into $Na_2Cr_2O_7$, or the co-precipitation of other compounds during the precipitation and crystallization of $K_2Cr_2O_7$, which reduced the purity of the final product. Therefore, employing more rigorous precipitation and crystallization techniques is recommended to prevent impurities from co-precipitating with the desired product.

6C.4.8 XRD Analysis of Reduced $K_2Cr_2O_7$

Potassium dichromate is reduced by carbon in a tube furnace at 1173K and the resultant product is analyzed using XRD. X-ray diffraction (XRD) pattern of the product is shown in Fig. 6C.15. The image shows that chromium oxide (Cr_2O_3) is the major phase along with potassium carbonate (K_2CO_3), chromium (II) carbide (Cr_2C_3), chromium dioxide (CrO_2) and unreacted carbon. The presence of Cr_2O_3 as a major phase suggests that Cr^{6+} underwent reduction to Cr^{3+} during the reduction process. The peak of CrO_2 in the XRD image indicates that the reduction process is incomplete, as Cr in CrO_2 is in a higher oxidation state compared to Cr in Cr_2O_3. There might have been insufficient reaction time to fully reduce all the Cr(VI) to Cr(III). The detection of carbon peaks indicates that some unreacted carbon is also present in the reduced sample. The formation of Cr_3C_2 indicates that some of the reduced chromium oxides reacted with excess carbon to form carbides. From the above observation, it is clear that the reduction of

$K_2Cr_2O_7$ at 1173K by carbon led to the formation of Cr_2O_3 as the primary phase, with Cr_3C_2 as a secondary phase due to excess carbon. This Cr_2O_3 and Cr_3C_2 are further used in industrial metallurgical applications.

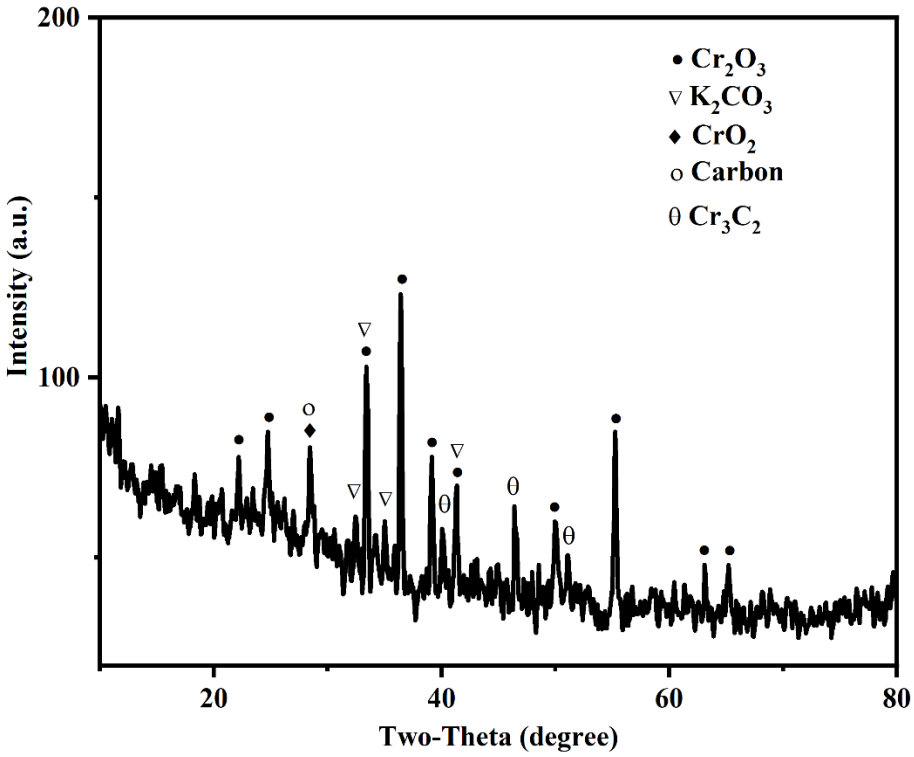

Figure 6C.15: XRD Analysis of Reduced $K_2Cr_2O_7$.

6C.4.9 Conclusion

Potassium dichromate and chromium oxide are effectively synthesized from low-grade chromite ore through oxidative roasting with sodium nitrate and sodium hydroxide. By significantly improving the efficiency of chromium extraction, $NaNO_3$ enables nearly complete recovery (99.52%) within just 120 minutes of roasting at 1073K, in contrast to the 80% recovery achieved without its inclusion. This highlights $NaNO_3$ as a crucial catalyst in enhancing potassium dichromate yield and purity, thereby optimizing the entire chromite ore processing procedure. Chromium extraction depends on alkali concentration, roasting time, and temperature. The experimental result shows that recovery of chromium increases with time and higher temperature. Higher NaOH concentrations enhance chromium recovery, with a 1:3 ratio offering optimal efficiency in time and resources. The kinetic study indicates that the roasting process

follows the D5 mechanism (anti-Jander). This mechanism implies that, during the leaching of chromite ore with $NaNO_3$ and NaOH, the rate-determining step is the diffusion of chromate ions through the solid product layer formed during roasting. The activation energy for this step is measured at 48.375 kJ/mol. The analysis of the leaching residue reveals that Fe_2O_3 is the predominant oxide, accompanied by other oxides including MgO, Al_2O_3, SiO_2, Na_2O, etc. Phases identified in the residue include Fe_2O_3 and $MgFe_2O_4$, along with intermediate phases such as $(Mg, Fe)(Cr, Al)_2O_4$, $MgCrAlO_4$, and $Al(OH)_3$. Aluminum from the chromite ore exhibits favorable leaching characteristics with NaOH. Under optimized conditions, aluminum recovery reaches 97.76%. However, the purity of the final $K_2Cr_2O_7$ is determined to be 90.76%, which does not meet analytical grade standards. Further purification is necessary through recrystallization techniques to achieve analytical-grade purity. The reduction of $K_2Cr_2O_7$ by carbon at 1173 K predominantly yields Cr_2O_3 as the major phase along with Cr_3C_2 phase. Cr_2O_3 is generally utilized in industrial metallurgical applications. These results suggest that at higher reduction temperatures, the process could lead to the formation of metallic chromium more efficiently for the metallurgical aspect.

6C.5 Reference

[1] B. Zhang, P. Shi, and M. Jiang, "Advances towards a clean hydrometallurgical process for chromite," Minerals, vol. 6, no. 7, pp. 1-12, 2016 doi:10.3390/min6010007.

[2] J. Sun, Y. Luo, J. Ye, C. Li, and J. Shi, "Chromium Distribution, Leachability and Speciation in a Chrome Plating Site," Processes, vol. 10, no. 1, Jan. 2022, doi: 10.3390/pr10010142.

[3] A. M. Amer and I. A. Ibrahim, "Leaching of a low grade Egyptian chromite ore," *Hydrometallurgy*, vol. 43, pp. 307-316, 1996. DOI https://doi.org/10.1016/0304-386X(96)00005-9.

[4] S. B. Shen, M. Bergeron, and M. Richer-Laflèche, "Effect of sodium chloride on the selective removal of iron from chromite by carbochlorination," *Int J Miner Process*, vol. 91, no. 3–4, pp. 74–80, May 2009, doi: 10.1016/j.minpro.2008.12.005.

[5] R. H. Nafziger, "A review of the deposits and beneficiation of lower-grade chromite." *Journal of The South African Institute of Mining and Metallurgy*, pp.205-226, 1982.

[6] L.A. Cramer, J. Basson, and L.R. Nelson "The impact of platinum production from UG2 ore on ferrochrome production." *The Journal of The South African Institute of Mining and Metallurgy,* pp. 517-527, 2004.

[7] Y. ZHANG, S. li ZHENG, H. DU, H. bin XU, and Y. ZHANG, "Effect of mechanical activation on alkali leaching of chromite ore," *Transactions of Nonferrous Metals Society of China (English Edition)*, vol. 20, no. 5, pp. 888–891, May 2010, doi: 10.1016/S1003-6326(09)60231-4.

[8] H. Bin Xu et al., "Development of a new cleaner production process for producing chromic oxide from chromite ore," *Journal of Cleaner Production*, vol. 14, no. 2, pp. 211–219, 2006, doi: 10.1016/j.jclepro.2004.09.001.

[9] Y. Zhang et al., "A new metallurgical process for the clean utilization of chromite ore," *Int J Miner Process*, vol. 131, no. 1, pp. 58–68, 2014, doi: 10.1016/j.minpro.2014.07.002.

[10] S. Zheng, Y. Zhang, Z. Li, T. Qi, H. Li, and H. Xu, "Green metallurgical processing of chromite," *Hydrometallurgy*, vol. 82, no. 3–4, pp. 157–163, Aug. 2006, doi: 10.1016/j.hydromet.2006.03.014.

[11] Z. Kowalski and K. Wieczorek-Ciurowa, "The Effect of Chromic Mud Graining on the Technological Parameters of the Sodium Chromate Production Process," *Polish Journal of Environmental Studies*, vol. 12, no. 1, pp.73-81, 2003.

[12] C. Arslan and G. Orhan, "Investigation of chrome(VI) oxide production from chromite concentrate by alkali fusion," *International Journal of Mineral Processing*, vol. 50, no 1–2, pp. 87-96, 1997.

[13] Y. Zhang et al., "A clean and efficient leaching process for chromite ore," *Miner Eng*, *vol.* 60, pp. 60–68, 2014, doi: 10.1016/j.mineng.2014.01.025.

[14] S. Parirenyatwa, L. Escudero-Castejon, S. Sanchez-Segado, Y. Hara, and A. Jha, "Comparative study of alkali roasting and leaching of chromite ores and titaniferous minerals," *Hydrometallurgy*, vol. 165, pp. 213–226, Oct. 2016, doi: 10.1016/j.hydromet.2015.08.002.

[15] Q. Zhao, C. Liu, B. Li, R. Zevenhoven, H. Saxén, and M. Jiang, "Recovery of chromium from residue of sulfuric acid leaching of chromite," *Process Safety and Environmental Protection*, vol. 113, pp. 78–87, 2018, doi: 10.1016/j.psep.2017.10.002.

[16] P. Ning, X. Lin, H. Cao, and Y. Zhang, "Selective extraction and deep separation of V(V) and Cr(VI) in the leaching solution of chromium-bearing vanadium slag with primary amine LK-N21," *Sep Purif Technol*, vol. 137, pp. 109–115, Nov. 2014, doi: 10.1016/j.seppur.2014.08.033.

[17] C. Liu, J. Qi, and M. Jiang, "Experimental study on sulfuric acid leaching behavior of chromite with different temperature," *Advanced Materials Research*, 2012, pp. 628–631. doi: 10.4028/www.scientific.net/AMR.361-363.628.

[18] A. Geveci, Y. Topkaya, and E. Ayhan, "Sulfuric acid leaching of Turkish chromite concentrate," *Minerals Engineering*, Nov. 2002, pp. 885–888. doi: 10.1016/S0892-6875(02)00159-0.

[19] Q. Zhao et al., "Sulfuric acid leaching kinetics of South African chromite," *International Journal of Minerals, Metallurgy and Materials*, vol. 22, no. 3, pp. 233–240, Mar. 2015, doi: 10.1007/s12613-015-1066-2.

[20] E. Vardar, R. H. Eric, and F. K. Letowski, "Acid leaching of chromite," *Minerals Engineering*, vol. 7, no. 5–6, pp. 605-617, 1994. DOI https://doi.org/10.1016/0892-6875(94)90093-0.

[21] Q. Zhao et al., "Cleaner production of chromium oxide from low Fe(II)-chromite," *Minerals*, vol. 10, no. 5, May 2020, doi: 10.3390/min10050460.

[22] Q. Zhao et al., "A cleaner method for preparation of chromium oxide from chromite," *Process Safety and Environmental Protection*, vol. 105, pp. 91–100, Jan. 2017, doi: 10.1016/j.psep.2016.09.017.

[23] Z. Kowalski and M. Gollinger-Tarajko, "Environmental evaluation of different variants of the chromium compound production model using chromic waste." *Waste Management*, vol. 23, no. 8, pp. 771-783, 2003. https://doi.org/10.1016/S0956-053X(02)00114-9.

[24] D. Deakin, L. J. West, D. I. Stewart, and B. W. D. Yardley, "Leaching behaviour of a chromium smelter waste heap." *Waste Management*, vol. 21, no. 3, pp. 265-270, 2011. https://doi.org/10.1016/S0956-053X(00)00099-4.

[25] S. C. Jagupilla, D. H. Moon, M. Wazne, C. Christodoulatos, and M. G. Kim, "Effects of particle size and acid addition on the remediation of chromite ore processing residue using ferrous sulfate," *J Hazard Mater*, vol. 168, no. 1, pp. 121–128, Aug. 2009, doi: 10.1016/j.jhazmat.2009.02.012.

[26] J. M. Tinjum, C. H. Benson, and T. B. Edil, "Mobilization of Cr(VI) from chromite ore processing residue through acid treatment," *Science of the Total Environment*, vol. 391, no. 1, pp. 13–25, Feb. 2008, doi: 10.1016/j.scitotenv.2007.10.041.

[27] X. Bin Li, W. Bin Xu, Q. S. Zhou, Z. H. Peng, and G. H. Liu, "Leaching kinetics of acid-soluble Cr(VI) from chromite ore processing residue with hydrofluoric acid," *Journal of Central South University of Technology (English Edition)*, vol. 18, no. 2, pp. 399–405, Apr. 2011, doi: 10.1007/s11771-011-0710-x.

[28] M. Hatzifotis, A. Williams, M. Muller, and S. Pegg, "Hydrofluoric acid burns," *Burns*, vol. 30, no. 2, pp. 156–159, 2004, doi: 10.1016/j.burns.2003.09.031.

[29] F. Spöler, M. Frentz, M. Först, H. Kurz, and N. F. Schrage, "Analysis of hydrofluoric acid penetration and decontamination of the eye by means of time-resolved optical coherence tomography," *Burns*, vol. 34, no. 4, pp. 549–555, Jun. 2008, doi: 10.1016/j.burns.2007.05.004.

[30] Y. Zhang, S. L. Zheng, H. Bin Xu, H. Du, and Y. Zhang, "Decomposition of chromite ore by oxygen in molten NaOH-$NaNO_3$," *Int J Miner Process*, vol. 95, no. 1–4, pp. 10–17, Jul. 2010, doi: 10.1016/j.minpro.2010.03.005.

Chapter-6D

Optimization of Bioleaching Parameters for Metal Extraction from Low-Grade Chromite Ore Using Pseudomonas putida

6D.1 Introduction

The demand for chromium in different industrial applications like stainless steel production increases, so extracting it from chromite ore ($FeCr_2O_4$) is very crucial in the present scenario. Conventionally, chromite ore processing is carried out through pyro-metallurgical and hydrometallurgical techniques. Both processes are (specially pyro-metallurgical process) energy-intensive and generate significant environmental waste [1]. At this condition, there is a pressing need to explore alternative, eco-friendly methods for chromite ore beneficiation and extraction. Bio-leaching has emerged as a promising approach. This process gives economical viability, reduced environmental impact with efficiency in extracting valuable metals from ores. This process is given importance when microorganisms are used to solubilize metals from ores through their metabolic activities. Different microbes are used in the bioleaching process as per the requirement of metal to be extracted from their respective ores. Due to its strong metabolism and versatility, Pseudomonas putida is used in the bioleaching process. Pseudomonas putida is a gram-negative bacterium. Pseudomonas putida is capable of degrading a wide range of organic compounds. But, the application of Pseudomonas putida in the bioleaching of chromite ore is still underexplored [2].

This study aims to investigate the feasibility of using Pseudomonas putida for the bioleaching of chromite ore. The ability of Pseudomonas putida to solubilize chromium from chromite has been investigated. This research tries to find the contribution to the development of more sustainable and environmentally friendly methods for chromite ore processing. The specific objectives are to evaluate how effectively Pseudomonas putida extracts chromium and to understand the underlying biochemical mechanisms of the process. The findings of this study could provide a valuable understanding of the application of microbial processes in mineral extraction, potentially leading to more sustainable practices in the mining industry and reduced environmental impact.

6D.2 Literature Review

Chromite ore, primarily composed of iron chromium oxide ($FeCr_2O_4$), is a key source of chromium, which is essential for diverse industrial purposes, including the creation of stainless steel, alloys, and chemicals. Traditional methods for chromite ore processing include pyrometallurgical techniques such as smelting and hydrometallurgical methods involving acidic or alkaline leaching. These conventional approaches, while effective, are often associated with high energy consumption, significant greenhouse gas emissions, and the generation of hazardous waste [3].

Bioleaching, the process of using microorganisms to extract metals from ores, has emerged as an environmentally friendly alternative to traditional extraction methods. This technique exploits the metabolic capabilities of microbes to solubilize valuable metals from mineral matrices. Various microorganisms, including bacteria, fungi, and archaea, have been investigated for their bioleaching potential. Acidophilic bacteria such as Thiobacillus ferrooxidans and Ferroplasma acidarmanus have been extensively studied for their role in the bioleaching of sulfide ores [4][5][6]. In bioleaching, microorganisms like bacteria or archaea facilitate the oxidation of metal sulfides to convert metals into a soluble form. These microbes get their energy from these oxidation reactions, creating an environment that breaks down metals from the mineral matrix. The metals in their soluble state can then be recovered in later processing steps. Bioleaching is widely used in industry to extract metals such as copper, gold, zinc, nickel, and cobalt [7][8][9][10][11]. This method is seen as a sustainable and innovative approach to mineral extraction, aligning with contemporary environmental and economic goals in mining. Bioleaching is chosen for several important reasons, highlighting its benefits compared to traditional mining and metal extraction methods [12]. Here are the key reasons why bioleaching is utilized:

1. Bioleaching significantly reduces environmental impact by minimizing or eliminating harsh chemicals like cyanide and mercury, commonly used in traditional mining, and pose risks to soil, water, and air. This method also reduces greenhouse gas emissions typically associated with high-temperature smelting processes. Furthermore, bioleaching operates at ambient temperatures and pressures, requiring less energy than conventional methods, leading to lower energy consumption and a reduced carbon footprint [13].

2. Bioleaching can be more cost-effective, especially for processing low-grade ores that aren't profitable with traditional techniques. It reduces expenses related to energy, chemicals, and waste management. Additionally, it often results in higher metal recovery rates, particularly for metals in low concentrations or within challenging mineral matrices, boosting overall mining efficiency and profitability [14][15].
3. Bioleaching allows for the selective extraction of specific metals from complex ores, which decreases the need for extra refining steps and reduces secondary waste. Its versatility means it can be adapted to various ores and minerals, offering flexibility for different geological conditions and mining scenarios [16][17].
4. By enhancing metal extraction efficiency and minimizing environmental impact, bioleaching supports sustainable resource management in mining. It also helps mining companies comply with increasingly strict environmental regulations and sustainability goals set by governments and international organizations [18].

The primary types of bioleaching are heap leaching, tank leaching, and in-situ leaching, each with distinct mechanisms and applications. Heap Leaching is widely used in the mining industry, particularly for low-grade ores. In this process, ores are piled into large heaps and irrigated with a leaching solution that contains microorganisms. As the solution percolates through the heap, it leaches out metals, which are collected at the base. This method is particularly effective for metals such as copper, gold, silver, uranium, and nickel [19][20]. Tank Leaching involves placing the crushed ore in tanks or reactors where leaching takes place under controlled conditions. Agitation and aeration ensure that the leaching solution, which may contain chemicals or microorganisms, thoroughly interacts with the ore. This method is highly efficient, especially for high-grade ores, as the controlled environment allows for the optimization of leaching conditions such as pH, temperature, and agitation. Tank leaching often results in higher recovery rates compared to heap leaching [21]. In-situ leaching (ISL), or solution mining, is a method where the leaching solution is injected directly into the ore body underground. The solution dissolves the target minerals in place, which are then pumped to the surface for recovery. This technique is particularly suited for ores that are difficult to access or too low in grade to be mined conventionally. ISL is widely used for the extraction of uranium, and to a lesser extent, copper and potash [22].

Among the diverse array of microorganisms explored for bioleaching, Pseudomonas putida stands out due to its metabolic versatility and environmental resilience. This gram-negative bacterium is known for its ability to degrade various organic pollutants and its potential for bioremediation [23]. Recent studies have demonstrated the efficacy of Pseudomonas putida in the bioleaching of non-sulfide ores and its role in the biotransformation of heavy metals, including lead and copper [24]. Pseudomonas putida can produce a range of organic acids and metabolites, which may enhance the solubilization of metals from ores through complexation and acidolysis. In the context of bioleaching, Pseudomonas putida offers several advantages. Its ability to adapt to various environmental conditions, including different pH levels and temperatures, makes it suitable for handling the diverse conditions found in ore processing. The bacterium's production of organic acids, such as citric and gluconic acid, enhances the dissolution of metal ions from ores, improving the efficiency of the leaching process [25]. Preliminary studies indicate that Pseudomonas putida can effectively solubilize metals such as chromium from chromite ores, showing promising results in terms of metal recovery and process optimization. These findings suggest that Pseudomonas putida could be a valuable tool in bioleaching applications, providing a potentially more sustainable and efficient approach compared to traditional methods of metal extraction.

Chromite ore, primarily composed of chromium and iron oxides, presents unique challenges for bioleaching due to its complex mineralogy and the harsh conditions typically associated with its processing. Research into the bioleaching of chromite ore is relatively limited compared to other ores. Most studies have focused on the use of acidophilic microorganisms, such as certain bacteria and fungi, which are well-suited to the acidic and oxidative environments necessary for effective bioleaching [26]. These microorganisms can enhance the solubilization of chromium and other metals from the ore by secreting organic acids and oxidizing agents, thereby facilitating metal extraction. Key studies highlight that acidophilic bacteria, such as Acidithiobacillus ferrooxidans, and fungi like Aspergillus niger have shown promise in leaching chromium from chromite ores [27]. These organisms not only adapt to harsh conditions but also significantly enhance the effectiveness of the leaching process by accelerating the breakdown of chromite and increasing metal recovery rates [24][28]. Bioleaching of chromite ore offers a viable and eco-friendly approach to extracting chromium, utilizing microbial processes to enhance metal recovery with a

lower environmental impact than conventional methods. Advancements in research and development could pave the way for wider adoption of bioleaching in mining and metallurgy.

The application of Pseudomonas putida for the leaching of chromite ore represents a novel approach with potential advantages. The bacterium's ability to produce organic acids and its adaptability to various environmental conditions suggest that it may offer an effective method for enhancing chromium recovery from chromite ores. Preliminary research into the use of Pseudomonas putida for similar applications indicates promising results in terms of metal solubilization and process efficiency [29][30]. However, detailed studies specifically targeting the bioleaching of chromite ore using Pseudomonas putida are scarce, warranting further investigation to optimize conditions and understand the underlying mechanisms involved. *Pseudomonas putida* demonstrates the power of microbial diversity in tackling environmental issues and driving progress in industrial biotechnology. Its ability to adapt, broad metabolic capabilities, and ease of genetic manipulation make it a key organism for innovations in bioprocessing, environmental protection, and other fields, solidifying its importance in both scientific research and industrial use [31].

While Pseudomonas putida shows great promise for bioleaching, there is still much to learn about its effectiveness specifically for chromite ore. This study explores the impact of pH, leaching time, and bacterial concentration on the leaching process of chromite ore.

6D.3 Materials and Methods

6D.3.1 Strain Preparation

For the bioleaching process, the initial step involves preparing the microbial culture solution. Pseudomonas putida is selected to treat the low-grade chromite ore, with the microorganism being purchased from ATCC Pune. To prepare a pure microbial culture solution, Luria broth medium (succinate medium) is autoclaved in 250 ml conical flasks. Once the autoclaved medium is cooled to room temperature, the Pseudomonas putida powder is added. The mixture is then incubated in a BOD shaker at 37°C and 110 rpm for 48 hours, after which the microbial culture solution is deemed ready for the bioleaching experiment.

6D.3.2 Experimental Setup

The 9 experimental setups, with additional blank experiments conducted (Blank 1 and Blank 2 which have numbers 10 and 11 respectively). The variable experimental parameters are pulp density and culture volume, where each parameter is evaluated at three levels: pulp density (1 g/L, 5.5 g/L, 10 g/L), and culture volume (4 ml/L, 8 ml/L, 12 ml/L). Table 1 outlines the 11 specific experimental setups with varying combinations of these parameters.

Table 6D.1: Summary of Experimental Setup.

Sl. No.	**Culture volume (ml/L)**	**Pulp Density (g/L)**
1	4	1
2	4	5.5
3	4	10
4	8	1
5	8	5.5
6	8	10
7	12	1
8	12	5.5
9	12	10
10	0	5.5
11	8	0

100ml of LB Broth medium is prepared in 11 glass conical flasks, each containing 250 ml. After that chromite ore samples are added based on the experimental setup. For bioleaching, the pH of the media is adjusted to 7 using 0.1 N HCl or NaOH, measured by a digital pH meter. The flasks are autoclaved at 121°C for 15 minutes. After sterilization, a 48-hour-old Pseudomonas putida culture is inoculated into the media. The flasks are incubated in a BOD shaker at 37°C and 110 rpm for the bioleaching process.

Samples are collected at intervals of 1, 5, 10, 15, 20, 25, and 30 days. For analysis, 10 mL aliquots are withdrawn from each flask and supplemented with autoclaved fresh broth medium every five

days to maintain the solid-liquid ratio. The pH of the leaching solutions is measured and recorded. The concentration of chromium, iron, and aluminium in the leached solutions is determined using atomic absorption spectroscopy (AAS) to assess the effectiveness of the bioleaching process.

6D.4 Results and Discussion

6D.4.1 Variation in pH

Figs. 6D.1 and 6D.2 present the variation of pH over the progression of bioleaching of chromite ore using Pseudomonas putida under changing pulp densities & culture volumes. The pH is observed to understand the interaction between the bacterial activity, chromite ore, and the bioleaching environment. In the Fig. 6D.1 and 6D.2, A represents blank 1 (contains only chromite ore in the absence of the culture), and blank 2 (control with only P. putida culture). In Fig. 6D.1 B, C, and D represent the pH profile for pulp density 1g/L, 5.5g/L, & 10g/L with variable culture volume. The pH in blank 1 shows a steady trend during the experimental time. This stability likely indicates the inherent chemical properties of the ore itself. But, in blank 2 the pH initially rises from 7 to 9 and then stabilizes, which is indicative of the metabolic activities of P. putida in the absence of chromite ore. The experiments involving blank 1 and blank 2 are conducted to establish a baseline for understanding pH changes during the bioleaching process in the presence of both the microorganism and the ore. It is observed from Figure 1 that changing the culture volume does not significantly impact the trend of pH change during the bioleaching process. In all cases, the pH initially rises from 7 to 9, followed by a flat terrain with no further significant changes. Notably, when the culture volume is high, a decrease in pH is observed after 25 days across all experiments. This decrease may be attributed to a saturation effect. The higher culture volume increases the microbial biomass, where the microbial population reaches a critical point beyond which it no longer significantly influences the pH.

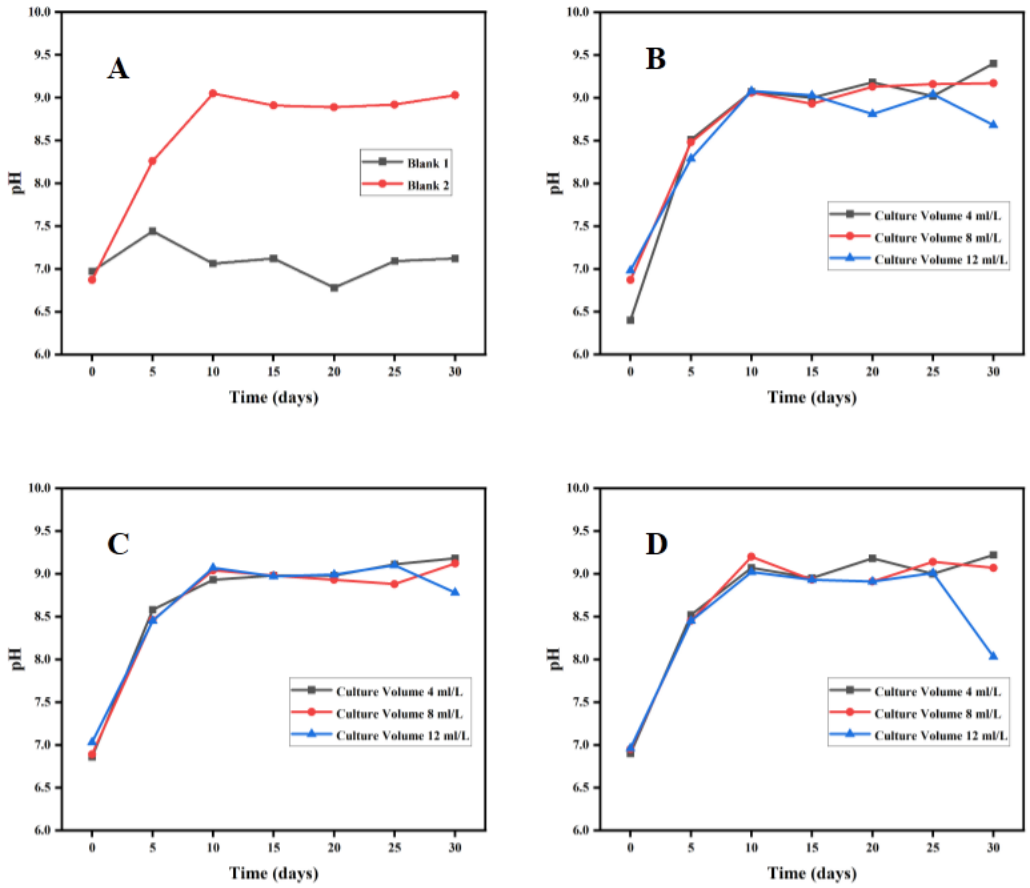

Figure 6D.1: Variation of pH During Leaching Experiment with Different Culture Volumes at a Fixed Pulp Density of (B) 1 g/L, (C) 5.5 g/L, (D) 10 g/L, Where (A) Represents the Blank Experiment.

A similar pH trend is observed when pulp density is changed remaining fixed culture volume. However, at higher pulp densities and culture volumes, the pH begins to decrease after a certain period. The expected reason behind it:

- Higher pulp densities provide more substrate availability for the Pseudomonas putida. This substrate may enhance their metabolic activities which helps to produce acidic by-products [32].
- Deficiency of nutrients, in the presence of higher culture volume may alter the metabolic processes of Pseudomonas putida which causes the generation of more acidic compounds [33].

- When the culture volume is high, the production of CO_2 during the metabolic processes of Pseudomonas putida increases accordingly. This CO_2 may dissolve in the leaching solution, forming carbonic acid, which ultimately leads to a reduction in pH [34].

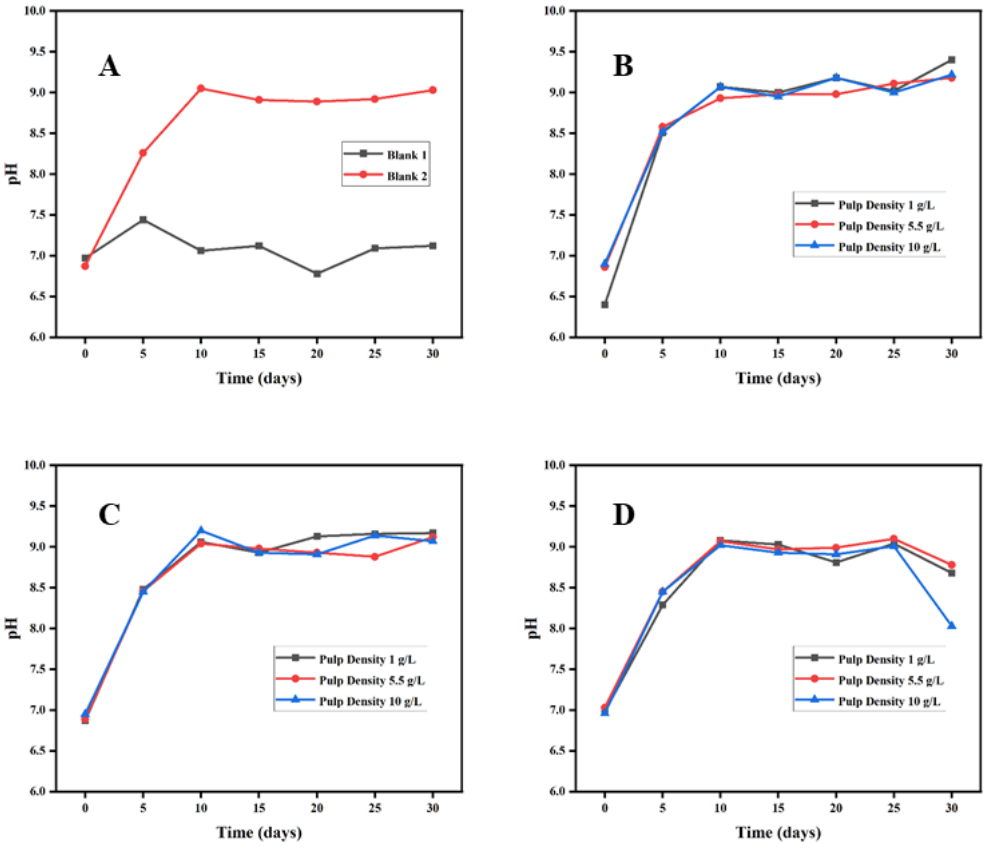

Figure 6D.2: Variation of pH During Leaching Experiment with Different Pulp Densities at a Fixed Culture Volume of (B) 4 mL/L, (C) 8 mL/L, (D) 12 mL/L, Where (A) Represents the Blank Experiment.

6D.4.2 Element Release during Leaching Studies

6D.4.2.1 Leaching Behavior of Chromium

Figs. 6D.3 and 6D.4 show the leaching behavior of chromium at different experimental setups. The blank sample 1 contained only chromite ore, resulting in a maximum chromium concentration of 4.28 mg/L which indicates minimal leaching of chromite ore in succinate media. Whereas, blank 2, which consisted only of Pseudomonas putida culture, showed no detectable chromium which confirms that leaching is driven by the bioleaching process facilitated by P. Pudida.

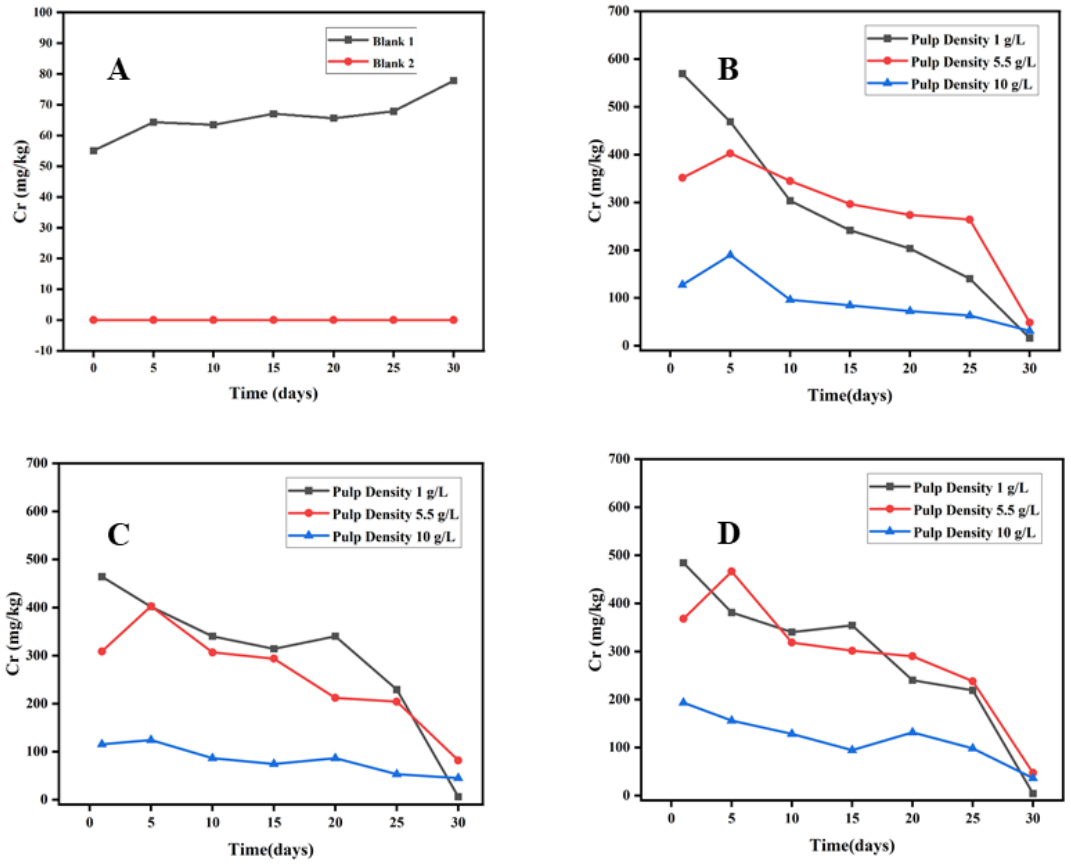

Figure 6D.3: Concentration of Chromium in Leachate During Leaching Experiment with Different Pulp Densities at a Fixed Culture Volume of (B) 4 mL/L, (C) 8 mL/L, (D) 12 mL/L, Where (A) Represents the Blank Experiment.

In Fig. 6D.3, images B, C, and D represent chromium leaching at culture volumes of 4 ml/L, 8 ml/L, and 12 ml/L, respectively. In all cases, the chromium concentration in the leachate decreased as the bioleaching process progressed. Remarkably, the maximum chromium concentrations are observed in the early stages of the leaching process.

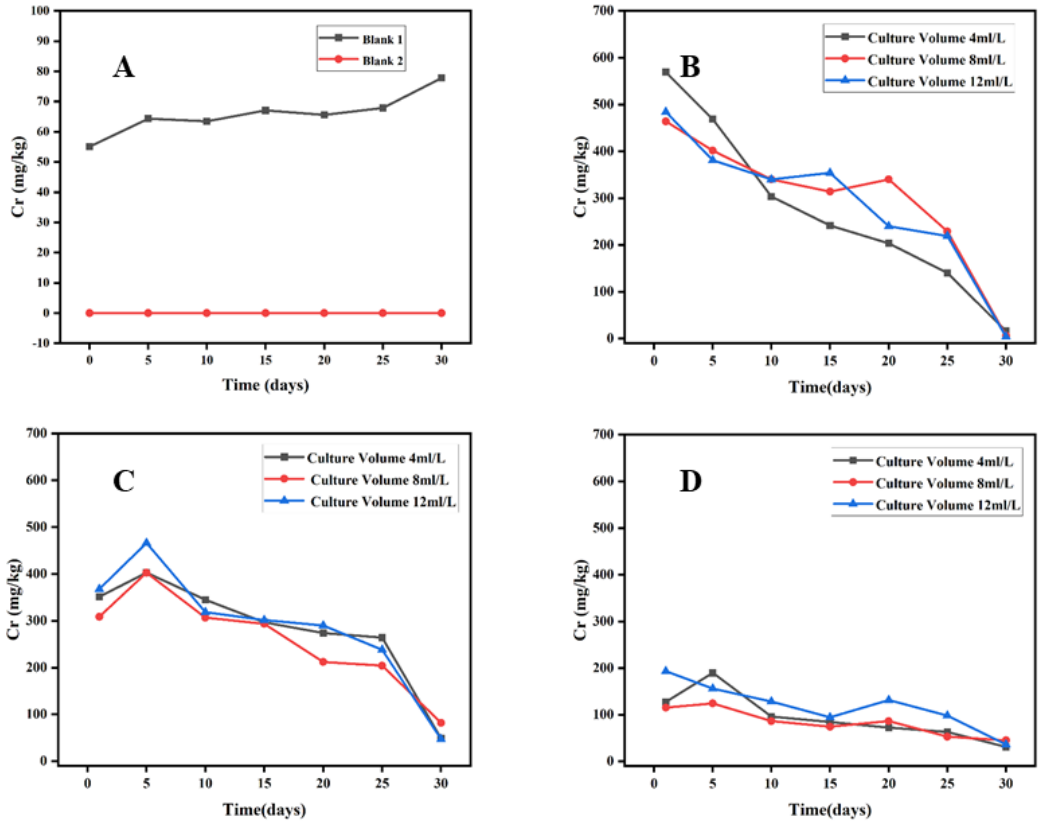

Figure 6D.4: Concentration of Chromium in Leachate During Leaching Experiment with Different Culture Volumes at a Fixed Pulp Density of (B) 4 g/L, (C) 8 g/L, (D) 12 g/L, Where (A) Represents the Blank Experiment.

The general trend of decreasing concentrations persisted for up to 30 days. It is observed that chromium (Cr) extraction is significantly higher at a density of 1 g/L compared to 5.5 g/L and 10 g/L, suggesting that chromium is either being taken up by bacteria or precipitating as insoluble compounds. The maximum concentration of chromium is found to be 569.50 mg/kg during the early stages of the leaching process, with a pulp density of 1 g/L and a culture volume of 4 mL/L. On the other hand, increasing culture volume decreases the Cr recovery, with the 12 ml/L volume showing no such significant chromium leaching behavior throughout the experiment. Control experiments confirmed that leaching is attributable to the microbial activity of P. Pudida. These findings highlight the importance of optimizing both pulp density and culture volume to enhance bioleaching efficiency.

6D.4.2.2 Leaching Behavior of Iron

Figs. 6D.5 and 6D.6 show the bioleaching of iron from chromite ore using P. putida. They show iron leaching results under various conditions, including controls, pulp densities, and culture volumes.

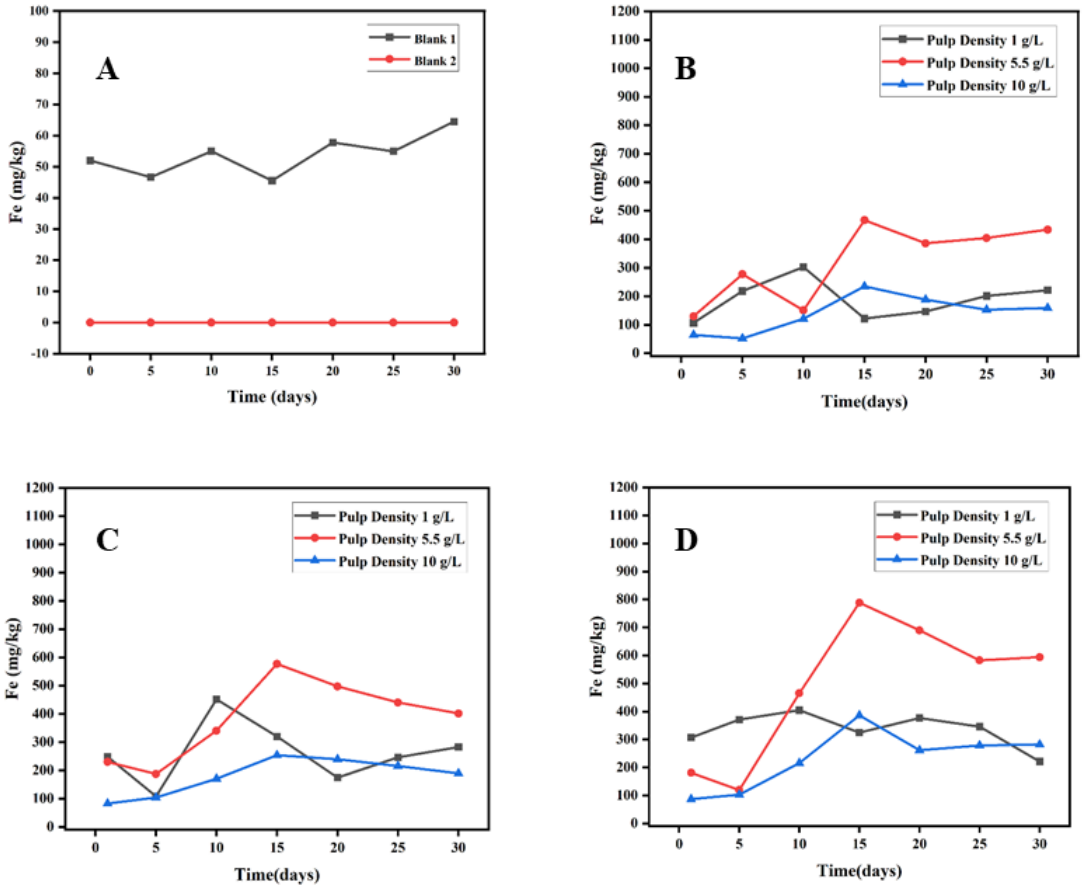

Figure 6D.5: Concentration of Iron in Leachate During Leaching Experiment with Different Pulp Densities at a Fixed Culture Volume of (B) 4 mL/L, (C) 8 mL/L, (D) 12 mL/L, Where (A) Represents the Blank Experiment.

Fig. 6D.5 shows leaching at different pulp densities with constant culture volumes of 4, 8, and 12 ml/L. Whereas Fig. 6D.6 shows leaching at different culture volumes with constant pulp densities of 1, 5.5, and 10 g/L. The leaching rate of iron increases with time. Images B, C, and D the concentration of iron gradually increases up to 15 days then declines slightly for the pulp density 5.5g/L and 10g/L. The most optimized result is observed at a pulp density of 5.5 g/L with a culture

volume of 12 mL/L, where maximum iron leaching reached 788.58 mg/kg after 15 days. A similar observation is also observed in Figure 6. Increasing the culture volume generally enhances the leaching efficiency, indicating that more bacteria can process higher amounts of iron. The results indicate the ability of iron to leach from chromite ore by P. Pudida.

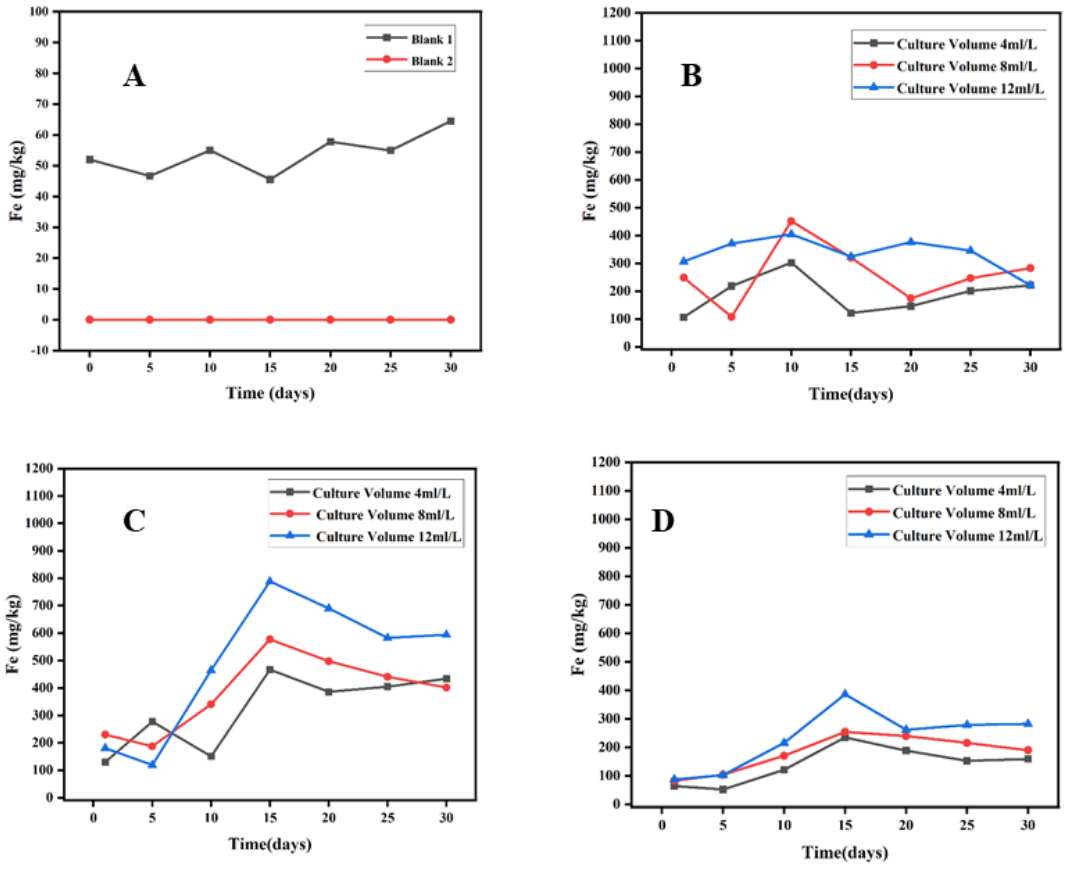

Figure 6D.6: Concentration of Iron in Leachate During Leaching Experiment with Different Culture Volumes at a Fixed Pulp Density of (B) 1 g/L, (C) 5.5 g/L, (D) 10 g/L, Where (A) Represents the Blank Experiment.

6D.4.2.3 Leaching Behavior of Aluminum

Figs. 6D.7 & 6D.8 reflect the influence of different experimental conditions on aluminum leaching from chromite ore using the bacterium P. Pudida. The aluminum leaching activity in blank, as well as chromite samples, is carried out for a period of 30 days. Same as earlier blank 1 contains only chromite ore with no bacteria and blank 2 contains only P. Pudida culture without chromite ore.

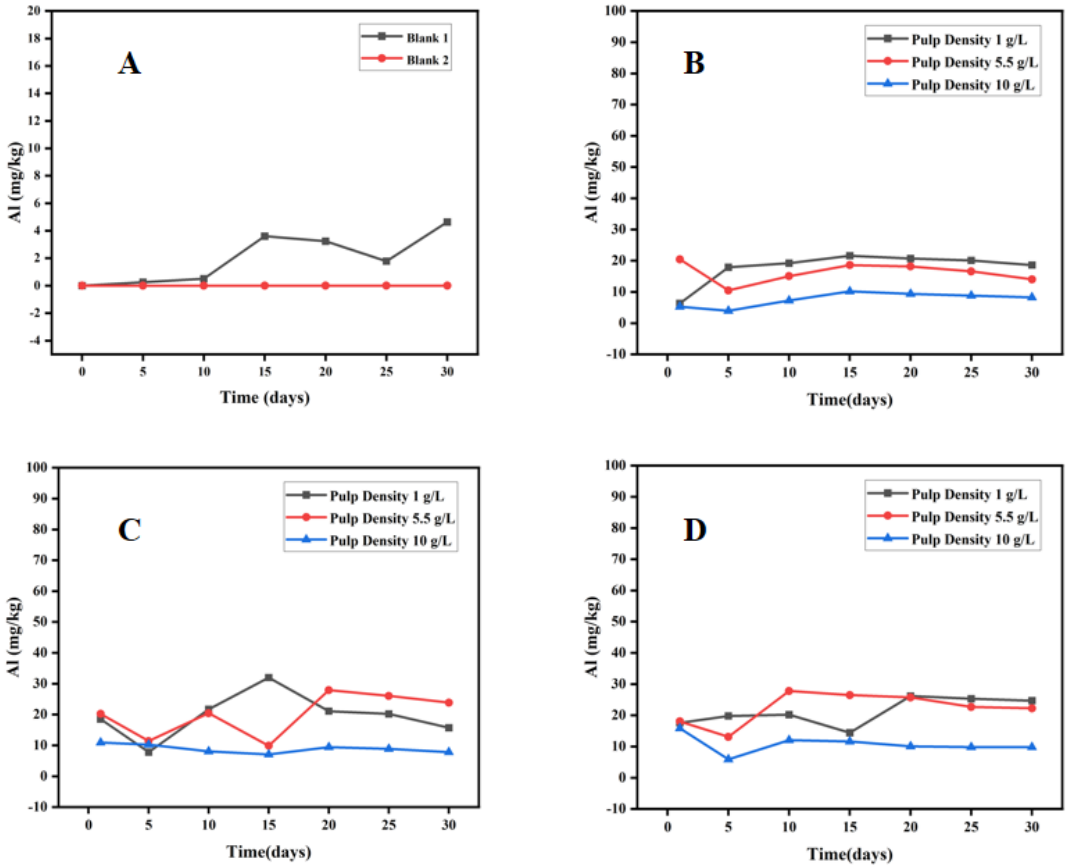

Figure 6D.7: Concentration of Aluminium in Leachate During Leaching Experiment with Different Pulp Densities at a Fixed Culture Volume of (B) 4 mL/L, (C) 8 mL/L, (D) 12 mL/L, Where (A) Represents the Blank Experiment.

It is observed from images B, C, and D in Fig. 6D.7, initially, aluminium leaching is quite an irregular manner but after 10 days aluminium concentration is increased in leachate then the concentration decreases as leaching time increases. On the other hand, when the ore concentration is increased while maintaining a fixed bacterial culture volume, the concentration of aluminum in the leachate decreases. It is observed that the highest aluminum recovery, peaking at 30.0 mg/kg, is achieved after 15 days under conditions with a pulp density of 1 g/L and a culture volume of 8 mL/L. It can be concluded that lower pulp densities favor higher Al dissolution, possibly due to better microbial activity and higher surface area availability for leaching reactions.

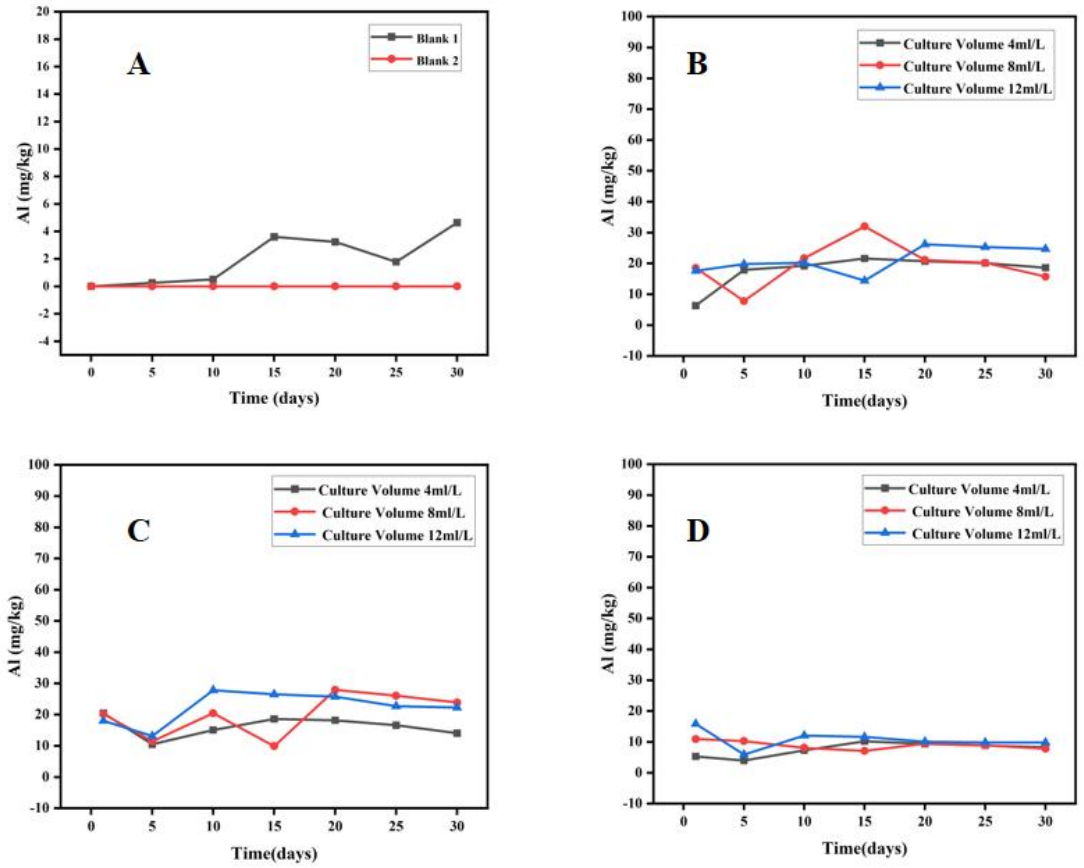

Figure 6D.8: Concentration of Aluminium in Leachate During Leaching Experiment with Different Culture Volumes at a Fixed Pulp Density of (B) 1 g/L, (C) 5.5 g/L, (D) 10 g/L, Where (A) Represents the Blank Experiment.

From Figs. 6D.8 and images B, C, and D, it can be observed that changes in culture volume do not significantly affect aluminum leaching. This indicates that at this low ore density, bacterial concentration is not a limiting factor. At the intermediate pulp density (5.5g/L), the trend might show slightly more variation in aluminum leaching with changes in culture volume. This suggests a more pronounced interaction between bacterial quantity and ore availability, potentially indicating an optimal culture volume for this specific pulp density. The overall data indicate that while low pulp densities do not require high bacterial volumes for effective leaching, intermediate and high densities might benefit from adjusted culture volumes. However, at higher pulp densities (10 g/L), the effect of increasing culture volume is reduced, indicating a threshold where pulp density becomes the dominating factor in limiting microbial access to the ore. This implies a

relationship between the available ore for leaching and the amount of bacteria needed to process that ore.

6D.5 Conclusion

In the present study, bioleaching of low-grade chromite ore using Pseudomonas putida is investigated where the effects of pulp density and culture volume on the leaching of chromium, iron, and aluminum are observed. Pseudomonas putida is chosen because it survives in harsh environments and produces acidic by-products that help with metal solubilization. The leaching results for chromium and iron showed that lower densities led to higher metal recovery. The low-grade chromite ore contains 18.39% chromium and 23.72% iron. But, during the leaching process, only 0.056% of chromium and 0.433% of iron are extracted, which is very low. These findings suggest that there is no significant bacterial effect on the release of chromium and iron from the chromite ore due to its complex mineralogy [17]. The production of acidic by-products during the leaching process is linked to changes in pH, with significant drops observed after extended incubation, particularly at higher culture volumes and densities. Crucial findings show that at low pulp densities (1 g/L), aluminum leaching is favored, with optimal recovery achieved at a culture volume of 8 mL/L. The results showed that higher bacterial concentrations are not necessary for effective leaching at this density, indicating that microbial activity is not limited by bacterial availability. In contrast, at intermediate pulp densities (5.5 g/L), slight variations in culture volume influenced aluminum leaching more significantly, suggesting a potential optimal culture volume for this density. Overall, this study underscores the importance of optimizing both pulp density and culture volume to enhance bioleaching efficiency. The relationship between ore availability and bacterial concentration suggests that careful calibration of these parameters can maximize the extraction of valuable metals from chromite ore, thereby improving the efficacy of microbial leaching processes. However, in the present investigation, it can be concluded that low pulp density (1 g/L) and higher culture volume (8 mL/L) are favorable conditions for the leaching of Cr, Fe, and Al.

6D.6 References

[1] M. Laputka and W. Xie, "A Review of Recent Advances in Pyrometallurgical Process Measurement and Modeling, and Their Applications to Process Improvement", Mining, Metallurgy & Exploration, vol. 38, pp. 1135–1165, 2021. doi: 10.1007/s42461-021-00386-y/Published.

[2] A. Weimer, M. Kohlstedt, D. C. Volke, P. I. Nikel, and C. Wittmann, "Industrial biotechnology of Pseudomonas putida: advances and prospects," Sep. 01, 2020, Springer. doi: 10.1007/s00253-020-10811-9.

[3] W. Liu et al., "Different Pathways for Cr(III) Oxidation: Implications for Cr(VI) Reoccurrence in Reduced Chromite Ore Processing Residue," Environ Sci Technol, vol. 54, no. 19, pp. 11971–11979, Oct. 2020, doi: 10.1021/acs.est.0c01855.

[4] G. G. Geesey, "Bacterial behavior at surfaces", Current Opinion in Microbiology, vol. 4, no. 3, 296-300, Jun. 2001. DOI: 10.1016/s1369-5274(00)00206-x.

[5] P. S. Kumar and P. R. Yaashikaa, "Recent trends and challenges in bioleaching technologies," in Biovalorisation of Wastes to Renewable Chemicals and Biofuels, Elsevier, 2019, pp. 373–388. doi: 10.1016/B978-0-12-817951-2.00020-1.

[6] W. Chingwaru, J. Vidmar, and C. Chingwaru, "Potential of biotechnology for metals extraction in Zimbabwe: A review," J South Afr Inst Min Metall, vol. 117, no. 4, pp. 381–386, Apr. 2017, doi: 10.17159/2411-9717/2017/v117n4a10.

[7] H. C. Liu, J. L. Xia, and Z. Y. Nie, "Relatedness of Cu and Fe speciation to chalcopyrite bioleaching by Acidithiobacillus ferrooxidans," Hydrometallurgy, vol. 156, pp. 40–46, Jun. 2015, doi: 10.1016/j.hydromet.2015.05.013.

[8] X. C. Chen, L. T. Chen, J. Y. Shi, W. X. Wu, and Y. X. Chen, "Immobilization of heavy metals by Pseudomonas putida CZ1/goethite composites from solution," Colloids Surf B Biointerfaces, vol. 61, no. 2, pp. 170–175, Feb. 2008, doi: 10.1016/j.colsurfb.2007.08.002.

[9] R. Naresh Kumar and R. Nagendran, "Fractionation behavior of heavy metals in soil during bioleaching with Acidithiobacillus thiooxidans," J Hazard Mater, vol. 169, no. 1–3, pp. 1119–1126, Sep. 2009, doi: 10.1016/j.jhazmat.2009.04.069.

[10] K. Bosecker, "Bioleaching: metal solubilization by microorganisms," FEMS Microbiol Rev, vol. 20, no. 3–4, pp. 591–604, Jul. 1997, doi: 10.1111/j.1574-6976.1997.tb00340.x.

[11] E. D. van Hullebusch et al., "Bio-alteration of metallurgical wastes by Pseudomonas aeruginosa in a semi flow-through reactor," J Environ Manage, vol. 147, pp. 297–305, Jan. 2015, doi: 10.1016/j.jenvman.2014.09.018.

[12] D. Borja et al., “Experiences and future challenges of bioleaching research in South Korea,” Dec. 01, 2016, MDPI AG. doi: 10.3390/min6040128.

[13] F. Echegaray, “Understanding stakeholders’ views and support for solar energy in Brazil,” J Clean Prod, vol. 63, pp. 125–133, Jan. 2014, doi: 10.1016/j.jclepro.2013.02.017.

[14] S. M. J. Koleini, H. Mehrpouya, K. Saberyan, and M. Abdolahi, “Extraction of indium from zinc plant residues,” Miner Eng, vol. 23, no. 1, pp. 51–53, Jan. 2010, doi: 10.1016/j.mineng.2009.09.007.

[15] R. Nkuna, G. N. Ijoma, T. S. Matambo, and N. Chimwani, “Accessing Metals from Low-Grade Ores and the Environmental Impact Considerations: A Review of the Perspectives of Conventional versus Bioleaching Strategies,” May 01, 2022, MDPI. doi: 10.3390/min12050506.

[16] H. Su, Y. Wen, F. Wang, Y. Sun, and Z. Tong, “Reductive leaching of manganese from low-grade manganese ore in H2SO4 using cane molasses as reductant,” Hydrometallurgy, vol. 93, no. 3–4, pp. 136–139, Aug. 2008, doi: 10.1016/j.hydromet.2008.01.001.

[17] K. Kremser et al., “Bioleaching and Selective Precipitation for Metal Recovery from Basic Oxygen Furnace Slag,” Processes, vol. 10, no. 3, Mar. 2022, doi: 10.3390/pr10030576.

[18] L. Rendón-Castrillón, M. Ramírez-Carmona, C. Ocampo-López, and L. Gómez-Arroyave, “Bioleaching Techniques for Sustainable Recovery of Metals from Solid Matrices,” Jul. 01, 2023, Multidisciplinary Digital Publishing Institute (MDPI). doi: 10.3390/su151310222.

[19] H. R. Watling, “Review of biohydrometallurgical metals extraction from polymetallic mineral resources,” Dec. 24, 2014, MDPI. doi: 10.3390/min5010001.

[20] T. Thenepalli, R. Chilakala, L. Habte, L. Q. Tuan, and C. S. Kim, “A Brief Note on the Heap Leaching Technologies for the Recovery of Valuable Metals,” Sustainability, vol. 11, no. 12, p. 3347, Jun. 2019, doi: 10.3390/su11123347.

[21] S. K. Behera and A. F. Mulaba-Bafubiandi, “Advances in microbial leaching processes for nickel extraction from lateritic minerals - A review,” Aug. 01, 2015, Springer New York LLC. doi: 10.1007/s11814-015-0085-z.

[22] G. M. Mudd, “Critical review of acid in situ leach uranium mining: 1. USA and Australia,” Dec. 01, 2001, Springer Verlag. doi: 10.1007/s002540100406.

[23] D. Kour et al., “Microbe-mediated bioremediation: Current research and future challenges,” J Appl Biol Biotechnol, vol. 10, pp. 6–24, 2022, doi: 10.7324/JABB.2022.10s202.

[24] V. Bolaños-Benítez et al., “(Bio)leaching behavior of chromite tailings,” Minerals, vol. 8, no. 6, Jun. 2018, doi: 10.3390/min8060261.

[25] A. Schippers, S. Hedrich, J. Vasters, M. Drobe, W. Sand, and S. Willscher, "Biomining: metal recovery from ores with microorganisms," Geobiotechnology I, vol. 141, pp. 1-47, 2014. doi: 10.1007/10_2013_216.

[26] S. Ghosh and A. K. Paul, "Heterotrophic leaching of metals from Indian chromite mining overburden," Int J Min Reclam Environ, vol. 31, no. 1, pp. 66–77, Jan. 2017, doi: 10.1080/17480930.2015.1118181.

[27] S. Biswas, S. Samanta, R. Dey, S. Mukherjee, and P. C. Banerjee, "Microbial leaching of chromite overburden from Sukinda mines, Orissa, India using Aspergillus niger," International Journal of Minerals, Metallurgy and Materials, vol. 20, no. 8, pp. 705–712, Aug. 2013, doi: 10.1007/s12613-013-0787-3.

[28] P. C. D L and H. L. Ehrlich, "Applied Microbiology Biotechnology Reduction of hexavalent chromium by Pseudomonas fluorescens LB300 in batch and continuous cultures," Applied Microbiology and Biotechnology, vol. 40, pp. 756–759, 1994.

[29] M. A. Kamran, S. Bibi, R. kou Xu, S. Hussain, K. Mehmood, and H. J. Chaudhary, "Phyto-extraction of chromium and influence of plant growth promoting bacteria to enhance plant growth," J Geochem Explor, vol. 182, pp. 269–274, Nov. 2017, doi: 10.1016/j.gexplo.2016.09.005.

[30] P. A. Wani, S. Wahid, M. S. A. Khan, N. Rafi, and N. Wahid, "Investigation of the role of chromium reductase for Cr (VI) reduction by Pseudomonas species isolated from Cr (VI) contaminated effluent," Biotechnology Research and Innovation, vol. 3, no. 1, pp. 38–46, Jan. 2019, doi: 10.1016/j.biori.2019.04.001.

[31] F. Rojo, "Carbon catabolite repression in Pseudomonas: Optimizing metabolic versatility and interactions with the environment," FEMS Microbiol Rev, vol. 34, pp. 658–684, Sep. 2010. doi: 10.1111/j.1574-6976.2010.00218.x.

[32] S. Sudarsan, S. Dethlefsen, L. M. Blank, M. Siemann-Herzberg, and A. Schmid, "The Functional Structure of Central Carbon Metabolism in Pseudomonas putida KT2440," Appl Environ Microbiol, vol. 80, no. 17, pp. 5292–5303, 2014, doi: 10.1128/AEM.01643-14.

[33] K. O'connor, W. Duetz, B. Wind, and A. D. W. Dobson, "The Effect of Nutrient Limitation on Styrene Metabolism in Pseudomonas putida CA-3," Applied and Environmental Microbiology, vol. 62, no. 10, pp. 3594-3599, 1996. DOI: 10.1128/AEM.62.10.3594-3599.1996.

[34] S. Zobel, J. Kuepper, B. Ebert, N. Wierckx, and L. M. Blank, "Metabolic response of Pseudomonas putida to increased NADH regeneration rates," Eng Life Sci, vol. 17, no. 1, pp. 47–57, Jan. 2017, doi: 10.1002/elsc.201600072.

Chapter-7

Overall Conclusion & Future Scope of Work

7.1 Characterization of Chromite Ore, Rductants, and Binders:

- Analysis shows that the collected ore has a chromium-to-iron ratio of 0.78.
- The major constituents of the ore are Cr_2O_3 (26.88%), Fe_2O_3 (33.88%), and Al_2O_3 (21.075). It is characterized as low-grade chromite ore with a significant iron content.
- The primary mineral phase identified is berezovskite $(Mg,Fe)(Al,Cr)_2O_4$, indicating a spinel structure.
- Chromite particles range in size from 75-200 μm.
- Microscopic analysis shows irregular particle shapes.
- Aluminum is distributed prominently across the chromite particles.
- Thermal analysis (TG-DTA) indicates a chemical dissociation occurring between 300°C and 350°C in the ore.

7.1.1 Reductants and Binders:

- Coke and boiler-grade coal are utilized as reductants. Coke contains 83.26% fixed carbon, whereas boiler-grade coal contains 30.52% fixed carbon.
- TG-DTA analysis in the characterization of reductants, corroborates the proximate analyses of coal and coke.
- Volatile matter in boiler-grade coal causes a notable weight loss when heated to 550°C.
- Two types of binders, bentonite (inorganic) and molasses (organic), are used.
- Molasses shows superior adhesive properties, while bentonite swells effectively.

In summary, the ore analyzed exhibits a complex nature with a spinel structure dominated by berezovskite. It is low-grade chromite ore with significant iron content and irregular particle shapes. Thermal analysis suggests phase transformations at specific temperatures, and the study evaluates reductants and binders for potential industrial applications.

7.2 Particle Size Distribution and Up-gradation of Chromite Ore:

- Adjusting particle size distribution significantly enhances the ratio of chromium to iron from 0.78 to 0.91, with an 86.90% Cr_2O_3 recovery.
- Using a wilfley Table for gravity separation in the lab is highly effective for the up-gradation of the ore.
- The tabling process is optimized through the application of the Box-Behnken Design (BBD) model.
- The tilt angle of the wilfley Table is the most influential parameter among those studied.
- Pre-heating the ore causes cracks and fissures, significantly boosting Cr_2O_3 recovery.

- Specific pre-heat temperatures improve the separation of gangue minerals from the chromite ore.

7.2.1 Experimental and Statistical Validation:

- High R^2 values for Cr/Fe ratio (0.96), Cr_2O_3 grade (0.91), and Cr_2O_3 recovery (0.96) indicate strong agreement between experimental results and BBD model predictions.
- ANOVA results confirm the reliability of these findings.

7.2.2 Optimal Conditions and Results:

- The best Cr/Fe ratio, Cr_2O_3 grade, and recovery achieved are 2.17, 48.50%, and 70.08% respectively.
- Optimal conditions for upgrading low-grade chromite ore:
    - Tilt angle: 8°
    - Water flow rate: 4 l/min
    - Pre-heat temperature: 443.72°C
- These conditions resulted in a Cr_2O_3 grade of 46.02%, a Cr/Fe ratio of 1.91, and a 65.95% recovery rate.

In conclusion, optimizing the wilfley table parameters, including tilt angle and pre-heat temperature, significantly enhances chromium recovery and the Cr/Fe ratio in chromite ore. The use of Box-Behnken Design (BBD) models confirms the effectiveness of these parameters, demonstrating their critical role in improving ore upgrading processes.

7.3 Agglomeration of Chromite Concentrate:

- Mechanical properties of chromite ore briquettes improve significantly with increased percentages of bentonite and molasses.
- The percentage of binders (bentonite and molasses) has a direct impact on the briquette's EOR (Extant of Reduction) and reducibility. Lower binder percentages improve EOR and reducibility, while higher binder percentages decrease them.
- Briquette stability increases with higher briquetting pressures.

7.3.1 Optimization of Briquette Composition:

- **Optimal Binder Composition**: 3% bentonite and 3% molasses yield the best mechanical strength and reducibility.
- **Optimal Pressure**: 450 Kg is the ideal briquetting pressure.
- **Overall Optimal Parameters**: 3% bentonite, 3% molasses, 3% water, and 450 Kg pressure provide the best combination of mechanical strength and reducibility.

In conclusion, the gravity separation technique using a wilfley Table coupled with optimized briquetting parameters provides a robust method for upgrading low-grade chromite ore and preparing it for efficient ferrochrome production.

7.4 Isothermal Reduction of Concentrate Chromite Briquettes:

- In the isothermal reduction of chromite ore, the extent of chromium and iron reduction is greatly impacted by the duration and temperature of the reduction process.
- Chromium reduction initiates at temperatures above 1573K, with the appearance of chromium carbide phase detected at 1623K.
- Chromium reduction follows iron reduction, indicating that metallic chromium is absent below 1573K, while iron metallization starts from 1373K.
- Increasing time and temperature progressively enhance the degree of metallization, reaching maximum levels of 75.50% for chromium and 75.71% for iron at 1723K over 120 minutes.
- Metallic fractions in reduced ore improve process efficiency and economic viability during smelting.
- Initially, the CG2 mechanism dominates at high temperatures, transitioning to the D3 mechanism with prolonged reduction time due to changes in thermodynamic stability and reaction kinetics.
- Activation energies for CG2 and D3 mechanisms are 165.357 KJ/mol and 179.36 KJ/mol, respectively.
- Ferrochrome obtained from smelting pre-reduced chromite briquettes contains 52.96% chromium, 28.72% iron, and minor amounts of carbon, silicon, sulfur, and phosphorus as per ICP-OES analysis.
- The slag generated in the smelting process is enriched with silica, alumina, and oxides of iron, primarily comprising silicate and aluminate phases such as forsterite ($MgSi_2O_4$) and magnesium aluminate ($MgAl_2O_4$).
- Despite achieving the desired chromium and iron content, further refinement is necessary to meet stringent industrial specifications for stainless steel production.

This conclusion summarizes the intricate processes and findings of chromite ore reduction, highlighting key parameters, mechanisms, and requirements for producing high-quality ferrochrome suitable for industrial applications.

7.5 Low-Grade Chromite Reduction in Gasification Furnace:

- **Pre-reduction Process:**
- Low-grade chromite ore undergoes effective pre-reduction in a gasification furnace using lean-grade coal.
- Maximum extent of reduction (EOR) occurs at 1473K over 2 hours.
- **XRD Analysis of Reduced Ore:**
- XRD analysis shows an increased intensity of metallic iron peak with higher reduction temperatures.
- Magnetic separation post-reduction enhances the Cr/Fe ratio from 0.775 to 1.18 in the ore fractions.

7.5.1 Product Characterization:

- XRD analysis of the product indicates that without blending, the major phase is $Cr_{1.36}Fe_{0.52}$. However, blending with a 20% magnetic fraction shifts this to the $CrFe_4$ phase.
- Higher blending ratios decrease the chromium concentration in the product.
- SEM imaging reveals a distinct lamellar structure of the ferroalloy.
- Two-phase distribution within the grain and numerous inclusions are observed in the product.
- Cr/Fe ratios in the smelting products are 0.92 and 0.70 for non-magnetic and magnetic fractions, respectively.
- Incorporating the magnetic fraction enhances the volume of the metalized phase.

In conclusion, the study demonstrates effective pre-reduction of low-grade chromite ore using lean-grade coal, leading to increased Cr/Fe ratios through magnetic separation. It identifies phases in the produced iron-chromium alloy and outlines steps for enhancing product quality through additional processing steps.

7.6 Hydrometallurgical Treatment of Low-Grade Chromite Ore:

- Chromium oxide and potassium dichromate are successfully produced from low-grade chromite ore through oxidative roasting with sodium nitrate ($NaNO_3$) and sodium hydroxide (NaOH).

- It is observed that sodium nitrate acts as a catalyst by enhancing the recovery of chromium by 99.52%, compared to 80% without it.
- The extraction of chromium depends upon some factors, such as alkali concentration, roasting time, and temperature.
- Optimal chromium recovery is achieved at a 1:3 NaOH to ore ratio.
- The kinetic study indicates that the process follows the D5 mechanism (anti-Jander), where the rate-limiting step is the transport of chromate ions across the solid product layer formed during roasting.
- The activation energy for the rate-determining step is found to be 48.375 kJ/mol.
- Leaching residue analysis identifies Fe_2O_3 as the predominant oxide along with other oxides like MgO, Al_2O_3, SiO_2, and Na_2O.
- Aluminum leaching from chromite ore with NaOH shows promising results, with a 97.76% recovery under optimized conditions.
- The purity of potassium dichromate is calculated to be 90.76%.
- Reduction of $K_2Cr_2O_7$ with carbon at 1173 K for 30 minutes predominantly produces Cr_2O_3 and Cr_3C_2 phases. The result indicates that metallic chromium can easily be obtained from Cr_2O_3 and Cr_3C_2 when reduction occurs at higher temperatures.

Further refinement through recrystallization and higher-temperature reduction processes may yield higher-purity potassium dichromate and chromium compounds for metallurgical applications.

7.7 Biohydrometallurgical Treatment of Low-Grade Chromite Ore:

- The bioleaching process of low-grade chromite ore in this research is performed using Pseudomonas putida, focusing on the effects of pulp density and culture volume on chromium, iron, and aluminum leaching.
- Pseudomonas putida is selected for its ability to survive in harsh environments and produce acidic by-products that help metal solubilization.
- Higher bacterial concentrations are not necessary for efficient aluminum leaching at low pulp density, suggesting microbial activity was not limited by bacterial availability.
- Chromium and iron leaching showed minimal bacterial impact due to the spinel structure of chromite ore.
- Aluminum leaching is more effective at lower pulp densities and optimized culture volumes.

- Optimization of pulp density and bacterial concentration is a key factor in improving bioleaching outcomes for valuable metals from chromite ore.

7.8 Interpretation:

In this thesis, efforts have been made to upgrade lean-grade chromite ore to produce ferrochrome and chromium-based alloys. Chromium compounds and alloys are crucial in modern technology, particularly in the steel industry. Upgrading lean-grade chromite ore can enhance the quality of steel products and improve their financial viability. This research successfully achieved the effective upgradation and utilization of lean-grade chromite through various process routes, including wilfley Table separation, direct and indirect carbothermic reduction, sodium hydroxide leaching, and bio-leaching.

Future Scope of Work

Future work will emphasize bridging the gap between laboratory research and industrial application through pilot-scale testing to validate findings under real-world conditions. This includes assessing the economic feasibility and scalability of optimized parameters. To enhance the briquetting process, alternative binders with improved performance or cost-efficiency will be explored, alongside a thorough evaluation of their environmental impact and sustainability. Additionally, efforts will focus on fine-tuning wilfley table parameters-such as tilt angle, water flow rate, and feed rate-for various ore types and conditions, while systematically studying the effects of pre-heating temperatures on separation efficiency and concentrate quality.

Looking ahead, future work could focus on refining technologies to enhance the purity of ferrochrome through advanced decarburization, desulfurization, and deoxidation techniques. These developments aim to meet increasingly stringent industrial standards and improve the overall quality and market competitiveness of the final alloy.

Future work will explore the potential of using Pseudomonas putida for the beneficiation of low-grade bauxite ore, leveraging its leaching capabilities demonstrated in chromite processing.

Future research should focus on enhancing the efficiency and purity of the iron-chromium alloy production process. This includes optimizing gasification furnace conditions to achieve higher EOR and investigating alternative reducing agents to improve metallurgical outcomes. The development of advanced magnetic separation techniques could further enhance the Cr/Fe ratio and streamline alloy production. Additionally, refining processes should aim to mitigate inclusions and achieve a uniform distribution of alloy phases through improved slag phase management and substitution of aluminum with Fe-Si reducers. These efforts will be crucial in meeting stringent industrial standards and expanding the application potential of the produced ferroalloy in high-value steel manufacturing.

Appendix I

1. Percentage Chromium Oxide (Cr_2O_3) Recovery:

Cr_2O_3 recovery (%) = $\frac{M1 \times C1 \times 100}{M2 \times C2}$

Where, M1 = Mass of chromite ore after tabling.

M2 = Mass of low-grade chromite ore introduced into the tabling process.

C1 = Percentage of Cr_2O_3 present in concentrate chromite sample.

C2 = Percentage of Cr_2O_3 present in low-grade chromite ore.

2. The Grade Chromium Oxide (Cr_2O_3) Percentage:

Cr_2O_3 grade (%) = $\frac{M \times 100}{W}$

M = Amount of Cr_2O_3 present in the chromite concentrate after the tabling process.

W = Total mass of the chromite concentrate obtained from the tabling process.

3. The shatter index (SI):

SI = $\frac{W1 \times 100}{W}$

Where W1 = Weight retained on the 0.5 mm sieve following the shatter test and subsequent sieving.

W = Total weight of the briquette.

4. The abrasion index (AI):

AI = $\frac{W2 \times 100}{W}$

Where W2 = Weight passing through a 0.5 mm sieve following the abrasion test and subsequent sieving.

W = Total weight of the briquette.

Appendix II

Calculation of Stoichiometric Carbon for Chromite ore Reduction:

WDXRF result of low grade chromite ore is given below:

Cr_2O_3	Fe(T)	Mn	Al_2O_3	SiO_2	TiO_2	K_2O	Ni	P	S	V_2O_5	CaO	MgO	LOI
26.88	23.72	0.55	21.07	0.92	0.29	0.004	0.1	0.02	ND	0.172	0.02	5.1	8.99

Where Fe (T) = Total iron content.

Molecular weight of Fe_2O_3 is 160 gm.

160 gm of Fe_2O_3 contains 112 gm of Fe.

23.72 gm of Fe present in (160/112)*23.72 = 33.88 gm of Fe_2O_3.

The maximum reduction temperature of chromite ore reduction is carried out at 1723K K. At that temperature, the reduction of magnesium oxide and aluminium oxide is thermodynamically unfavorable. Only chromium and iron oxides are reduced. So the reaction that occurs during the reduction process is given below:

For chromium oxide

$Cr_2O_3 + 3C = 3CO + 2Cr$

36 gm of carbon is required to reduce 152 gm Cr_2O_3.

100 gm Cr_2O_3 is reduced by 23.68 gm of carbon.

26.88 gm Cr_2O_3 is present in 100 gm chromite ore.

100 gm Cr_2O_3 is present in 372.02 gm chromite ore.

372.02 gm chromite ore required 23.68 gm of carbon for Cr_2O_3 reduction.

100 gm chromite ore required 6.37 gm of carbon for Cr_2O_3 reduction.

For iron oxide

$Fe_2O_3 + 3C = 3CO + 2Fe$

36 gm of carbon is required to reduce 160 gm Fe_2O_3.

100 gm Fe_2O_3 is reduced by 22.5 gm of carbon.

33.88 gm Fe_2O_3 is present in 100 gm chromite ore.

100 gm Fe_2O_3 is present in 295.16 gm chromite ore.

295.16 gm chromite ore required 22.5 gm of carbon for Fe_2O_3 reduction.

100 gm chromite ore required 7.62 gm of carbon for Fe_2O_3 reduction.

Total carbon required to reduce 100 gm ore (6.37+7.62) = 13.99 gm.

84.96 gm fixed carbon is present in 100 gm of coke.

13.99 gm of fixed carbon is present in 16.46 gm of coke.

To reduce 100g of chromite ore 16.46 gm of coke is required.

Appendix III

Percentage Extent of Reduction (EOR) Calculation:

Carbothermic reduction of chromite ore is carried out using metallurgical grade coke which contains 84% of fixed carbon. The extent of reduction is the ratio of percentage oxygen loss during reduction and total oxygen loss expected for the complete (100%) reduction.

Percentage extent of reduction = $\frac{Weight\ loss\ of\ oxygen\ after\ reduction \times 100}{Weight\ loss\ of\ oxygen\ for\ complete\ reduction}$

Chromite concentrate contains 46.02% Cr_2O_3 and 23.54% Fe_2O_3.

The composition of briquette is = 3% bentonite + 3% molasses + 3% water + rest chromite ore.

Before taking initial weight for the reduction, the briquettes are dried in hot air oven at 105 ºC for one hour. During this process moisture has been removed.

Dried briquettes contains 3% bentonite + 3% molasses + rest chromite ore.

Reactions occur during the reduction:

$Cr_2O_3 + 3C = 3CO + 2Cr$ 1

$Fe_2O_3 + 3C = 3CO + 2Fe$ 2

From equation 1:

36 gm carbon is required to remove complete oxygen from 152 gm Cr_2O_3.

Carbon required to remove complete oxygen from 46.02 gm Cr_2O_3 = $\frac{36 \times 46.02}{152}$= 10.90 gm.

From equation 2:

36 gm carbon is required to remove complete oxygen from 160 gm Fe_2O_3.

Carbon required to remove complete oxygen from 23.54 gm Fe_2O_3 = $\frac{36 \times 23.54}{160}$= 5.29 gm.

Total fixed carbon is required for complete reduction of 100 gm chromite ore = (10.90+5.29) =16.19 gm.

100 gm coke contain 84 gm of fixed carbon.

16.9 gm fixed carbon present in 19.27 gm coke.

19.27 gm coke is required to reduce 100 gm of chromite ore.

The initial weight of briquette is 10 gm and final weight (after reduction) of the briquette is 7.5 gm.

If weight of the chromite ore in the briquette is X then:

Coke present in the briquette = X × 0.1927 gm.

Bentonite present in the briquette = X × 0.03 gm.

Molasses present in the briquette = X × 0.03 gm.

So, 10 = X+ 2(X × 0.03) + X × 0.1927

or, X = 7.983 gm

10 gm briquette contains 7.983 gm chromite ore + 0.239 gm molasses + 0.239 gm bentonite + 1.539 gm coke.

7.983 gm ore contain (7.983 × 0.4602) = 3.674 gm Cr_2O_3.

Weight loss due to the complete reduction of Cr_2O_3 = 1.16 gm

7.983 gm ore contain (7.983 × 0.2354) = 1.879 gm Fe_2O_3.

Weight loss due to the complete reduction of Fe_2O_3 = 0.563 gm.

Weight loss for complete oxygen removal = (1.16+0.563) = 1.723 gm.

Weight loss of bentonite at 1673 K is 18.90%.

Weight of bentonite during reduction = (0.239 × 0.1890) = 0.045 gm.

Weight loss of molasses at 1673 K is 96.16%.

Weight of molasses during reduction = (0.239 × 0.9612) = 0.230 gm.

Ash content of coke = 13.64%.

Weight loss of coke during reduction = (1.539 × 0.8636) =1.328 gm.

Fixed weight loss due to coke, bentonite, and molasses = (1.328 + 0.045 + 0.230) = 1.603 gm.

Weight loss due to oxygen removal during reduction = [(10-7.5)-1.603] = 1.39 gm.

Percentage extent of reduction = $\frac{1.39 \times 100}{1.723}$ = 80.67%.